Probing the Reactivity of Lattice Nitrogen in Transition Metal Nitrides

Anne-Marie C. Alexander

A Thesis Presented to the University for the Degree of

Doctor of Philosophy

School of Chemistry

The University of Glasgow

April 2011

Abstract

Reactions involving nitrogen transfer are of great industrial interest. Utilizing nitrides in this manner, in principle, could help industries overcome the increasing challenges which they face to meet economic and environmental targets. An example of this is the possible application of metal nitrides in the direct synthesis of aniline from benzene, which could potentially remove the need for the lengthy, uneconomical, and environmentally unfriendly process which is currently employed.

In the work presented in this thesis a screening study has been undertaken which explores the reactivity of lattice nitrogen within bulk and supported transition metal nitride catalysts. The experimental work has been conducted with the aim of developing a potential nitrogen transfer reagent in order to synthesise aniline via the direct conversion of benzene and has focussed on three main objectives: the first being to determine the most active transition metal nitride catalysts for ammonia synthesis, in the absence of N_2, in order to determine the reactivity of "lattice" nitrogen. It was necessary at this point to establish which materials were reactive and lost nitrogen from the metal lattice at or below $400^{o}C$, the maximum temperature for the envisaged process.

Secondly, those materials which demonstrated a subsequent loss of lattice nitrogen upon reaction with H_2/Ar were then screened to establish whether it was possible to restore the original nitrogen content in the materials in order for the nitrides to function in a Mars-van Krevelen type capacity. Finally the reaction of benzene and hydrogen over bulk binary nitrides was conducted in an attempt to trap reactive NH_x species for the production of aniline. It was found that no aniline was produced in these reactions. However, some interesting results were obtained over a selection of nitride materials, namely Co_3Mo_3N, Cu_3N, Zn_3N_2, Re_3N and a metallic Co-4Re compound where low quantities of, as yet unidentified, reaction products were formed.

To the author's knowledge, this is the largest systematic study of bulk nitrides and related materials which has been investigated on this scale and which has been directed towards this specific, novel, target process.

Contents

List of Tables

List of Figures

Publications

A.-M. Alexander, J. S. J. Hargreaves 'Alternative catalytic materials: carbides, nitrides, phosphides and amorphous boron alloys' Chemical Society Reviews, 39 (2010) 4388-4401

Future publications anticipated.

Acknowledgements

I am deeply grateful to my supervisor Dr. Justin Hargreaves. His enthusiasm, inspiration and his enormous amount of patience over the last 4 years has helped make chemistry a much more enjoyable experience for me.   Throughout my thesis-writing period, he provided encouragement and sound advice and I would have been lost without him. I have really enjoyed working with Justin for the last four years, and can't stress enough how much I appreciate his help. Thanks must also go to my supervisor at Huntsman Polyurethanes in Brussels, Chris Mitchell, for his input and continuing interest in this thesis.

I am also very grateful to various other people who have helped me to make this project successful. These include Ron Spence for his help with the GC analysis; Mr. Jim Gallagher for his help with the SEM; Mrs. Kim Wilson for her assistance in performing the CHN analysis and a big thank-you must also go to Andy Monaghan for his friendship, help and the numerous debates over a cup of coffee, which were very much appreciated.

I would also like to specially thank Stuart Hunter for all his help in the last 4 years, moving cylinders, assisting with some of the conductivity readings for the 18+ hour experiments, which allowed me to get a few hours sleep and generally being a good friend. I wish him all the best on the career front. I hope we keep in touch scouting or otherwise.

Thanks also to the remaining members of the Hargreaves and Jackson research group: Liam France, Alex Munnoch, Fiona Wigzell, Lynsey Pugh, Javeed Ali, Muhammad Bilal, Alisa Lynch, Claire Gillian, Stuart Blain and Mark Facchini for making the last four years an interesting and memorable experience.

I owe a huge thanks to my parents and grandparents who have been a constant source of support – both emotionally and morally throughout my undergraduate and postgraduate years. This thesis most certainly would not exist -especially since my mum accepted my PhD on my behalf!! - if it had not been for all their love, encouragement and support during my time at university and throughout my life.

Finally I want to thank Ian, who has been there for me over the last 5 years, for his patience, support and words of encouragement when I needed them most.

Author's Declaration

The work contained in this thesis, submitted for the degree of Doctor of Philosophy, is my own original work, except where due reference is made to other authors. No material within has been previously submitted for a degree at this or any other university.

To Mum, Shaun and Ian

1. Introduction.

1.1 Catalysis with Nitrides.

The chemistry of inorganic nitrides has progressed rapidly over the last two decades, due to advances in preparation methods, which has meant many nitrides have become much more easily accessible.[1-5]   However, the stability of the N_2 molecule, when compared, for example to oxygen or halogens, has meant that the production of nitrides from the direct reaction with nitrogen is often difficult due to the thermodynamic barriers associated with the breaking of the N-N bond (945 kJ mol^{-1}).[6] This also implies that nitriding conditions are generally high temperature and often involve nitrogen containing species such as ammonia, which are more reactive than molecular nitrogen. Many nitrides are air and moisture sensitive forming oxides and ammonia on contact with oxygen or moisture; this is particularly apparent with Group I and II nitrides.[7]

Generally the transition metal nitrides are more stable and are characterised by their high melting points, hardness and resistance to corrosion. These materials often have very desirable physical properties under catalytic reaction conditions and it has been well-documented that they possess catalytic advantages over their parent metals in activity, selectivity and their resistance to poisoning.[5, 8-10] Many have been found to be effective catalysts for a wide range of reactions and some, in particular molybdenum and tungsten, are often reported to exhibit catalytic properties comparable to that of traditional noble metal catalysts as initially proposed in the work by Levy and Boudart.[10-14]

All transition metals form nitrides with the exception of the second and third row Group VIII-X metals (Ru, Os, Rh, Ir, Pd and Pt), although thin films of these have been prepared.[1,14]   Many of the catalytic studies reported in the literature have focused mainly on the application of the nitrides of Group IV-VI metals.[15-19] This is partly due to their increased stability when compared to the nitrides of Group VII-X metals, which have been relatively little studied and have limited applications for catalytic reactions.[20,21] Nevertheless in recent years the number of reactions catalysed by nitrides has increased, as has their application in optoelectronic devices (TiN, BN, GaN and InN),[22-25] semiconductors (Cu_3N, GaN)[26,27] and high temperature ceramics (BN, Si_3N_4).[28,29] Despite the expansion in nitride chemistry the catalytic behaviour of many established nitride compounds remains unknown. This is mostly due to the fact that efforts have

predominantly focused on preparative methods rather than their properties and catalytic ability.

Nitrides are typically classified as ionic, covalent and interstitial,[7] although metallic nitrides have also been described.[30,31] Ionic nitrides generally possess a formula which would be expected by the combination of a metal ion with N^{3-} and are typically formed by elements found in Groups I, and II such as Li, Mg, Ca, Sr, and Ba. However, metals such as Cu, Zn and Hg also form ionic or salt-like nitrides. Nitrides of the Group III metals are also salt like but are either metallic conductors, or at least semi-conductors, and therefore represent the transition to the metallic or interstitial nitrides. Interstitial nitrides are formed by some transition metals and generally refer to those which have structures in which the nitrogen atoms reside in the interstitial space in close packed metal structures. In moving from left to right along the 1st row transition series, the size of the metal atom decreases and it becomes increasingly difficult for the nitrogen atom to be accommodated into the metal lattice; hence the thermal stability of the nitride also decreases. As a consequence of the smaller atomic radii, nitrides of Group VII -X transition metals do not form interstitial compounds but are generally classed with the ionic or salt-like nitrides (e.g. Cu_3N as mentioned above). Non-metallic Group XIII and XIV elements, such as B, Si, P and C, form nitrides which are characterised predominately by their covalent bonding. Due to the chemical inertness and the high heat capacity of these materials, many covalent type nitrides, in particular BN and Si_3N_4, have been investigated as catalyst supports and are used within the ceramic industry.[29] However it is quite often that more than one type of bond exists within the compound which can make classification by this method somewhat arbitrary. Nitrides can be further categorized according to the number of metal atoms present in the main structure; these are binary (one metal), ternary (two metals) and quaternary (three metals). Table 1.1-1 provides an overview of the nitrides of Groups IV-X which may be most relevent for heterogenous catalysis.[31]

Group IV	Group V	Group VI	Group VII	Group VIII	Group IX	Group X
Ti_2N $TiN_{0.9}$ TiN	V_2N VN	Cr_2N CrN	Mn_4N Mn_2N Mn_3N_2	Fe_4N Fe_3N Fe_2N	Co_4N Co_3N Co_2N	Ni_3N
ZrN	Nb_4N_5 Nb_2N NbN	Mo_2N MoN	$TcN_{0.75}$	Ru	Rh	Pd
Hf_3N_2 HfN	Ta_3N_5 Ta_2N TaN	W_2N WN	Re_3N Re_2N	Os	Ir	Pt

Table 1.1-1 Table of Group IV-X metal nitrides which may be most relevent for heterogenous catalysis.[31]

1.2 Preparation methods.

Before Volpe and Boudart reported the synthesis of nitride catalysts via the temperature programmed reaction method, transition metal nitrides had long been known as hard, refractory materials possessing the electronic and magnetic properties of metals. Traditionally, the synthesis of many metal nitrides involved the direct reaction of the metal with nitrogen gas, typically operated at elevated temperatures and pressures, which often resulted in materials with low surface areas. Hence they were not considered as catalytic materials and as a consequence historically the use of nitrides has been fairly limited.[31]

In the innovative work of Volpe and Boudart, it was shown that high surface area metal nitrides and carbides (reportedly 225 m^2g^{-1} in the case of γ-Mo_2N) could be prepared by the treatment of a metal oxide precursor with ammonia using carefully controlled temperature ramp conditions.[32] In this method, which is generally described as ammonolysis, the high ammonia flow rates and low temperature ramp rates are of significant importance in the preparation of high surface area materials.[33] The use of high flow rates reduces the partial pressure of the H_2O generated during transformation of the oxide precursors and subsequently minimises the effect of hydrothermal sintering which occurs at high temperatures. This method generally results in products which are pseudomorphic with the oxide precursor and is now very common in the preparation of different nitride materials.[34] However, oxynitrides may form in the case of incomplete transformation, which may be difficult to identify by powder X-ray diffraction.[35] The major concern with this method, however, is the pyrophoric nature of the freshly prepared materials. Passivation procedures employing low concentrations of O_2 are generally applied leading to the generation of a protective oxide layer to facilitate handling. This layer can

subsequently be removed by treatment with H_2 or H_2/N_2 mixtures.[36,37] Ammonolysis of different precursors can yield different phases, examples of which can be observed within the literature related to the preparation of molybdenum nitrides.[38-40] For instance, ammonolysis of MoS_2 or $MoCl_5$ generates the δ-MoN phase, as opposed to the γ-Mo_2N phase which is formed via the oxide precursor. Ammonolysis has also been applied to the preparation of various supported nitride materials. Several studies have examined how preparation conditions can affect the phase purity of the molybdenum nitride obtained; Marchand and co-workers have demonstrated the effect of heating rates on surface areas of the γ-Mo_2N phase prepared by ammonolysis of MoO_3, as shown in Table 1.2-1.[33]

	γ-Mo₂N–A	γ-Mo₂N–B	γ-Mo₂N Volpe and Boudart
Amount of commercial MoO_3 precursor (g) (S_g = 2 m^2g^{-1})	2-3	2-3	1
Rate of temperature increase (K min^{-1})			
-from 293K to 633K	10	20	6
-from 633K to 723K	1	20	0.6
-from 723K to final temperature	-	20	-
Final temperature (K)	700	780	710
Step time (h)	10-12	0.5	1
Ammonia flow rate (l h^{-1})	35	35	1
Specific surface area (m^2g^{-1})	115-120	15-20	170-220

Table 1.2-1 The influence of ammonolysis parameters on the surface area of gamma molybdenum nitride (S_g : mass normalised surface area).[33]

As can be observed from Table 1.2-1, sample γ-Mo_2N-A and the γ-Mo_2N sample, reported by Volpe and Boudart, have both been prepared using relatively low temperature ramp rates and it is apparent that these samples have a much higher surface area with respect to the γ-Mo_2N-B sample prepared using higher ramp rates. The high flow rates of NH_3 documented in the table should also be noted.

Although temperature programmed ammonolysis has a number of benefits, including reduced sintering and increased surface areas, in large scale applications problems arise due to heat transfer issues associated with the endothermic decomposition of ammonia. Wise and Markel proposed an alternative nitridation procedure using mixtures of H_2/N_2 in

order to eliminate these problems.[41] In addition to this, they also reported that γ-Mo$_2$N phase could be prepared with reproducible surface areas using mixtures of H$_2$/N$_2$. There is a degree of dispute within the literature in terms of phases reported using this method. Some authors have reported the formation of the γ-Mo$_2$N phase whilst others observe the formation of the body centred tetragonal β-Mo$_2$N$_{0.78}$ phase (which can also be prepared by the partial decomposition of γ-Mo$_2$N).[42] More recent reports have focused on the β-Mo$_2$N phase and the influence of Mo precursors and heating rates on phase purity. [42-44] These investigations highlight the effect that nitriding procedures can have on morphology and phases obtained and also illustrate the importance of final nitriding temperatures, ramp rates, H$_2$/N$_2$ ratio and MoO$_3$ precursor source.

Within the literature, there have been a number of studies which have investigated the thermal decomposition of nitrogen containing single source precursors to afford nitride products. For example, Afanasiev[45,46] has reported that the thermal decomposition of (HMTA)$_2$(NH$_4$)$_4$Mo$_7$O$_{24}$ (where HMTA = hexamethalentetramine) under an argon atmosphere yields a high surface area molybdenum nitride and a recent study by Wu demonstrated a single source route to nanocrystalline TiN through the decomposition of (NH$_4$)$_2$TiF$_6$.[47] The route employed by Afanasiev provides a unique advantage over conventional methods in the fact the precursor acts as the reducing agent with release of CO during the decomposition and nitridation occurs by utilising the nitrogen present in the precursor. This method offers a convenient alternative for the preparation of nitride materials. Solid state metathesis, in which nitrogen transfer occurs between a donating and a receiving phase, is also a feasible method in which to synthesise both binary and ternary nitrides. Examples of this strategy can be observed in studies by Song and co-workerson the preparation of GaN, TiN, CrN and VN[48] and more recently in the synthesis of Li$_2$SiN$_2$ in which Li$_3$N was shown to be an effective nitridation agent with both single metal elements and metal oxides.[49] Reactions using hydrazine as a nitriding agent have also been investigated by Jacob and co-workers.[50] It was found that hydrazine is a more effective nitriding agent than ammonia when reacted with oxide, sulfide or chloride precursors and many nitrides that cannot be synthesised by ammonia can be prepared by this method (for example HfN and Th$_3$N$_4$). Hydrazine needs to be introduced to the reaction using a water cooled lance to prevent its decomposition to ammonia and hydrogen prior to introduction to the reactor. Due to the risks associated with this method, hydrazine has not been employed on a large scale. Solvothermal and sol-gel methods are also a useful means of nitride synthesis wherein high surface areas are required. These methods have

been frequently used for the preparation of ceramic nitrides like GaN, Si_3N_4, BN and AlN and ZrN.[51]   They are generally used in the synthesis of binary nitrides, although they can be also be employed for the formation of ternary based systems which can be more difficult to synthesise. In a different approach, Jacobsen and co-workers have demonstrated the use of mechanochemical routes as an effective method to ternary nitrides wherein metals are ball-milled with binary nitrides.[52]

Despite the range of nitridation procedures, temperature controlled ammonolysis is still currently the method of choice, notwithstanding the thermal implications associated with it. It is often the case that partial de-nitridation occurs during ammonolysis and the incorporation of oxygen into the structure due to either passivation or partial nitridation can occur. It should be noted therefore that many of the materials investigated in the literature should be viewed as oxynitrides, which are difficult to distinguish from the nitride phase by powder x-ray diffraction.   However, the use of alternative synthetic procedures can lead to unusual phases of nitrides and in this respect such routes are therefore of interest in themselves.

1.3 Catalytic Reactions with Nitrides.

Metal nitrides have attracted significant attention as heterogeneous catalysts over the last decade. As discussed previously, this is mainly due to the development of temperature programmed synthesis techniques consequently enabling materials with high surface areas to be synthesised. Additionally it has been reported that some nitride materials have similar catalytic properties to the platinum group metals which has resulted in increased efforts to develop cheaper alternatives to the traditional platinum type catalysts. Metal nitrides have been shown to catalyse a range of reactions including applications in hydrotreating, ammonia synthesis and applications in fuel cells. Table 1.3-1 summarises the range of catalytic applications for which nitrides have been reported.

As can be seen in Table 1.3-1, different nitrides have attracted significant attention as active catalysts for hydrotreating reactions within the petroleum refining industry. This process requires removal of heteroatoms from feedstream molecules and involves hydrodenitrogenation (HDN), hydrodesulfurisation (HDS) and hydrodeoxygenation (HDO). Studies have been conducted using model heterocyclic compounds such as thiophene, pyridine, quinolone and benzofuran, and it was shown that nitrides are particularly effective in HDN type reactions, which requires high temperature and pressure

with commercial $Co-Mo/Al_2O_3$ and $Ni-Mo/Al_2O_3$ hydrotreating catalysts. When transition metal nitrides of Groups IV-VI were compared for HDS and HDN activity, it was shown that the activity follows the order of Group VI > Group V > Group IV with Mo_2N showing the highest activity for both types of reaction.[75] Bulk Co_4N and Fe_3N showed higher pyridine HDN removal than Mo_2N, but these nitrides are difficult to prepare and often have low surface areas.[76] These studies illustrate the potential that bulk nitrides may have to replace commercial hydrotreating catalysts. Another exciting area in which nitrides may be utilised is in both PEM (proton exchange membrane) and DM (direct methanol) fuel cells.[86-89] There have recently been investigations into the prospect of replacing noble metals such as Pt and Ru with less expensive but durable compounds such as CrN and TiN as coatings for the stainless steel cathodes and anodes. Mo_2N/C has been investigated as an alternative cathode material by Zhong and co-workers, and it was shown to have activity for the oxygen reduction reaction in the presence of methanol.[89]

Application	Catalyst
Ammonia Synthesis	γ- Mo_2N[53] V_2O_2N[54,55], VN[56] UN[57], Re_3N[59], Cs/Co_3Mo_3N[60-68]
Ammonia Decomposition	VN[69,70]
Amination	VN , Mo_2N, W_2N, TiN, NbN[18] , $VAlON$[71]
NO Removal	$Co_4N/\gamma-Al_2O_3$[72] ,
Hydrotreating and Hydrogenation	Re_3N[73], Mo_2N,[11,74] $NiMo_2N/Al_2O_3$[11,73], VN[74], TiN[74], Co_4N[75], Fe_3N[75], YbN[77], EuN[77]
Photocatalysis	TiO_2 (nitrogen doped anatase)[78-81], GaN[82], Ta_3N_5[83], $TaON$[84,85]
Fuel Cell Applications	TiN[86], CrN[87], CN[88] , Mo_2N/C[89]

Table 1.3-1 Range of catalytic applications to which nitride materials have been applied.

Although the number of applications in which nitrides are utilised has grown significantly, these are still somewhat limited and it is apparent that much work is needed to develop other potential uses. Interest in nitride materials in terms of catalysis has generally been directed on either the acid base properties or the noble metal like properties; there is very little evidence within the literature which has alluded to the use of nitrides as potential carriers in nitrogen transfer reactions and their possible application seems to have been largely overlooked in this respect. The potential reactivity of lattice nitrogen was first referred to in early ammonia synthesis studies by Segal and Sebba.[57] It was reported that 'extra' nitrogen was incorporated into the surface layers of a uranium nitride catalyst, under a H_2/N_2 gas mixture, and which was subsequently found to participate in the

ammonia synthesis reaction. One of the main issues associated with potential nitrogen transfer materials is the ability for the material to reversibly adsorb and desorb the reacting species. Studies by Itoh and Machida have reported on the ability of rare earth intermetallic compounds to reversibly store large amounts of nitrogen.[90-92] These compounds form the corresponding nitrides by heating in either N_2 or NH_3 at elevated temperatures, with the nitrogen being incorporated into the interstitial sites within the crystal lattice. The stored nitrogen can subsequently be lost in the form of ammonia when the systems are heated under hydrogen. This is one of the first examples in which nitride based materials have been shown to regenerate to their original phase, once depleted, by reaction with a gas phase nitrogen source. This demonstrates the potential ability for metal nitrides to participate in Mars-van Krevelen type processes, which are more commonly associated with oxygen transfer.[93]

In the well-established Mars-van Krevelen oxidation mechanism an organic substrate is directly oxidised by the transfer of lattice oxygen from an oxide catalyst, thus generating a temporary vacancy in the metal lattice, which is replenished by a gas-phase oxygen source. This general type of mechanism has also been observed for sulfide and carbide catalysts. In the latter case, Green and co-workers have reported the direct lattice carbon transfer to carbon monoxide produced in the partial oxidation of methane catalysed by molybdenum carbide.[94] In this investigation it was shown, through isotopic labelling, that surface carbon in the molybdenum carbide takes an active part in partial oxidation. The oxygen in the reactants initially reacts with surface carbon species on the molybdenum carbide to yield CO and the partially oxidised carbide is subsequently regenerated to the original phase by methane in the feedstream, liberating product H_2.
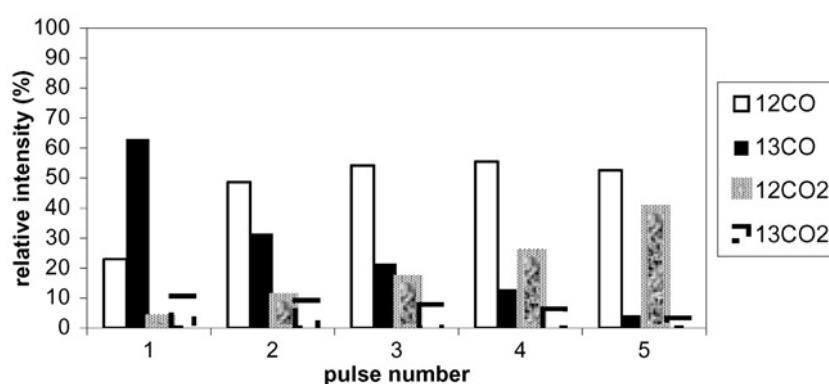
Figure 1.3-1 ^{13}C exchanged carbon oxide distribution while pulsing the mixture of ($2^{12}CH_4+O_2$) over $Mo_2^{13}C$ at 1130 K and 1 bar.[94]

From Figure 1.3-1 it is apparent that on the first pulse the reaction is selective to CO over the labelled molybdenum carbide, however, over half of the CO produced is ^{13}CO. This is clearly a result of the oxidation of lattice carbon species in the molybdenum carbide. On subsequent pulses the amount of ^{13}CO produced deminishes relative to the loss of labelled lattice species. These results highlight the potential ability for molybdenum carbides to participate in Mars van-Krevelen like processes.

Although there is a limited amount of literature investigating nitride materials for nitrogen transfer reactions, recent studies by Olea *et al* have demonstrated one of the first examples of using lattice nitrogen transfer for the direct ammoxidation of propane to acrylonitrile using a vanadium aluminium oxynitride (VAlON) catalyst in a double Mars-van Krevelen process.[71] In those studies, isotopically labelled NH_3 was employed in order to distinguish between adsorbed ammonia and lattice nitrogen species. It was reported that even in the absence of co-fed NH_3 propane ammoxidation to acroylonitrile was evident. Measurements were conducted via temporal analysis of products (TAP) experiments. The consumption of gaseous ammonia in the reaction was documented to be involved in the re-nitridation of the catalyst surface instead of its direct participation in the reaction with propane.

In this thesis, the reactivity of lattice nitrogen in a range of binary and ternary nitrides have been investigated with the aim of directly synthesising aniline from benzene. Aniline is one of the most fundamentally important intermediate products and it is extensively used within organic synthesis and in large scale applications.[95-99] It is used as a feedstock for a variety of different industries leading to a wide range of industrial and commercial applications. The majority of global aniline, between 80-85%, is consumed in the production of MDI (methylene di-para-phenylene isocyanate), for which the demand is steadily growing at an annual rate of between 6-8%.[95,97] MDI is subsequently polymerised and used in the synthesis of polyurethanes, which are versatile polymers used in the manufacture of rigid and semi-rigid foams, elastomers and coating resins.[95-97, 99] These materials are typically used within the construction industry for building insulation and the automotive industry for car interiors.

The remainder of the aniline manufactured is used in the production of a range of different products specifically pharmaceuticals, aniline dyes and rubber additives. Additionally aniline is also utilised in the agricultural industry to synthesise fungicides and pesticides.[98]

Large scale aniline production occurs via the hydrogenation of nitrobenzene in the following sequence of reactions:

$$N_2 + 3H_2 \longleftrightarrow 2NH_3$$

$$NH_3 + 2O_2 \longrightarrow HNO_3 + H_2O$$

$$HNO_3 + 2H_2SO_4 \longrightarrow NO_2^+ + H_3O^+ + 2HSO_4^-$$

$$C_6H_6 + NO_2^+ \longrightarrow C_6H_5NO_2 + H^+$$

$$C_6H_5NO_2 + 3H_2 \longrightarrow C_6H_5NH_2 + 2H_2O$$
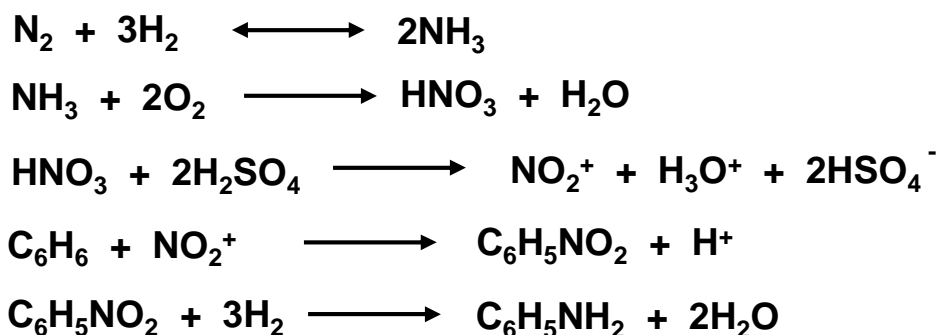
Viewed in terms of the nitrogen conversion steps, i.e. initial reduction followed by partial re-oxidation and then re-reduction, the inefficiency and indirect nature of this process is readily apparent. Given that ammonia synthesis, the first step of the process, is very energy intensive (reportedly being responsible for 1% of global energy demand) and that much of the hydrogen used in the process is indirectly converted to H_2O, the desirability of alternative routes is obvious.

In this thesis, a screening study has been undertaken whereby the reactivity of lattice nitrogen in a range of binary and ternary nitrides has been assessed. Initial studies investigate the ambient pressure ammonia production activity of the nitrides using both H_2/N_2 and H_2/Ar feeds and comparisons have been made with ruthenium based systems, which are generally recognized to have the greatest efficacy for this reaction. Those which have the greatest efficacy for ammonia production and/or demonstrate a loss of nitrogen at 400^oC or below have been investigated in a Mars-van Krevelen type capacity for the production of aniline via the direct and indirect amination of benzene. The approach taken is novel and highly speculative. No comparable studies of this nature has been documented in the literature

2.   Experimental.

2.1 Introduction.

The experimental techniques employed within this research are reported in distinct sections; preparation, characterisation and testing.

2.2 Preparation.

A large number of materials have been prepared and tested in this work. They are primarily bulk binary nitrides, although ternary nitrides, mixed metal phases and supported ruthenium catalysts were also prepared.

2.2.1 Preparation of Precursors and Nitride Materials.

(i) Ammonolysis Reactor.

Most of the nitride materials were prepared using temperature programmed ammonolysis similar to that first reported in the work of Volpe and Boudart.[32] The gases used were NH_3 (BOC grade N 3.8), N_2 (BOC oxygen free, 99.998 %) and 2 % O_2/Ar (BOC purity). These gases were introduced into a vertical quartz glass reactor (10.5 mm internal diameter), fitted with a sintered disc, via ¼ inch stainless steel tubing (Swagelok). Gas flow was controlled using a series of Brooks 5850 TR mass flow controllers and the effluent gas was flowed through a dilute sulfuric acid solution to neutralise any remaining ammonia present. All experiments were carried out within a well-ventilated fume cupboard. The quartz reactor was located in the centre of a Carbolite tube furnace, and the temperature was controlled using a Eurotherm temperature controller which was programmed to go through various heating regimes for the nitriding process, dependent on the target nitride. Figure 2.2-1 shows the experimental set-up for nitriding.
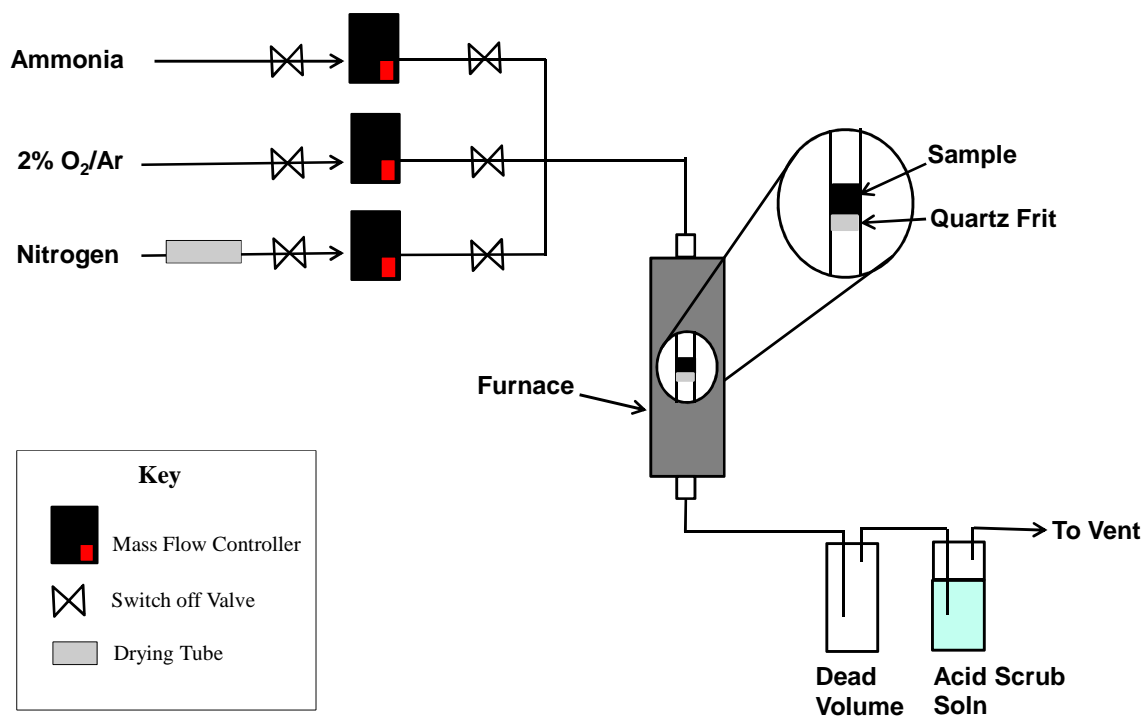
Figure 2.2-1 Apparatus used for preparing nitrides by ammonolysis

(ii) Nitridation of materials.

The typical experimental conditions used for nitriding are outlined below. Approximately 0.5 g of the material to be nitrided was placed into the vertical quartz reactor and a 94 ml min^{-1} flow of NH$_3$ was introduced. The furnace was programmed to heat the material in accordance with previously reported methods specific to the nitride, as discussed in more detail in the relevant preparation sections, and this is shown in Table 2.2-1. Once the furnace had reached the final nitriding temperature a dwell period was applied. Following this, the nitrided material was left to cool in flowing ammonia, and upon reaching ambient temperature, nitrogen gas was flushed through the system at 100 ml min^{-1} for 30 minutes to remove any residual ammonia from the system. Some materials are known to be sensitive towards oxygen and in order to prevent pyrolysis on exposure of the nitrided material to air, these materials (VN, Fe$_2$N, W$_2$N, Co$_3$Mo$_3$N) were passivated using a mixture of 2 % O$_2$/Ar flowing at 5 ml min^{-1} and N$_2$ (passed through an oxygen trap) at 95 ml min^{-1} so as to obtain a gas mixture containing < 0.1 % O$_2$. This allowed a protective oxide skin to form on the surface of the nitride material which could be subsequently removed prior to testing by treatment with a 3:1 H$_2$/N$_2$ gas mixture.

Material	Precursor	Nitriding Temperature (^{o}C)	Nitriding Duration (hours)	Nitriding Gas
Mg_3N_2	as purchased			
TiN	TiO_2 (anatase)	900	6	NH_3
VN	V_2O_5	700	2	NH_3
CrN	$CrCl_3$	700	5	NH_3
Fe_2N	Fe powder	500	6	NH_3
Co_4N	Co_3O_4	700	2	NH_3
Co_4N/Al_2O_3	Co_3O_4/Al_2O_3	700	2	NH_3
Ni_3N	$NiCl_2$	480	6	NH_3
Cu_3N	CuF_2	300	6	NH_3
Cu_3N/SiO_2	CuO/SiO_2	300	6	NH_3
Zn_3N_2	Zn powder	600	6	NH_3
$\beta\text{-}Mo_2N_{0.78}$	MoO_3	700	3	3:1 H_2/N_2
Ta_3N_5	Ta_2O_5	900	9	NH_3
W_2N	WO_3	700	2	NH_3
Re_3N	NH_4ReO_4	350	2	NH_3
Co_3Mo_3N	$CoMoO_4.nH_2O$	785	6	NH_3
$TiFe_2Nx$	Ti shots Fe wire	450	3	NH_3
Co-4Re	Co-Re oxide	700	3	NH_3

Table 2.2-1 Summary of preparation conditions for nitride materials

2.2.2 Preparation of Mg$_3$N$_2$.

Mg_3N_2 was purchased from Sigma Aldrich and no further treatment was required. [100]

2.2.3 Preparation of TiN.

Anatase nanopowder (TiO$_2$ 99.97 % Sigma –Aldrich) was used as the precursor for TiN. The material was heated to 900 ^{o}C, at a rate of 5 ^{o}C min^{-1} under the conditions outlined above. The diffraction pattern of the nitrided material was crystalline and similar to that of pure phase TiN reported in the literature.[23]

2.2.4 Preparation of VN.

Ammonolysis of V$_2$O$_5$ (Aldrich) was undertaken so as to obtain VN using the method described by Shi and co-workers.[17]   The sample was linearly heated from room temperature to 350 °C over a period of 30 minutes, followed by a rise in temperature from

350 to 450 °C at a rate of 0.5 °C min^{-1}, and a further increase from 450 to 700 °C at a rate of 1.25 °C min^{-1}. The temperature was then kept at 700 °C for 2 h before cooling in a flow of NH$_3$ and subsequently passivating as previously described.

2.2.5 Preparation of CrN.

CrN was synthesised by the reaction of CrCl$_3$ (Sigma Aldrich 95%) with NH$_3$ (94ml min^{-1}) at 700 °C for 5 h as described in the literature.[101]

2.2.6 Preparation of Fe$_2$N.

Iron nitrides were prepared following the method outlined by Goodeve and Jack.[102,103] They reported that it was possible to obtain different phases of iron nitride ranging from Fe$_2$N, Fe$_3$N and Fe$_4$N through ammonoylsis of Fe powder at various temperatures. In this study Fe$_2$N was prepared by heating Fe powder to 500 °C using a ramp rate of 5 °C min^{-1} under conditions previously described. Powder X-ray diffraction confirmed that the only phase present in the sample was Fe$_2$N. Other temperatures were also employed but resulted in mixed phase materials.

2.2.7 Preparation of Co$_4$N and Co$_4$N/ γ-Al$_2$O$_3$.

Bulk cobalt nitride and the γ-Al$_2$O$_3$ supported cobalt nitride were generated by means of temperature programmed ammonolysis. The oxide precursors were loaded into the quartz reactor, and a flow of NH$_3$ was introduced to the reactor. The temperature was increased from room temperature to 300 °C over a period of 30 minutes, followed by a rise in temperature from 300 to 450 °C at a rate of 0.7 °C m and a further increase to 700 °C at which point it was held for 2 hours.[72]

Supported Co$_4$N was prepared by nitriding the supported oxide precursor (Co$_3$O$_4$/Al$_2$O$_3$, as confirmed by XRD). The precursor was prepared by method of incipient wetness impregnation via stirring γ-Al$_2$O$_3$, in an aqueous cobalt nitrate (Co(NO$_3$)$_2$.6H$_2$O, Sigma Aldrich 98+ %) solution so as to obtain a Co loading of 20 wt.%. The precipitate was dried at 110 °C overnight and calcined at 500 °C for 3 hours.

2.2.8 Preparation of Ni$_3$N.

Baiker reported the synthesis of pure Ni$_3$N through ammonolysis of NiO within a narrow temperature range of 200-500 ^{o}C, below or above which the nitride phase co-existed with nickel metal.[22]   Initially nickel oxide was employed as the precursor, and ammonolysis took place over a range of temperatures. However, the resultant material was mixed phase Ni$_3$N with impurities from Ni metal as shown by XRD. NiCl$_2$ (Koch Light Laboratories Ltd) was therefore utilized as the precursor and apparently pure phase Ni$_3$N formed at 480°C. A ramp rate of 15 ^{o}C min^{-1} and dwell time of 6 hours was used.

2.2.9 Preparation of Cu$_3$N and Cu$_3$N/SiO$_2$.

Cu$_3$N powders were synthesised at 300 ^{o}C using anhydrous CuF$_2$ (Aldrich 98 %) as a starting material and NH$_3$ gas (BOC, 99.98 %) as a nitriding agent.[21,22,104] It was found that this material is very temperature sensitive and starts to decompose rapidly at temperatures above 320 ^{o}C forming metallic copper.

Supported Cu$_3$N was prepared by nitriding the supported oxide precursor (CuO/SiO$_2$, as confirmed by XRD).   The precursor was prepared by method of incipient wetness impregnation via stirring SiO$_2$ (200 m^2), in an aqueous copper nitrate (Cu(NO$_3$)$_2$.6H$_2$O, Sigma Aldrich 98+ %) solution so as to obtain a Cu loading of 20 wt.%. The precipitate was dried at 110 ^{o}C overnight and calcined at 250 ^{o}C for 3 hours.

2.2.10 Preparation of Zn$_3$N$_2$.

The Zn$_3$N$_2$ powders were synthesised by reacting Zn powder (British Drug Houses) with NH$_3$ gas at 600 ^{o}C using a ramp rate of 15 ^{o}C min^{-1}.[105,106] Powder X-ray diffraction of the resultant material confirmed that Zn$_3$N$_2$ had been obtained and trace impurities of ZnO were also observed, which is accordance with previous literature.

2.2.11 Preparation of β-Mo$_2$N$_{0.78}$ and 1.5% Fe/ β-Mo$_2$N$_{0.78}$, 1.5% Cu/ β-Mo$_2$N$_{0.78}$ and 1.5% Bi/ β-Mo$_2$N$_{0.78}$.

β-Mo$_2$N$_{0.78}$ was prepared *in-situ* in a fixed bed microreactor. 0.5 g of MoO$_3$ (sigma Aldrich 99.5 %) was charged to the reactor and treated with 60 ml min^{-1} of a 3:1 H$_2$/N$_2$ (BOC, H$_2$ 99.998 %, N$_2$ 99.995 %) mixture at 750 ^{o}C for 3 hours.[107]

Iron, copper and bismuth were used as dopants and doped β-Mo$_2$N$_{0.78}$ was prepared were prepared by impregnating MoO$_3$ using Fe(NO$_3$)$_3$.9H$_2$O (Sigma Aldrich 98 %), Cu(NO$_3$)$_2$.3H$_2$O (Sigma Aldrich 99 %), and   Bi(NO$_3$).5H$_2$O (Sigma Aldrich >98 %), respectively, so as to achieve a metal loading of 1.5 wt.% on the MoO$_3$ (i.e. using 0.109 g of Fe(NO$_3$)$_3$.9H$_2$O, 0.057 g of Cu(NO$_3$)$_2$.3H$_2$O and 0.026 g of Bi(NO$_3$).5H$_2$O respectively per gram of catalyst prepared). The doped materials were then dried in an oven at 120 ^{o}C and calcined at 500 ^{o}C for 5 hours. Samples were subsequently nitrided following the same conditions previously described.

2.2.12 Preparation of Ta$_3$N$_5$.

Ta$_3$N$_5$ was synthesised by the reaction of Ta$_2$O$_5$ (Sigma Aldrich 99 %) with NH$_3$ (94 ml min^{-1}) at 900 ^{o}C for 9 hours as described in the literature.[109]

2.2.13 Preparation of W$_2$N.

W$_2$N was prepared using the same temperature programmed nitridation method as described for VN (section 1.2.4).[17] WO$_3$ (Sigma Aldrich) was treated with NH$_3$ gas in order to produce the tungsten nitride.

2.2.14 Preparation of Re$_3$N.

Clark and co-workers have reported that rhenium nitride can be formed by one of two methods, either from ammonium perrhenate (NH$_4$ReO$_4$) or rhenium trichloride (ReCl$_3$) through ammonia reduction at temperatures between 300 and 350 ^{o}C, above which it starts to decompose to the metal.[73] Re$_3$N is relatively unstable and hence cannot be prepared by direct reaction of the elements due to the high temperatures required, nor can it be formed from the oxides because their reduction temperatures are above the decomposition temperature of the nitride. Thus, the application of rhenium nitride for the reactions of interest must be studied below 370 ^{o}C.

NH$_4$ReO$_4$ (Sigma-Aldrich, 99.5 %) was used as the precursor for Re$_3$N.   NH$_4$ReO$_4$ was nitrided in accordance with the conditions, outlined by Clark -350 ^{o}C for 2 hours. Powder X-ray diffraction (XRD) confirmed the phase of the resultant material as Re$_3$N which is in agreement with previous literature.[59,73]

2.2.15 Preparation of Co-4Re.

Co-4Re was prepared by reduction of a cobalt rhenium oxide precursor. The precursor was prepared by impregnating ammonium perrhenate (NH_4ReO_4 Sigma Aldrich 99+ %) with cobalt nitrate ($Co(NO_3)_2.6H_2O$ Sigma Aldrich 98+ %) using incipient wetness and it was then dried overnight at 110 ^{o}C. The resulting powder was calcined at 500 ^{o}C for 3 hours and reduced in ammonia at 700 ^{o}C for 2 hours. The higher temperature was required in order to reduce the cobalt metal.[59]

2.2.16 Preparation of Co$_3$Mo$_3$N.

Co$_3$Mo$_3$N was prepared by nitriding a cobalt molybdate hydrate precursor ($CoMoO_4.nH_2O$, as confirmed by XRD). The precursor was prepared by adding aqueous solutions of cobalt nitrate (4.5 g $Co(NO_3)_2.6H_2O$, Sigma Aldrich, 98+ %) and ammonium heptamolybdate (7.2 g $(NH_4)_6Mo_7O_{24}.4H_2O$ Sigma Aldrich 81-83 % as MoO_3) then heating the mixture to approximately 80 ^{o}C for 3 hours. A purple precipitate was collected after vacuum filtration and the precipitate washed with distilled water and ethanol, and subsequently dried overnight at 120 ^{o}C. The resulting powder was calcined at 500 ^{o}C for 5 hours and then nitrided by ammonolysis using the following temperature regime, from ambient to 357 ^{o}C at a rate of 5.6 ^{o}C min^{-1}, then to 447 ^{o}C at 0.5 ^{o}C min^{-1} then to 785 ^{o}C at 2.1 ^{o}C min^{-1}. [111] The material was then cooled and passivated following the general procedure described previously.

2.2.17 Preparation of TiFe$_2$N$_x$ Laves Phase.

TiFe$_2$N$_x$ materials were prepared by heating 0.5 g Fe wire (Goodfellow, 99.95 %) and 0.5 g Ti metal shots (Goodfellow, 99.96 %) to 1150 ^{o}C under argon and dwelling at this temperature for 48 hours. After cooling in the flowing gas, the material was then crushed into a fine powder and heated to 1150 ^{o}C for a further 48 hours in Ar, and crushed into fine particles.[90,91] The material was then nitrided by temperature programmed ammonolysis in which it was heated to 450 ^{o}C at 5.6 ^{o}C min^{-1} and held at this temperature for 3 hours, before being allowed to cool to room temperature in ammonia gas.

2.2.18 Preparation of Ru/AlMg$_2$O$_4$ and Ba/Ru/ AlMg$_2$O$_4$.

Supported ruthenium catalysts have been prepared as they are known to be an excellent catalyst for ammonia synthesis. Some Ru-based catalysts have been shown to be

significantly more active than conventional, multipromoted iron system[112-114] and these are being used for comparative purposes within this body of work.

The support material ($AlMg_2O_4$) was prepared by drop-wise addition of 100 ml of a 0.05M solution of aqueous ammonium carbonate, ($(NH_4)_2CO_3$, Sigma Aldrich > 99.99 %) to a 100ml aqueous mixture of $Mg(NO_3)_2.6H_2O$ (0.05M, Sigma Aldrich > 98 %) and $Al(NO_3)_3.9H_2O$ (0.02 M, Sigma Aldrich 98 %). A white precipitate was obtained after vacuum filtration and the precipitate was washed twice with distilled water and dried in an oven overnight at 120 ^{o}C. The Mg-Al complex oxide was prepared by calcinating the compound at 800 ^{o}C for 6 hours in air.

Triruthenium dodecacarbonyl ($Ru_3(CO)_{12}$, Sigma Aldrich 99 %) was added by impregnation to the AlMgO support after the calcination step, so as to obtain a 5 wt.% metal loading, and dried at 70 ^{o}C. The resulting orange-grey powder was crushed and sieved to < 250 microns and subsequently heated in 3:1 H_2/N_2 (60 ml min^{-1}) at 400 ^{o}C for 2 hours in order to reduce the Ru precursor and was then cooled under H_2/N_2.

Barium nitrate, was introduced to the $Ru/AlMg_2O_4$ system by incipient wetness impregnation from aqueous solution, followed by drying the samples in air at 70 ^{o}C overnight and reduced as described above.[115,116]

2.3 Characterisation.

The following techniques were used to characterise, describe and verify the properties of pre- and post-reaction samples and to evaluate the results of various reactions carried out.

2.3.1 Powder X-ray Diffraction (PXRD).

Powder X-ray diffraction was carried out on all synthesised materials to identify the crystalline phases of the pre- and post-reaction samples. XRD patterns were obtained using a Siemens D5000 X-ray diffractometer (40 kV, 40 mA) operating with a CuK_α X-ray source (λ-1.5418 Å). The scanning range used was 5 $^\circ$- 85 $^\circ$ with a step size of 0.02 $^\circ$ and a scan rate of 1 second per step.

2.3.2 Surface Area Determination.

The surface area of the catalysts was determined by applying the Brunauer, Emmett and Teller (BET) method to nitrogen physisorption isotherms which were determined at liquid nitrogen temperatures. Isotherms were measured using a Micromeritics Flow Prep 060 and Gemini BET machine. Prior to analysis, the samples (0.1 g) were degassed in N_2 at $110^{o}C$ overnight to remove any adsorbed moisture.

2.3.3 Elemental Analysis.

CHN analysis was performed to determine changes in the pre- and post- reaction materials with the kind assistance of Mrs Kim Wilson at the University of Glasgow using an Exeter Analytical CE-440 elemental analyser.

2.3.4 Scanning Electron Microscope (SEM).

SEM micrographs of pre and post reaction samples were acquired using a Philips XL30E-scanning electron microscope (25 kV, Spot Size 5, Working Distance 10 mm). Samples were dispersed onto carbon stubs before being inserted into an inert atmosphere.

2.3.5 Nuclear Magnetic Resonance (^{1}H NMR).

^{1}H NMR spectroscopy was conducted on liquid samples (dissolved in a $CDCl_3$ and THF-d_8) using a Bruker Advance III 400 MHz spectrometer. Samples were run under automation using the standard default programme settings in the 'Brooker data library' as supplied with the spectrometer.

2.3.6 Fourier Transform Infrared Spectroscopy (FTIR).

Fourier Transform Infrared Spectroscopy was performed on a Shimadzu FTIR-8400S spectrometer. Liquid samples were scanned 20 times at a resolution of 2 cm^{-1} in the region 600-4000 cm^{-1}

2.3.7 Gas Chromatography / Mass Spectroscopy (GCMS).

GC analysis was conducted on liquid samples (dissolved in 1:10 v:v ratio with methanol) using a Thermo Finnigan Focus GC fitted with an AS2000 autosampler. The column that was used in the instrument was a CP- Sil8CB 50 meter, 0.32 ID, 5 µm film thickness run at

a constant pressure of 14.5 p.s.i. The injector was heated to 200 ^{o}C and the split ratio used was 30:1. The initial oven temperature was 60 ^{o}C and this was held for 1 minute and subsequently increased to 260 ^{o}C using the following ramp profile, 30 ^{o}C min^{-1} to 110 ^{o}C, 9 ^{o}C min^{-1} to 135 ^{o}C and finally 30 ^{o}C min^{-1} to 260 ^{o}C where it was held for 2 minutes. The total acquisition time was 11.6 minutes. Samples were also sent to the EPSRC National Mass Spectrometry Service Centre, Swansea, for characterisation.

2.4 Testing.

Figure 2.4-1 illustrates the reactor set up which was used to conduct the ammonia production and lattice nitrogen studies. This was a fixed bed, continuous flow reactor and a quartz glass reactor tube (10.5 mm internal diameter) was used to contain the sample. The powdered sample was held centrally between silica wool plugs within the reactor tube which itself was held in a Carbolite furnace. The feed gas mixtures were introduced through ¼ inch stainless steel tubing (Swagelok), and a total flow rate of 60 ml min^{-1} which was controlled via Brooks 5850 TR mass flow controllers, was used for both reactions. The vent gas from the reactor was passed through a sulfuric acid bubbler (200 ml 0.0018 mol L^{-1}) and the decrease in conductivity, corresponding to the consumption of H$^+$ by NH$_3$, was measured by a conductivity meter. Conductivity calibration data can be found in the following section. All gases were vented into a fume hood.
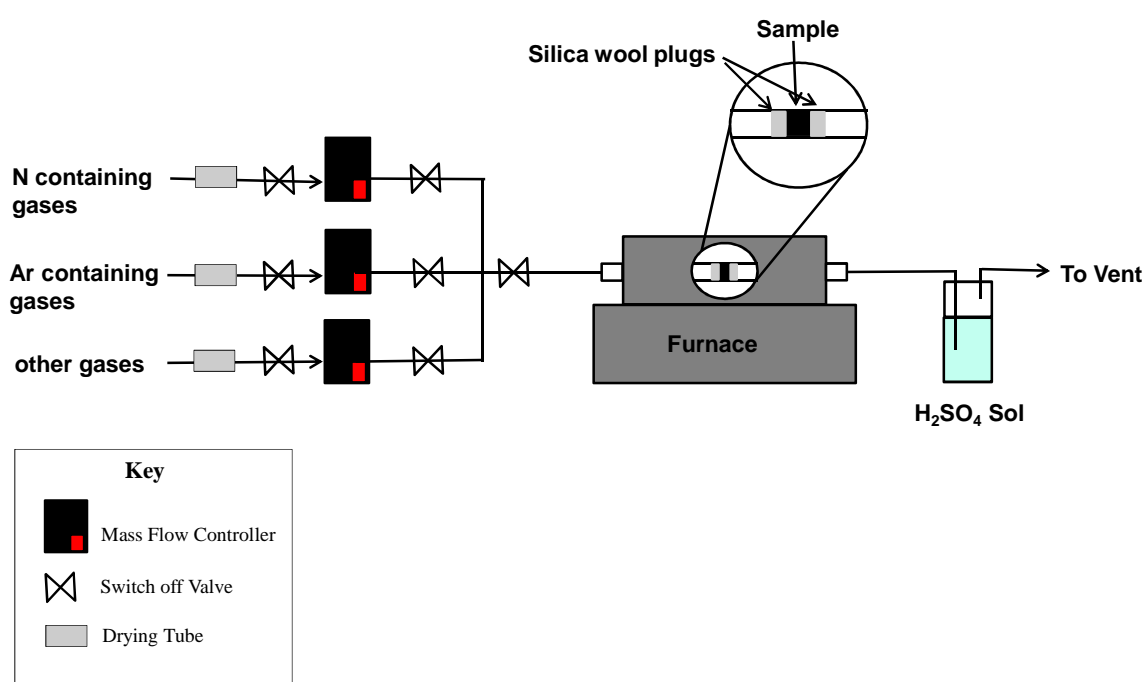
Figure 2.4-1 Apparatus used to conduct ammonia synthesis and lattice nitrogen experiments.

2.4.1 Ammonia Synthesis Calculations and Conductivity Calibration Data.

During ammonia production and lattice nitrogen studies, the formation of ammonia was monitored through a decrease in the conductivity of a dilute sulphuric acid solution (200 ml 0.0018 mol L^{-1}).   As previously mentioned this decrease corresponds to the consumption of H^+ ions by NH_3, forming NH_4^+ ions. It is the difference in the relative size of these ions H^+ and NH_4^+ which results in the conductivity change of the solution.

To establish upper and lower conductiviy values the mean conductivity of six different 0.0018 mol L^{-1} solutions of H_2SO_4 and $(NH_4)_2SO_4$ was determined. Table 2.4-1 below shows the conductivities which were observed.

Conductivity of H_2SO_4 solution($\mu S\ cm^{-1}$)	Conductivity of $(NH_4)_2SO_4$ solution($\mu S\ cm^{-1}$)
959	313
953	301
943	302
949	307
934	308
951	304
Mean ~ 948	Mean ~ 305

Table 2.4-1 Conductivity values which were observed for 0.0018 mol L^{-1} solutions of H_2SO_4 and $(NH_4)_2SO_4$.

The calculation shown below illustrates how the ammonia production rates were calculated with respect to the conductivity versus time plot for every ammonia synthesis experiments.

Moles of H_2SO_4 = Concentration (H_2SO_4) x Volume (H_2SO_4)

= 0.00108 mol L^{-1} x 0.2 L

= 2.16 x 10^{-4} moles

Due to stoichiometric considerations 4.32 x10^{-4} moles of ammonia are required to completely react with H_2SO_4

Change in conductivity for reaction $H_2SO_4 + 2NH_3 \longrightarrow (NH_4)_2SO_4$

$$= 948 \ \mu Scm^{-1} - 305 \ \mu Scm^{-1}$$

$$= 643 \ \mu Scm^{-1}$$

Number of moles of ammonia required / Total change in conductivity

$$= \ 4.32 \ x10^{-4} \ moles \ / \ 643 \ \mu Scm^{-1}$$

$$= 6.72x10^{-7} \ mol \ /\mu S \ cm^{-1}$$

The gradient of the conductivity (μScm^{-1}) versus time plots are determined. By multiplying the resultant value by the calibration value ($6.72x10^{-7}$ mol/μS cm^{-1}) and dividing by the mass of the material investigated (generally 0.3 g) the mass normalised ammonia production rate is determined.

Under reaction conditions using a 3:1 H_2/N_2 gas mixture and operated at 400 ^oC and 1 atm pressure, NH_3 has a limiting yield of 0.4 mol%.[20]

From the above information a theoretical equilibrium NH_3 synthesis rate can be calculated as shown below:

$$0.4 \ mol \ \% \ \ x \ 60 \ ml \ min^{-1} \ = 0.24 \ ml \ min^{-1}$$

$$\frac{0.24 \ ml \ min^{-1}}{22400 \ ml \ (molar \ gas \ volume)} \ = 1.07 \ x10^{-5} \ moles \ min^{-1}$$

$$1.07 \ x10^{-5} \ moles \ min^{-1} x \ 60 \ min \ = 6.4285 \ x \ 10^{-4} \ moles \ hour^{-1}$$

$$\frac{6.4285 \ x \ 10^{-4} \ moles \ hour^{-1}}{0.3g \ (weight \ of \ material)} \ \ \begin{array}{l} = 2.142 \ x \ 10^{-3} \ mol \ g^{-1} \ h^{-1} \\ = 2142 \ \mu mol \ g^{-1} \ h^{-1} \end{array}$$

It is worth noting that during ammonia production and lattice nitrogen reactivity studies that a change in the conductivity value may not be truly representative of the rate of NH_3 formation. It is assumed within this thesis that NH_3 is the only nitrogen containing species produced under reaction conditions so as to cause a decrease in the conductivity of the acid solution. Other nitrogen containing species, such as N_2H_4, N_2H_2, N_3H, may also form during the reaction and would have a similar effect of lowering the conductivity of the solution. Furthermore it is also assumed that any NH_3 species formed during reaction

subsequently reacts with H^+ ions to form NH_4^+. It may be possible that only a limited amount of NH_3 species reacts in solution (i.e. are trapped) and the remainder is vented, thus any decrease which is observed in the conductivity readings would not be illustrative of the total NH_3 produced during reaction.

2.4.2 Ammonia Production.

0.3 g of material was placed into the quartz reactor tube and so that it was held centrally within the heated zone of the furnace. Generally the nitrides were pre-treated at 700 ^{o}C with the reactant gas (H_2/N_2 (BOC, H_2 99.998 %, N_2 99.99 %) in a ratio of 3:1 respectively) at 60 ml min^{-1} for 2 hours, in order to remove the passivation layer, with the exception of the less stable nitrides; Co_4N, Ni_3N, Cu_3N, Re_3N and Zn_3N_2, which were not pre-treated. The samples were then cooled to reaction temperature, 400 ^{o}C (250 ^{o}C for the less stable nitrides), in flowing gas and held at this temperature for 6 hours. On reaching reaction temperature, the vent gas from the reactor was bubbled through a sulfuric acid solution (200 ml 0.0018 mol L^{-1}) at ambient temperature. The conductivity of the solution was measured every 30 minutes and the production of ammonia was measured by monitoring the change in conductivity of a sulfuric acid solution with respect to time and compared with the theoretical equilibrium NH_3 synthesis rate which was calculated to be 2142 µmol g^{-1} h^{-1} for the above reaction conditions with a limiting yield of 0.4 mol. % as discussed previously.[133]

2.4.3 Lattice Nitrogen Reactivity.

The reactivity of the lattice nitrogen, within the bulk nitrides, was assessed with H_2/Ar as a function of temperature in order to evaluate the temperature range at which nitrogen was lost from the metal lattice.

0.3 g of nitride was placed into the silica reactor tube and held between quartz wool plugs centrally in the heated zone of the furnace. As described for ammonia synthesis studies, most of the nitrided materials were pre-treated at 700 ^{o}C for 2 hours with 3:1 H_2/N_2 to remove any residual oxide present and then cooled to 400 ^{o}C (or lower for the unstable nitrides). At this point the feed gas was switched from H_2/N_2 to 3:1 H_2/Ar (BOC, H_2 99.998 %, Ar min 99.99 %) and conductivity measurements were taken at 400 ^{o}C for 4 hours. The temperature of the reaction was then increased and held in the following increments, 500 ^{o}C (1 hour dwell), 600 ^{o}C (1.5 hour dwell) and finally 700 ^{o}C (1 hour

dwell). Nitrides of Groups IX-XII had a marginally different temperature regime (starting at 200 ^{o}C) due to their thermal instability. From conductivity calibration data, the percentage of nitrogen species, lost from the nitride resulting in the formation of ammonia could be determined and compared with the total amount of nitrogen lost from the nitride as determined by combustion analysis.

2.4.4 Benzene Flow Test Reactor.

Experiments investigating the potential synthesis of aniline from benzene, phenol and chlorobenzene were carried out using the experimental set-up as shown in Figure 2.4-2 with some slight modifications. 0.3 g of reagent was placed into a silica reactor tube and held centrally in the heated zone of the furnace. Those nitrides which were passivated following the procedure described in section 2.2.1 were pre-treated at 700 ^{o}C under 3:1 H_2/N_2 gas (60 ml min^{-1}) for 2 hours and allowed to cool to room temperature before the solvent was charged to the reactor. The system was then flushed with H_2/N_2 at room temperature to ensure traces of oxygen were removed after exposure to air. A bubbler held at ambient temperature was used to introduce a flow of benzene/chlorobenzene/phenol over the materials. Assuming equilibrium, it is calculated that the proportion of benzene and chlorobenzene in the gas stream corresponds to 9 and 1% respectively.

The reagents were tested at different temperatures, primarily 300 ^{o}C and 400 ^{o}C, (unless otherwise stated) and a temperature ramp rate of 100 ^{o}C min^{-1} was used to attain the reaction temperature. The temperature was then held for 1-4 hours. An ice bath was used at the exit of the reactor to condense products which were subsequently analysed by ^{1}H NMR spectroscopy, mass spectroscopy and FTIR spectroscopy. Below is a schematic of the set-up for benzene experiments on the plug flow reactor.
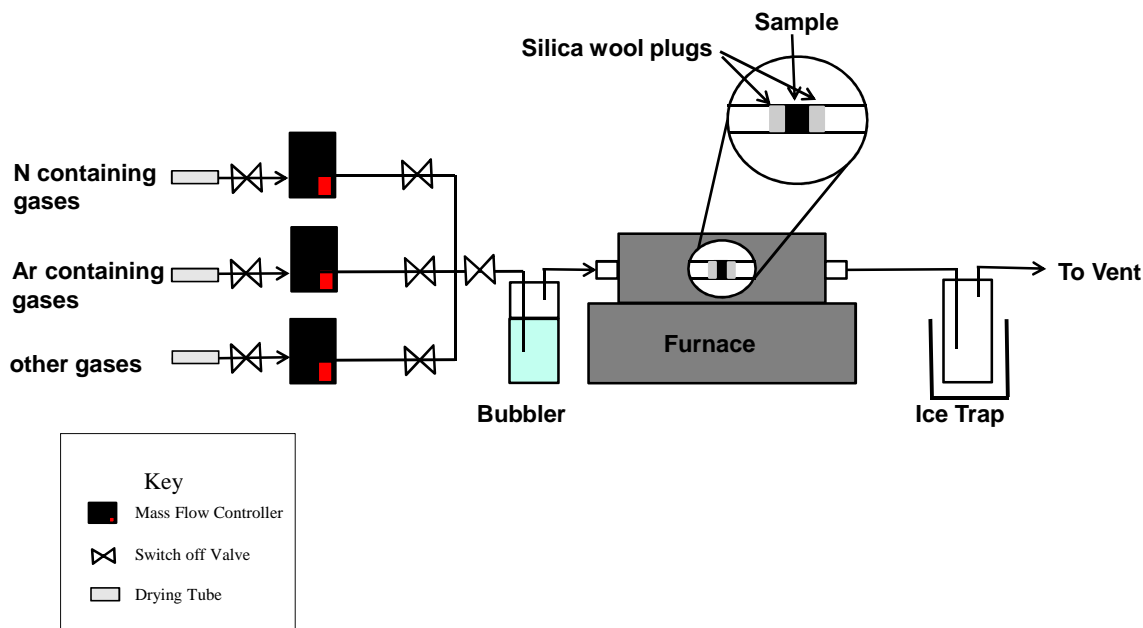
Figure 2.4-2 Apparatus used to for benzene /nitrogen experiments.

2.4.5 Benzene - Ammonia Pulse Reactor.

Benzene and ammonia pulse reactions have been undertaken with the ultimate aim of overcoming the limitation posed by direct reaction of ammonia and benzene. Direct amination of benzene is an equilibrium limited dehydrogenation.[117] By pulsing ammonia and benzene alternatively, the dehydrogenation stage can be separated from the amination stage. NH_x residues are adsorbed onto the surface of the reagent and may react with the following pulse of benzene. In doing so, this may lift the equilibrium limitation by the sequential removal of hydrogen from the reaction and potentially enables increased benzene conversion to aniline.

Pulse reactions were conducted under three different feed gas regimes, (a) 5 % H_2/N_2 (BOC), (b) 5 % H_2/Ar (BOC) and (c) Ar (BOC) only. The samples were initially exposed to the 5 % H_2/N_2 gas mix and also the 5 % H_2/Ar and Ar only gas feeds if there was evidence of coking on the lower packing granules after reaction with the 5 % H_2/N_2 gas mix as discussed later. Figure 2.4-3 is a schematic of the experimental set-up for the pulse reactions. Both NH_3 and C_6H_6 were injected into a carrier gas through an injection port fitted into the Swagelok steel tubing. The carrier gas was delivered to the steel reactor tube through ¼" Swagelok steel tubing and the flow set to 60 ml min^{-1} using a rotameter. The effluent gas was passed to an online mass spectrometer (Varian Quadrupole Mass Spectrometer) via a needle valve, whilst excess gas sent to a vent flow line.

The reactor volume used was 3.69 cm^3 and catalyst bed length was 0.13 cm^3. In order for the sample to be located centrally in the heater the reactor is packed with 1.78 cm^3 boiling chips both above and below the nitrided sample.

Before bringing the catalyst to reaction temperature, the reactor and gas lines were purged for 1 hour at ambient temperature using the H$_2$/N$_2$ carrier gas in order to remove any air from the reaction system prior to passing into the on-line mass spectrometer.   The materials were then heated to reaction temperature, 400 ^{o}C and held at this temperature for 3 hours. Upon reaching reaction temperature and after a period of 20 minutes to allow for catalyst stabilisation, 2 µl (2.3x10^{-5} moles) of benzene was injected into the reactor every 15 minutes followed by 5ml (2.2x10^{-4} moles) NH$_3$ gas. These injections were also performed in reverse, i.e. NH$_3$ followed by benzene, in a series of different experiments.
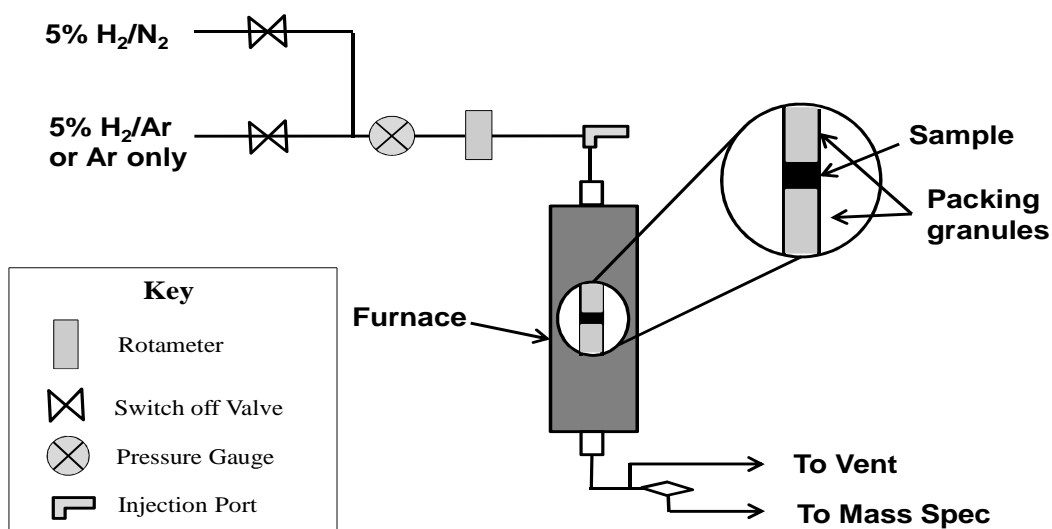
Figure 2.4-3 Apparatus used for conducting pulse experiments

3. The Reactivity of "Lattice" Nitrogen in Nitrides as Probed by H_2/N_2 and H_2/Ar Reactions.

3.1 Introduction.

Interest in nitrides, as previously discussed, has generally focussed on their catalytic ability for reactions such as hydrotreating, photocatalysis and ammonia synthesis. However within this project metal nitrides are investigated as potential nitrogen transfer reagents, in which the nitrides could be viewed as reservoirs for 'active' molecular nitrogen. This approach is akin to the Mars-van Krevelen mechanism which often occurs for catalytic oxidation reactions catalysed by metal oxides. In this mechanism an organic reactant is oxidized by the transfer of lattice oxygen from the catalyst generating the vacancies which are subsequently replenished by a gas-phase oxygen source.[93] Figure 3.1-1 illustrates this general type of process.

$$S \ + \ \tfrac{1}{2}\,O_2 \longrightarrow SO$$
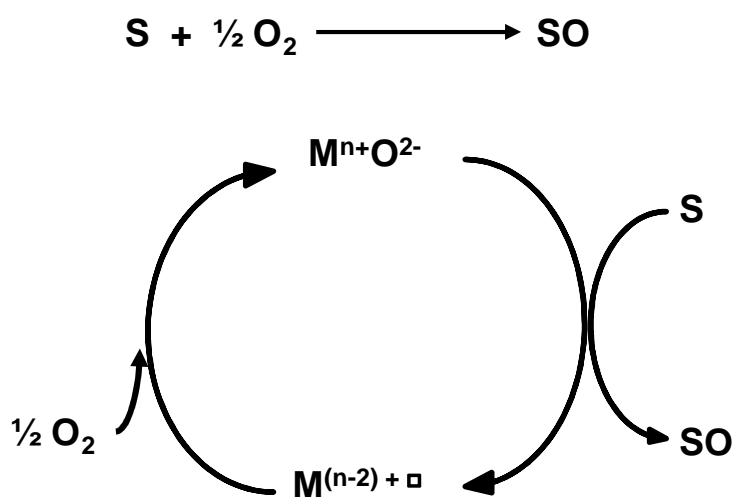
Figure 3.1-1 Schematic of Mars-van Krevelen oxidation mechanism (S = a substrate)

As well as being a mechanism, Mars-van Krevelen type oxidation can be viewed in process terms. In doing so, the substrate oxidation and catalyst re-oxidation phases can be performed in separate isolated stages. This could result in significant thermodynamic and / or kinetic advantages - for example in partial oxidation reactions where the desired products are more susceptible to oxidation than the reactants, it is possible to enhance their yields by performing the reaction in the absence of gas-phase oxygen. In the initial stage, the desired product is formed by direct reaction with the "catalyst" resulting in a reduced phase which can be re-oxidised in a separate stage. This type of approach has been applied

on the industrial scale by Du Pont for maleic anhydride production from butane oxidation using a vanadium phosphate based catalyst.[118-120]

In mechanistic terms, Mars-van Krevelen oxidation is found to occur in a wide range of systems. One example is the partial oxidation of propylene to acrolein over bismuth molybdate, which has been shown to occur in two steps, the activation of the propylene molecule, followed by the insertion of O atoms into the hydrocarbon.[121] Isotopic labelling studies have demonstrated that the sites located on the bismuth atoms, activate and dissociate O_2. Oxygen atoms subsequently fill vacancies which occur in the lattice as a consequence of acrolein desorption. This general type of mechanism has also been observed for sulfide and carbide transfer reactions. In the latter case, Gracia and co-workers have proposed a mechanism, demonstrated through computational methods, for the direct lattice carbon transfer from carbon dioxide hydrogenation to methane on an iron carbide surface.[122] Similarly Green and co-workers have reported the direct lattice carbon transfer to carbon monoxide produced in the partial oxidation of methane which is catalysed by molybdenum carbide.[94]

There is little evidence within the literature that suggests nitrogen participates in analogues of the Mars-van Krevelen type mechanism. Metal nitrides have been largely over-looked in this respect, despite early reports by Segal and Sebba which alluded to the possibility of lattice nitrogen being active in synthesis of ammonia catalysed by uranium nitride.[56-57] Examples can also be found in the Russian literature, where Panov and co-workers have investigated isotopic nitrogen exchange and ammonia synthesis with uranium and barium nitride systems.[123] More recently studies by Grange and co-workers have demonstrated one of the first examples of using lattice nitrogen transfer for the direct ammoxidation of propane to acrylonitrile using a vanadium aluminium oxynitride (VAlON) catalyst in a double Mars-van Krevelen process, which is illustrated in Figure 3.1-2.[71]
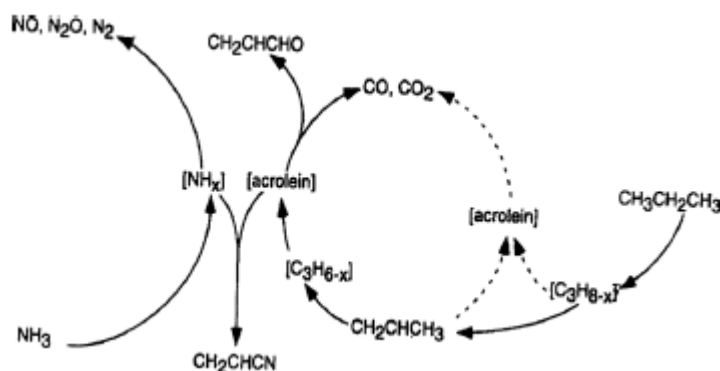
Figure 3.1-2 Reaction mechanism for propane ammoxidation over VAlON catalysts. Solid lines indicate reaction paths involving lattice oxygen, and dashed lines donate pathways with adsorbed oxygen. Square brackets are used to symbolize surface intermediates.[71]

One of the fundamental issues for this type of system is the ability for the material to reversibly uptake and release the reacting species. It is well known that intermetallic compounds, such as $LaNi_5$ and TiFe, can reversibly take-up and lose large amounts of hydrogen under mild conditions and it has been shown in the work of Itoh and Machida, that interstitial type metal nitrides behave in a similar manner, as shown below:[90-92]
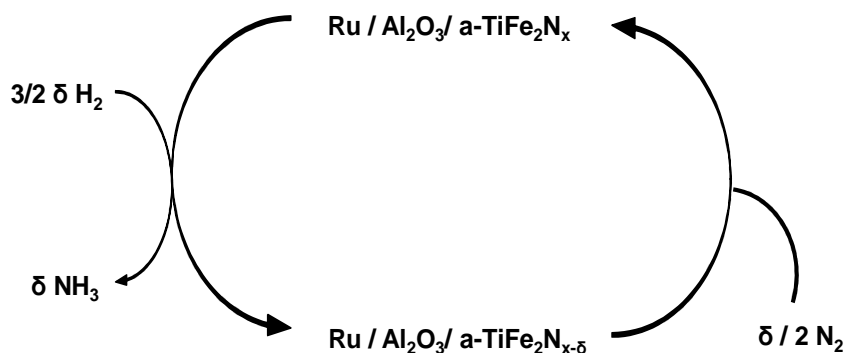
Figure 3.1-3 Schematic of the nitrogen uptake / removal system described by Itoh _et al._ [90]

Further to this, recent studies on Co_3Mo_3N have shown that there is a reversible loss of 50% of nitrogen from the structure under a H_2/Ar atmosphere, with the residual nitrogen moving to a different crystallographic site. The original stoichiometry can then be subsequently restored under a nitrogen atmosphere. [124-126] In many large scale processes, ammonia is used as a nitrogen carrier molecule and when viewed in terms of the nitrogen conversion process, they appear very inefficient. For example, as discussed in the

introduction, large scale aniline synthesis is performed in the following sequence of reactions:

$$N_2 + 3H_2 \longleftrightarrow 2NH_3$$

$$NH_3 + 2O_2 \longrightarrow HNO_3 + H_2O$$

$$HNO_3 + 2H_2SO_4 \longrightarrow NO_2^+ + H_3O^+ + 2HSO_4^-$$

$$C_6H_6 + NO_2^+ \longrightarrow C_6H_5NO_2 + H^+$$

$$C_6H_5NO_2 + 3H_2 \longrightarrow C_6H_5NH_2 + 2H_2O$$
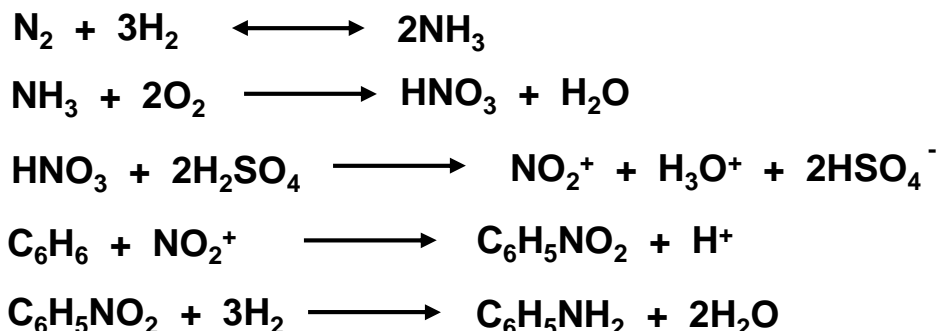
When broken down into the nitrogen transfer steps, it can be seen that N_2 is initially reduced to produce NH_3 from which HNO_3 is prepared by its re-oxidation (and effectively the corresponding oxidation of much of the H_2 used in the NH_3 synthesis stage). Nitration is eventually performed by nitronium cations in which the nitrogen is subsequently re-reduced. Given that it has been estimated that large scale ammonia synthesis consumes in excess of 1% of the global energy demand, the desirability of alternative, more direct routes is obvious.[95-99]

The use of nitrides for the ammonia synthesis reaction has been well documented, with first examples of uranium and osmium nitrides being reported in the initial work of Haber.[128] The conventional catalyst for ammonia synthesis is iron-based with the addition of alkali promoters, and more recently a promoted ruthenium based catalyst was introduced into commercial operation.[129-132] However as demand grows for nitrogen containing materials, the need to develop a more cost effective and highly efficient catalytic process for ammonia synthesis has become of great significance over the last 70 years. Among these, the invention of novel catalysts plays a leading role. Many elements, other than iron, have been examined in order to obtain a more active catalyst. One of the first being reported was molybdenum, documented by Mittasch in 1937. Molybdenum is, generally, known to dissociate N_2 more easily than iron or ruthenium. However, catalysts containing molybdenum or other transition metals have not been studied extensively when compared to iron or ruthenium based catalysts which are well understood. Many of these studies investigate the nitrogen adsorption steps, and the extent to which promoters affect the activity of the catalyst. Jacobsen and co-workers have rationalized the activity of Co_3Mo_3N in terms of a volcano relationship with the alloying of Co (which has a low N_2

adsorption energy) with Mo (which has a high N_2 adsorption energy) producing an optimal binding adsorption strength, and recent developments have involved the identification of Cs^+ promoted Co_3Mo_3N as a highly active catalyst for ammonia synthesis with an activity reportedly exceeding commercial based catalysts.[52, 60-68]

The work conducted in this chapter focuses on the reactivity of lattice nitrogen over a range of binary and ternary nitride materials and this is established via the comparison of ammonia synthesis activities using stoichiometric H_2/N_2 mixtures with H_2/Ar mixtures, as described in the experimental section. Eighteen different systems were prepared, characterised and screened and activities were compared to a supported Ru catalyst, which is known to be one of the most active systems for catalytic ammonia synthesis. Some supported nitrides have also been investigated to elucidate whether increasing the surface area of the material, via dispersion of the active phase, effects the ammonia synthesis activity. The effects of dopants on the activities of some bulk nitride phases have also been investigated. However, as previously mentioned, in order to function as a nitrogen transfer reagent it must be possible to replenish the depleted lattice nitrogen within the nitride, which will be discussed later in this thesis. The proposed nitrogen adsorption and transfer cycle, in theory could be conducted as separate steps and at different temperatures, which may prove to be advantageous in the development of a novel nitrogen transfer process, overcoming thermodynamic and kinetic limitations imposed by such systems. This general type of approach has been documented in the work of van Santen using a carbide based system.[133,134]

For this purposes of this chapter, the nitrides which have been investigated are divided into three groups – early transition metal nitrides, later transition metal nitrides and miscellaneous systems.

3.2 Early Transition Metal Nitrides.

3.2.1 Introduction to Early Transition Metals.

This section investigates the reactivity of lattice nitrogen of group IV-VI transition metal nitrides. The metal nitrides that will be discussed here include TiN, VN, CrN, β-$Mo_2N_{0.78}$, Ta_3N_5 and W_2N.

Group IV-VI transition metal nitrides are generally described as metallic nitrides because of their metallic conductivity, lustre and general metallic behaviour. These compounds are

characterised by their high melting points, hardness and resistance to corrosion, like their corresponding carbides and borides, they are often referred to as refractory hard metals.[31] They have traditionally found applications in ceramics, cutting tools and as structural components.   In the pioneering work of Levy and Boudart,[10] and which has been summarised by Oyama,[9] transition metal nitrides have been shown to be efficient catalysts. As a result, binary nitrides have attracted significant attention. In particular those of vanadium, molybdenum and tungsten have been applied to a range of reactions such as CO hydrogenation and NO dissociation, with resultant rates which are reportedly comparable to traditional 'platinum- like' catalysts.[9,10,11,17,54,75]   Suggestions have been made that this behaviour is attributed to the alloying the electron deficient parent metal with nitrogen.[134] The nitrogen atoms occupy the interstitial space created within the metal lattice and in doing so increase the electron count; hence the chemical properties of the nitride reportedly bear resemblance to the platinum group metals.   The description of interstitial occupancy of N atoms cannot be so easily applied to Ta_3N_5 since it forms an orthorhombic unit cell and the nitrogen atoms are either three-fold or four-fold co-ordinated to Ta.[136] However it is important to note that the level of similarity between nitrides and platinum group metals remains unclear, and much debate has arisen around this.[137-141]

There is a substantial amount of catalytic literature available for binary nitrides.   However, these generally focus on Mo or W based systems whilst other nitrides remain little studied. In addition to this, a large proportion of the literature concerning binary nitrides is primarily focussed upon synthesis techniques and the electronic and structural properties. Nevertheless, of the binary nitrides reported in the literature, molybdenum has been studied in greatest detail in terms of its catalytic applications and it is understood in the greatest detail. γ-Mo_2N and β-$Mo_2N_{0.78}$ have been shown to be active ammonia synthesis catalysts as have other binary nitrides such as vanadium nitride, uranium nitride and tungsten nitrides.

Furthermore, indirectly related to this, within the organic literature early transition metals such as Zr, Mo and Ti have been used for molecular nitrogen fixation with the aim to incorporate nitrogen into organic compounds. This approach can be illustrated by the work of Mori and others.[142,143] Mori reported the application of titanium-nitrogen based compounds, synthesised directly from dinitrogen, for the preparation of nitrogen heterocycles from organic compounds under ambient conditions.

The nitrides, which are investigated in this section, are stable under ammonia synthesis conditions and some can exist in a wide variety of stoichiometric forms, which could be envisaged to play a key role in facilitating Mars-van Krevelen type mechanisms/processes in which the reversible uptake and loss of N from the metal lattice may be facilitated. Despite ammonia synthesis activities of a number of the individual transition metal nitrides being known, there is not a comparative study of these materials within the literature and so this chapter also presents a general overview of this area. In addition, comparative studies of de-nitridation employing H_2/Ar have not been documented. In this chapter, individual systems will be described separately and then comparisons drawn later. Also, it should be emphasised that reaction data has been normalised to sample mass rather than surface area. The reason for this is that most of the systems which have been investigated are air sensitive and therefore, since areas are not measured *in-situ*, use of this parameter may introduce artefacts.

Ammonia production rates were derived from conductivity versus time plots, and a calculation applied to the gradient from the calibration data detailed in section 2.4-1. These are used to provide an indication of NH_3 formation during various phases of time on stream and are not meant to imply that steady state rates pertain. The general approach taken throughout this section, and indeed this chapter, has been to make comparisons of ammonia synthesis using H_2/N_2 and H_2/Ar feedstreams. The latter has been employed to determine the reactivity of "lattice" N species, including sorbed NH_x residues.

3.2.2 TiN.

Much of the literature surrounding titanium nitride either focuses on preparative methods or the electronic and optical properties associated with it for use as photocatalysts.[144-149] For the titanium group nitrides there are few catalytic applications which have been documented, although recently Kaskel *et al* reported the use of titanium nitride for the catalytic decomposition of complex aluminium hydrides, which led to subsequent studies for the use of TiN as a co-catalyst in hydrogen transfer reactions.[150] In addition to this, titanium complexes have also found use within organic chemistry as nitrogen transfer agents. As mentioned earlier, Mori developed a titanium–nitrogen complex from a titanium chloride precursor and applied it to the synthesis of nitrogen containing heterocycles.[142,143] In the same study it was also observed, that via this method, the titanium nitrogen complex could be used to synthesise imines from keto-carbonyls, and pyrrole derivatives from 1,4 – diketones.
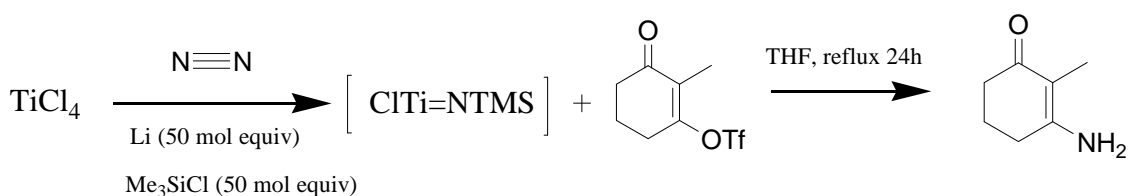
An early study by Lotz and Sebba reported the ammonia decomposition activities of the first row transition metal nitrides,[151] and it was shown that titanium nitride possessed little activity towards ammonia decomposition. Other than this, titanium nitride has only been studied for ammonia synthesis in combination with iron.[152] Titanium nitride (TiN_x) has been reported to exist in a variety of stoichiometric forms with x ranging from 0.53 to greater than 1.00.[23,24,153] The colour of TiN_{1-x} is an indicator of stoichiometry. The colours exhibited range from metallic grey to a yellow/gold, with yellow coloured TiN being the stoichiometric form. The resulting sample that was prepared in the current study was black in colour, which would suggest it was sub-stoichiometric. This colour of TiN has been previously observed in studies by Kaskel *et al* where they also produced a black powder with surface areas reported to be in excess of 200 $m^2 g^{-1}$.[154]

3.2.2.1   Reaction Data.

The H_2/N_2 and H_2/Ar reaction studies were conducted as outlined in the experimental section. Figure 3.2-1 illustrates the conductivity versus time plot for the ammonia production reaction at 400 ^oC using H_2/N_2 and H_2/Ar feeds.

It can be seen that under H_2/N_2 that there is a steady decrease in the conductivity value for TiN in the first 2.5 hours after which the NH_3 production rate drops off. In the reaction with H_2/Ar there is a sharp initial decrease in the conductivity within the first 30 minutes on stream, followed by a diminished rate of NH_3 evolution. As evident in the latter stages of the reaction, very little ammonia is produced.

Ammonia synthesis TiN
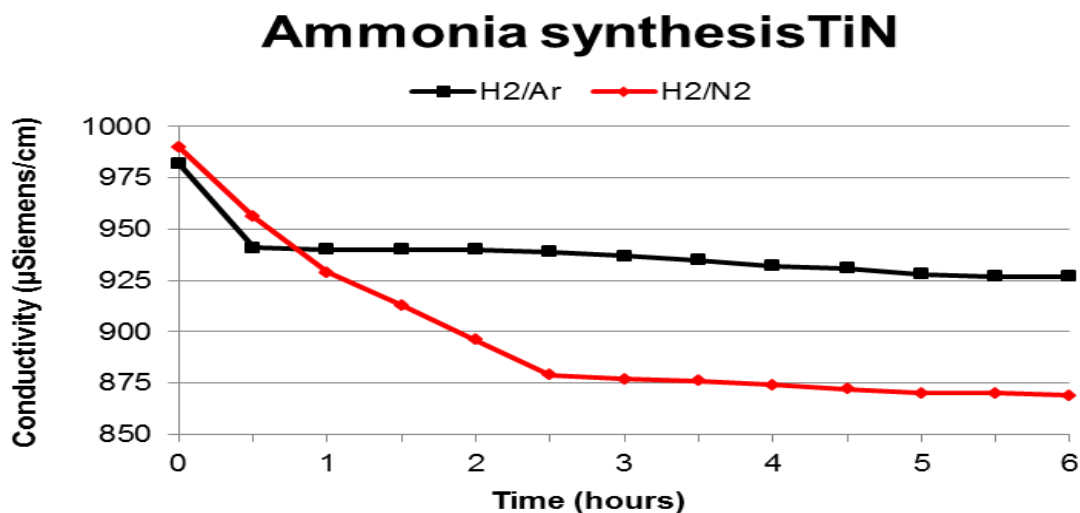
Figure 3.2-1 Comparison of conductivity for TiN ammonia production using H_2/N_2 vs. H_2/Ar at 400 ^{o}C.

The ammonia which is produced, during either reaction, may be as a result of the hydrogenation of surface NH_x species formed either during the preparation of the nitride by ammonolysis or in the initial two hour pre-treatment with H_2/N_2. The relatively rapid initial production of ammonia followed by a slower phase is a common trend which is observed in most of the nitrides that have been investigated in this work. The rates of ammonia synthesis at various time intervals for both the H_2/Ar and H_2/N_2 reactions conducted at 400 ^{o}C are presented in Table 3.2-1

It is worth noting that even under H_2/N_2 the ammonia production rates during the first 30 minutes of reaction are almost double that of the succeeding reaction rate, again, as mentioned above, may be due to the hydrogenation of adsorbed NH_x surface species. Indeed it is possible that the difference between the H_2/N_2 and H_2/Ar profiles relate to differences in the concentration of NH_x between the two samples.

Sample and Reaction Conditions	NH_3 Synthesis Rate (μmol h^{-1} g^{-1})
TiN, 400 ^{o}C (H_2/N_2, 0-0.5 h)	152
TiN, 400 ^{o}C (H_2/N_2, 1.0-2.5 h)	74
TiN, 400 ^{o}C (H_2/N_2, 3.0-6.0 h)	6
TiN, 400 ^{o}C (H_2/Ar, 0.-0.5 h)	183
TiN, 400 ^{o}C (H_2/Ar, 1-6 h)	6

Table 3.2-1 Ammonia production rates of TiN under both H_2/Ar and H_2/N_2 at 400 ^{o}C.

Temperature programmed H_2/Ar experiments were undertaken in order to assess the reactivity of the lattice nitrogen or NH_x species as a function of temperature.   This experiment was carried out in a similar manner to the H_2/Ar ammonia synthesis experiments but after ammonia production ceased the temperature was increased in 100 ^{o}C increments up to 700 ^{o}C.   The reaction profile (as well as the temperature profile) for TiN is illustrated in Figure 3.2-2:
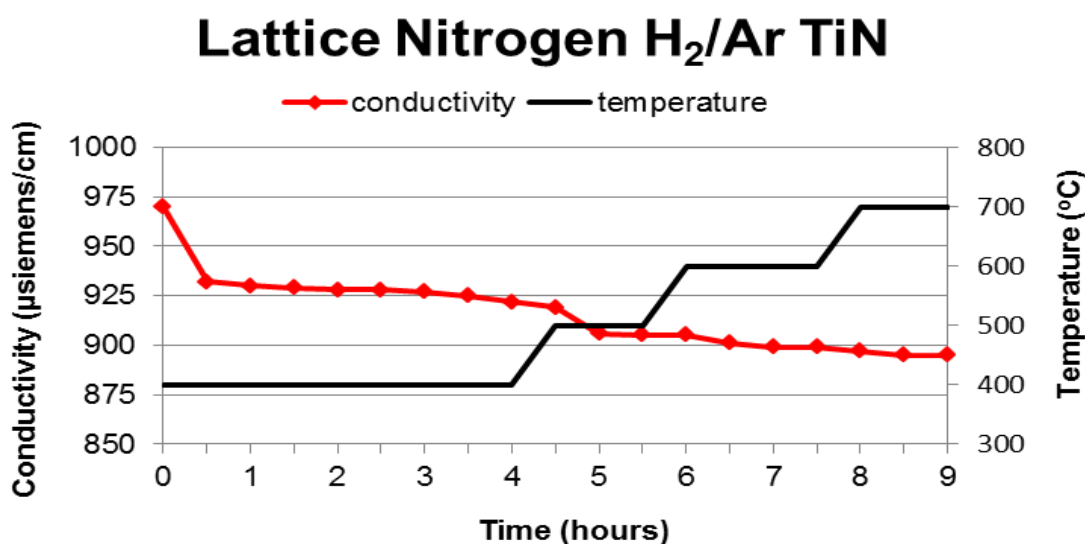
Figure 3.2-2 Conductivity data for NH$_3$ synthesis over TiN as a function of increasing temperature.

Again there is an initial decrease in conductivity within the first 30 minutes on stream and is comparable to the rate reported in Table 3.2-1, after which the ammonia production rate decreases rapidly with time on stream at 400 ^{o}C. After 4 hours, the reaction produces very little ammonia. The temperature was increased to 500 ^{o}C and it is clear that there was a further burst of ammonia production, which was not sustained. Further increases in temperature led to short lived NH_3 production. These surges of ammonia production upon temperature increase indicate that the nitrogen associated with the TiN phase prepared has various degrees of reactivity.   This could be attributed to different binding strengths between bulk and/or surface nitrogen species. It was calculated that only 1.29 % of the lattice nitrogen within TiN lost, as determined by CHN analysis, resulted in the formation of ammonia in this reaction. The ammonia production rates of TiN (under H_2/Ar) at temperatures between 400 ^{o}C and 700 ^{o}C are presented in Table 3.2-2:

Reaction Temperature and Time	NH$_3$ Synthesis Rate (μmol h^{-1} g^{-1})
400 $^{\circ}$C (0.0-0.5 h)	170
400 $^{\circ}$C (1.0-4.5 h)	6
500 $^{\circ}$C (4.5-5.0 h)	58
500 $^{\circ}$C (5.0-6.0 h)	2
600 $^{\circ}$C (6.0-7.5 h)	9
700 $^{\circ}$C (7.5-9.0 h)	4

Table 3.2-2 Ammonia production activity of TiN under H$_2$/Ar as a function of increasing temperature.

3.2.2.2 Nitrogen Analysis

The results of pre- and post-reaction nitrogen analysis of the TiN sample are presented in Table 3.2-3, along with calculated stoichiometric nitrogen content of the material.

Sample and Reaction Conditions	Calculated Stoichiometric N content (wt.%)	Pre-Reaction N Content (wt.%)	Post-Reaction N Content (wt.%)
TiN (H$_2$/N$_2$) after 6 h at 400 $^{\circ}$C	22.63	19.74	18.81
TiN (H$_2$/Ar) after 6 h at 400 $^{\circ}$C	22.63	19.74	18.76
TiN (H$_2$/Ar) using temperature profile as shown in Fig. 3.2-2	22.63	19.74	18.45

Table 3.2-3 Nitrogen content of TiN samples pre- and post-reaction.

The pre-reaction nitrogen content of the TiN is below that of the calculated stoichiometric value, which corresponds to a sub-stoichiometric form of TiN with a formula of TiN$_{0.87,}$ assuming there is no influence of surface oxidation. When considering the post-reaction data it is evident that in all cases the nitrogen content is slightly lower than that of the pre-reaction samples. In the case of the reactions at 400 $^{\circ}$C (H$_2$/N$_2$ and H$_2$/Ar), both materials after reaction have comparable nitrogen content (within 0.05 wt.%) and which indicates that there is limited consumption of nitrogen, which is possibly consistent with the reaction and loss of surface NH$_x$ species. Similarly in the case of the material treated under H$_2$/Ar using the temperature profile illustrated in Figure 3.2-2 with a maximum of 700 $^{\circ}$C, the post-reaction results indicate that very little additional nitrogen has been removed. The results show that only 1.29 wt.% of nitrogen has been lost which is in good correspondence

with the amount of ammonia produced in the reaction, as determined from the NH_3 production data (1.25 wt.%).

These results suggest that TiN is a relatively stable phase which would have very limited applicability as a nitrogen transfer reagent. Since several studies investigating bonding energy in TiN and sub-stoichiometric TiN_x have suggested that bonding energy between titanium and nitrogen is a function of nitrogen concentration within the metal lattice (i.e. with increasing nitrogen concentration as x approaches 1 the bond energy also increases) it is possible that the relatively inert behaviour observed in this study could be altered by changing the stoichiometry. However, in practice, targeted synthesis of specific stoichiometries may prove difficult using ammonolysis.

3.2.2.3 XRD Patterns.

The pre-and post- reaction X-ray diffraction patterns of the titanium nitride samples, which have been studied under the reaction conditions described in section 3.2.2.1, are shown in Figure 3.2-3
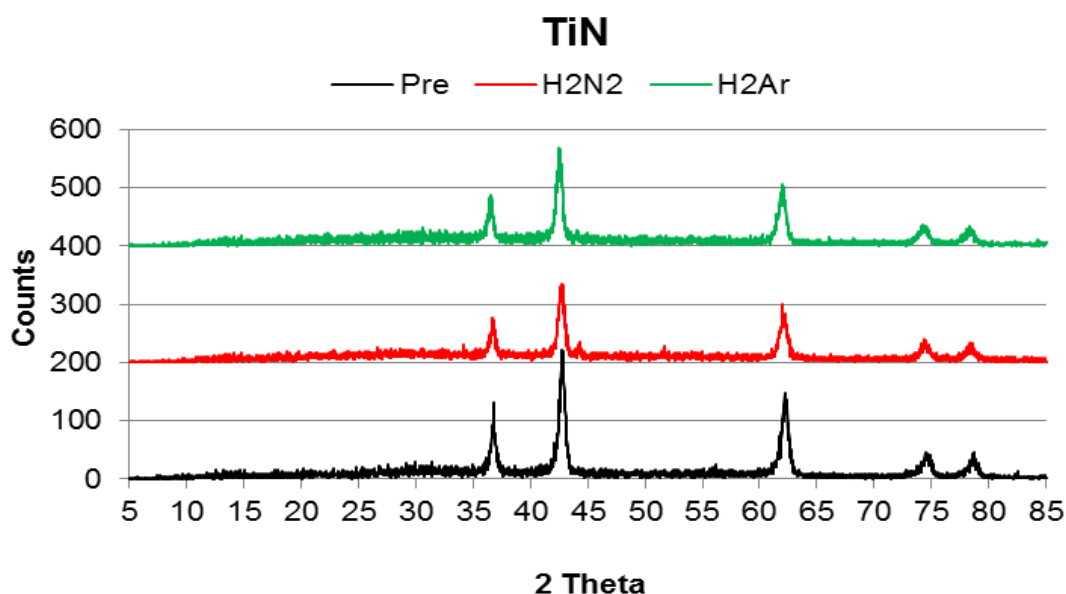
Figure 3.2-3 Pre- and post-reaction XRD patterns of TiN under H_2/N_2 and H_2/Ar (700 ^{o}C) gas mixtures (JCPDS 038-1420 TiN).

All three samples match to face centred cubic TiN. From the XRDs it is apparent that the reflections are quite broad, which is typical of high surface area materials, and possibly results from small particle size and/or disordered material. There are no apparent lattice shifts generated upon reaction which would suggest no significant loss of nitrogen from the crystal lattice. However, upon inspection of the post-reaction pattern obtained under H_2/Ar

it is evident that some small additional reflections are present.   These peaks are characteristic of rutile (TiO_2) which are most likely a result of aerobic oxidation when discharging the slightly more reduced material from the reactor.

3.2.3 VN.

Vanadium complexes are known to participate in biological nitrogen fixation, and are found in nitrogenase enzymes, where they show activity for the reduction of N_2 to either hydrazine or ammonia.[155] Similar non-biological mechanisms have been demonstrated in the work of Shilov *et al,* whereby vanadium (II)-catechol systems were prepared and the rate of ammonia formation was monitored and compared with a nitrogenase active centre.[156] Despite this, very little is known regarding the potential catalytic applications of vanadium nitride. However, as stated earlier reports by Sebba *et al* have demonstrated that vanadium nitride is catalytically active for both ammonia decomposition and ammonia synthesis reactions.[55,151]   In the study by Lotz and Sebba, it was suggested that the ammonia produced was a result of hydrogenation of loosely bound surface nitrogen which subsequently decreased with time on stream, affecting the activity of the material, as a consequence of the slow diffusion rates of nitrogen from bulk to the surface.[151]   More recent studies have suggested that vanadium carbides and nitrides may be more active for ammonia decomposition than platinum based catalysts. Oyama investigated the high temperature kinetics of ammonia decomposition over cubic VN.[70,157] This study highlighted that vanadium nitride exhibited similar behaviour to molybdenum and tungsten nitrides for ammonia decomposition.   Besides studies for ammonia synthesis and decomposition, vanadium nitride has also been shown, by Thompson *et al,*[158] to be active for the dehydrogenation of butane.

3.2.3.1 Reaction Data.

Previous literature has suggested that vanadium nitride has a higher activity towards ammonia synthesis than either of its neighbouring metal nitrides, TiN and CrN, at elevated pressures and temperatures.[151] This was also observed in the current ammonia production study conducted at ambient pressure and 400 $^{\circ}$C, and the conductivity versus time plots for VN are presented in Figure 3.2-4.
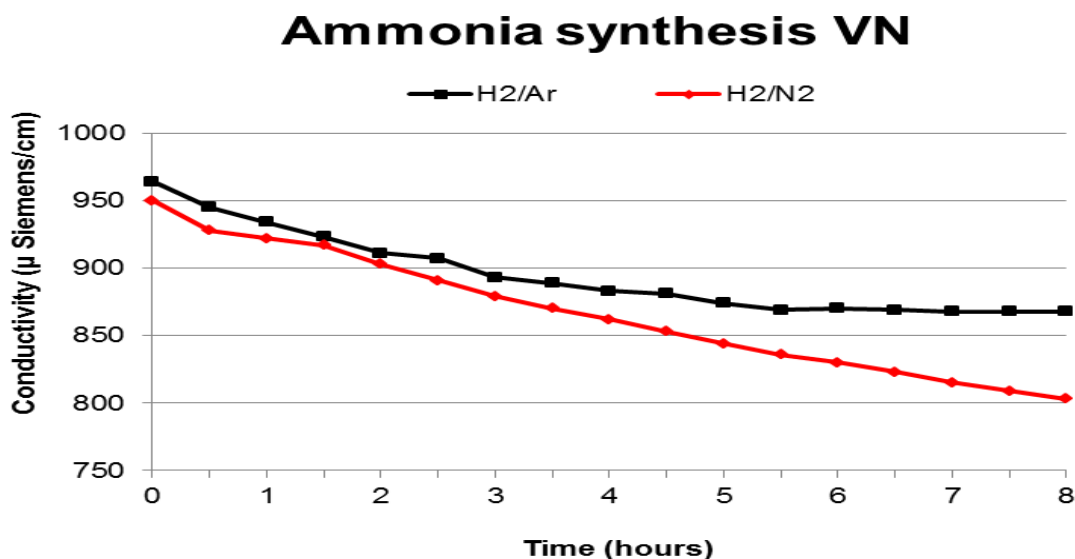
Figure 3.2-4 Comparison of conductivity for VN ammonia production using H_2/N_2 vs. H_2/Ar at 400 ^{o}C.

From Figure 3.2-4, it can be seen that after about 90 minutes on stream under a H_2/N_2 atmosphere the reaction exhibits an apparently steady state synthesis rate. However it can also be observed that under a H_2/Ar environment there too is a relatively steady decrease in the conductivity with time.   However, in this case activity appears to drop off after 5.5 h and very little additional ammonia is produced after this period. Hence an extended reaction time run (as shown in Figure 3.2-4) was undertaken so as to distinguish whether or not catalytic ammonia formation occurs under a H_2/N_2 atmosphere, as up until 5.5 h this could still be ambiguous. For most other metal nitride systems investigated a sharp drop in the conductivity has been observed within the first 30 minutes on stream, which may possibly be attributed to the removal of loosely bound surface NH_x species. In the case of VN, however, it is apparent that there is not the same sharp drop in conductivity but rather a gradual decrease. It may be the case that, as has been alluded to by King and Sebba,[55] surface species are removed before being replaced by bulk nitrogen diffusing to the surface which eventually ceases in leading to loss of activity. Conversely in H_2/N_2 the surface nitrogen which is hydrogenated can continuously be replaced from the nitrogen in the feed gas and steady state conditions can be maintained.   The ammonia production rates for VN under H_2/Ar and H_2/N_2 at 400 ^{o}C are presented in Table 3.2-4.

Sample and Reaction Conditions	NH$_3$ Synthesis Rate (μmol h^{-1} g^{-1})
VN, 400 ^{o}C (H$_2$/N$_2$, 0-0.5 h)	98
VN, 400 ^{o}C (H$_2$/N$_2$, 0.5-1.5 h)	24
VN, 400 ^{o}C (H$_2$/N$_2$, 1.5-8 h)	40
VN, 400 ^{o}C (H$_2$/Ar, 0.0-0.5 h)	85
VN, 400 ^{o}C (H$_2$/Ar, 0.5-1.5 h)	49
VN, 400 ^{o}C (H$_2$/Ar, 1.5-5.5 h)	31
VN, 400 ^{o}C (H$_2$/Ar, 5.5-8 h)	trace

Table 3.2-4 Ammonia production rates of VN under both H$_2$/Ar and H$_2$/N$_2$ at 400 ^{o}C.

As for TiN, studies under H$_2$/Ar were also conducted using the same temperature ramp profile as previously described. The ammonia production rates for each temperature are quoted in Table 3.2-5.

Reaction Temperature and Time	NH$_3$ Synthesis Rate (μmol h^{-1} g^{-1})
400 ^{o}C (0-0.5 h)	84
400 ^{o}C (1.0-4.5 h)	38
500 ^{o}C (4.5-5.0 h)	31
500 ^{o}C (5.0-6.0 h)	9
600 ^{o}C (6.0-7.5 h)	40
700 ^{o}C (7.5-9.0 h)	27

Table 3.2-5 Ammonia production activity of VN under H$_2$/Ar as a function of increasing temperature.

3.2.3.2 Nitrogen Analysis.

From comparison of the pre- and post-reaction N analysis, it is evident that there is a significant loss of nitrogen from the samples upon reaction under both H$_2$/N$_2$ and H$_2$/Ar. However, it is notable that the extent of nitrogen loss appears to be relatively independent of the reaction conditions. Whilst the loss of N from the sample reacted isothermally with H$_2$/Ar at 400 ^{o}C is greater than that of the corresponding H$_2$/N$_2$ reaction, as might be expected, the influence of employing the temperature programme up to 700 ^{o}C (using the

temperature profile shown for TiN in Figure 3.2-2) appears rather limited. Whilst the nitrogen content in the temperature-programmed H_2/Ar sample is lower than its isothermal counterpart, the difference is relatively small. The loss observed has been compared with that calculated on the basis of ammonia production experiments and it was found that around 1.8 % of the total nitrogen lost, as found by CHN analysis, formed ammonia in the H_2/Ar experiments.

Sample and Reaction Conditions	Calculated Stoichiometric N content (wt.%)	Pre-Reaction N Content (wt.%)	Post-Reaction N Content (wt.%)
VN (H_2/N_2) after 6 h at 400 ^{o}C	21.55	18.39	14.88
VN (H_2/Ar) after 6 h at 400 ^{o}C	21.55	18.39	14.15
VN (H_2/Ar) using temperature profile as shown in Fig. 3.2-2	21.55	18.39	14.06

Table 3.2-6 Nitrogen content of VN samples pre- and post-reaction.

3.2.3.3 XRD Patterns.

From XRD, all samples were confirmed to be cubic VN, matching JCPDS file number 00-035-0768. Post-reaction XRD analysis again illustrates that the VN undergoes no phase change under H_2/N_2. However, as with TiN, traces of an oxide, (in this case V_2O_3) are present in the post H_2/Ar (700 ^{o}C) reaction sample, as highlighted in Figure 3.2-7 and indicated by small stars. It is known that the early transition metals are sensitive towards oxygen, and readily react to form their oxides. As discussed, this oxidation may occur on discharge of the material, which could be a result of the sample becoming more reduced at the higher temperatures, employed during the temperature programmed H_2/Ar reactions, causing the material to subsequently become more sensitive towards oxygen and hence increasing susceptibility towards oxidation.
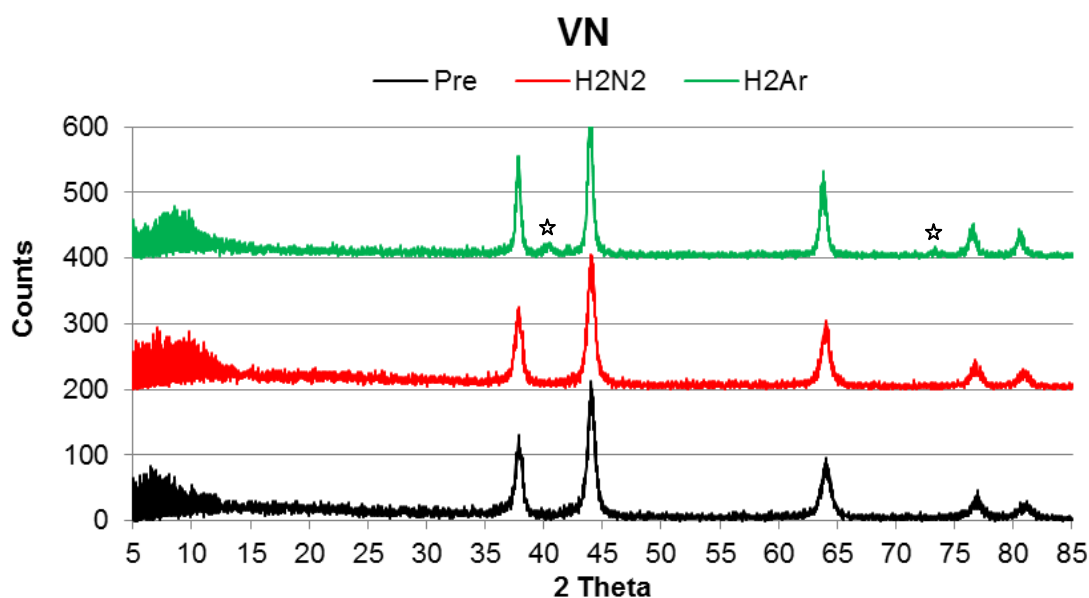
Figure 3.2-5 Pre- and post-reaction XRD patterns of VN under H$_2$/N$_2$ and H$_2$/Ar (700 ^{o}C) gas mixtures. ☆ indicate V$_2$O$_3$ reflections. (JCPDS 00-035-0768 VN).

3.2.4 CrN.

Like titanium nitride (section 3.2.2), chromium nitride is considered to have properies similiar to refactory metals, such as hardness and resistance to corrosion, and it has been investigated as a replacement for TiN for use as coatings on steel cutting and drilling tools due to its stability.[159-162] Chromium nitride is one of the more difficult nitrides to prepare and is not readily synthesised from the oxide precursor.   Much of the literature surrounding preparation techniques concentrate on a variety of vapour deposition techniques, such as magnetron sputtering, vacuum arc evaporation and reactive ion plating.[162-165] Various phases of CrN$_x$, such as Cr$_2$N and CrN can be observed using these deposition techniques and their formation is dependent on the partial pressure of the reactive nitrogen gas. In comparison, preparation of chromium nitride by ammonolysis is less well documented. Herle and co-workers reported the synthesis of CrN by ammonolysis of a chromium sulfide precursor (Cr$_2$S$_3$) and it was shown that a pure phase nitride could be synthesised under a flow of NH$_3$ gas at 725 ^{o}C for 12 hours.[166] More recently Zhang *et al*, discussed the effects of temperature and time on the morphology of chromium nitride prepared using a chromium halide precursor and ammonia gas.[101]   It was concluded that as the nitriding temperature is increased from 500 ^{o}C to 800 ^{o}C larger particles form and this effect was also observed to occur when the nitridation duration was increased (in the range of 2-5 hours). The catalytic literature on CrN is very sparse, with the bulk of the literature concentrating on material properties and novel preparation techniques. Despite this, Lotz and Sebba investigated this material as an ammonia

decomposition catalyst, along with the other first row transition metal nitrides, and its activity was found to be minimal.[151]

3.2.4.1 Reaction Data.

As can be seen from Figure 3.2-6, the decrease in conductivity does not follow the same pattern as has been previously observed, with the loss of nitrogen being somewhat erratic under both feed streams.   During the first 30 minutes on stream, there a drop in conductivity, in both instances.   However beyond this time, there does not appear to any consistency to the conductivity observed, although the general trend is a decrease.   It is apparent that in both instances very little ammonia is produced. At most only 0.7 % of the lattice nitrogen contributes to the formation of ammonia in the case of the H_2/Ar feed. Similar ammonia production was observed in duplicate H_2/Ar and H_2/N_2 studies with a maximum difference in each conductivity reading of 10 µS/cm and 6 µS/cm respectively, which are represented by error bars in Figure 3.2-6.   As the production of ammonia is somewhat unstable, it has not been possible to calculate the ammonia production rates in the same manner as has been for materials, for this reason only the ammonia production rates for the first 30 minutes on stream are presented in Table 3.2-7.

As can be seen, the rates for H_2/N_2 that are presented in Table 3.2-7 are comparable to that of vanadium nitride within first 30 minutes on stream. However beyond this initial phase, the two systems behave differently.
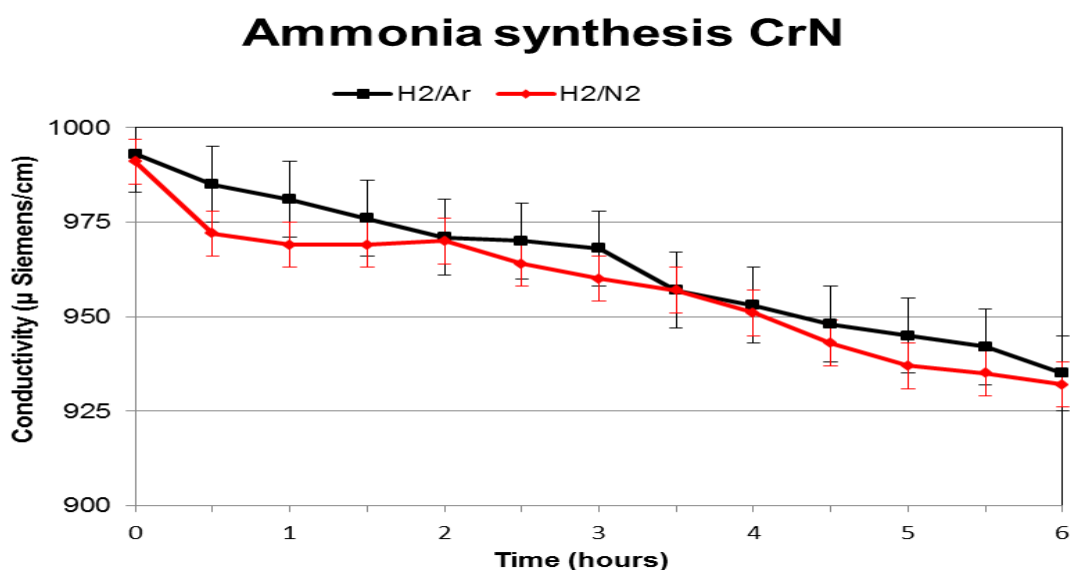
Figure 3.2-6 Comparison of conductivity for CrN ammonia production using H_2/N_2 vs. H_2/Ar at 400°C (error bars of ± 10 µS/cm H_2/Ar and ± 6 µS/cm H_2/N_2).

Sample and Reaction Conditions	NH$_3$ Synthesis Rate (μmol h^{-1} g^{-1})
CrN, 400 ^{o}C (H$_2$/N$_2$, 0-0.5 h)	86
CrN, 400 ^{o}C (H$_2$/Ar, 0-0.5 h)	36

Table 3.2-7 Ammonia production rates of CrN under both H$_2$/Ar and H$_2$/N$_2$ at 400 ^{o}C.

It may be anticipated that chromium nitrides would have activity rates comparable to either molybdenum or tungsten nitride, since Cr, Mo and W are from the same group in the periodic Table. This is not the case. Even at temperatures up to 700 ^{o}C in the temperature programmed studies employing H$_2$/Ar, very little ammonia production is observed with a total of *ca.* 1% of the total nitrogen, as determined by CHN analysis, being lost as ammonia. The ammonia production rates at various times on stream are presented in Table 3.2-8.

Reaction Temperature and Time	NH$_3$ Synthesis Rate (μmol h^{-1} g^{-1})
400 ^{o}C (0-0.5 h)	27
400 ^{o}C (1.0-4.5 h)	24
500 ^{o}C (4.5-5.0 h)	36
500 ^{o}C (5.0-6.0 h)	18
600 ^{o}C (6.0-7.5 h)	5
700 ^{o}C (7.5-9.0 h)	2

Table 3.2-8 Ammonia production activity of CrN under H$_2$/Ar as a function of increasing temperature.

3.2.4.2 Nitrogen Analysis.

As can be seen in Table 3.2-9 there is a large decrease in the post-reaction nitrogen content, with a loss of almost 13-14 wt. % in each case. When this is compared to the calculated amount of total nitrogen lost as ammonia (*ca.* 1%) it is evident that the nitrogen lost is in a form which does not manifest itself in a change of conductivity of the H$_2$SO$_4$ solution. It is most likely that loss occurs as N$_2$. In this instance it is particularly curious that this amount of nitrogen has been lost from the system, when it is considered that CrN is supposed to be a thermally resistant material, and even when compared to TiN where only a small decrease in the nitrogen content is observed. However this was reproducibly found to be the case.

Sample and Reaction Conditions	Calculated Stoichiometric N content (wt.%)	Pre-Reaction N Content (wt.%)	Post-Reaction N Content (wt.%)
CrN (H_2/N_2) after 6 h at 400 ^{o}C	21.21	19.66	6.57
CrN (H_2/Ar) after 6 h at 400 ^{o}C	21.21	19.66	5.98
CrN (H_2/Ar) using temperature profile as shown in Fig. 3.2-2	21.21	19.89	5.60

Table 3.2-9 Nitrogen content of CrN samples pre- and post-reaction.

3.2.4.3 XRD Patterns.

Chromium nitride exists in two phases; γ-CrN and β-Cr_2N. with calculated nitrogen stoichiometric values of 21.21 wt.% and 11.81 wt.% respectively.[166]   This led to ambiguity in terms of the phases present in the post-reaction samples. Using XRD samples were confirmed to be γ-CrN, with minor reflections corresponding to β-Cr_2N reflections which are present in both the starting phase and the post H_2/Ar reaction sample (as indicted by stars in Figure 3.2-7).

It is interesting to note that these peaks are not observed in the post-reaction H_2/N_2 sample. Given the large, and reproducible, nitrogen loss from these samples it would be anticipated that there would be shifts in the position of the post-reaction reflections. If crystalline Cr metal was formed reflections would be anticipated to occur at 39 ^{o}, 44 ^{o}, 49 ^{o}, 57 ^{o}, 67 ^{o} and 71° 2θ. Furthermore, if oxidation occurred upon discharge of these samples from the reactor it is probable that chromium oxide phases would be evident. The origin of this apparent discrepancy is not clear.

 In both post H_2/Ar and H_2/N_2 reaction samples, there is evidence of a broad reflection between 17 ^{o} and 28 ^{o} 2θ, which is not observed in the pre-reaction XRD, which could potentially be an amorphous material and may explain the reason for the significant difference in nitrogen contents between the pre- and post-reaction samples. However its intensity is very low.

CrN
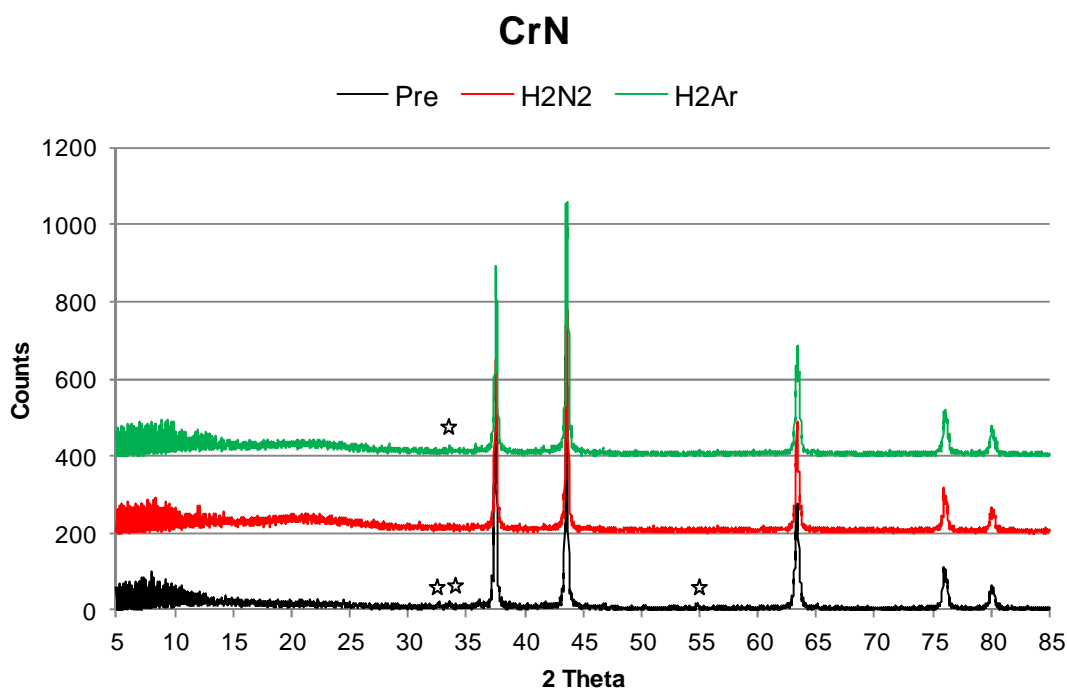
Figure 3.2-7 Pre- and post-reaction XRD patterns of CrN under H_2/N_2 and H_2/Ar gas mixtures. (JCPDS 003-1157 CrN) β-Cr_2N is indicated by a (☆)

3.2.5 β-$Mo_2N_{0.78}$.

Of the binary nitrides reported in the literature, molybdenum and tungsten nitrides have been studied in the greatest depth in terms of their catalytic applications. Molybdenum nitride is well recognised as a catalyst for ammonia synthesis.[53] Latterly most catalytic interest in nitride materials has largely arisen due to the easily accessible synthesis of high surface area γ-Mo_2N by means of temperature programmed ammonolysis of an oxide precursor, as first reported by Volpe and Boudart.[32,107] High space velocities of ammonia and carefully controlled temperature ramp rates are an important requirement in this method. These specific parameters are thought to be significant in achieving high surface area materials by reducing the partial pressure of water generated from the oxide precursor, which is understood to reduce the surface area of the material through hydrothermal sintering, and to control the extent of thermal sintering at crucial stages of the temperature process.[32] Wise and Markel demonstrated that high surface area γ-Mo_2N could also be prepared using H_2/N_2 mixtures, rather than NH_3, by applying similar conditions as described by Volpe and Boudart, involving controlled temperature ramp rates and high space velocities.[41] Wise and Markel compared both nitridation methods and concluded that, in terms of industrial applications, application of a H_2/N_2 gas mixture is favoured with respect to NH_3 due to the problems associated with heat transfer at elevated temperatures in the latter case. Although Wise and Markel report on the synthesis of γ-Mo_2N under H_2/N_2

mixtures, other studies which have also adopted this approach have shown that β-$Mo_2N_{0.78}$ (which can also be prepared by partial decomposition of γ-Mo_2N at temperatures above 800 ^{o}C in an inert atmosphere)[42,43] is the resultant phase. Although there are discrepancies in terms of the phases which are reported using this route, it was this method which was applied for the preparation of bulk and doped molybdenum nitrides in the current study, as described in the experimental section.

Molybdenum nitride has been investigated as a potential catalyst for a range of different reactions including CO hydrogenation, ammonia synthesis, hydrotreating and amination reactions and has been reported to display similar catalytic activities to the platinum group metals. Thompson and co-workers have demonstrated that a range of early metal nitrides are active for ethanol amination and also reported that molybdenum nitride is more selective than Ni/SiO_2 for the production of di- and tri-ethylamine.[18] Although molybdenum nitride has been studied in great detail, most catalytic applications have generally focused on the γ-Mo_2N phase whilst other phases such as β-$Mo_2N_{0.78}$ and δ-Mo_2N have not been studied to the same extent. β-$Mo_2N_{0.78}$ is the only phase which is examined in this study. As well as being relatively easy to prepare, inspection of the Mo-N phase diagram shows that variable stoichiometry may be possible and a number of different stoichiometries have been reported.[167] Therefore, it is arguable that this phase could be of more interest than the more commonly investigated γ-Mo_2N, in terms of the objective of this study. Studies of the effect of metal dopants upon de-nitridation have also been conducted. These include Fe, Cu and Bi at a 1.5 wt. % loading. Previous studies have indicated that addition of low level metal dopants may have an effect on the morphology and the de-nitridation characteristics.[168] The metals which are employed as dopants in this study have either been found to be active for amination reactions or to activate the C-H bond in hydrogen abstraction.[169-179]

3.2.5.1   Reaction Data.

From previous investigations by Mckay *et al*, it is known that the beta phase is active for ammonia synthesis.[34] Figure 3.2-8 presents a typical conductivity versus time plot which was obtained for the undoped β-$Mo_2N_{0.78}$ phase.

Ammonia synthesis β- $Mo_2N_{0.78}$
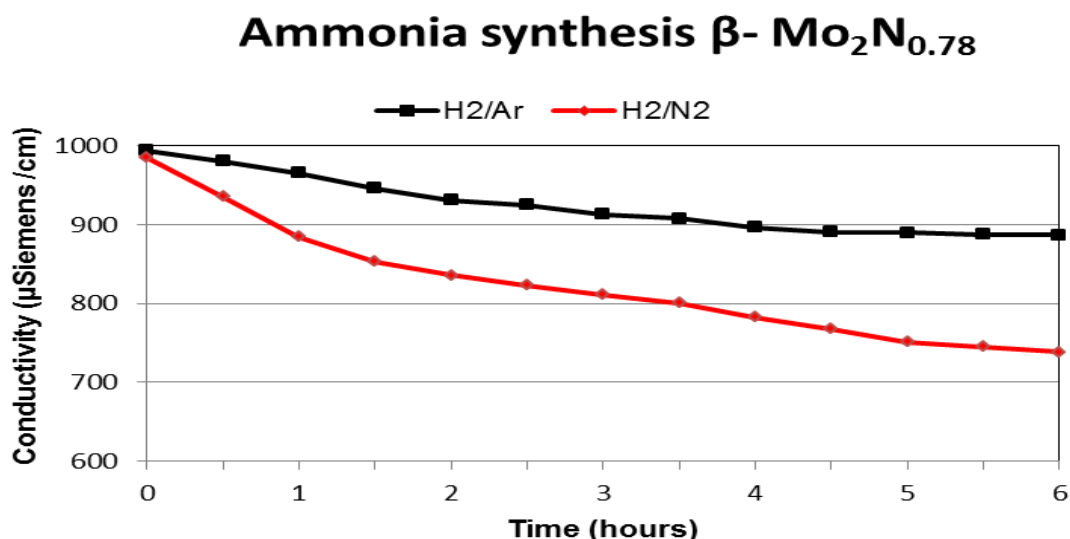
Figure 3.2-8 Comparison of conductivity for β-$Mo_2N_{0.78}$ ammonia production using H_2/N_2 vs. H_2/Ar at 400 ^{o}C.

From Figure 3.2-8 it is evident that ammonia production occurs over β-$Mo_2N_{0.78}$ under H_2/N_2 and it would appear that steady state conditions are reached beyond 1.5 h on stream Figure 3.2-9 highlights that the addition of metal dopants has little effect on the rate at which ammonia is produced, although it appears that Bi perhaps hinders the synthesis slightly and that iron perhaps enhances it slightly. Table 3.2-10 provides the ammonia synthesis rates for the above conductivity versus time plot and comparable data for doped samples can be found in Table 3.2-11.

Sample and Reaction Conditions	NH$_3$ Synthesis Rate (μmol h^{-1} g^{-1})
β-$Mo_2N_{0.78}$, 400 ^{o}C (H_2/N_2, 0.0-0.5 h)	222
β-$Mo_2N_{0.78}$ 400 ^{o}C (H_2/N_2, 1.0-6.0 h)	66
β-$Mo_2N_{0.78}$, 400 ^{o}C (H_2/Ar, 0.0-0.5 h)	224
β-$Mo_2N_{0.78}$, 400 ^{o}C (H_2/Ar, 1.0-6.0 h)	35

Table 3.2-10 Ammonia production rates of β-$Mo_2N_{0.78}$ under both H_2/Ar and H_2/N_2 at 400°C.

Ammonia synthesis doped β-Mo₂N₀.₇₈
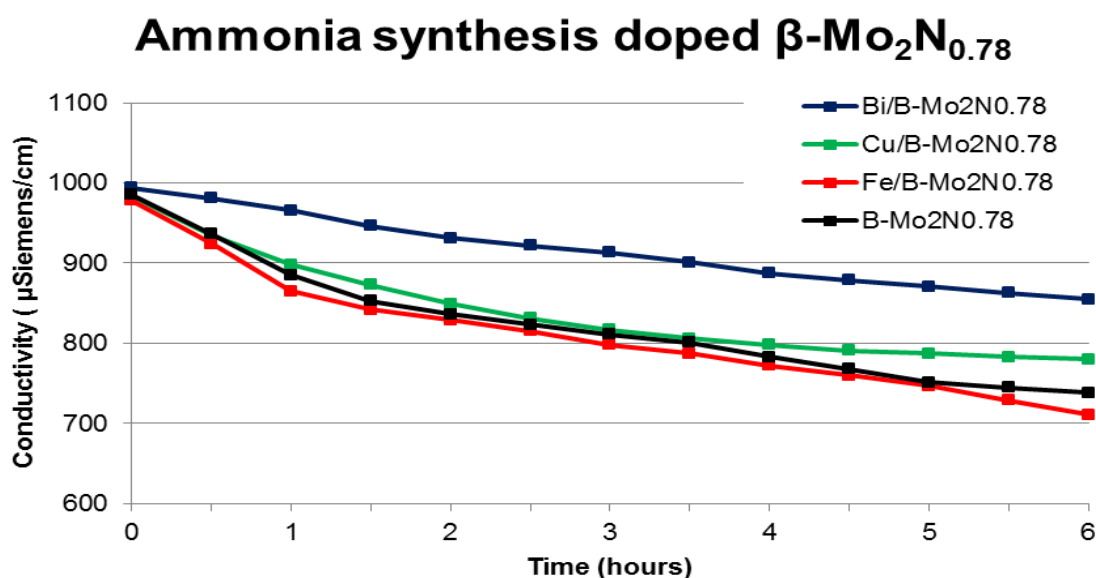
Figure 3.2-9 Comparison of conductivity for β-Mo$_2$N$_{0.78}$ and doped β-Mo$_2$N$_{0.78}$ ammonia production using H$_2$/N$_2$ at 400 ^{o}C.

Sample	NH$_3$ Synthesis Rate (µmol h^{-1} g^{-1})			
	H$_2$/N$_2$		H$_2$/Ar	
	0.0-0.5 h	1.0-6.0 h	0.0-0.5 h	1.0-6.0 h
β-Mo$_2$N$_{0.78}$	222	66	224	35
1.5% Fe / β-Mo$_2$N$_{0.78}$	242	69	122	22
1.5% Cu / β-Mo$_2$N$_{0.78}$	214	54	107	18
1.5% Bi / β-Mo$_2$N$_{0.78}$	59	50	78	6

Table 3.2-11 Ammonia production rates of β-Mo$_2$N$_{0.78}$ and doped β-Mo$_2$N$_{0.78}$ under both H$_2$/Ar and H$_2$/N$_2$ at 400 ^{o}C.

In the case of H$_2$/Ar, the conductivity steadily decreases over time, which would either suggest that there is a 'bank' of reactive surfaces species which are not strongly bound or that nitrogen species slowly diffuse out of the metal lattice at this temperature (400 ^{o}C). It was neccessary to determine if the metal dopants facilated this and results are presented in Table 3.2-12.

Reaction Temperature and Time	NH$_3$ Synthesis Rate (µmol h^{-1} g^{-1})			
	β-Mo$_2$N$_{0.78}$	1.5% Fe / β-Mo$_2$N$_{0.78}$	1.5% Cu / β-Mo$_2$N$_{0.78}$	1.5% Bi / β-Mo$_2$N$_{0.78}$
400 ^{o}C (0-0.5 h)	220	122	107	78
400 ^{o}C (1-4.5 h)	56	32	24	36
500 ^{o}C (4.5-5 h)	85	82	89	77
500 ^{o}C (5-6 h)	34	38	49	43
600 ^{o}C (6-7.5 h)	54	63	42	47
700 ^{o}C (7.5-9 h)	7	13	11	9

Table 3.2-12 Ammonia production activity of β-Mo$_2$N$_{0.78}$ and doped β-Mo$_2$N$_{0.78}$ under H$_2$/Ar with increasing temperature

From these results, it is evident that the addition of metal dopants has a relatively small effect on the production of ammonia, with synthesis rates being comparable to the undoped sample. However it is evident that the addition of bismuth hinders the production of ammonia, despite complete removal of lattice nitrogen (as detailed below).

3.2.5.2 Nitrogen Analysis.

Table 3.2-13 indicates the pre- and post- reaction nitrogen contents within the sample. As can be seen, both the undoped and Fe-doped pre-reaction samples are consistent with the calculated stoichiometric values; however the Cu and Bi samples appear to be slightly lower than expected. In the case of Bi it is apparent that after 6 hours at 400 ^{o}C, under H$_2$/Ar not all nitrogen has been removed, which is unlike the other samples studied, where all nitrogen is apparently removed.

On examining the H$_2$/N$_2$ post-reaction nitrogen content, all samples have slightly lower values than the pre- reaction sample, which is further evidence to suggest the removal of surface species. Despite this, the Fe doped material only lost 0.05 wt.% N compared with ~1.5 wt.% observable in the other materials, this would suggest that under H$_2$/N$_2$ reaction conditions molybdenum nitride doped with Fe could more resistant to hydrogenation of the nitrogen in the metal lattice. It may also be the case that the Fe facilitates a nitrogen spill over effect, replenishing nitrogen loss from the molybdenum nitride phase. This suggestion is consistent with the fact that iron is known to be an effective ammonia synthesis catalyst.[139,217,218]

Sample and Reaction Conditions	Calculated Stoichiometric N content (wt.%)	Pre-Reaction N Content (wt.%)	Post-Reaction N Content (wt.%)
β-$Mo_2N_{0.78}$, (H_2/N_2) after 6 h at 400 ^{o}C	5.38	5.58	3.83
β-$Mo_2N_{0.78}$, (H_2/Ar) after 6 h at 400 ^{o}C	5.38	5.58	0
β-$Mo_2N_{0.78}$, (H_2/Ar) using temperature profile as shown in Fig. 3.2-2	5.38	5.58	0
1.5% Fe / β-$Mo_2N_{0.78}$, (H_2/N_2) after 6 h at 400 ^{o}C	5.38	5.31	5.26
1.5% Fe / β-$Mo_2N_{0.78}$, (H_2/Ar) after 6 h at 400 ^{o}C	5.38	5.31	0
1.5% Fe / β-$Mo_2N_{0.78}$, (H_2/Ar) using temperature profile as shown in Fig. 3.2-2	5.38	5.31	0
1.5% Cu / β-$Mo_2N_{0.78}$, (H_2/N_2) after 6 h at 400 ^{o}C	5.38	4.39	3.14
1.5% Cu / β-$Mo_2N_{0.78}$, (H_2/Ar) after 6 h at 400 ^{o}C	5.38	4.39	0
1.5% Cu / β-$Mo_2N_{0.78}$, (H_2/Ar) using temperature profile as shown in Fig. 3.2-2	5.38	4.39	0
1.5% Bi / β-$Mo_2N_{0.78}$, (H_2/N_2) after 6 h at 400 ^{o}C	5.38	4.66	4.17
1.5% Bi / β-$Mo_2N_{0.78}$, (H_2/Ar) after 6 h at 400 ^{o}C	5.38	4.66	3.37
1.5% Bi / β-$Mo_2N_{0.78}$, (H_2/Ar) using temperature profile as shown in Fig. 3.2-2	5.38	4.66	0

Table 3.2-13 Ammonia production activity of β-$Mo_2N_{0.78}$ and doped β-$Mo_2N_{0.78}$ under H_2/Ar as a function of increasing temperature.

3.2.5.3 XRD Patterns.

Figures 3.2-10 to 3.2-13 confirm that the nitride formed is consistent with the β-$Mo_2N_{0.78}$ phase reported in the literature. These figures also highlight that small amounts of Mo metal is observed as an impurity in the pre-reaction materials, which is again consistent with previous studies.[44,168] After reaction in the H_2/N_2 mixture, it is evident that there are some shifts present in the post-reaction diffraction pattern with respect to that determined

pre-reaction. This accords with the reduced N content of the post-reaction as reported in Table 3.2-13. On the other hand in a H_2/Ar environment under the temperature programming regime employed, the nitride is completely reduced to the Mo metal in all cases. In all doped systems there are no reflections present corresponding to metal dopants.
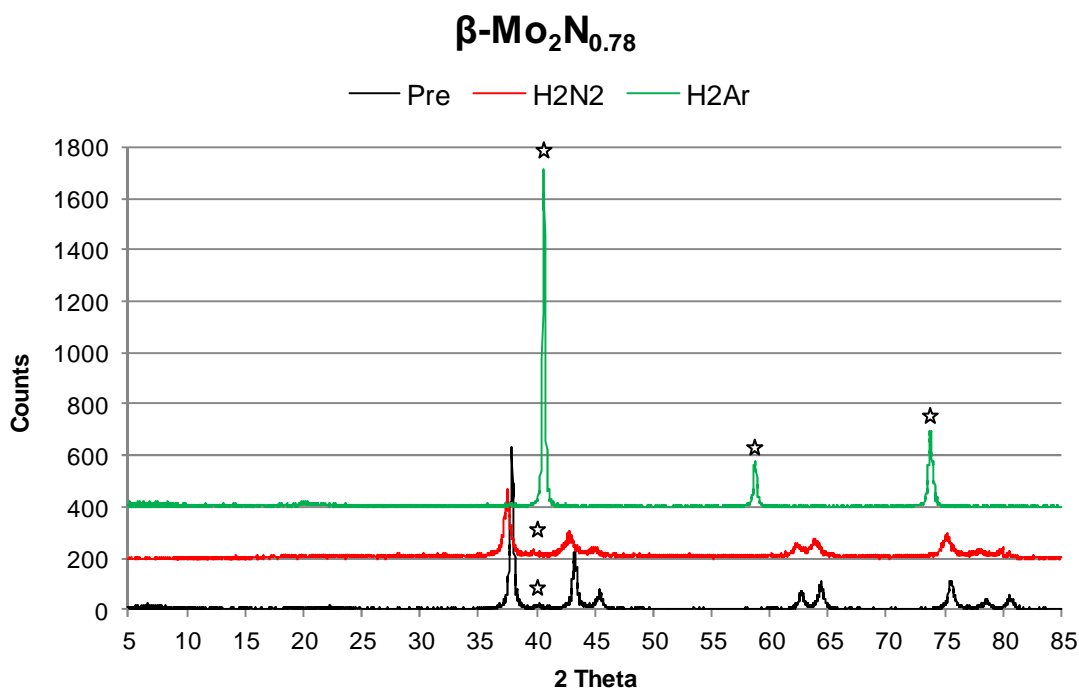
Figure 3.2-10 Pre- and post-reaction XRD patterns of β-Mo$_2$N$_{0.78}$ under H$_2$/N$_2$ and H$_2$/Ar gas mixtures. (JCPDS 023-1256 β-Mo$_2$N$_{0.78}$). Mo metal (☆)
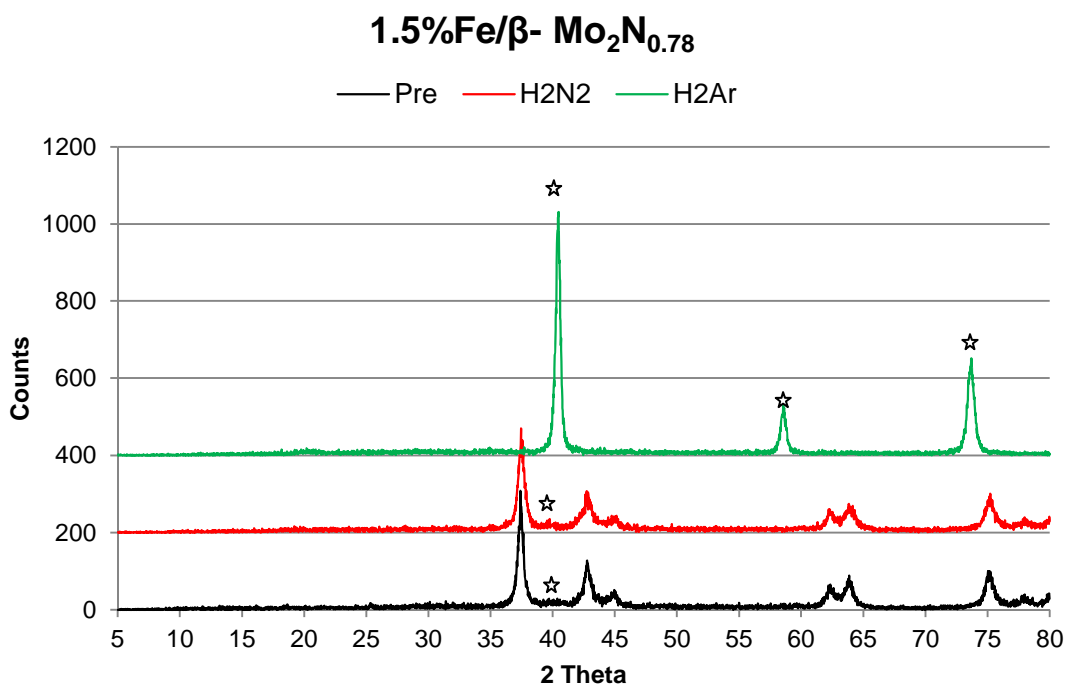
Figure 3.2-11 Pre- and post-reaction XRD patterns of 1.5%Fe/β-Mo$_2$N$_{0.78}$ under H$_2$/N$_2$ and H$_2$/Ar gas mixtures. (JCPDS 023-1256 β-Mo$_2$N$_{0.78}$). Mo metal (☆)
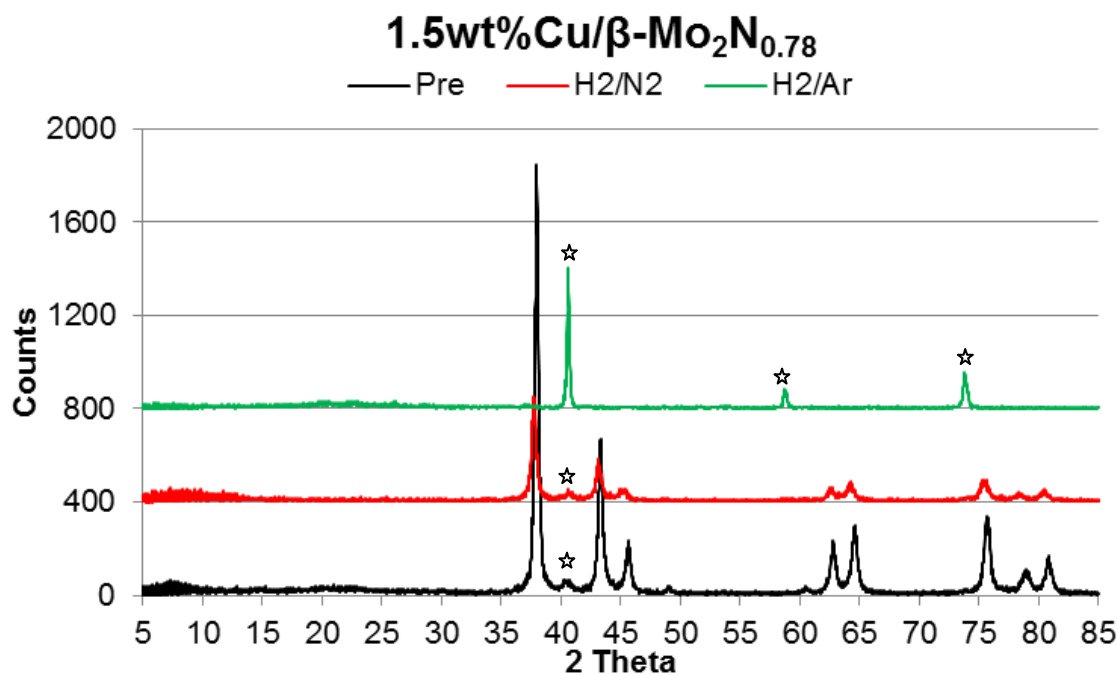
Figure 3.2-12 Pre- and post-reaction XRD patterns of 1.5%Cu/β-Mo$_2$N$_{0.78}$ under H$_2$/N$_2$ and H$_2$/Ar gas mixtures. (JCPDS 023-1256 β-Mo$_2$N$_{0.78}$). Mo metal (☆)
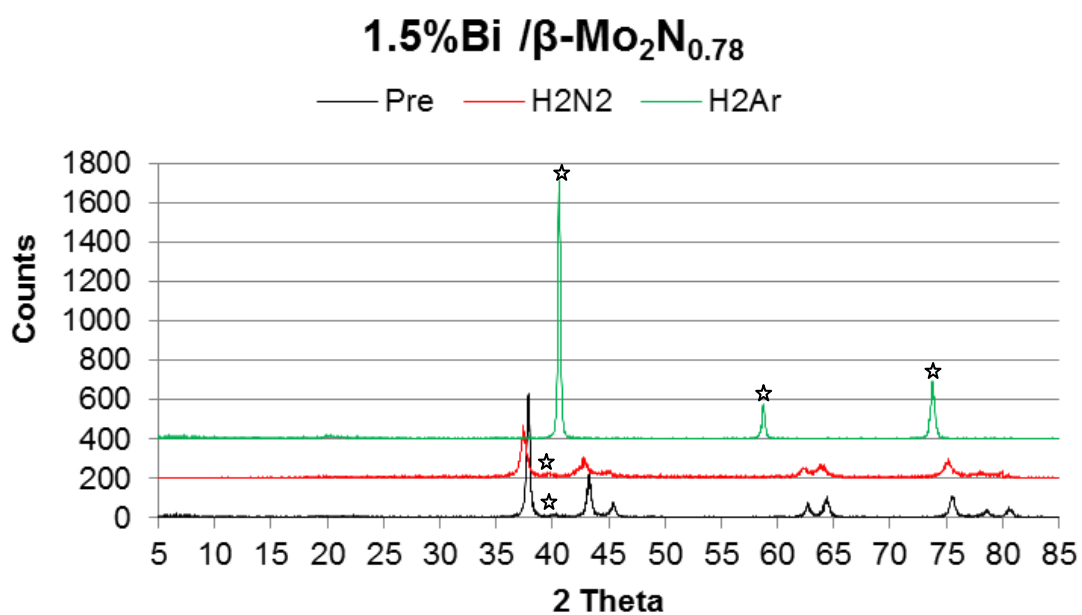
Figure 3.2-13 Pre- and post-reaction XRD patterns of 1.5%Bi/β-Mo$_2$N$_{0.78}$ under H$_2$/N$_2$ and H$_2$/Ar gas mixtures. (JCPDS 023-1256 β-Mo$_2$N$_{0.78}$). Mo metal (☆)

3.2.6 Ta$_3$N$_5$.

Tantalum nitride and tantalum oxynitride have attracted considerable attention recently, with many studies focusing on their activity for visible light induced photocatalytic splitting of water to produce H$_2$.[180-182]   Although there is a limited amount of literature

available on Ta_3N_5 regarding ammonia synthesis, there are reports of tantalum oxides being utilized for these types of reactions. Studies by Antonelli and co-workers have investigated tantalum oxide based catalysts for ammonia synthesis reactions.[183,184] In one particular study, it was found that by doping tantalum oxide with ruthenium, ammonia could be synthesised from a 3:1 H_2/N_2 gas mixture, with initial activity rates comparable to more traditional catalysts. However it was found that the activation energy for cleavage of the N_2 bond was much lower for these materials being only 10% of previously reported activation energies with using standard catalysts. It was suggested that reduced tantalum metal played a significant role in splitting dinitrogen, in which a lower activation energy threshold was recorded for the cleavage of N_2 on the Ru/Ta oxide surface. This was not observed for the other supports which were investigated (MgO and Al_2O_3). Tantalum systems have also been found to be catalytically active for ammonia decomposition reactions.[185] Ta_3N_5 can exist in a variety of sub-stoichiometric forms and like TiN, subject to the nitrogen content, a series of different colours can be observed.[109] These range from brown/black through to orange/red. Stoichiometric tantalum nitride (Ta_3N_5) is bright red when formed and this is often a good visual indication of phase purity.

3.2.6.1 Reaction Data.

Figure 3.2-14 illustrates the conductivity versus time plot for Ta_3N_5 using H_2/N_2 and H_2/Ar. As can be observed from the plot, the ammonia production activities are significantly different.

Figure 3.2-14 reports the rate of ammonia production for Ta_3N_5 under H_2/N_2 at 400 ^{o}C. In the comparable reaction, using H_2/Ar, there is a relatively sharp initial decrease in the conductivity of the H_2SO_4 solution. This would suggest that within the first hour on stream there is ammonia produced. This production quickly diminishes, with only a small amount of ammonia being produced subsequently. The ammonia production rates for Ta_3N_5 during various time intervals on stream are given in Table 3.2-14.

Ammonia synthesis Ta$_3$N$_5$
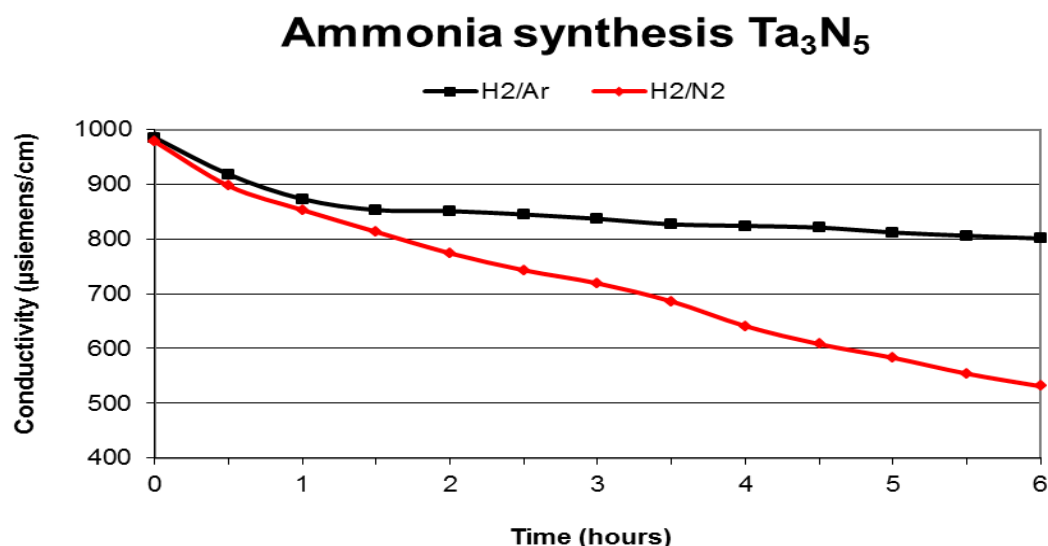
Figure 3.2-14 Comparison of conductivity for Ta$_3$N$_5$ ammonia production using H$_2$/N$_2$ vs. H$_2$/Ar at 400 ^{o}C.

Sample and Reaction Conditions	NH$_3$ Production Rate (μmol h^{-1} g^{-1})
Ta$_3$N$_5$ 400 ^{o}C (H$_2$/N$_2$, 0.0-0.5 h)	366
Ta$_3$N$_5$, 400 ^{o}C (H$_2$/N$_2$, 1.0-6 h)	239
Ta$_3$N$_5$, 400 ^{o}C (H$_2$/Ar, 0.0-0.5 h)	315
Ta$_3$N$_5$, 400 ^{o}C (H$_2$/Ar, 1.0-6 h)	35

Table 3.2-14 Ammonia production rates of Ta$_3$N$_5$ under both H$_2$/Ar and H$_2$/N$_2$ at 400 ^{o}C.

Further studies were conducted to assess the reactivity of the lattice nitrogen with H$_2$/Ar as a function of temperature and again it was found that upon increasing the temperature by 100 ^{o}C increments (to a maximum of 700 ^{o}C) ammonia production occurred in steps associated with the temperature increases. The ammonia production rates are presented in Table 3.2-15.

Compared to all other systems investigated in this study, the production of ammonia under H$_2$/Ar is significant. However, there is a small degree of variability in the 0.0-0.5 h rates of the two H$_2$/Ar reaction runs (400 ^{o}C isothermal and temperature programmed). This may possibly arise from different concentrations of surface NH$_x$ introduced during the H$_2$/N$_2$ pre-treatment procedure. Accordingly, in terms of the relatively high ammonia production rates in the absence of N$_2$, it was especially of interest to determine the reactivity of surface NH$_x$ versus lattice N species in this system.

Reaction Temperature and Time	NH$_3$ Production Rate (μmol h^{-1} g^{-1})
400 ^{o}C (0-0.5 h)	300
400 ^{o}C (1.0-4.5 h)	37
500 ^{o}C (4.5-5.0 h)	188
500 ^{o}C (5.0-6.0 h)	4
600 ^{o}C (6.0-7.5h)	154
700 ^{o}C (7.5-9.0h)	87

Table 3.2-15 Ammonia production activity over Ta$_3$N$_5$ under H$_2$/Ar with increasing temperature.

Additional experiments were preformed to investigate the effect of temperature on the lattice nitrogen in an inert atmosphere and the extent to which hydrogen influenced the ammonia synthesis. Figure 3.2-15 illustrates a study in which Ar (60 ml min^{-1}) is initially passed over the material and the temperature raised up to 700 ^{o}C using the same temperature profile which has been previously applied in standard lattice nitrogen studies. After this pre-treatment, the sample was cooled to 400 ^{o}C and the reaction gas was subsequently switched to the H$_2$/Ar mix and the previous temperature profile was applied. Surface NH$_x$ decomposition should occur under the Ar only pretreatment procedure, and thus subsequent NH$_3$ production with H$_2$/Ar gives an indication of the behaviour of lattice N species.
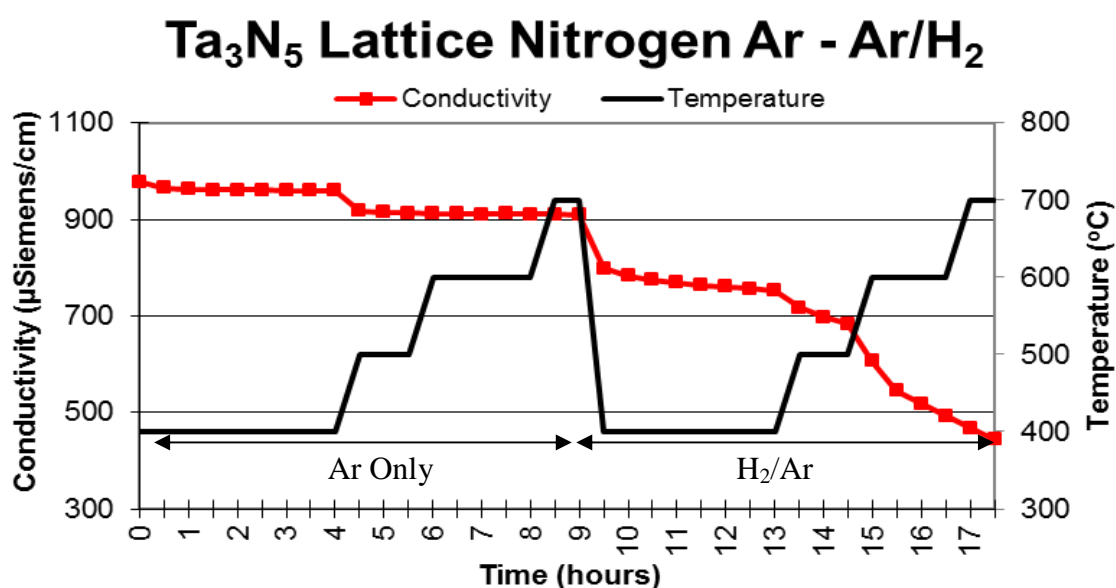
Figure 3.2-15 Conductivity vs. Time plot for Ta$_3$N$_5$ studying effects of temperature and H$_2$ on lattice nitrogen removal. Feed gas switched from Ar to H$_2$/Ar at 9 h on stream.

Figure 3.2-15 details an experiment in which temperature programmed Ar pre-treatment was applied prior to cooling the sample and subsequently switching the feed to H$_2$/Ar and

repeating the temperature programmed regime. Whilst it is clear that a degree of NH_3 production is evident in the case of Ar feed, the presence of H_2 results in a much more significant loss. This indicates the high degree of lattice nitrogen reacting in this sample.

3.2.6.2 Nitrogen Analysis.

The pre- and post-reaction nitrogen contents of Ta_3N_5 are presented in Table 3.2-16, along with the stoichiometric nitrogen content value. In the case of H_2/Ar studies it is interesting to note that although a substantial amount of nitrogen is lost (almost 33 % at 700 ^{o}C) only 20 % of the total nitrogen lost contributes to the formation of ammonia. In the H_2/N_2 and Ar only studies, there is only a relatively small change between the nitrogen content of the post-reaction samples compared to those of the pre-reaction samples. This may suggest that only loosely bound NH_x species are removed from the surface of the material and, in the case of Ar only treatment, relatively small loss of nitrogen is in good correlation with the conductivity versus time plot, where there is only a small apparent change in the conductivity values.

Sample and Reaction Conditions	Calculated Stoichiometric N content (wt.%)	Pre-Reaction (wt.%)	Post-Reaction (wt.%)	Calculated Post-reaction Stoichiometry
Ta_3N_5 (H_2/N_2, 400 ^{o}C)	11.42	11.23	10.60	$Ta_3N_{4.64}$
Ta_3N_5 (H_2/Ar, 400 ^{o}C)	11.42	11.23	7.98	$Ta_3N_{3.49}$
Ta_3N_5 (H_2/Ar, 700 ^{o}C)	11.42	11.23	7.83	$Ta_3N_{3.43}$
Ta_3N_5 (Ar -H_2/Ar, 700 ^{o}C)	11.42	11.23	7.65	$Ta_3N_{3.35}$
Ta_3N_5 (Ar, 700 ^{o}C)	11.42	11.23	10.73	$Ta_3N_{4.70}$

Table 3.2-16 Nitrogen content of Ta_3N_5 samples pre- and post-reaction.

Figure 3.2-16 (a-d) shows the different colours observed for the post-reaction tantalum nitride samples.
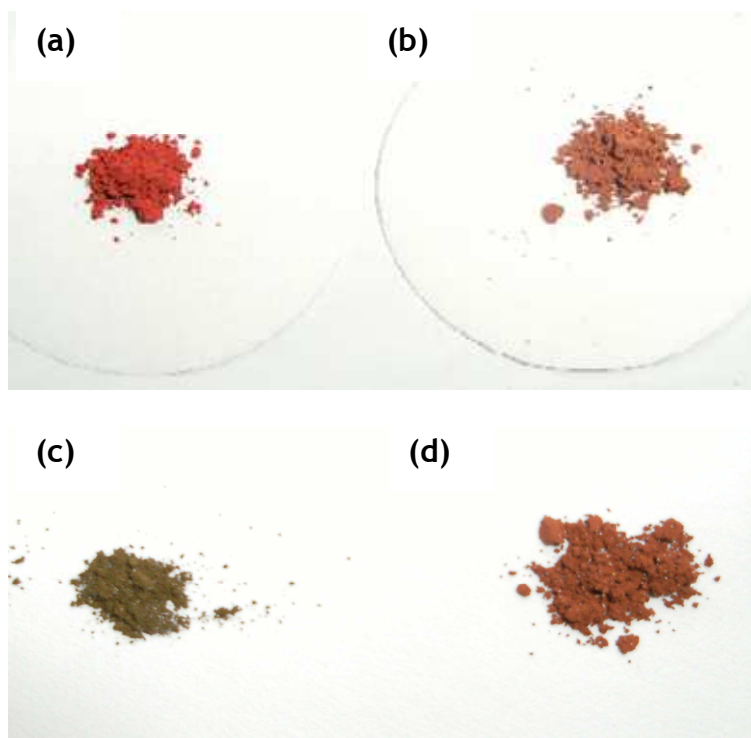
Figure 3.2-16 Post- reaction tantalum nitride samples (a) H_2/N_2 400 ^{o}C (b) Ar 700 ^{o}C (c) H_2/Ar 700 ^{o}C (d) H_2/Ar 400 ^{o}C.

3.2.6.3 XRD Patterns.

Since Ta_3N_5 is bright red and the sample colour is related to stoichiometry, visual inspection provides a good indicator of phase purity. Samples which are brown or orange in colour usually consist of an amorphous material or contain traces of TaON. It was also found that as heating times were increased during ammonolysis, the nitrogen content in the material decreased giving rise to orange or burnt red products. It was shown that the optimum heating time and temperature was 900 ^{o}C for 9 hours, in relation to achieving the desired Ta_3N_5 stoichiometry, although Henderson *et al* have quoted that much longer heating times should be applied.[109]

As can be seen from Figure 3.2-16, the colours of the H_2/Ar post-reaction samples were either burnt orange, in the sample treated at 400 ^{o}C, or green/black when treated to 700 ^{o}C. Although the green/black colour has not been reported in the literature, it would appear that a phase change may have occurred. However, upon inspection of the XRD patterns, it is apparent that the phase remains unchanged, although slight alterations in reflection widths can be observed. Nonetheless the XRD pattern is in accordance with previously reported literature [109] and the phase is confirmed as Ta_3N_5 matching to JCPDS file 019-1291.   In the case of the post- H_2/Ar treated sample it is apparent that there is an increase

in the intensity of the background which is consistent with a greater content of amorphous phase, possibly arising from the loss of N observed.
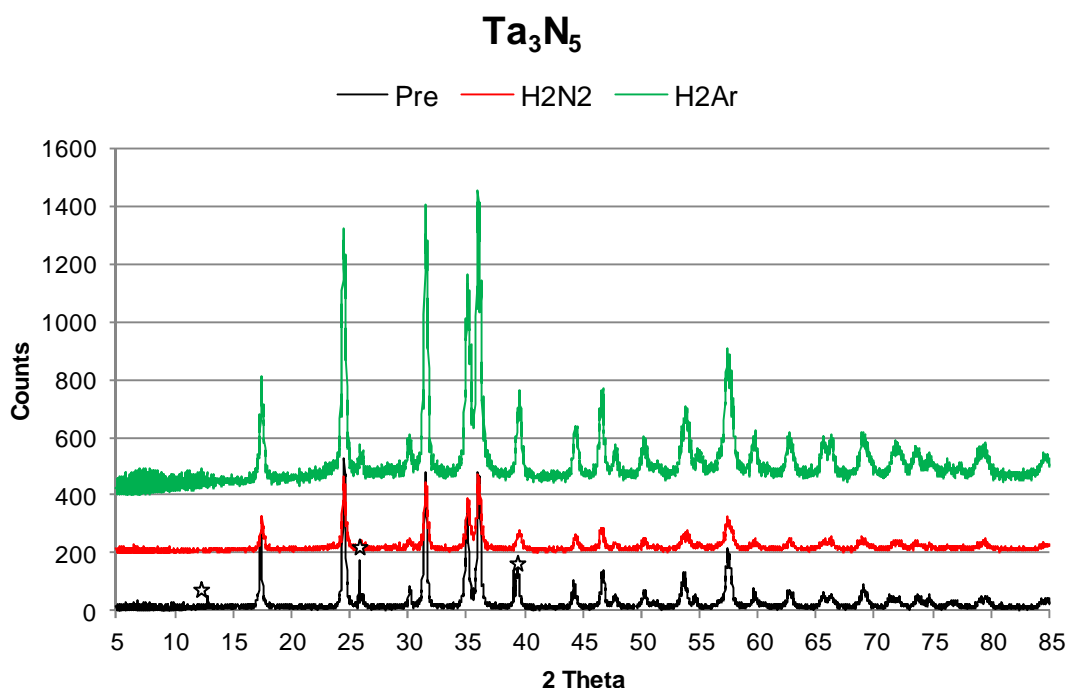
Figure 3.2-17 Pre and Post-reaction XRD patterns of Ta$_3$N$_5$ (JCPDS 019-1291) Small reflections that are indicated by (☆) correspond to TaN.

3.2.7 W$_2$N

The first reports of catalytic activity over tungsten carbide were by Böhm and co-workers[186] which subsequently led on to further studies using tungsten carbide as a catalyst for the isomerization reaction of neo-pentane to isopentane.[10] This reaction had only previously been known to occur in the presence of a platinum or iridium catalyst and led to notion that tungsten carbides may in fact behave like platinum group metals.[9] Since then, resulting primarily from subsequent studies by Volpe and Boudart, on the preparation of high surface area materials, and the perceived similarity in behaviour of carbides and nitrides, tungsten nitrides have been a focus of attention. There is a range of literature concerning tungsten nitride, which describes preparation techniques and the mechanical and structural properties of the material. Tungsten nitride is known to exist in two main forms: W$_2$N, which has a cubic structure, and WN which has a hexagonal structure.[186] Both phases are difficult to form, and W does not react readily with N$_2$ directly. However W$_2$N is perhaps more difficult to prepare in pure phase, with W metal often appearing as an impurity.[187] Despite this, tungsten nitrides have been explored for a wide range of catalytic applications including ethanol amination,[18] NO reduction,[17,189] isomerisation

reactions[19] and hydrotreating.[11,190,191] Like molybdenum nitride, tungsten nitride is also known to be one of the more active nitrides for ammonia synthesis.[198] There is currently little evidence to suggest that tungsten nitrides have been utilized in a nitrogen transfer type reaction, despite the fact that it is a good ammonia synthesis catalyst. Studies by Knor have investigated the effect of Pd doped tungsten on nitrogen dissociation.[193] In that work, it was proposed that Pd would prevent the strong binding between tungsten and nitrogen and thus make it possible to react the surface nitrogen species more easily at room temperature.

3.2.7.1 Reaction Data.

As stated above, tungsten nitride is documented for its ammonia synthesis capabilities. Ammonia synthesis under essentially steady state conditions was apparent under H_2/N_2 at 400 ^{o}C as shown in Figure 3.2-18. Under a H_2/Ar feed gas, as expected, there was an initial decrease in the conductivity of which was short lived and after 90 minutes little or no ammonia is observed. Figure 3.2-18 compares the activity of W_2N under both feed streams, whilst the corresponding ammonia production rates are presented in Table 3.2-17.
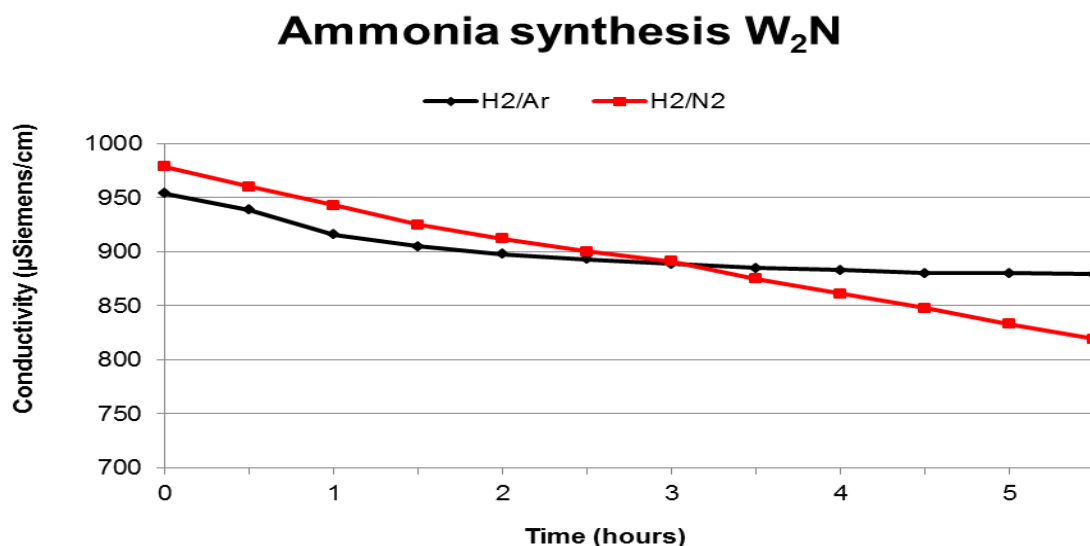
Figure 3.2-18 Comparison of conductivity for WN ammonia production using H_2/N_2 vs. H_2/Ar at 400 ^{o}C.

Sample and Reaction Conditions	NH$_3$ Production Rate (μmol h^{-1} g^{-1})
W$_2$N, 400 ^{o}C (H$_2$/N$_2$, 0.0-0.5 h)	84
W$_2$N 400 ^{o}C (H$_2$/N$_2$, 1.0-6.0 h)	60
W$_2$N, 400 ^{o}C (H$_2$/Ar, 0.0-0.5 h)	66
W$_2$N, 400 ^{o}C (H$_2$/Ar, 1.0-6.0 h)	12

Table 3.2-17 Ammonia production rates of W$_2$N under both H$_2$/Ar and H$_2$/N$_2$ at 400 ^{o}C.

Further experiments were conducted to remove nitrogen from within the lattice as a function of temperature, under H$_2$/Ar. The results are presented in Table 3.2-18. It is apparent that the rate of ammonia production decreases as the reaction proceeds, although there is a further burst of ammonia produced after a temperature increase to 600°C, before ammonia production ceases completely. It may be possible that this additional burst of ammonia is a result of more strongly absorbed surrface NH$_x$ species desorping from the material.

Reaction Temperature and Time	NH$_3$ Production Rate (μmol h^{-1} g^{-1})
400 ^{o}C (0.0-0.5 h)	66
400 ^{o}C (1.0-4.5 h)	24
500 ^{o}C (4.5-5.0 h)	35
500 ^{o}C (5.0-6.0 h)	18
600 ^{o}C (6.0-7.5 h)	74
700 ^{o}C (7.5-9.0 h)	2

Table 3.2-18 Ammonia production activity over W$_2$N as a function of increasing temperature under H$_2$/Ar.

3.2.7.2   XRD Patterns.

As discussed earlier, tungsten nitride can occur as cubic W$_2$N or as hexagonal WN phases. The samples prepared in this study corresponded to cubic W$_2$N. Again under H$_2$/N$_2$ no shift was observed in the post-reaction sample's XRD pattern. However, under H$_2$/Ar, tungsten nitride undergoes a partial decomposition with W metal reflections, as indicated by a star in Figure 3.2-19, being evident. This is somewhat expected due to the similar

nature of tungsten and molybdenum nitrides, where complete reduction of β-$Mo_2N_{0.78}$ to Mo was observed. The observed reflections are particularly broad which would be indicative of materials with high surface area and very small particle size and/or disorder.
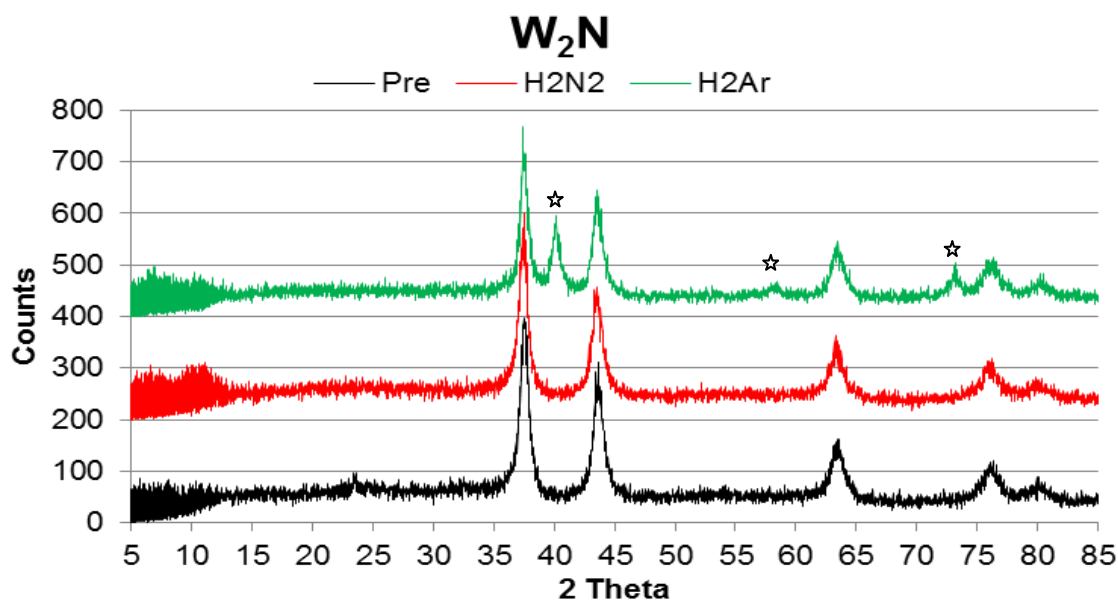
Figure 3.2-19 Pre and Post-reaction XRD patterns of W_2N (JCPDS 025-1257 W_2N) W metal reflections are indicated by (☆)

3.2.7.3   Nitrogen Analysis.

The N content in the pre-reaction sample is almost double that of the calculated stoichiometric value, and would suggest that perhaps WN (7.07 wt.% N) is formed instead of W_2N. However, the XRD reflections correspond to those of W_2N. Another explanation for the high nitrogen content may be that a large amount of loosely bound NH_x species is present on the surface of the material. It is evident that there is a loss of nitrogen from the material after reaction and it is also evident that there is less nitrogen in the samples treated with H_2/Ar than those exposed to H_2/N_2. If the excess nitrogen content is a result of surface bound NH_x, reactions could be undertaken with longer times on stream to enhance depletion. Furthermore, the similarity between the N content values between the isothermally reacted and temperature programmed samples under H_2/Ar suggest that the influence of higher temperature reduction is minimal. In addition, the occurrence of W metal in the post-reaction XRD pattern indicates that loss of lattice N does occur to some extent. Comparison of the production of NH_3 with the loss of nitrogen indicates that only 7 % of the total lost nitrogen, as determined by CHN analysis, results in the formation of ammonia.

Sample and Reaction Conditions	Calculated Stoichiometric N content (wt.%)	Pre-Reaction N Content (wt.%)	Post-Reaction N Content (wt.%)
W_2N (H_2/N_2) after 6 h at 400 ^{o}C	3.66	6.13	5.62
W_2N (H_2/Ar) after 6 h at 400 ^{o}C	3.66	6.13	4.24
W_2N (H_2/Ar) using temperature profile as shown in Fig. 3.2-2	3.66	6.13	4.18

Table 3.2-19 Nitrogen content of W_2N samples pre- and post-reaction.

3.2.8 Summary of Early Transition Metal Nitrides.

Tables 3.2-20 and 3.2-21 give a summary of the nitrides investigated so far in this chapter. Ammonia production rates under selected conditions are presented in Table 3.2-20 whilst Table 3.2-21 presents the nitrogen content pre- and post-reaction of each material as well as the surface areas of the pre-reaction material. Caution must be exercised in the latter respect since materials may be air sensitive and so the areas measured may not correspond to those exhibited *in-situ*

3.2.8.1 Summary of Ammonia Production Rates.

It is apparent from Table 3.2-20 that the ammonia production rates during the initial 30 minutes on stream, for samples treated under both H_2/N_2 and H_2/Ar, are higher than those observed between 1-6 hours on stream. As previously discussed this initial high ammonia production rate may be attributed to the removal of loosely bound surface NH_x species. In the case of TiN and CrN it was observed that after the intial 30 minutes on stream that very little or no ammonia was produced with further heat treatment, indicating that these materials do not lose nitrogen from the metal lattice at temperatures at or below 400°C and may therefore be unsuitable for the envisaged process. It is also evident that Ta_3N_5 has a much higher ammonia production rate under H_2/N_2 reaction conditions, when compared to the other materials investigated in this section. Most of the materials investigated in this section, with the exception of TiN and CrN, exhibit almost steady state ammonia synthesis conditions under H_2/N_2 at 400°C, the target temperature for the target process, and will be investigated further in subsequent chapters.

Material	NH$_3$ Production Rate (μmol h^{-1} g^{-1})		
	H$_2$/N$_2$, 400 °C 1-6 h	H$_2$/N$_2$, 400 °C, 0.5 h	H$_2$/Ar, 400 °C, 0.5 h
TiN	-	152	183
VN	40	98	85
CrN	-	86	36
β-Mo$_2$N$_{0.78}$	66	222	224
Fe/ β-Mo$_2$N$_{0.78}$	69	242	122
Cu/ β-Mo$_2$N$_{0.78}$	58	214	107
Bi/ β-Mo$_2$N$_{0.78}$	50	59	78
Ta$_3$N$_5$	239	366	315
W$_2$N	60	84	66

Table 3.2-20 Summary of NH$_3$ production rates for the early transition metal nitride materials.

3.2.8.2 Summary Pre/Post-Reaction N Data and Surface Areas

Material	BET Surface Area (m^{2}g^{-1})	Nitrogen Content (wt.%)			
		Calculated Stoichiometric	Pre-reaction	Post-reaction (H$_2$/Ar) 700°C	Post-Reaction (H$_2$/N$_2$) 400°C
TiN	116	22.63	19.74	18.45	18.66
VN	39	21.55	18.39	14.06	14.88
CrN	53	21.21	15.40	5.60	6.57
β-Mo$_2$N$_{0.78}$	8	5.38	5.58	0	3.83
Fe/ β-Mo$_2$N$_{0.78}$	10	5.38	5.31	0	5.26
Cu/ β-Mo$_2$N$_{0.78}$	5	5.38	4.39	0	3.14
Bi/ β-Mo$_2$N$_{0.78}$	4	5.38	4.66	0	4.17
Ta$_3$N$_5$	8	11.42	11.23	7.83	8.40
W$_2$N	76	3.66	6.13	4.18	5.62

Table 3.2-21 Summary of pre- and post-reaction nitrogen content, and surface area of pre reaction samples for the early transition metal nitride materials.

3.3 Later Transition Metal Nitrides

3.3.1 Introduction to Later Transition Metals.

When compared to the nitrides of early transition metals, nitrides of Groups VII –X have been far less well studied. This may possibly be attributed to the fact that these nitrides have very poor thermal stability and mostly decompose to the corresponding metal at relatively low temperatures. For this reason, the later transition metal nitrides have found limited application.

It is perhaps only within the last two decades that there has been a resurgent interest in these materials due to their potential application in the microelectronics industry and also for use in optical and magnetic storage devices. As these materials are becoming more extensively studied in terms of their structural and electronic properties, an increase in the catalytic literature is becoming available. For example only recently it was documented that cobalt nitrides have been found to be catalytically active for CO oxidation and NO decomposition reactions.[72,194]

On the other hand some nitrides investigated in this section, such as Fe_2N, Re_3N, have long been recognised for their catalytic activity. These materials have been documented to be active for dehydrogenation reactions[195] ammonia decomposition,[196] ammonia synthesis [197] and CO hydrogenation.[198, 199]

3.3.2 Fe_2N.

Iron has been well documented as an ammonia synthesis catalyst, with initial reports reporting ammonia formation over iron at atmospheric pressure.[200,201] This was confirmed in the work of Haber. Further work by Mittasch led to the discovery of a doubly promoted iron catalyst, which was significantly more active and this was subsequently put into commercial operation for ammonia synthesis, where it remains the catalyst of choice. One of the key ideas behind the development of the iron catalyst was the formation of a metastable iron nitride intermediate.[202,203]

The iron-nitrogen system has received considerable attention not only for catalytic purposes but also for magnetic storage devices and for use within the coating industry.[204-209] Binary iron nitrides are classified as interstitial compounds and a wide range of

different phases are known, with the first phase diagram of iron nitrides being documented by Goodeve and Jack, as presented in Figure 3.3-1:[102,103]
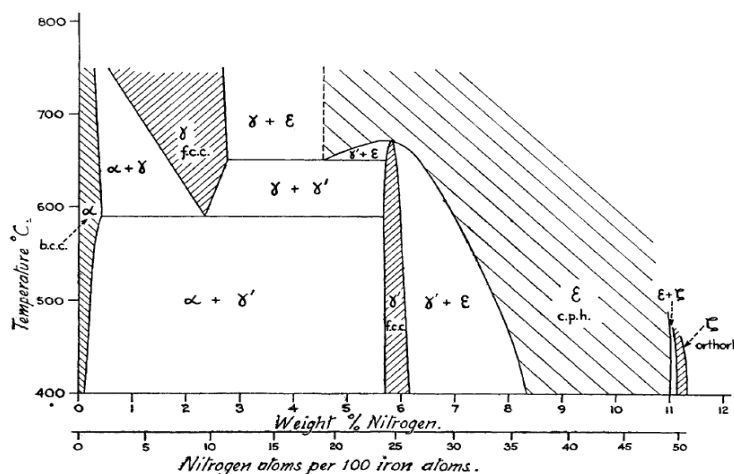
Figure 3.3-1 Iron nitride phase diagram.[103]

Goodeve and Jack also investigated the evolution of nitrogen from iron nitrides in order to determine their structure. In this investigation, it was demonstrated that iron nitrides undergo phase transitions upon increasing temperature and decompose from Fe_2N or Fe_3N into lower phases such as Fe_4N, as N_2 is eliminated from the metal lattice. Despite the phase transformation associated with the loss of nitrogen, it was found that the relative positions of the Fe atoms in the crystal lattice remain unchanged although distortion occurs due to the rearrangement of the nitrogen atoms. In addition, it was reported that between 250 ^{o}C and 450 ^{o}C, ammonia was evolved from the decomposition of the iron nitride under hydrogen, which is of obvious relevance to the current study.

Iron nitrides appear to be promising candidates for nitrogen transfer reactions, due to the fact the nitrogen is evolved from the metal lattice at the temperatures of interest. Furthermore the nitride can be prepared directly from the Fe metal and it would therefore be possible to renitride reduced phases.

3.3.2.1 Reaction Data.

As previously mentioned, Fe based catalysts are currently used in commercial ammonia synthesis. It was therefore expected that the Fe_2N prepared in this study would exhibit production of ammonia as was observed under H_2/N_2 and H_2/Ar and shown in Figure 3.3-2.

From Figure 3.3-2 it is evident that the reaction profile for Fe_2N follows a similar trend to that which was previously observed in some of the early transition metal nitrides as discussed in section 3.2. Under both reaction gases, there is a sharp initial decrease in conductivity, indicating the formation of ammonia due to loosely bound surface NH_x species, which occurs for the first hour on stream. This subsequently tails off in the case of H_2/Ar. The ammonia production rates for Fe_2N at 400 °C for the reactions under H_2/Ar and H_2/N_2 are presented in Table 3.3-1.
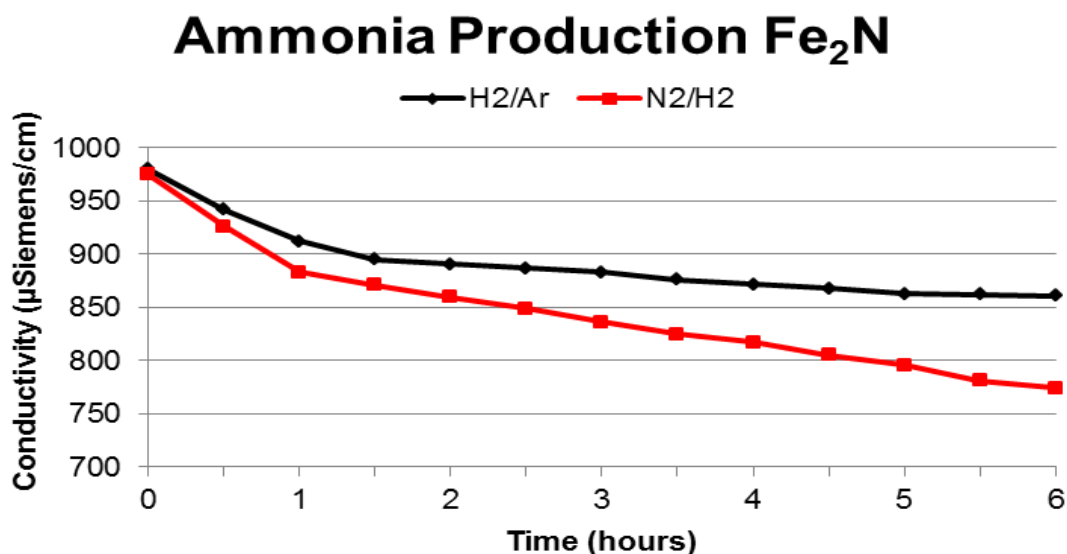
Figure 3.3-2 Comparison of conductivity for Fe₂N ammonia production using H₂/N₂ vs. H₂/Ar at 400 °C.

Sample and Reaction Conditions	NH_3 Production Rate (μmol h^{-1} g^{-1})
Fe_2N, 400 °C (H_2/N_2, 0.0-0.5 h)	213
Fe_2N 400 °C (H_2/N_2, 1.0-6.0 h)	47
Fe_2N, 400 °C (H_2/Ar, 0.0-0.5 h)	170
Fe_2N, 400 °C (H_2/Ar, 1.0-6.0h)	17

Table 3.3-1 Ammonia production rates of Fe₂N under both H₂/Ar and H₂/N₂ at 400 °C.

Table 3.3-1 shows the rates which were attained for the production of ammonia under H_2/Ar using the temperature profile in Figure 3.2-2. It is apparent that the rate of ammonia production decreases as the reaction proceeds.

Reaction Temperature and Time	NH$_3$ Production Rate (μmol h^{-1} g^{-1})
400 ^{o}C (0.0-0.5h)	170
400 ^{o}C (1.0-4.5 h)	77
500 ^{o}C (4.5-5.0 h)	67
500 ^{o}C (5.0-6.0 h)	13
600 ^{o}C (6.0-7.5 h)	15
700 ^{o}C (7.5-9.0 h)	7

Table 3.3-2 Ammonia production activity over Fe$_2$N with increasing temperature under H$_2$/Ar.

3.3.2.2 Nitrogen Analysis.

Inspection of the data presented in Table 3.3-3 highlights that more than half of the nitrogen is removed from the sample in the case of the H$_2$/N$_2$ reaction and almost two thirds in the case of H$_2$/Ar at 400 ^{o}C and at higher temperature. It is interesting to note that at increased temperatures (maximum of 700 ^{o}C) under H$_2$/Ar that the nitride has not fully been reduced to Fe metal (as shown later). Table 3.3-3 also shows that the nitride is not stoichiometric to Fe$_2$N and has a lower than expected nitrogen content. In fact, the initial N content is has a closer nitrogen content to that expected for Fe$_3$N which would contain 7.71 wt.%. However the powder XRD analysis suggested that Fe$_2$N was formed, Figure 3.3-3.

Sample and Reaction Conditions	Calculated Stoichiometric N content (wt.%)	Pre-Reaction N Content (wt.%)	Post-Reaction N Content (wt.%)
Fe$_2$N (H$_2$/N$_2$) after 6 h at 400 ^{o}C	11.13	8.65	3.57
Fe$_2$N (H$_2$/Ar) after 6 h at 400 ^{o}C	11.13	8.65	2.43
Fe$_2$N (H$_2$/Ar) using temperature profile as shown in Fig. 3.2-2	11.13	8.59	2.40

Table 3.3-3 Nitrogen content of Fe$_2$N samples pre- and post-reaction.

3.3.2.3 XRD Patterns.

The reflections present in the pre-reaction sample in Figure 3.3.2-2 are indicative of those of cubic Fe$_2$N, with the (100) reflection at 43° 2θ, being the most prominent. Small reflections that correspond to Fe$_3$N phase can also be observed in the pre-reaction sample and are indicated by blue diamonds. Numerous attempts were made to achieve a pure phase material, following methods described by Goodeve and Jack. However this proved

extremely difficult with resulting samples displaying additional phases, namely Fe_3N, Fe_4N and Fe metal impurities. These samples were prepared at 350, 400 and 450 ^{o}C over a range of dwell periods; the samples used in this study were prepared at 500 ^{o}C for 6 hours.

The XRD patterns of the post-reaction samples demonstrate the different phases which are obtained via the decomposition of the nitride. The post-reaction H_2/N_2 sample contains a mixture of iron nitride phases where Fe_2N has partially decomposed into Fe_3N and a small Fe reflection can be observed at 64° 2θ. In addition to this, a small shift can be observed in the remaining Fe_2N reflections to a lower 2θ value indicative of increasing unit cell volume. The reflections are also slightly broadened which may result from increased disorder.
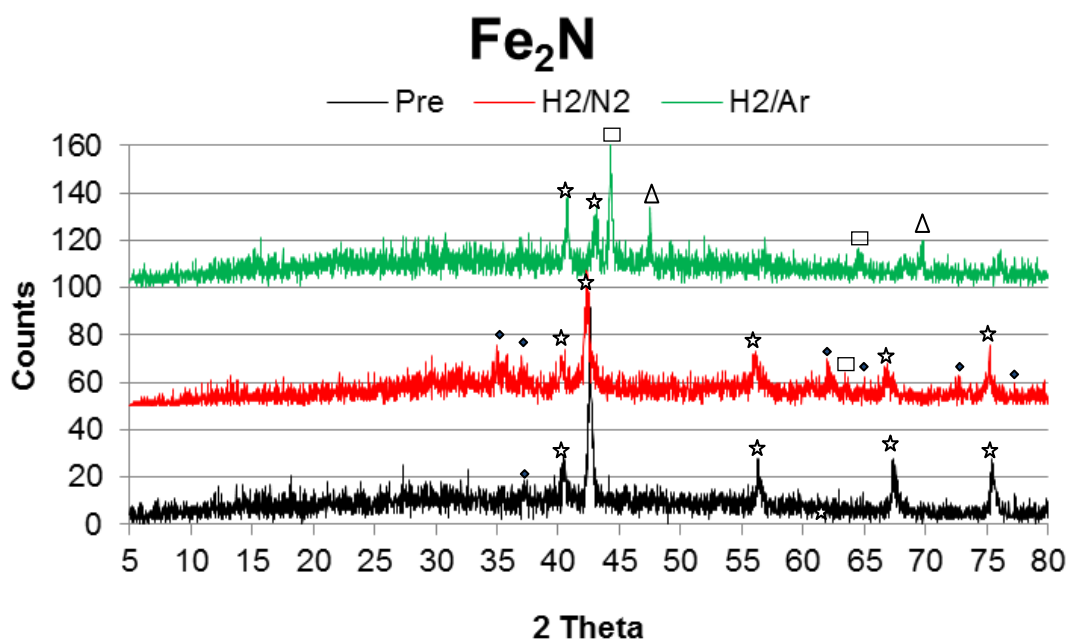
Figure 3.3-3 Pre- and Post-reaction XRD patterns of Fe₂N. (Fe₂N ☆ ,Fe₃N ♦,Fe₄N △,Fe □).

The XRD pattern of the post-reaction H_2/Ar sample indicates that Fe_2N has partially decomposed into a combination of the lower Fe_4N nitride and Fe metal, as indicated in Figure 3.3-3 by triangle and square markers respectively. Overall the changes evident in the post-reaction samples are small in comparison to the significant loss of nitrogen observed for these samples. However, in this context, it is important to note that there are amorphous backgrounds evident in all samples and hence N loss may occur from phases not visible by XRD.

3.3.3 Re$_3$N.

The catalytic properties of rhenium metal and the few rhenium nitride compounds that exist have been the subject of limited studies, and so far no commercial use has been made of the results.   Most of the literature that is available concentrates on the catalytic properties of the metal itself, which to date has been investigated for a variety of different reactions, including dehydrogenation reactions,[195] ammonia decomposition,[196] and ammonia synthesis.[197] Reports of the catalytic activity of rhenium nitride have been more recent, with Clark and co-workers reporting its use for hydroprocessing reactions, where it was found that Re$_3$N appears to be active for hydrodenitrogenation reactions.[73] Additionally, Kojima and Aika have investigated Re$_3$N as an ammonia synthesis catalyst, comparing it with Re metal to determine whether the formation of the nitride is beneficial. In that study it was shown that Re$_3$N is active for ammonia synthesis with initial rates being higher than those previously reported for Mo$_2$N, W$_2$N, VN and NbN.[59]   However it was shown this activity was short lived and that deactivation occurs with time on steam. Despite this deactivation, thought to occur due to decomposition to Re metal, ammonia synthesis rates were higher than those reported for pure Re metal.

3.3.3.1 Reaction Data.

Like the rest of the nitrides discussed in this section, Re$_3$N is unstable and decomposes to the metal at elevated temperatures. Re$_3$N is known to decompose above 370 ^{o}C and for this reason it was necessary to investigate rhenium nitride at a lower reaction temperature. Initially H$_2$/Ar studies were conducted with increasing temperature to establish the temperature at which lattice nitrogen became "active", as illustrated in Figure 3.3-4. From the conductivity shown in Figure 3.3-4, it can be seen that ammonia is produced at 300 ^{o}C before reaching a plateau, as soon as the temperature is increased to 350 ^{o}C and then 400°C there is an increase in the amount of ammonia produced. Ammonia production rates corresponding to the conductivity versus time plot, Figure 3.3-4, are presented in Table 3.3-4.
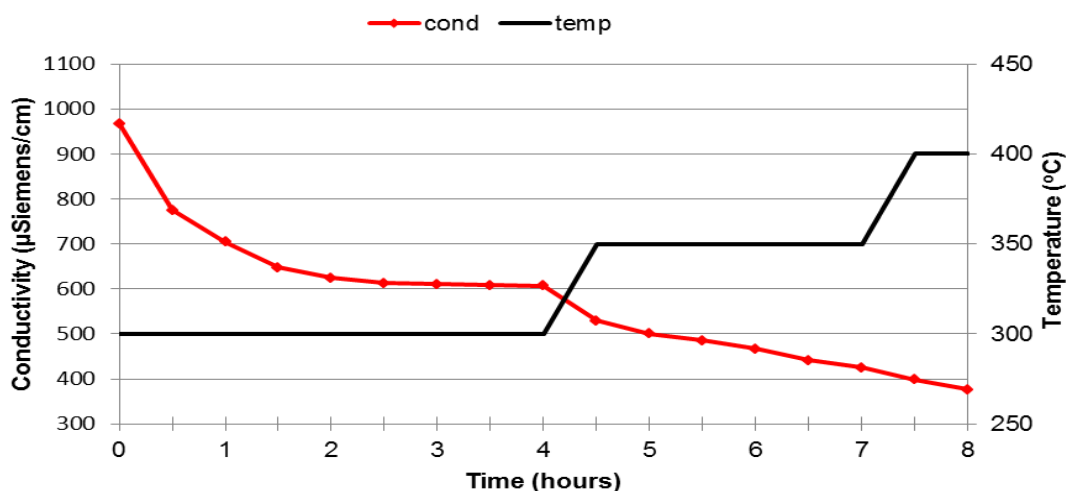
Figure 3.3-4 Conductivity data for NH$_3$ production over Re$_3$N with increasing temperature under H$_2$/Ar.

Reaction Temperature and Time	NH$_3$ Production Rate (μmol h^{-1} g^{-1})
300 $^{\circ}$C (0.0-0.5 h)	930
300 $^{\circ}$C (0.5-2.0 h)	243
300 $^{\circ}$C (2.0-4.0 h)	21
350 $^{\circ}$C (4.0-4.5 h)	371
350 $^{\circ}$C (4.5-7.0 h)	101
400 $^{\circ}$C (7.0-8.0 h)	116

Table 3.3-4 Ammonia production activity of Re$_3$N under H$_2$/Ar with increasing temperature.

On conducting the above study, the standard H$_2$/Ar and H$_2$/N$_2$ reactions were performed at 350 $^{\circ}$C, which is the same temperature used by Aika and Kojima in their investigation of ammonia synthesis. In their study it was found that at 350 $^{\circ}$C Re$_3$N had an initial high activity over the first 30 minutes, and a subsequent deactivation after 2 hours on stream. From the activity plot that is presented in Figure 3.3-5 there is also an initial burst of activity during the first 30 minutes on stream with an ammonia production rate comparable to that reported by Aika and Kojima[59] (initial activity 430 µmol h^{-1} g^{-1} at 350 $^{\circ}$C), Table 3.3-5. However in the case of H$_2$/N$_2$, the conductivity continues to steadily decrease, long after the 2 hours at which deactivation was previously reported. It is also apparent that the rate of ammonia formation is generally lower at 350 $^{\circ}$C as compared to 300 $^{\circ}$C under H$_2$/Ar. This may possibly be due to the fact that NH$_3$ decomposition is more favoured at higher reaction temperature.

Ammonia Production Re$_3$N
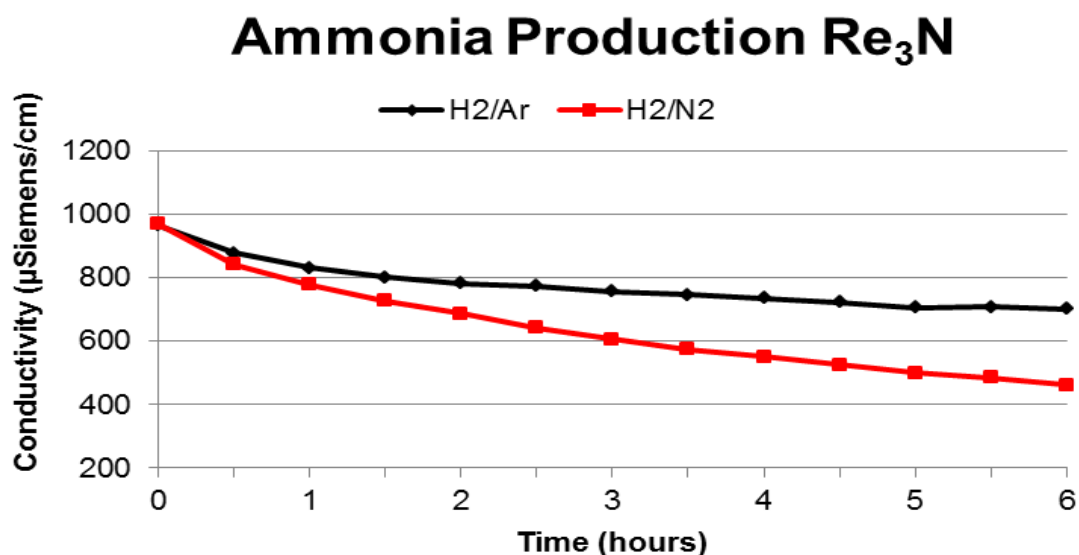
Figure 3.3-5 Comparison of conductivity for Re$_3$N ammonia production using H$_2$/N$_2$ vs. H$_2$/Ar at 350 ^{o}C.

Sample and Reaction Conditions	NH$_3$ Production Rate (μmol h^{-1} g^{-1})
Re$_3$N, 350 ^{o}C (H$_2$/N$_2$, 0.0-0.5 h)	580
Re$_3$N, 350 ^{o}C (H$_2$/N$_2$, 1.0-6.0 h)	133
Re$_3$N, 350 ^{o}C (H$_2$/Ar, 0.0-0.5 h)	419
Re$_3$N, 350 ^{o}C (H$_2$/Ar, 1.0-6.0 h)	53

Table 3.3-5 Ammonia production rates of Re$_3$N under both H$_2$/Ar and H$_2$/N$_2$ at 350 ^{o}C.

3.3.3.2 Nitrogen Analysis.

As can be seen from Table 3.3-6, the pre-reaction samples are in fairly good agreement with the calculated stoichiometric value for Re$_3$N. The slightly elevated values may be a result of residual NH$_x$ species that are adsorbed on the surface during subsequent cooling after ammonolysis of the precursor. Conversely, in both the H$_2$/N$_2$ and H$_2$/Ar reactions conducted at 350 ^{o}C, there is only a small amount of nitrogen remaining in the sample. Likewise there is a loss of nitrogen in the sample that underwent the temperature profile shown in Figure 3.3-4. However this did not appear to become fully reduced, with almost half of the nitrogen remaining in the sample, which may be due to the sample being exposed to temperatures of 350 ^{o}C and above for only 3.5 hours as compared with the 6 hours in the other studies.

Sample and Reaction Conditions	Calculated Stoichiometric N content (wt. %)	Pre-Reaction N Content (wt. %)	Post-Reaction N Content (wt. %)
Re_3N (H_2/N_2) after 6 h at 350 ^{o}C	2.44	2.52	0.47
Re_3N (H_2/Ar) after 6 h at 350 ^{o}C	2.44	2.52	0.32
Re_3N (H_2/Ar) using temperature profile as shown in Fig. 3.3-4	2.44	2.46	1.10

Table 3.3-6 Nitrogen content of Re₃N samples pre- and post-reaction.

3.3.3.3 XRD Patterns.

The "Re_3N" starting material appears to be largely amorphous with a very broad reflection centring upon $40^o \, 2\theta$. This is in accordance with the previously mentioned studies of Aika and Kojima. Under H_2/N_2 at 350 ^{o}C for 6 hours almost total de-nitridation is apparently related to the possible formation of crystalline Re metal, although there are shifts evident, as shown in Figure 3.3-6. The H_2/Ar sample subjected to the temperature programme, partially de-nitrides, as shown by the data, and a mixture of Re reflections (again shifted) and the original broad reflection is evident in the post-reaction XRD pattern which is consistent with this observation. It should be noted that the XRD pattern of the isothermal H_2/Ar reaction is very similar to that of the H_2/N_2 sample which is consistent with its similar post-reaction N content.

The apparent similarity in the shifts of the Re metal reflections between the H_2/N_2 and the temperature programed H_2/Ar samples suggests that Re-N phases of identical stoichiometry result in each case. This could be due to the formation of Re_4N. However, since this phase is not included on the XRD search and match database, it was not possible to definitely match it.
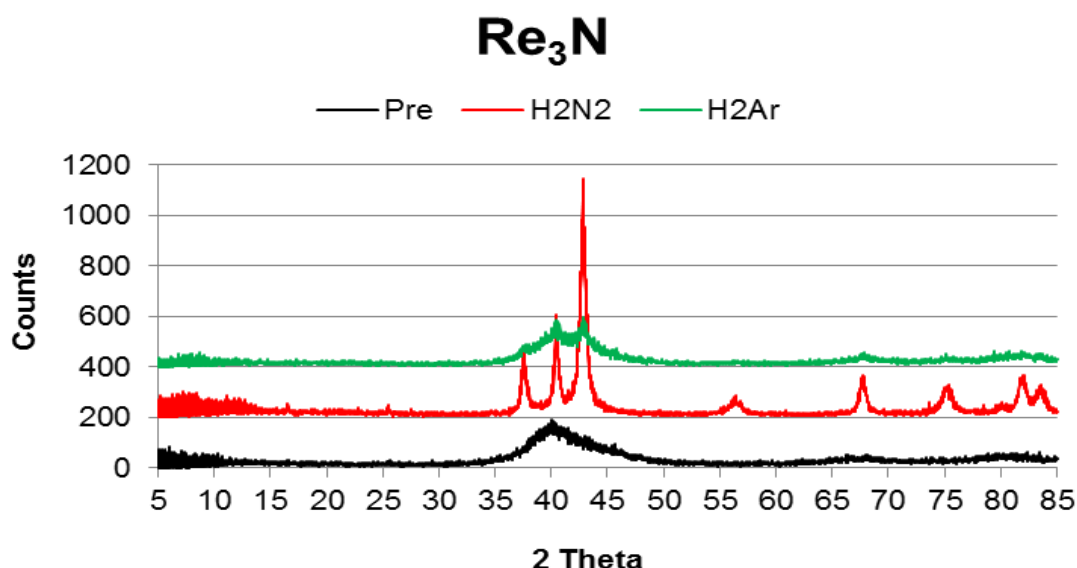
Figure 3.3-6 Pre- and Post-reaction XRD patterns of Re₃N.

3.3.4 Co₄N.

The literature available on cobalt nitrides is very limited with only a few studies of Co_4N having been reported, and nitrogen rich Co_2N and CoN systems only being recently investigated.[72,210-212]   Much of the catalytic literature on cobalt nitride, specifically Co_4N, is found in the work of Yao and co-workers, where it has been reported that bulk and supported Co_4N are active catalysts for NO decomposition and CO oxidation.[72, 194] Little work on cobalt nitrides which investigates the ammonia synthesis properties has been documented, aside from the early work conducted by Lotz and Sebba in which the ammonia decomposition activity of Co_2N was examined.[151]   Studies by Fang and co-workers have shown that cobalt nitride can exist in large range of different stoichiometries which undergo stepwise decomposition in the order Co_4N to Co_3N to Co_2N and ultimately CoN.[213]

3.3.4.1 Reaction Data.

From the conductivity versus time plot illustrated below, it is evident that there is a sharp decrease in conductivty, corresponding to the formation of ammonia, however it is uncertain whether this is due to reactive lattice species or surface NH_x species, and it is most probably a combination of both. Further decreases in conductivity are very small, even after an increase in temperture, and the formation of ammonia effectively ceases after 1.5 hours on stream as shown in Table 3.3-7. This is also evident in the reactions involving H_2/N_2 and H_2/Ar, as shown in Figure 3.3-8.

Lattice Nitrogen H$_2$/Ar Co$_4$N
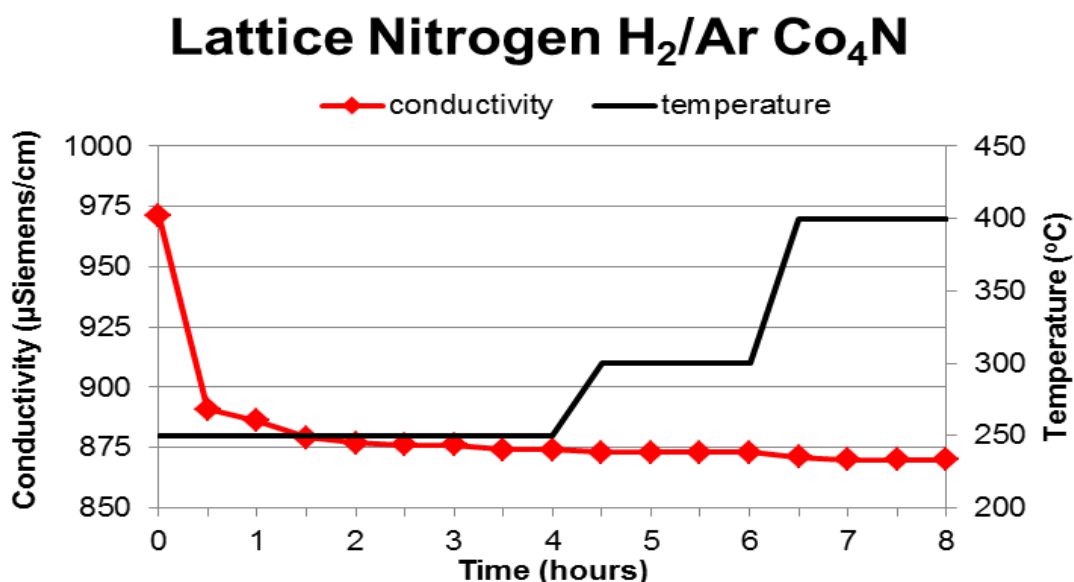
Figure 3.3-7 Conductivity data for NH$_3$ production over Co$_4$N with increasing temperature under H$_2$/Ar.

Reaction Temperature and Time	NH$_3$ Production Rate (μmol h^{-1} g^{-1})
250 ^{o}C (0.0-0.5 h)	357
250 ^{o}C (1.0-4.0 h)	13
300 ^{o}C (4.0-4.5 h)	4
300 ^{o}C (4.5-6.0 h)	0
400 ^{o}C (6.0-6.5 h)	9
400 ^{o}C (6.5-8.0 h)	2

Table 3.3-7 Ammonia production activity of Co$_4$N under H$_2$/Ar as a function of increasing temperature.

The reactions under H$_2$/Ar and H$_2$/N$_2$ were conducted at 250 ^{o}C, and follow a similar reaction profile as observed for the H$_2$/Ar reaction with increasing temperature. There is a sharp decrease in the conductivity, which subsequently stabilises in the first hour on stream and little further change in the conductivity is detected, resulting in a plateau. The decrease in conductivity is not as large as one might expect from complete decomposition. However, much of the nitrogen lost from the nitride is in the form of N$_2$ with 5.6 % of the total nitrogen, as found by CHN analysis, lost forming ammonia.

Ammonia Production Co$_4$N
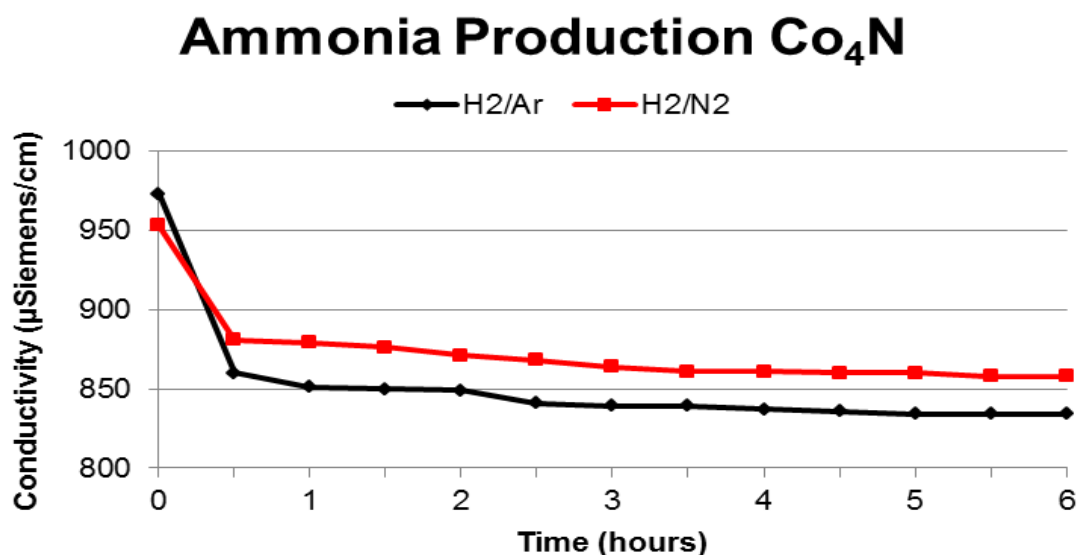
Figure 3.3-8 Comparison of conductivity for Co$_4$N ammonia production using H$_2$/N$_2$ vs. H$_2$/Ar at 250 ^{o}C.

Sample and Reaction Conditions	NH$_3$ Production Rate (μmol h^{-1} g^{-1})
Co$_4$N, 250 ^{o}C (H$_2$/N$_2$, 0.0-0.5 h)	321
Co$_4$N, 250 ^{o}C (H$_2$/N$_2$, 1.0-6.0 h)	10
Co$_4$N, 250 ^{o}C (H$_2$/Ar, 0.0-0.5 h)	477
Co$_4$N, 250 ^{o}C (H$_2$/Ar, 1.0-6.0 h)	8

Table 3.3-8 Ammonia production rates of Co$_4$N under both H$_2$/Ar and H$_2$/N$_2$ at 250 ^{o}C.

3.3.4.2 Nitrogen Analysis.

The pre-reaction sample contains a lower amount of nitrogen than the calculated stoichiometric value, as seen in Table 3.3-9. However this material was extremely difficult to prepare, and was constrained to very narrow synthesis conditions, requiring a specific temperature and time of formation. Even altering these conditions slightly resulted in Co metal. In the post-reaction samples it was surprising to see that some residual nitrogen remained in the sample treated under H$_2$/N$_2$, despite the production of ammonia apparently ceasing during the reaction. As for the samples treated under H$_2$/Ar, no nitrogen is detected within the material, indicating complete decomposition to yield to Co metal.

Sample and Reaction Conditions	Calculated Stoichiometric N content (wt.%)	Pre-Reaction N Content (wt.%)	Post-Reaction N Content (wt.%)
Co_4N (H_2/N_2) after 6 h at 250 ^{o}C	5.60	3.39	0.89
Co_4N (H_2/Ar) after 6 h at 250 ^{o}C	5.60	3.09	0.00
Co_4N (H_2/Ar) using temperature profile as shown in Fig. 3.3-7	5.60	3.17	0.00

Table 3.3-9 Nitrogen content of Co$_4$N samples pre- and post-reaction.

3.3.4.3 XRD Patterns.

Cobalt nitride proved more difficult to synthesise than originally envisaged and it was found that the nitride had to be ammonolysed within a 20 ^{o}C temperature window, and that pro-longed exposure to ammonia resulted in decomposition to Co metal. Yao had previously reported the difficulties in identifying the Co$_4$N phase from Co metal by XRD, as the reflections are identical, which is shown in Figure 3.3-9. Both the H_2/N_2 and H_2/Ar post-reaction samples have decomposed into the corresponding Co metal, however it is impossible to distinguish the Co phase from the Co$_4$N phase which is present in the pre-reaction sample by XRD analysis and so assignments are made solely on the basis of CHN data.
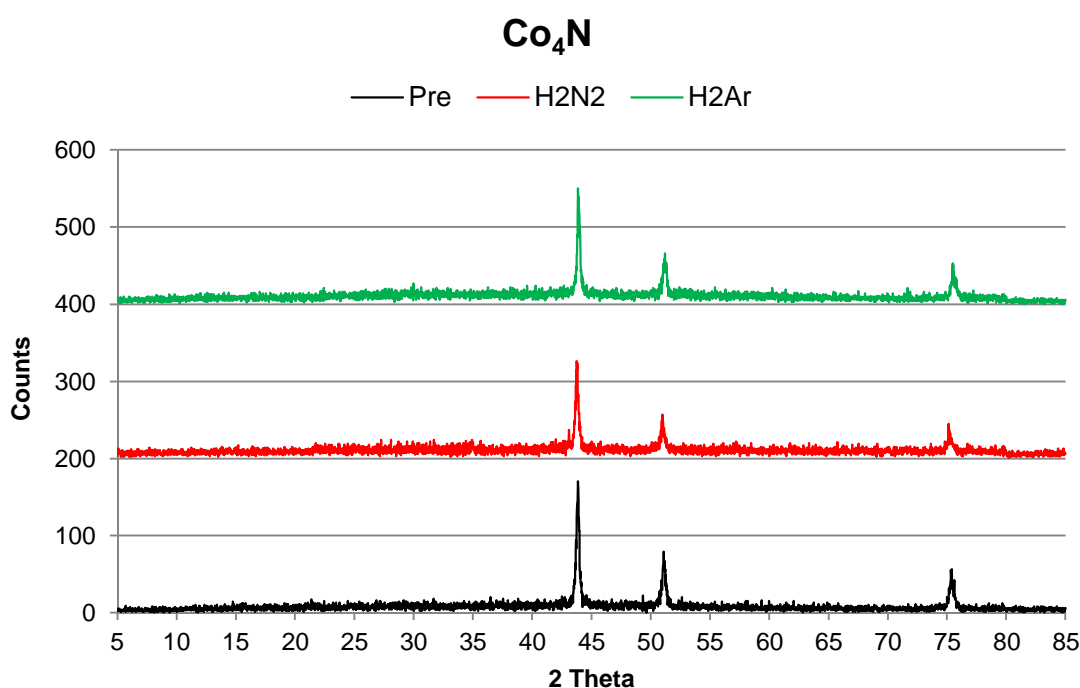
Figure 3.3-9 Pre and Post-reaction XRD patterns of Co$_4$N.

3.3.5 Ni$_3$N.

The first reported synthesis of Ni$_3$N was that documented by Juza in which Ni powder was treated under flowing ammonia at 450 ^{o}C.[214] This method, however, does not generally yield a pure phase material with unreacted Ni metal impurities often being observed. Since then a variety of different preparation techniques have been reported in attempts to achieve a pure phase material. These include exothermic solid state metathesis, synthesis in supercritical ammonia, sputtering of nickel films in Ar/N$_2$ mixed gases and also ion bombardment of nickel thin films with N$^+$ ions.[215-218] These methods require strict synthesis conditions without which impurities from the starting materials, and or by-products may be observed. It has been stated that nickel nitride is the final interstial nitride that forms in the 3d metals and it has been reported to have a hexagonal close packed crystal structure.[218]

Nickel nitride, along with cobalt and copper nitrides, has been shown to be metastable and decompose to the corresponding metal at relatively low temperatures. This was highlighted in the work of Baiker and co-workers where the thermal stability of copper and nickel nitrides under different atmospheres was examined.[22,219] These studies were conducted after it was found that the formation of nitrides on metal catalysts severely hindered their activity in amination type reactions. From this study it was concluded that Ni$_3$N, is stable in an ammonia atmosphere up to around 400 ^{o}C. Furthermore it was also reported that in a hydrogen environment the nitride is only stable up to 110 ^{o}C.[22] Perhaps due to the instability of this material, it has seldom been investigated for catalytic applications.

3.3.5.1 Reaction Data.

As with Co$_4$N, Ni$_3$N is known to decompose to the corresponding metal at low temperatures. A similar reaction profile, shown below, was obtained. However the decrease in conductivity for Ni$_3$N was much more pronounced and after the first 30 minutes on stream the H$_2$SO$_4$ solution required to be exchanged with a fresh solution, due to complete consumption of H$_3$O$^+$ by reaction with the evolved NH$_3$. Measurements were subsequently continued and hence the conductivity is reported in arbitrary units as seen in Figure 3.3-10. Following this large decrease, further activity was minimal. Ammonia production rates for Ni$_3$N under H$_2$/Ar and H$_2$/N$_2$ at 250 ^{o}C are presented in Table 3.3-10.

Ammonia Production Ni$_3$N
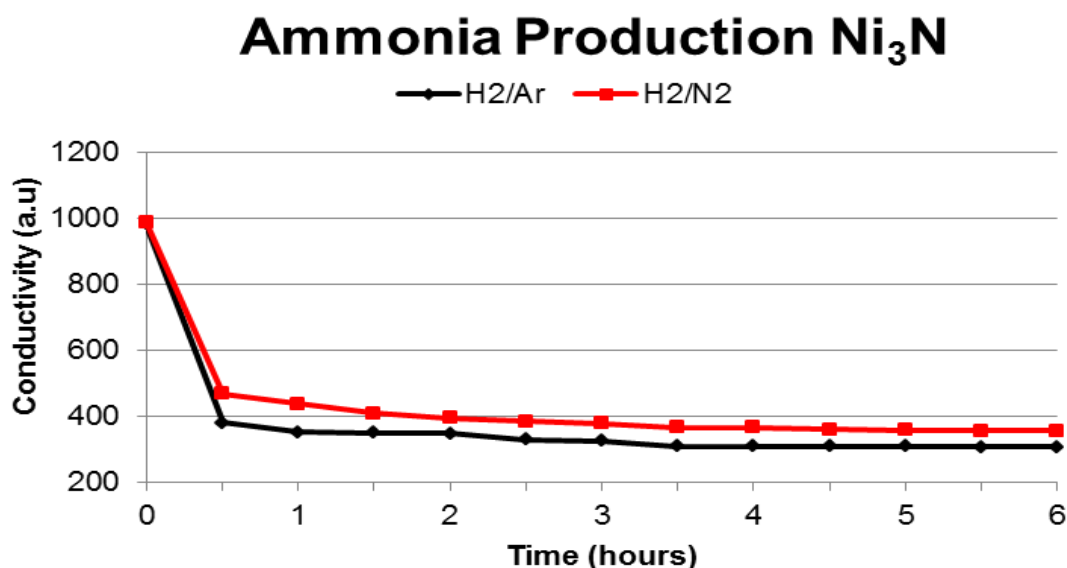
Figure 3.3-10 Comparison of conductivity for Ni$_3$N ammonia production using H$_2$/N$_2$ vs. H$_2$/Ar at 250 ^{o}C.

Sample and Reaction Conditions	NH$_3$ Production Rate (μmol h^{-1} g^{-1})
Ni$_3$N, 250 ^{o}C (H$_2$/N$_2$, 0.0-0.5 h)	2335
Ni$_3$N, 250 ^{o}C (H$_2$/N$_2$, 1.0-6.0 h)	36
Ni$_3$N, 250 ^{o}C (H$_2$/Ar, 0.0-0.5 h)	2702
Ni$_3$N, 250 ^{o}C (H$_2$/Ar, 1.0-6.0 h)	20

Table 3.3-10 Ammonia production rates of Ni$_3$N under both H$_2$/Ar and H$_2$/N$_2$ at 250 ^{o}C.

In the case of the temperature programmed H$_2$/Ar experiments, Ni$_3$N was observed to react in a similar manner to Co$_4$N. However, as seen under H$_2$/N$_2$ and the isothermal H$_2$/Ar experiments, a significant amount of ammonia is produced within the first 30 minutes on stream, which quickly subsides. In the temperature programmed H$_2$/Ar experiments, a further small burst of ammonia is observed after the temperature is increased to 400°C, which is in agreement with previous findings, where it has been observed that nitrogen desorbs from nickel at two different temperatures, similar to those observed in this study. [150, 154]

Reaction Temperature and Time	NH$_3$ Production Rate (μmol h^{-1} g^{-1})
250 ^{o}C (0-0.5 h)	2743
250 ^{o}C (1.0-4.0 h)	31
300 ^{o}C (4.5-5.0 h)	36
300 ^{o}C (5.0-6.0 h)	5
400 ^{o}C (6.0-6.5 h)	95
400 ^{o}C (6.5-8.0 h)	11

Table 3.3-11 Ammonia production activity of Ni$_3$N under H$_2$/Ar with increasing temperature.

3.3.5.2 Nitrogen Analysis.

Although it is evident that all nitrogen is removed from the pre-reaction samples during reactions with H$_2$/Ar and H$_2$/N$_2$, only around 31 % and 28 % of the lattice nitrogen accounts for the formation of ammonia under the H$_2$/Ar (up to 400 ^{o}C) and H$_2$/Ar (at 250 ^{o}C) respectively. The remaining *ca.* 70 % of nitrogen is thought to be lost as N$_2$.

Sample and Reaction Conditions	Calculated Stoichiometric N content (wt.%)	Pre-Reaction N Content (wt.%)	Post-Reaction N Content (wt.%)
Ni$_3$N (H$_2$/N$_2$) after 6 h at 250 ^{o}C	7.36	6.88	0
Ni$_3$N (H$_2$/Ar) after 6 h at 250 ^{o}C	7.36	6.88	0
Ni$_3$N (H$_2$/Ar) using temperature profile as shown in Fig. 3.3-7	7.36	7.24	0

Table 3.3-12 Nitrogen content of Ni$_3$N samples pre- and post-reaction.

3.3.5.3 XRD Patterns.

Ni$_3$N was inherently difficult to prepare. Initial attempts to prepare pure-phase Ni$_3$N, following the method reported by Juza, using a Ni powder and heating it under ammonia gas for 6 hours at 450 ^{o}C proved unsuccessful, resulting in a mixture of unreacted Ni and Ni$_3$N. [214] It was then decided to follow a method outlined by Baiker and co-workers, in which a NiO precursor was used in temperature-programmed adsorption and desorption studies conducted in an ammonia atmosphere.[22] It was reported that the formation of Ni$_3$N was observed at 350 ^{o}C and by about 400 ^{o}C the formation and decomposition reactions of Ni$_3$N were in equilibrium. With this in mind, an *in-situ* XRD was performed

on NiO, although under a 6 % H_2/N_2 gas mixture, from room temperature up to a maximum of 700 ^oC and it was found that the NiO precursor did not form the nitride but instead decomposed directly into the Ni metal. These studies were repeated with ammonia (albeit these were not conducted *in-situ*) as feed gas. Whilst Ni_3N reflections were evident, these were weak in comparison to those observed for Ni metal represented as stars in Figure 3.3-11.
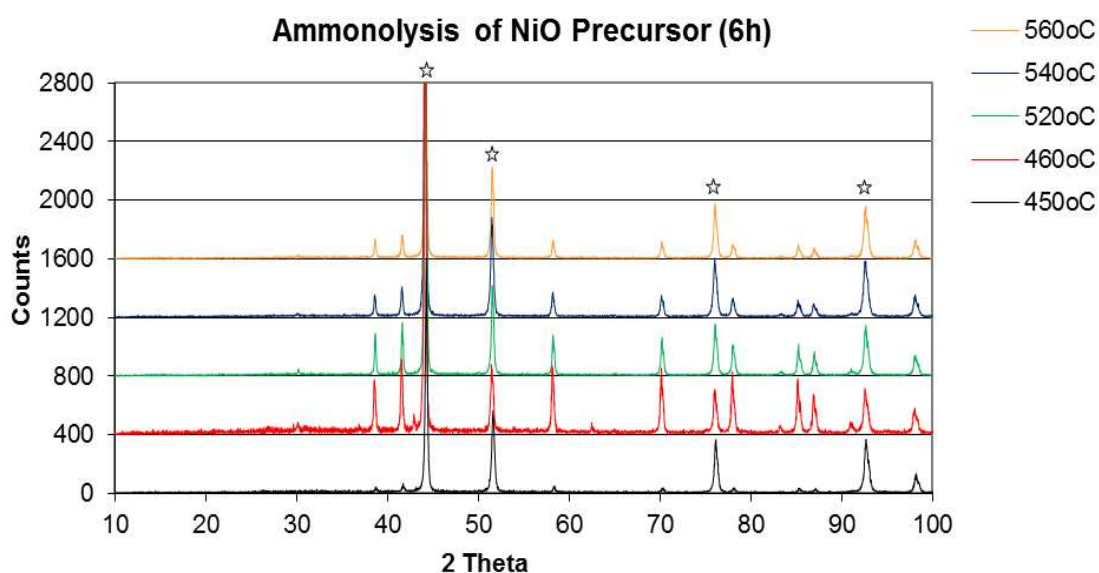
Figure 3.3-11 XRD patterns of ammonolysis of NiO at various temperatures, Ni reflections are represented by (☆) other reflections correspond to Ni₃N.

Ultimately Ni_3N was synthesised using a nickel chloride precursor, as described in the experimental chapter, which yielded hexagonal Ni_3N with a relatively high nitrogen content and only minor Ni impurities are observed in the pre-reaction material, as shown in Figure 3.3-11.

Ni_3N is fully reduced to the Ni metal, as confirmed by XRD, by both H_2/Ar and H_2/N_2 reaction gases.
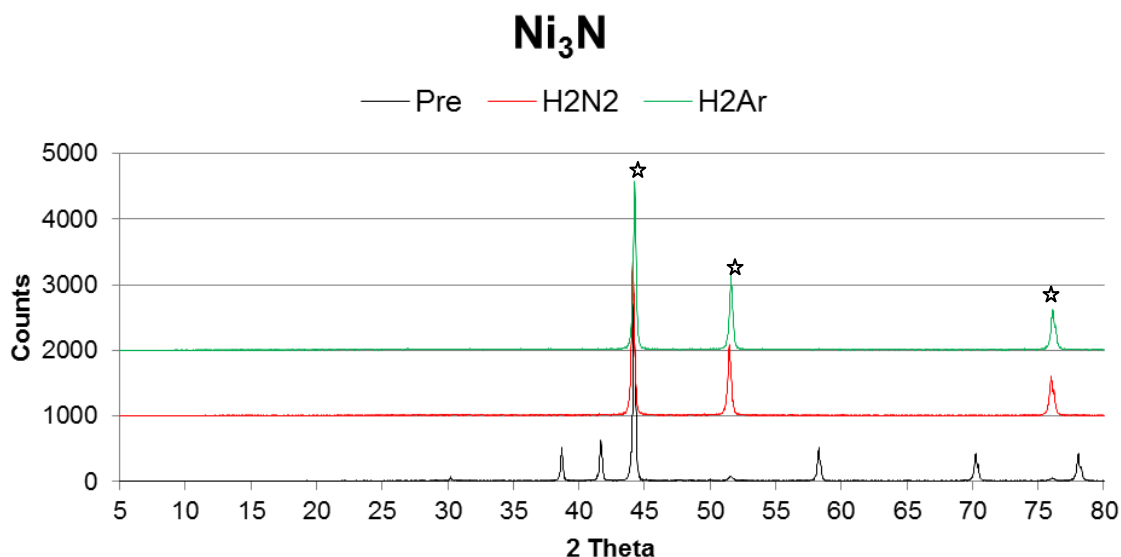
Figure 3.3-12 Pre- and Post-reaction XRD patterns of Ni₃N (JCPDS 010-0280 hexagonal Ni₃N). Ni metal reflections are indicated by (☆)

3.3.5.4   SEM Micrographs.

On viewing the SEM micrographs, it was interesting to note the apparent 'holes' that appeared in the post-reaction material, which has also been observed in studies by Kieda and Messing.[221] It is thought that these 'holes' form by the bursting of sub-surface N_2 occlusions. This would be a possible explanation why a low percentage of the nitrogen in the material forms ammonia in the reactions. Since sub-surface N_2 is formed, this also implies that there is a possible structure sensitivity, in that the surface area to volume ratio of crystallites may influence the amount of lattice nitrogen which forms NH_3.
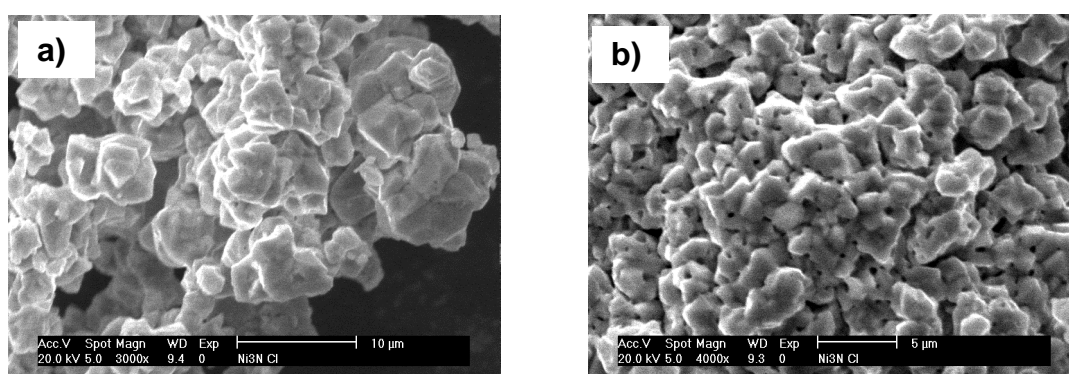
Figure 3.3-13 SEM micrographs images a) pre-reaction b) Post-reaction.

3.3.6 Cu₃N.

Recent interest in copper nitrides, motivated by its possible applications in the optoelectronic industry, has been documented.[222-224] This material crystallizes in a cubic anti-ReO$_3$ type structure.[225-230] In this arrangement, the copper atoms occupy the middle of the cube edges and the nitrogen atoms occupy the corners of the cell. This structure is unusual since Cu atoms do not occupy the face centred cubic close packing sites. As a result, this crystal structure has many vacant interstitial sites and therefore it may be a possible host to other transition metal atoms. Both lithium and palladium atoms have been reported to been successfully incorporated into this structure.[229,231,232] These ions have a similar size to Cu and as a result can be easily accommodated by the crystal lattice. Previous studies performed by Moreno-Armenta and co-workers[233] demonstrated that copper nitride has a small indirect band gap and can act as a semi-conductor, however when an extra ion is added to the lattice metallic like behavior is observed, which is in agreement with previous work by Hahn.[234] This provides an interesting means of perhaps stabilizing, or at least modifying the behavior of, Cu$_3$N which has a rather low decomposition temperature. Most of the studies that have investigated the intercalation of other metals into the Cu$_3$N framework have focused on enhancing the electronic properties of the material; however the focus of this study is to develop a nitrogen transfer reagent, and it is relevant to point out that from other literature studies copper itself is a good aminating agent with examples being found in the patent literature and documented in organic synthesis.[169-173, 236,237]

3.3.6.1 Reaction Data.

Copper nitride, like rhenium, cobalt and nickel nitrides, is metastable and decomposes to the Cu metal with increasing temperature. It therefore follows that Cu$_3$N displays a similar reaction profile to that observed for both cobalt and nickel nitrides. The ammonia production rates for the H$_2$/Ar experiment with increasing temperature are presented in Table 3.3-13.

Reaction Temperature and Time	NH$_3$ Production Rate (μmol h^{-1} g^{-1})
250 ^{o}C (0.0-0.5 h)	2109
250 ^{o}C (1.0-4.0 h)	36
300 ^{o}C (4.5-5.0 h)	18
300 ^{o}C (5.0-6.0 h)	22
400 ^{o}C (6.0-6.5 h)	9
400 ^{o}C (6.5-8.0 h)	1

Table 3.3-13 Ammonia production activity of Cu$_3$N under H$_2$/Ar as a function of increasing temperature.

As indicated in Table 3.3-13, Cu$_3$N displays a high activity for ammonia production within the first 30 minutes. However, as in the case of Co$_4$N and Ni$_3$N, this is not sustained and a rapid deactivation of the nitride is observed. The most likely cause for this is complete de-nitridation and the formation of the copper metal. In the case of H$_2$/N$_2$ and H$_2$/Ar studies, conducted at 250 ^{o}C, a comparable plot is obtained to that of the Ni$_3$N, Figure 3.3-14.

Figure 3.3-14 demonstrates that there is a rapid decrease in the conductivity in the first 30 minutes on stream with both H$_2$/Ar and H$_2$/N$_2$ feedstreams, and after approximately 1 hour on stream this activity is no longer observed. Table 3.3-14 demonstrates that between 1.0 and 6.0 hours on stream only a very small amount of ammonia is produced and is significantly lower (almost 300 x) than that produced in the first 30 minutes of the reaction. Despite the large drop in the conductivity value, only 45 % of the nitrogen lost from Cu$_3$N can be attributed to the formation of NH$_3$.

Ammonia Production Cu$_3$N
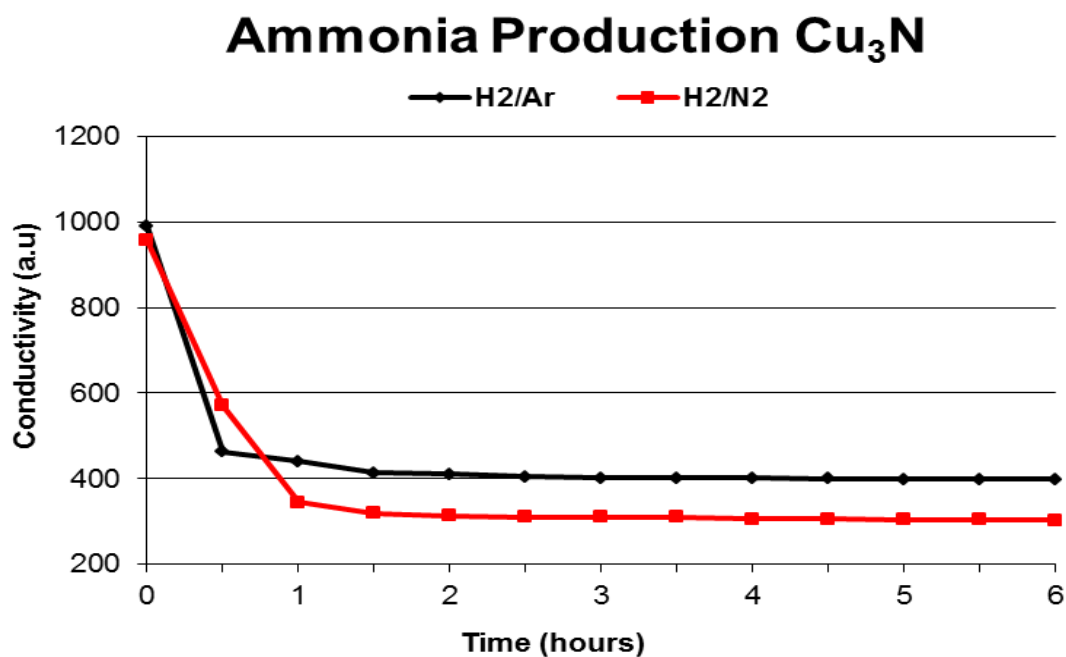
Figure 3.3-14 Comparison of conductivity for Cu$_3$N ammonia production using H$_2$/N$_2$ vs. H$_2$/Ar at 250 ^{o}C (H$_2$SO$_4$ solution changed after 30 minutes on stream).

Sample and Reaction Conditions	NH$_3$ Production Rate (μmol h^{-1} g^{-1})
Cu$_3$N, 250 ^{o}C (H$_2$/N$_2$, 0.0-0.5 h)	1732
Cu$_3$N, 250 ^{o}C (H$_2$/N$_2$, 1.0-6.0 h)	8
Cu$_3$N, 250 ^{o}C (H$_2$/Ar, 0.0-0.5 h)	2350
Cu$_3$N, 250 ^{o}C (H$_2$/Ar, 1.0-6.0 h)	8

Table 3.3-14 Ammonia production rates of Cu$_3$N under both H$_2$/Ar and H$_2$/N$_2$ at 250 ^{o}C.

3.3.6.2 Nitrogen Analysis.

Table 3.3-15 presents the nitrogen content found in the pre- and post-reaction samples via microanalysis. As can be seen from the table the pre-reaction samples correlate well to the calculated stoichiometric values for Cu$_3$N, and as expected the post-reaction samples contain no nitrogen.

Sample and Reaction Conditions	Calculated Stoichiometric N content (wt.%)	Pre-Reaction N Content (wt.%)	Post-Reaction N Content (wt.%)
Cu_3N (H_2/N_2) after 6 h at 250 °C	6.84	6.52	0
Cu_3N (H_2/Ar) after 6 h at 250 °C	6.84	6.87	0
Cu_3N (H_2/Ar) using temperature profile as shown in Fig. 3.3-7	6.84	6.63	0

Table 3.3-15 Nitrogen content of Cu₃N samples pre- and post-reaction.

3.3.6.3 XRD Patterns.

Like Ni_3N, Cu_3N was also difficult to prepare and a number of different synthesis methods were attempted. Originally a CuO precursor was used, as described by Baiker.[22] CuO was treated under H_2/N_2 and NH_3 at various temperatures, as indicated in Figures 3.3-15 and 3.3-16.

In the case of H_2/N_2, the resultant material was copper coloured, which was a visual indication that CuO had been reduced to Cu metal. This was confirmed by XRD, Figure 3.3-15. The increasing background as a function of angle is due to fluorescence effects associated with the use of a copper x-ray source.

Upon ammonolysis, as shown in Figure 3.3-16, it is clear that most samples result in a mixed phase material, with CuO, Cu and Cu_3N reflections being evident. The Cu_3N phase starts to be apparent at 200 °C, becoming more pronounced at 300°C. However reflections which correspond to CuO are also present in these samples. On increasing the temperature to 350 °C, these reflections disappear and are subsequently replaced by Cu metal reflections, which would indicate that the material decomposes somewhere between 300 and 350 °C, and that the temperature range for synthesis of Cu_3N is very narrow.
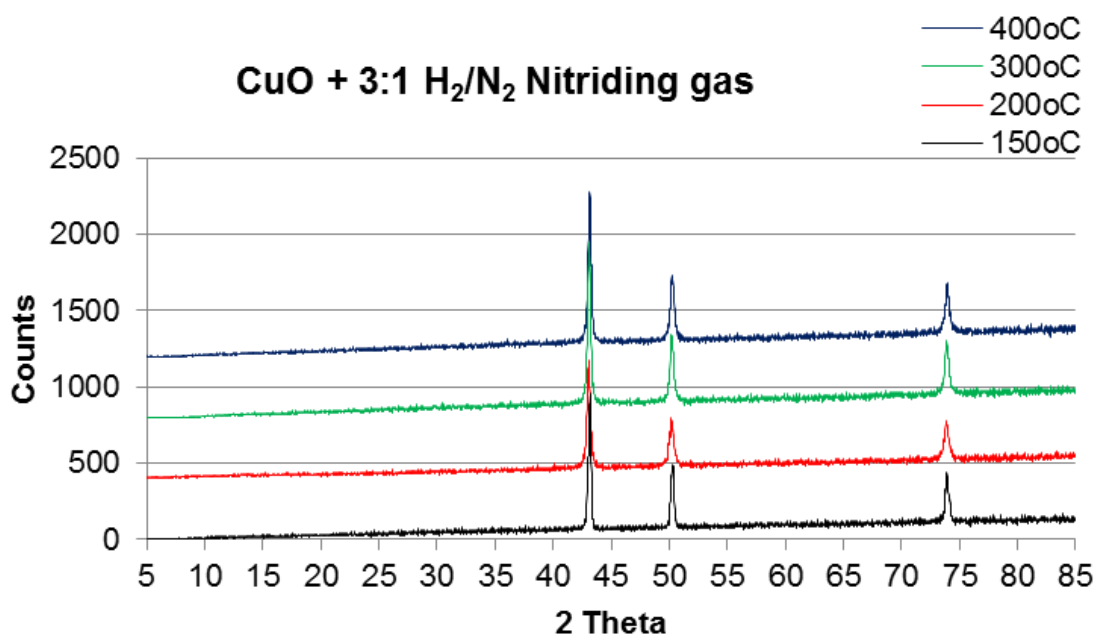
Figure 3.3-15 XRD patterns of CuO reacted under 3:1 H_2/N_2 at various temperatures. Reflections correspond to Cu metal.
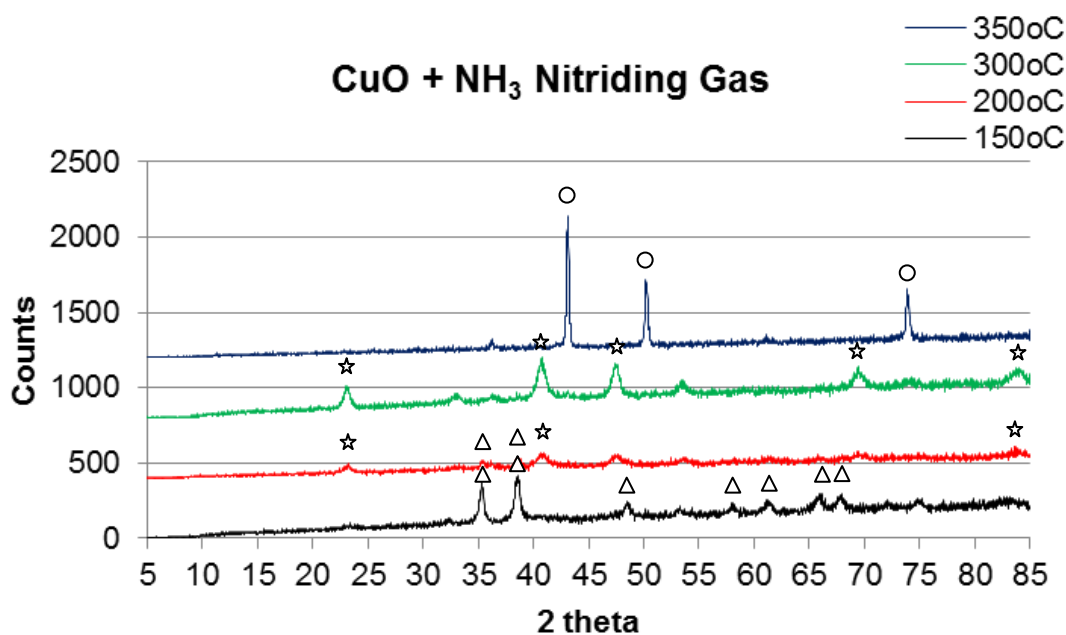
Figure 3.3-16 XRD patterns of ammonolysis of CuO at various temperatures, Cu reflections are represented by (○); CuO reflections are represented by (△); Cu_3N reflections are represented by (☆). These are the only reflections that can be identified with some certainty.

Since these attempts were unsuccessful in the synthesis of a single phase Cu_3N, CuF_2 was used as the precursor. This is undesirable to use due to the formation of HF gas on contact with ammonia and care had to be taken to ensure that all necessary precautions were made. This synthesis method was first reported by Juza in which ammonolysis of CuF_2 resulted in pure phase Cu_3N being obtained, as is evident in the current studies presented in Figure

3.3-17 where the pre-reaction material corresponds to a pure phase Cu_3N (JCPDS 00-002-1156).[228] Post-reaction reflections are characteristic of copper metal and on visual inspection the material is copper coloured.
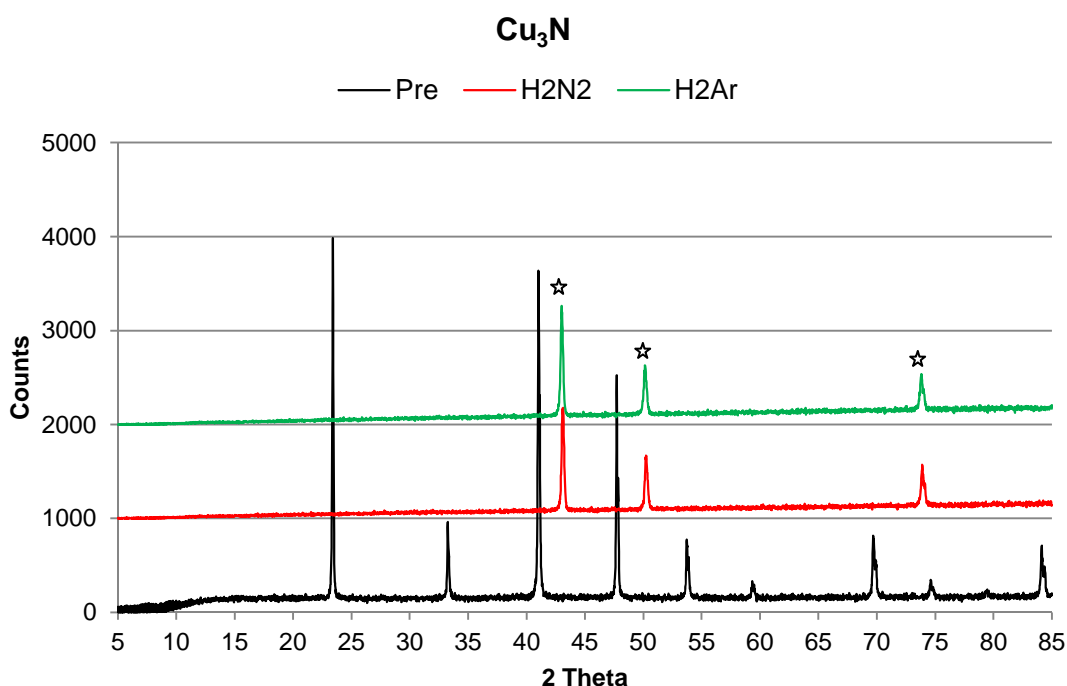
Figure 3.3-17 Pre- and Post-reaction XRD patterns of Cu₃N. (JCPDS: 00-002-1156 Cu₃N). Cu metal reflections are indicated by (☆)

3.3.6.4   SEM Micrographs.

As for Ni_3N post-reaction samples, Cu_3N also exhibits a change in morphology from the pre-reaction samples. In the post-reaction samples, it is again very evident that 'holes' have developed, possibly to a greater extent than observed for the Ni_3N samples. As has previously been stated, these 'holes' are thought to correspond with loss of nitrogen from the material via bursting of sub-surface N_2 occlusions. These types of holes are not evident in other materials which have been investigated, apart from Ni_3N, and may be a consequence of the materials being less thermally stable when compared to others such as Fe_2N and $\beta\text{-}Mo_2N_{0.78}$.   Again this suggests that there may be a possible relationship between sample morphology and the amount of NH_3 formed as a proportion of the lattice N.
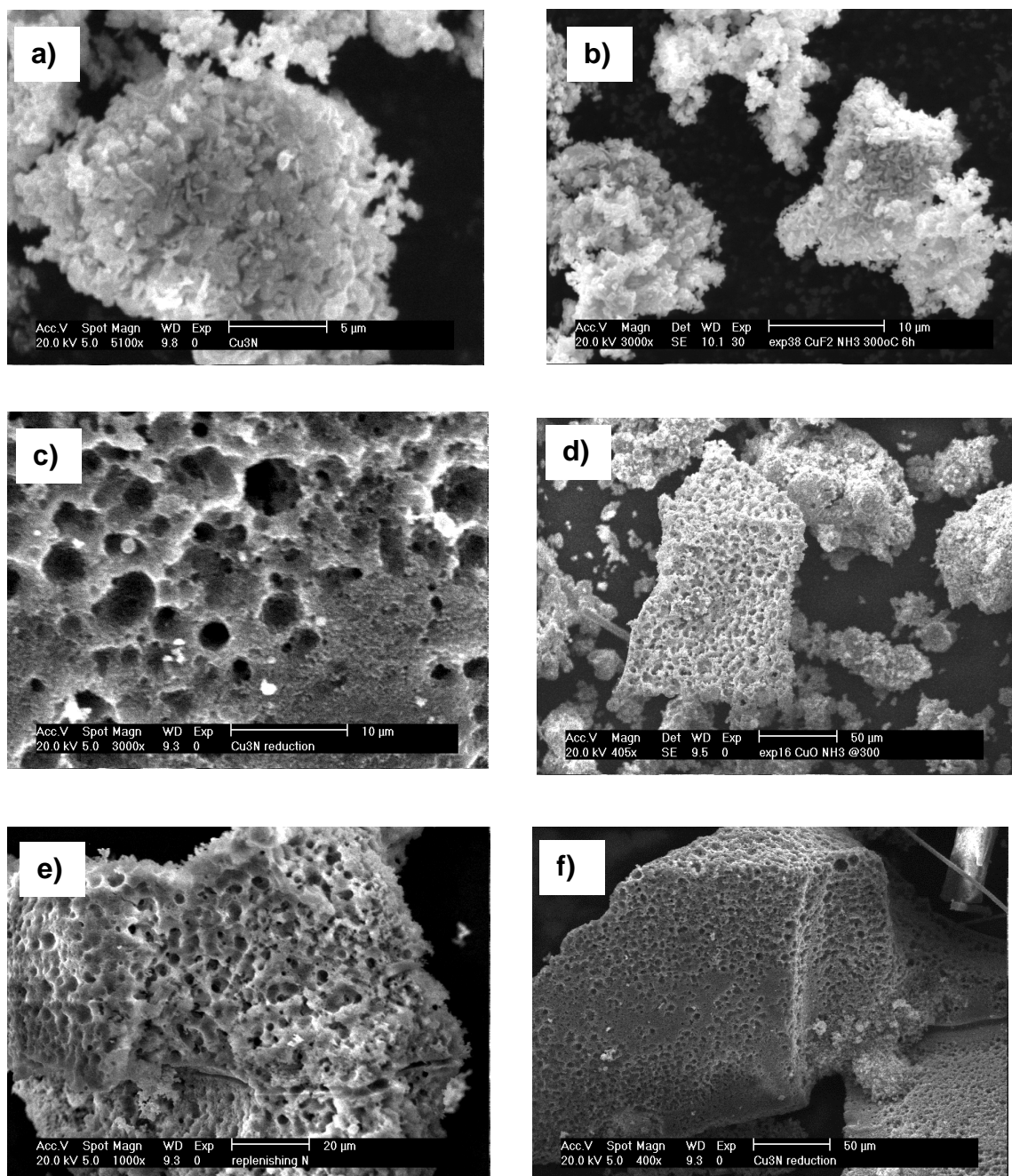
Figure 3.3-18 SEM micrographs images a-b) pre-reaction Cu$_3$N c- f) Post-reaction Cu$_3$N

3.3.7 Zn$_3$N$_2$.

Zinc is not strictly a transition metal because its 3d orbitals are completely filled in the element and also its highest common oxidation state. Its nitride, Zn$_3$N$_2$, is generally categorised with the Group III nitrides, such as BN, AlN and GaN. Zn$_3$N$_2$ was first synthesised by Juza and Hahn in 1940, and since then has rarely been studied.[237] Much of the recent interest in Zn$_3$N$_2$ focuses on the structure and optical and electronic properties of the material and how they may be applied to optoelectronic devices such as light emitting diodes and laser diodes.[105,238-240] The catalytic literature on Zn$_3$N$_2$ is sparse and it is

unknown how the material will act under ammonia synthesis conditions, with it being grouped with refractory nitrides which are inactive for ammonia synthesis. However it also has similar properties to that of copper, which decomposes to the metal at relatively low temperatures. A structural study by Partin and co-workers has shown that the nitrogen atoms within Zn_3N_2 occupy two different crystallographic sites, which may prove to be advantageous in terms of a Mars-van Krevelen mechanism.[241]

3.3.7.1 Reaction Data.

Figure 3.3-19 highlights that although there is a small decrease in conductivity during the first 30 minutes on stream it is not the same sharp decrease as seen with the neighbouring cobalt, nickel and copper nitrides. This would suggest that Zn_3N_2 is more stable at 250 ^{o}C than the preceding nitrides. However as the temperature is increased to 400 ^{o}C, the reaction appears to proceed at an increased rate. Ammonia production rates for the below conductivity versus time plot are presented in Table 3.3-16.
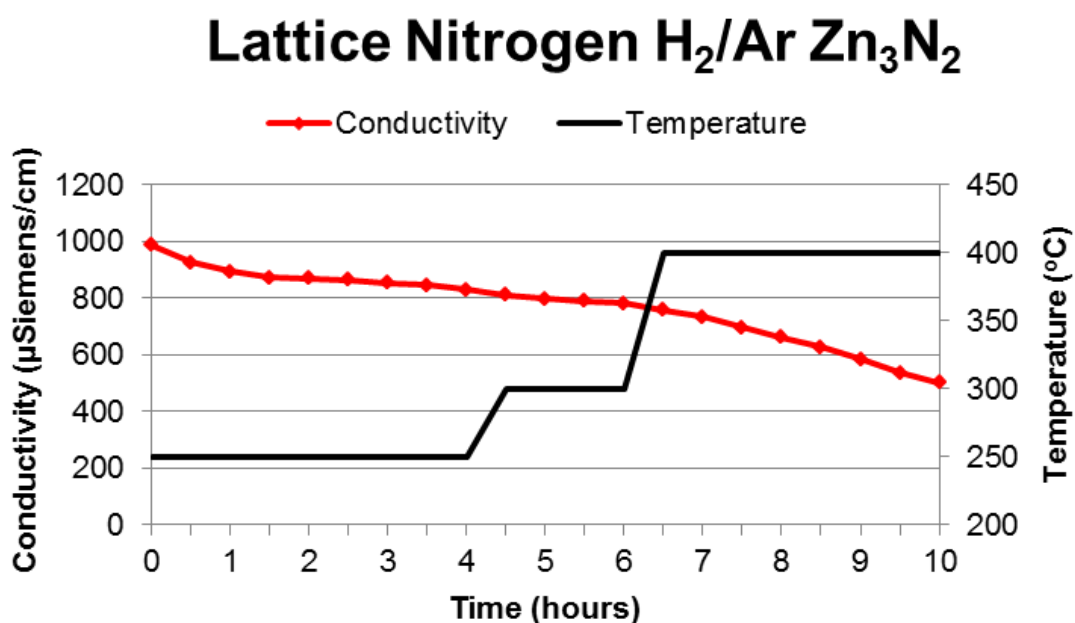
Figure 3.3-19 Conductivity data for NH$_3$ production over Zn$_3$N$_2$ as a function of increasing temperature under H$_2$/Ar.

Reaction Temperature and Time	NH$_3$ Production Rate (μmol h^{-1} g^{-1})
250 ^{o}C (0.0-0.5 h)	270
250 ^{o}C (1.0-4.0 h)	46
300 ^{o}C (4.0-4.5 h)	88
300 ^{o}C (4.5-6.0 h)	40
400 ^{o}C (6.0-6.5 h)	106
400 ^{o}C (6.5-10.0 h)	162

Table 3.3-16 Ammonia production activity of Zn$_3$N$_2$ under H$_2$/Ar as a function of increasing temperature.

Following the temperature programmed H$_2$/Ar experiments, subsequent H$_2$/N$_2$ and H$_2$/Ar studies were conducted at 400 ^{o}C. It can be seen in Figure 3.3-20 that the initial decrease in conductivity, for both H$_2$/Ar and H$_2$/N$_2$ reactions, is not as sharp as previously seen in other systems. However it is apparent that under both reaction gases, a plateau is reached - after 2.5 hours on stream in the case of H$_2$/Ar and around 5.5 hours in the case of H$_2$/N$_2$ - where the reaction ceases and either little or no ammonia is produced. Ammonia production rates at various time intervals in the reaction are presented in Table 3.3-17.
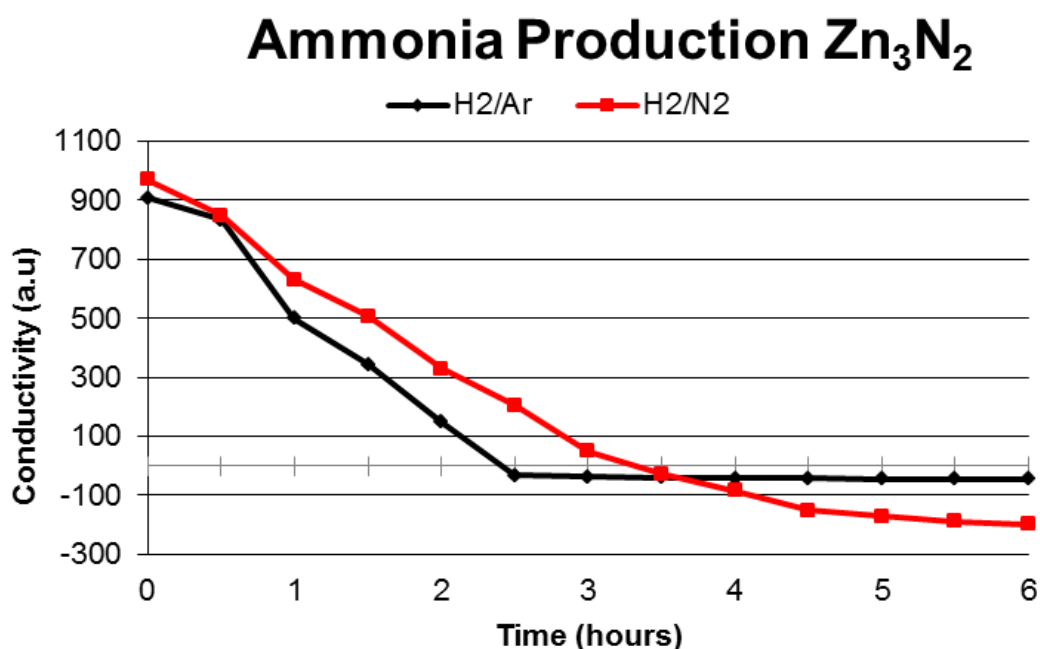
Figure 3.3-20 Comparison of conductivity for Zn$_3$N$_2$ ammonia production using H$_2$/N$_2$ vs. H$_2$/Ar at 400 ^{o}C (arbitrary units are used as the conductivity in the dilute H$_2$SO$_4$ solution does not decrease below ~350 μS/cm, on reaching this point the solution was changed and readings were continued).

Sample and Reaction Conditions	NH_3 Production Rate (μmol h^{-1} g^{-1})
Zn_3N_2, 400 ^{o}C (H_2/N_2, 0.0-0.5 h)	536
Zn_3N_2, 400 ^{o}C (H_2/N_2, 0.5-4.5 h)	498
Zn_3N_2, 400 ^{o}C (H_2/N_2, 4.5 -6.0 h)	70
Zn_3N_2, 400 ^{o}C (H_2/Ar, 0.0-0.5 h)	327
Zn_3N_2, 400 ^{o}C (H_2/Ar, 0.5-2.5 h)	785
Zn_3N_2, 400 ^{o}C (H_2/Ar, 2.5-6.0 h)	8

Table 3.3-17 Ammonia production rates of Zn_3N_2 under both H_2/Ar and H_2/N_2 at 400 ^{o}C.

3.3.7.2 Nitrogen Analysis.

From Table 3.3-18 it is apparent that the pre-reaction samples have slightly lower nitrogen contents, than would be expected from stoichiometric Zn_3N_2. However these values are comparable to that reported by Gregory and co-workers (10.91 wt.%).[105] On examination of the post-reaction material, it is evident that not all nitrogen is removed from the samples, and less than half is removed from the post-reaction sample treated under H_2/N_2. This may or may not be attributed to the fact that the N atoms, in Zn_3N_2, occupy two different crystallographic sites within the lattice, and it may be the case that these different nitrogen species become active at different temperatures.

Sample and Reaction Conditions	Calculated Stoichiometric N content (wt.%)	Pre-Reaction N Content (wt.%)	Post-Reaction N Content (wt.%)
Zn_3N_2 (H_2/N_2) after 6 h at 400 ^{o}C	12.49	10.04	5.99
Zn_3N_2 (H_2/Ar) after 6 h at 400 ^{o}C	12.49	10.14	2.50
Zn_3N_2 (H_2/Ar) using temperature profile as shown in Fig. 3.3-19	12.49	9.46	2.29

Table 3.3-18 Nitrogen content of Zn_3N_2 samples pre- and post-reaction.

3.3.7.3 XRD Patterns.

The pre-reaction sample, had a relatively high nitrogen content, however the lower than expected nitrogen content might be attributed to the presence of ZnO. This was confirmed by XRD with a ZnO reflection observed at *ca.* 36 $^{\circ}$ 2θ. In addition to this a small Zn metal impurity was detected at *ca.* 39 $^{\circ}$ 2θ. However, the remaining reflections matched those of cubic Zn_3N_2. This Zn reflection increases in intensity in the post-reaction XRD patterns, which would be expected in the case of decomposition of the nitride. The formation of ZnO is apparent in the post-reaction XRD patterns and it is more evident in the post-reaction H_2/Ar sample that underwent temperature increase up to 400 $^{\circ}$C. In this instance the characteristic nitride reflection is not apparent and the intensity of the ZnO reflection at 39 $^{\circ}$ 2θ increases. This may indicate that the Zn_3N_2 phase becomes more reduced to Zn metal upon reaction, which subsequently oxidises forming larger ZnO crystallites with respect to those present in the pre-reaction sample.
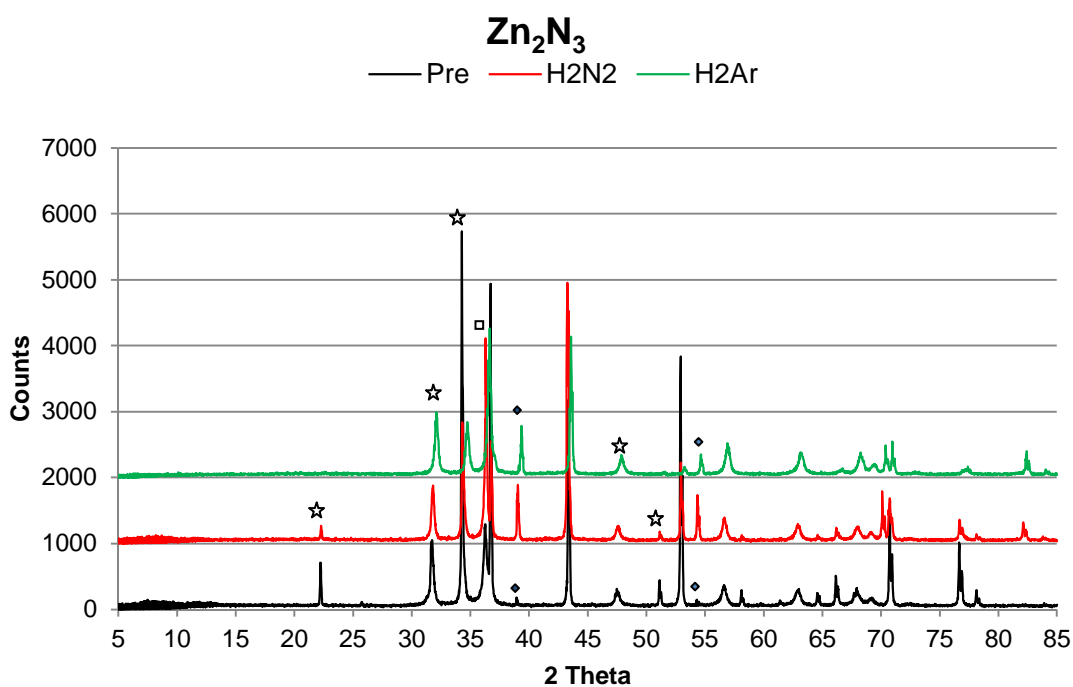
Figure 3.3-21 Pre- and Post-reaction XRD patterns of Zn_2N_3. The symbols used show characteristic reflections of Zn_2N_3 (☆) Zn metal (♦) and ZnO (▫) that can be clearly identified without ambiguity. (JCPDS 035-0762 Zn_2N_3).

3.3.8 Summary of Later Transition Metal Nitrides.

Tables 3.3-19 and 3.3-20 give a summary of the nitrides investigated within this section. Ammonia production rates are presented in Table 3.3-19, and only the ammonia production rates for the first 30 minutes on stream are included in the table due to the instability of many of the materials. Table 3.3-20 presents the nitrogen content pre- and post-reaction of each material as well as the surface areas of the pre-reaction material.

3.3.8.1 Summary of Ammonia Production Rates.

As previously mentioned many of the materials investigated within this section are thermally unstable and for this reason only the ammonia production rates within the first 30 minutes have been included in Table 3.3-19. It is evident that during the first 30 minutes on stream, Ni_3N and Cu_3N exhibit a significantly higher ammonia production rates when compared to the other materials investigated within this section, however as discussed in the relevent sections (3.3.5 and 3.3.6 respectively) this ammonia production is short lived and ammonia production ceases with these materials being reduced to their corresponding metals, under reaction conditions at relatively low temperatures *c.a* 300 ^{o}C. Co_4N was observed to reduce to Co metal under reaction conditions, as confirmed by elemental analysis, with no further ammonia production observed after the first 30 minutes on stream.

As discussed in the relevent sections Fe_2N, Re_3N and Zn_3N_2 exhibit ammonia production activities, under H_2/N_2, even after the initial 30 minutes on stream. Of these three materials, Zn_3N_2 displayed the highest ammonia production rates, under H_2/N_2 after 30 minutes on stream, followed by Re_3N and lastly Fe_2N.   However it is also apparent that during isothermal H_2/Ar reaction conditions, a steady decrease in the conductivities is also observed for all three samples, which may suggest that these materials undergoe decomposition rather than functioning as true ammonia synthesis reagents. This was confirmed by elemental analysis and the results are shown in Table 3.3-20. This however, may prove to be advantageous for the develpment of a novel nitrogen transfer reagent if the regeneration of the material can be preformed in a seperate step to that of the nitrogen transfer process and will be discussd further in Chapter 4.

Material	NH$_3$ Production Rate (μmol h^{-1} g^{-1})	
	H$_2$/N$_2$, 400 ^{o}C, 0.5 h	H$_2$/Ar, 400 ^{o}C , 0.5 h
Fe$_2$N	213	170
Re$_3$N	580	419
Co$_4$N	321	477
Ni$_3$N	1702	2335
Cu$_3$N	1732	2350
Zn$_3$N$_2$	536	327

Table 3.3-19 Summary of NH$_3$ production rates for the later transition metal nitride materials

3.3.8.2   Summary Pre/Post-Reaction N Data and Surface Areas.

Material	BET Surface Area (m^{2}g^{-1})	Nitrogen Content (wt.%)			
		Calculated Stoichiometric	Pre-Reaction	Post-Reaction (H$_2$/Ar) 700°C	Post-Reaction (H$_2$/N$_2$) 400°C
Fe$_2$N	13	11.13	8.65	2.4	3.57
Re$_3$N	2	2.44	3.52	1.10	0.47
Co$_4$N	4	5.60	3.39	0	0.89
Ni$_3$N	3	7.36	7.24	0	0
Cu$_3$N	4	6.84	6.63	0	0
Zn$_3$N$_2$	1	12.49	10.04	2.29	5.99

Table 3.3-20 Summary of pre- and post-reaction nitrogen content, and surface area of pre reaction samples for the later transition metal nitride materials.

3.4 Miscellaneous systems.

3.4.1 Introduction to Miscellaneous systems.

The materials which are investigated in this section have been examined for a number of different reasons and do not necessarily 'fit' with the binary nitrides categories that have been discussed in preceding sections. Most of these materials, with the exception of Co-4Re, have been reported to exhibit nitrogen transfer properties. For example, Mg_3N_2 has recently been reported by Ley and co-workers to be an active nitrogen source for the transformation of ester into amides.[100] Co_3Mo_3N has recently been reported to exhibit reversible nitrogen loss and regeneration properties.[111] Re-nitridation is one of the significant problems associated with the development of a novel nitrogen transfer reagent and as Co_3Mo_3N exhibits the ability to re-nitride under N_2 gas, this may have significant advantages for commercial type processes.

In addition to this, ruthenium based systems are included at the end of this section in order to draw a comparison between activity rates and also to assess how active each material is with respect to ruthenium based catalysts, which are known to exhibit very high activity rates for ammonia synthesis reactions.[113-115, 242,243]

3.4.2 Mg₃N₂.

Magnesium nitride is a well-known solid material which has been used as an additive for a variety of different applications including ceramics, catalytic cross-polymerization and hydrogen storage materials. Mg_3N_2 has recently applied in the formation of other nitrides such as boron nitride, scandium and lanthanum nitrides.[244-246] Magnesium nitride is reported to have a similar structure to that of zinc nitride. It forms an anti-bixbyite structure where the nitrogen atoms occupy two different crystallographic sites.[241] As mentioned earlier in the chapter, this may prove to be advantageous in terms of a Mars-van Krevelen type process.

Mg_3N_2 is known to be moisture sensitive, releasing ammonia when exposed to water.[253] Ley and co-workers have recently demonstrated that ammonia is also released from magnesium nitride when it is reacted with other protic solvents such as methanol or ethanol.[100] They subsequently investigated magnesium nitride as a nitrogen source for the transformation of esters to primary amides. The release of ammonia from magnesium nitride was accompanied by a color change from brown to yellow-white.

3.4.2.1 Reaction Data.

Group II metal nitrides are generally known to be unstable in air and also when exposed to moisture.   Despite this, it was unclear how the nitride would react under a H_2/Ar atmosphere and it was therefore necessary to initially conduct a temperature programmed reaction under H_2/Ar to determine the temperature range in which to conduct subsequent H_2/N_2 and isothermal H_2/Ar reactions. From Figure 3.4-1 it is evident that low levels of ammonia are formed at 300 ^{o}C. As the temperature is increased to 400 ^{o}C, there is a large steady decrease in the conductivity value, which persists for the duration of the reaction. This significant decrease in conductivity has not been observed in other systems which have been subjected to temperature programmed H_2/Ar reaction.   Ammonia production data for various phases of the reaction are presented Table 3.4-1
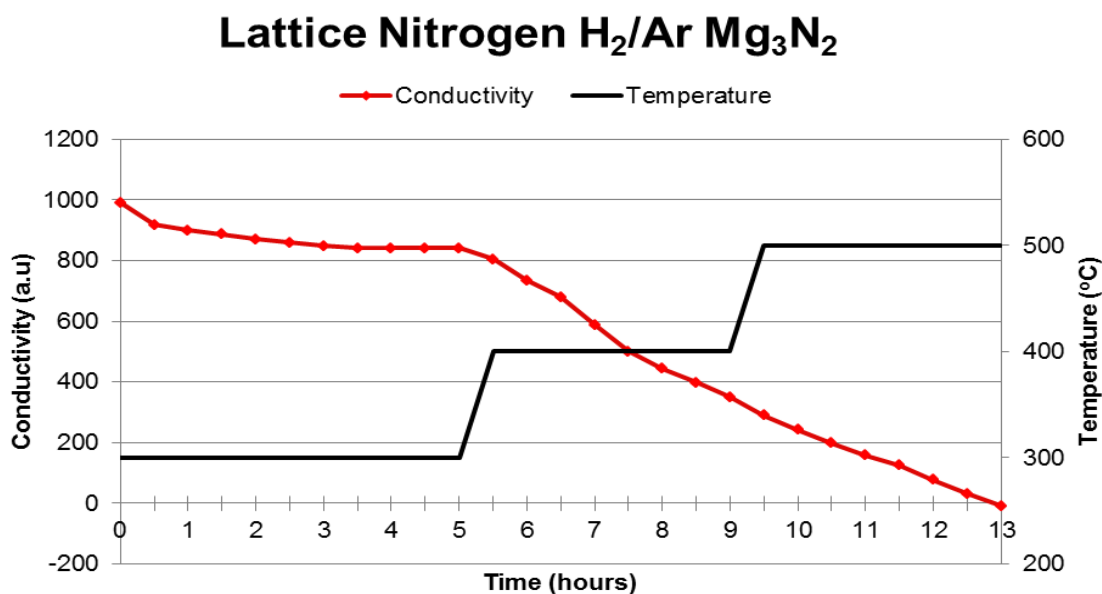

Figure 3.4-1 Conductivity data for NH$_3$ production over Mg$_3$N$_2$ as a function of increasing temperature under H$_2$/Ar.

Reaction Temperature and Time	NH$_3$ Production Rate (μmol h^{-1} g^{-1})
300 $^{\circ}$C (0.0-0.5 h)	332
300 $^{\circ}$C (1.0-5.0 h)	33
400 $^{\circ}$C (5-5.5.0 h)	157
400 $^{\circ}$C (5.5-9.0 h)	291
500 $^{\circ}$C (9.0-9.5 h)	269
500 $^{\circ}$C (9.5-13.0 h)	191

Table 3.4-1 Ammonia production activity of Mg$_3$N$_2$ under H$_2$/Ar as a function of increasing temperature.

H$_2$/N$_2$ and isothermal H$_2$/Ar reactions were conducted at 400 $^{\circ}$C, following these results. It is clear from Figure 3.4-2 that the resultant conductivity versus time plots for H$_2$/Ar and H$_2$/N$_2$ are comparable, with only a slight degree of variation in the ammonia production rates. This may be attributed to the fact that Mg$_3$N$_2$ undergoes decomposition at 400 $^{\circ}$C rather than exhibiting catalytic activity. However, for the purposes of this study, the evolution of nitrogen from Mg$_3$N$_2$ at 400 $^{\circ}$C may be beneficial, as this is the temperature range of interest for the target Mars-van Krevelen process which is the main focus of this thesis. This study was repeated, although a longer reaction time of 13 hours was investigated, with rates for ammonia production comparable to those presented in Table 3.4-2.
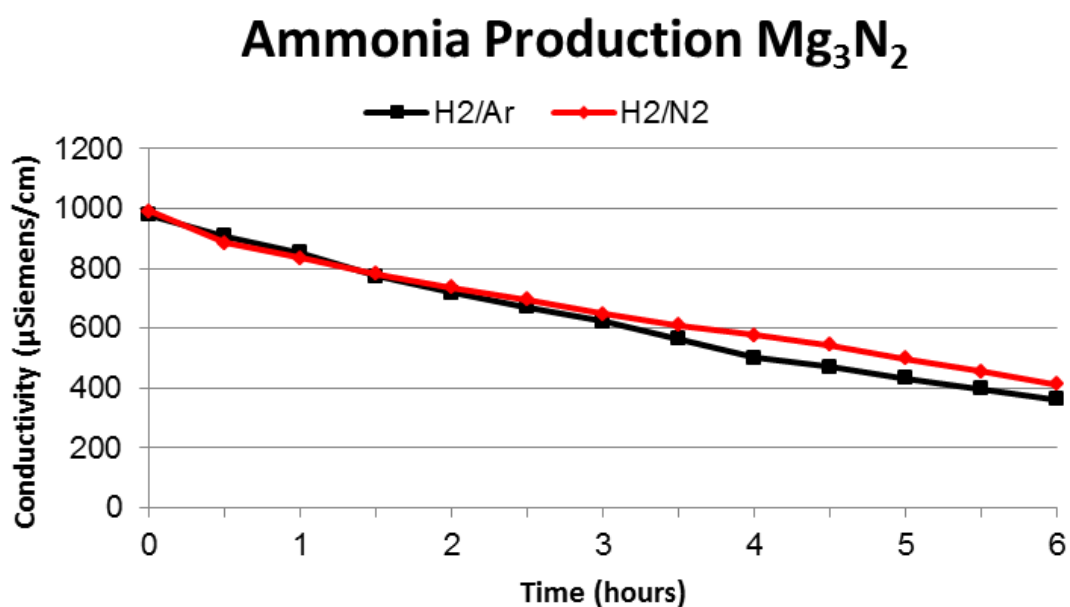
Figure 3.4-2 Comparison of conductivity for Mg$_3$N$_2$ ammonia production using H$_2$/N$_2$ vs. H$_2$/Ar at 400 $^{\circ}$C.

Sample and Reaction Conditions	NH_3 Production Rate ($\mu mol\ h^{-1}\ g^{-1}$)
Mg_3N_2, 400 ^{o}C (H_2/N_2, 0.0-0.5 h)	481
Mg_3N_2, 400 ^{o}C (H_2/N_2, 1.0-6.0 h)	190
Mg_3N_2, 400 ^{o}C (H_2/Ar, 0.0-0.5 h)	323
Mg_3N_2, 400 ^{o}C (H_2/Ar, 1.0-6.0 h)	226

Table 3.4-2 Ammonia production rates of Mg_3N_2 under both H_2/Ar and H_2/N_2 at 400 ^{o}C.

3.4.2.2 Nitrogen Analysis.

As has been previously mentioned, Mg_3N_2 is sensitive to air and moisture, and as a consequence the values obtained from nitrogen analysis may contain some degree of error due to the fact that the samples will have been exposed to an air atmosphere prior to analysis.

Pre-reaction samples were used as purchased from Sigma-Aldrich, without any further treatment. It is evident that there are differences in the nitrogen content between the pre- and post-reaction samples. It was found by CHN analysis that the post-reaction isothermal and temperature programmed H_2/Ar experiments samples, lost around 6.9 wt.% and 9.4 wt.% of nitrogen respectively. Subsequent calculations found that only 6.96 % and 11.41% of the total lattice nitrogen lost from the respective materials could be attributed to ammonia formation.

Sample and Reaction Conditions	Calculated Stoichiometric N content (wt.%)	Pre-Reaction N Content (wt.%)	Post-Reaction N Content (wt.%)
Mg_3N_2 (H_2/N_2) after 6 h at 400 ^{o}C	27.74	23.50	19.80
Mg_3N_2 (H_2/Ar) after 6 h at 400 ^{o}C	27.74	23.50	16.59
Mg_3N_2 (H_2/Ar) using temperature profile as shown in Fig. 3.4-1	27.74	23.50	14.10

Table 3.4-3 Nitrogen content of Mg_3N_2 samples pre- and post-reaction

3.4.2.3 XRD Patterns.

All three samples match to that of cubic Mg_3N_2, and it is apparent from the XRD patterns that the reflections are sharp and indicative of highly crystalline material. There are no

apparent lattice shifts between the pre- and post-reaction samples. This was not expected on the basis of the significant loss of nitrogen observed for these samples, as shown in Table 3.4-3.

It is also evident in the temperature programmed H_2/Ar samples' XRD pattern that the reflections observed at 43 ^{o}, 62 ^{o} and 78° 2θ, are slightly broader than observed for both the pre-reaction and the H_2/N_2 post-reaction samples, which would suggest that there is an increase in disorder. However, upon inspection of the post-reaction pattern obtained under H_2/Ar it is evident that some small additional reflections are present. In addition to these, very weak reflections can be observed at 17 ^{o} and 25° 2θ. These are characteristic of magnesium oxide (MgO) which is most likely a result of aerobic oxidation upon discharging the slightly more reduced material from the reactor.
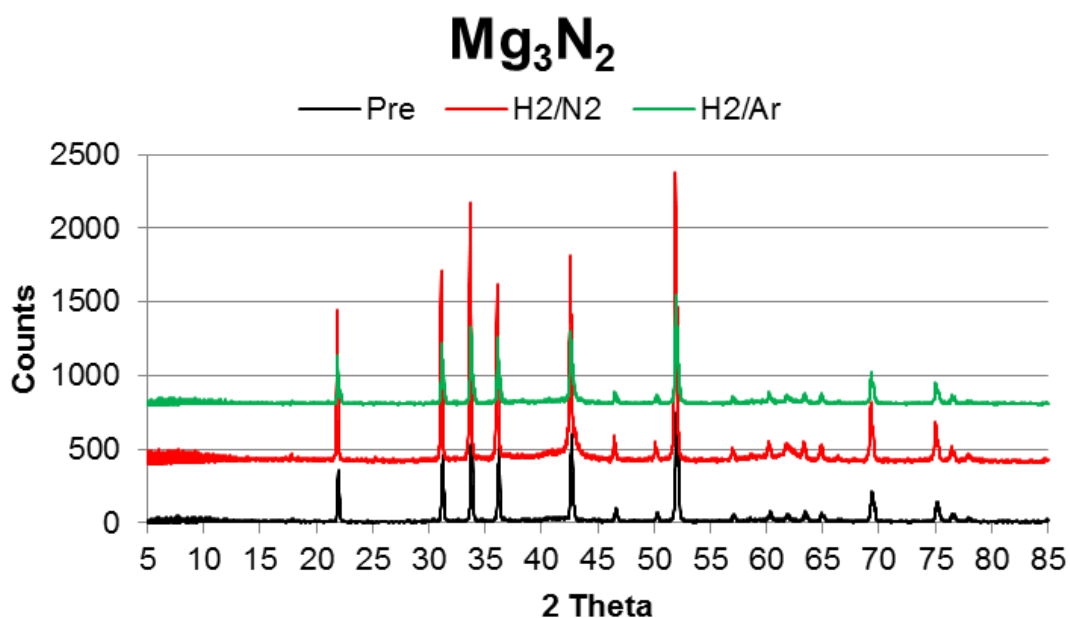
Figure 3.4-3 Pre- and Post-reaction Mg₃N₂ (JCPDS 035-0778 Mg₃N₂).

3.4.3 TiFe₂Nₓ.

The Laves type $TiFe_2$ phase has been reported to exhibit reversible nitrogen uptake and loss behaviour.[91]   Itoh and co-workers have demonstrated that intermetallic $TiFe_2$ compounds, amongst others, absorb large amounts of nitrogen, when heated either in an ammonia or nitrogen atmosphere. The nitrogen taken up can subsequently be released as ammonia upon heating under a hydrogen atmosphere.

Similar approaches can be seen in earlier work by Schwab and Wicke, and also Biewer and Bernasek which document the use of titanium-iron nitrides for ammonia synthesis.[248,249] In the study by Schwab and Wicke, it was reported that upon nitridation of a Cs-Cl structured TiFe compound, enhanced catalytic activity was displayed. The diffraction pattern from that study suggested that the material formed small iron particles which were supported on a TiN matrix. However subsequent studies have shown that this material only absorbs a limited amount of nitrogen compared with the $TiFe_2N_x$ Laves phase.

3.4.3.1 Reaction Data.

Initially H_2/Ar studies were conducted with increasing temperature to establish the temperature at which lattice nitrogen became "active", as illustrated in Figure 3.4-4. From this conductivity versus time plot, it is evident that very little ammonia is produced between the temperature ranges of 250 ^{o}C to 400 ^{o}C. On increasing the temperature to 500°C, a much larger decrease in the conductivity is observed. This is consistent with the formation of ammonia, and is in good agreement with the temperature at which Itoh observed significant ammonia formation (450 ^{o}C) by de-nitridation of $TiFe_2$. Further temperature increases to 600 ^{o}C and 700 ^{o}C result in a subsequent decrease in the conductivity value, with formation of ammonia particularly occurring at 700 ^{o}C, as illustrated in Table 3.4-4. The reaction was run over an extended period as a result of the uncertainty of the de-nitriding temperature.

Although there is very little nitrogen lost from the Laves phase $TiFe_2N_x$ material at 400 ^{o}C, subsequent H_2/N_2 and isothermal H_2/Ar studies were conducted at this temperature due to the fact that the target nitrogen transfer process which is the primary aim of this thesis should occur at this temperature.

Lattice Nitrogen TiFeN$_x$
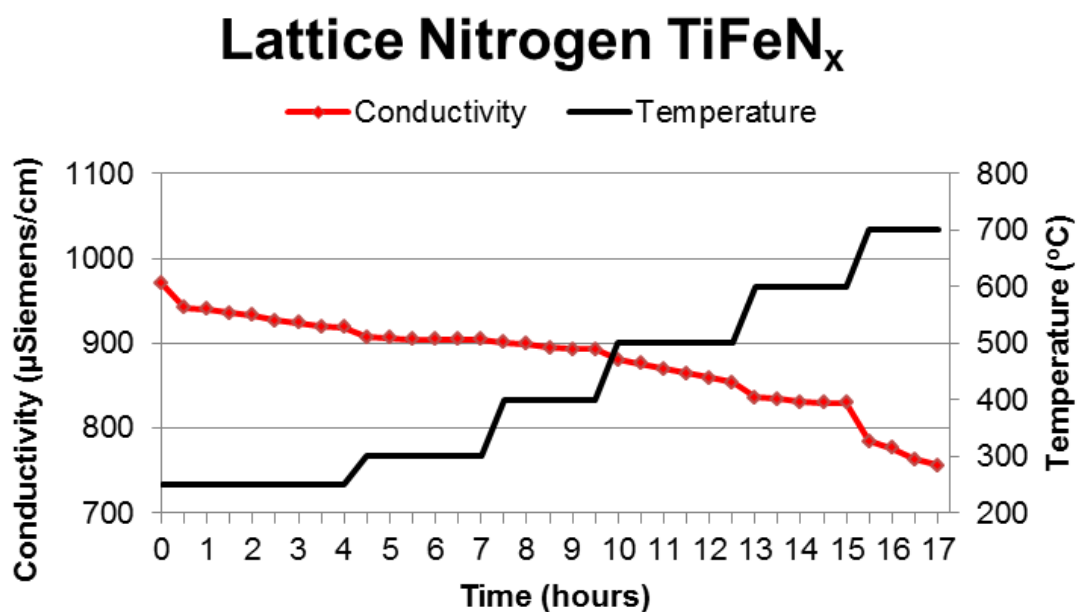
Figure 3.4-4 Conductivity data for NH$_3$ production over TiFe$_2$N$_x$ as a function of increasing temperature under H$_2$/Ar.

Figure 3.4-5 indicates that there is an initial decrease in the conductivity for the H$_2$/N$_2$ reaction studies which is only sustained for 1.5 hours, and subsequent ammonia production is limited. This is also evident in the isothermal H$_2$/Ar studies, where ammonia production ceases after 3.5 hours on stream.

Reaction Temperature and Time	NH$_3$ Production Rate (μmol h^{-1} g^{-1})
250 ^{o}C (0.0-0.5 h)	130
250 ^{o}C (0.5-4.0 h)	15
300 ^{o}C (4.0-4.5 h)	56
300 ^{o}C (4.5-7.0 h)	2
400 ^{o}C (7.0-7.5 h)	19
400 ^{o}C (7.5-9.5 h)	9
500 ^{o}C (9.5-10.0 h)	56
500 ^{o}C (10.0-12.5 h)	25
600 ^{o}C (12.5-13.0 h)	84
600 ^{o}C (13.0-15.0 h)	7
700 ^{o}C (15.0-15.5 h)	210
700 ^{o}C (15.5-17.0 h)	34

Table 3.4-4 Ammonia production activity of TiFe$_2$N$_x$ under H$_2$/Ar as a function of increasing temperature.
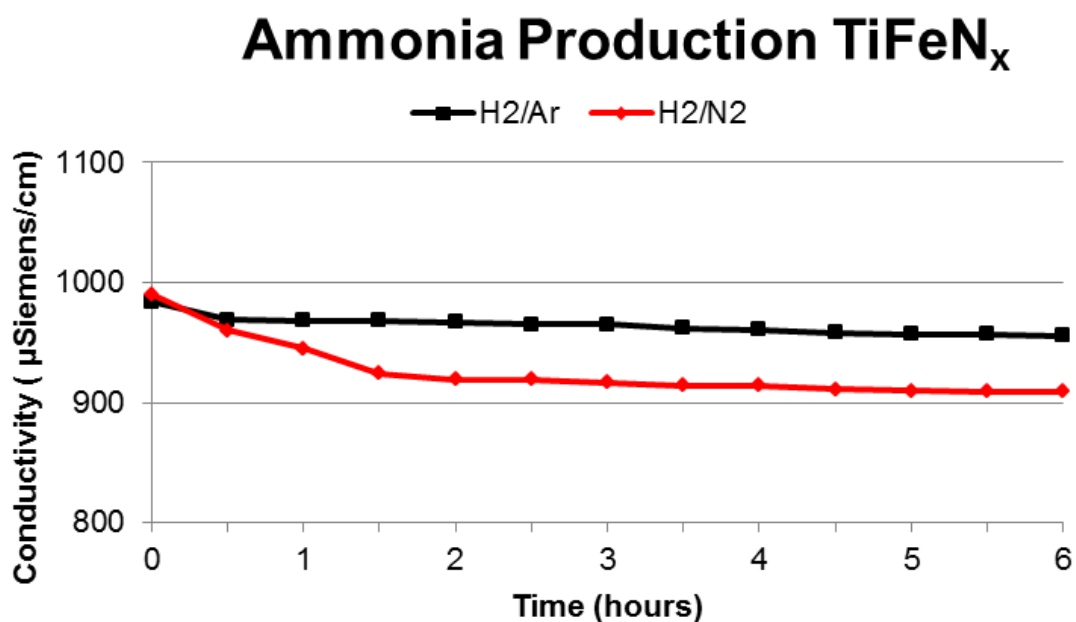
Figure 3.4-5 Comparison of conductivity for TiFe$_2$N$_x$ ammonia production using H$_2$/N$_2$ vs. H$_2$/Ar at 400 ^{o}C.

These results are in contrast to those documented by Itoh, in which it was found that after 1 absorption-desorption cycle 324 µmol g^{-1} of ammonia was produced, albeit at 450 ^{o}C.[91] Table 3.4-5 presents the rates of ammonia formation for H$_2$/N$_2$ and isothermal H$_2$/Ar reactions

Sample and Reaction Conditions	NH$_3$ Production Rate (µmol h^{-1} g^{-1})
TiFe$_2$N$_x$, 400 ^{o}C (H$_2$/N$_2$, 0.0-0.5 h)	135
TiFe$_2$N$_x$, 400 ^{o}C (H$_2$/N$_2$, 1.0-6.0 h)	16
TiFe$_2$N$_x$, 400 ^{o}C (H$_2$/Ar, 0.0-0.5 h)	67
TiFe$_2$N$_x$, 400 ^{o}C (H$_2$/Ar, 1.0-6.0 h)	5

Table 3.4-5 Ammonia production rates of TiFe$_2$N$_x$, under both H$_2$/Ar and H$_2$/N$_2$ at 400 ^{o}C.

3.4.3.2   Nitrogen Analysis.

Laves phase TiFe$_2$N$_x$ has been reported to exist in a variety of different stoichiometries ranging from x= 0.53 to x=1.44 corresponding to 4.44 wt.% and 11.22 wt.% nitrogen respectively. As illustrated in Table 3.4-6, the pre–reaction sample has a very low nitrogen content when compared to the possible stoichiometric values. This may be due to the difficulty in the preparation technique and the evidence of multiple phases in the

diffraction patterns. Despite this, the material has lost a limited amount of nitrogen and does not completely decompose to the metal. A possible reason for this may lie in the fact that TiN reflections are evident in the diffraction pattern. As has been previously observed in section 3.2.2, titanium nitride does not undergo substantial de-nitridation. Another possibility may be that the formation of TiFe has occurred instead of the Laves $TiFe_2N_x$ phase. This material has been reported to take-up only very small amounts of nitrogen.

Sample and Reaction Conditions	Calculated Stoichiometric N content (wt.%)	Pre-Reaction N Content (wt.%)	Post-Reaction N Content (wt.%)
$TiFe_2N_x$ (H_2/N_2) after 6 h at 400 ^{o}C	4.44-11.22	1.31	1.09
$TiFe_2N_x$ (H_2/Ar) after 6 h at 400 ^{o}C	4.44-11.22	1.31	1.01
$TiFe_2N_x$ (H_2/Ar) using temperature profile as shown in Fig. 3.4-4	4.44-11.22	1.31	0.94

Table 3.4-6 Nitrogen content of $TiFe_2N_x$ samples pre- and post-reaction.

3.4.3.3   XRD Patterns.

From the diffraction patterns obtained for the pre- and post-reaction samples, Figure 3.4-6, it is apparent the samples are largely amorphous. This is in agreement with the previously mentioned studies by Itoh. However, it is also evident there are multiple phases which exist within the material. These correspond to $TiFe_2$, TiN, Fe_4N and Fe metal and due to the overlap of some reflections not all can be unambiguously assigned. TiN and Fe metal reflections are represented by a triangle and star respectively, in Figure 3.4-6.

This may be further evidence to suggest the formation TiFe. Schwab and Wicke documented that upon nitridation of TiFe, that the diffraction pattern suggested the formation of small iron particles within a titanium nitride matrix.[248] It has also been found in the work of Itoh that TiFe does not form a single phase material. This would be a possible explanation as to why TiN and Fe metal reflections are present in the both the pre- and post-reaction samples and may also be, in part, an explanation, as to why apparent ammonia production rates were much lower than those quoted by Itoh were observed.
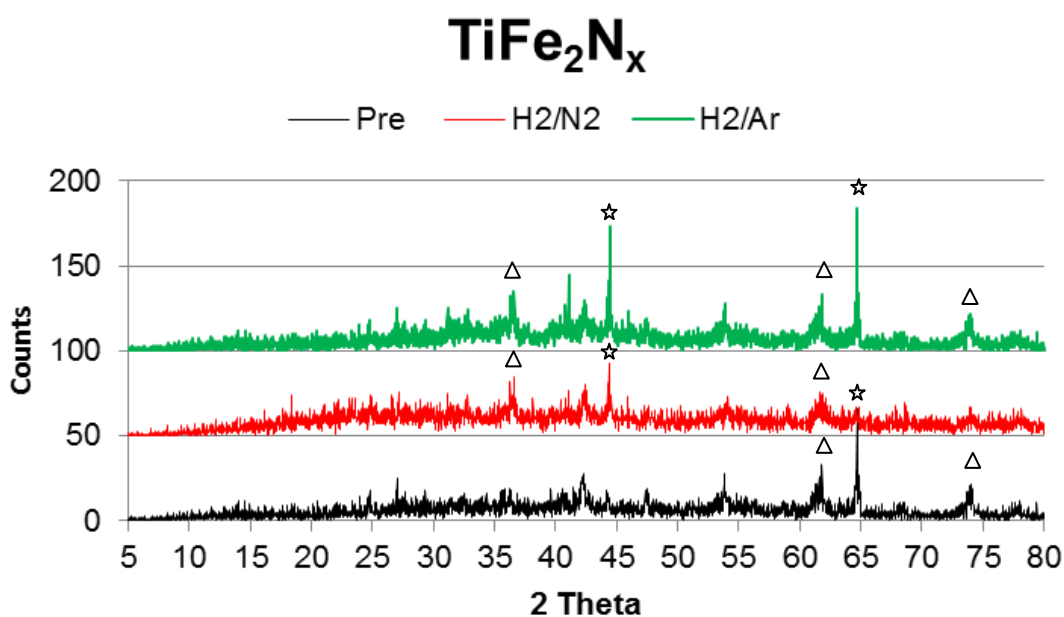
Figure 3.4-6 Pre- and Post-reaction XRD patterns of TiFe₂Nₓ (JCPDS 015-0336 TiFe₂). (Fe metal ☆ TiN △)

3.4.4 Co-4Re.

Aika and Kojima have recently described the synthesis of a bimetallic Co-Re system which was found to be active for ammonia synthesis.[59] The reported rate (2371 µmol h^{-1} g^{-1} at 350 ^{o}C and 3.1 MPa) was found to be higher than those found over traditional ammonia synthesis catalysts, promoted iron (Fe-K$_2$O-Al$_2$O$_3$), as well as Co$_3$Mo$_3$N, for which the rates are 2010 and 2113 µmol h^{-1} g^{-1} respectively, under similar conditions.[250]   In these studies rhenium nitride was initially investigated, as described in section 3.3.3, but was found to be unstable above 350 ^{o}C as was also reported in the findings of the current study. Cobalt was added in order to improve the stability of the material and in order to reduce the cobalt nitrate precursor a higher nitriding temperature is employed (700 ^{o}C) and hence the resultant phase is not the nitride which decomposes below this temperature.   Aika and Kojima also investigated the Co-Re system as a function of Re content and found that maximum ammonia synthesis activities were achieved with an 80 % Re content giving rise to a Co-4Re catalyst.

3.4.4.1   Reaction Data.

The current study temperature programmed H$_2$/Ar studies were undertaken to investigate the effect, if any, of the presence of sorbed NH$_x$ species on the bimetallic Co-4Re compound. It was found that low levels of NH$_3$ were produced within the first 30 minutes

on stream.   Table 3.4-7 presents the ammonia production activity which occurred at various points throughout the reaction.
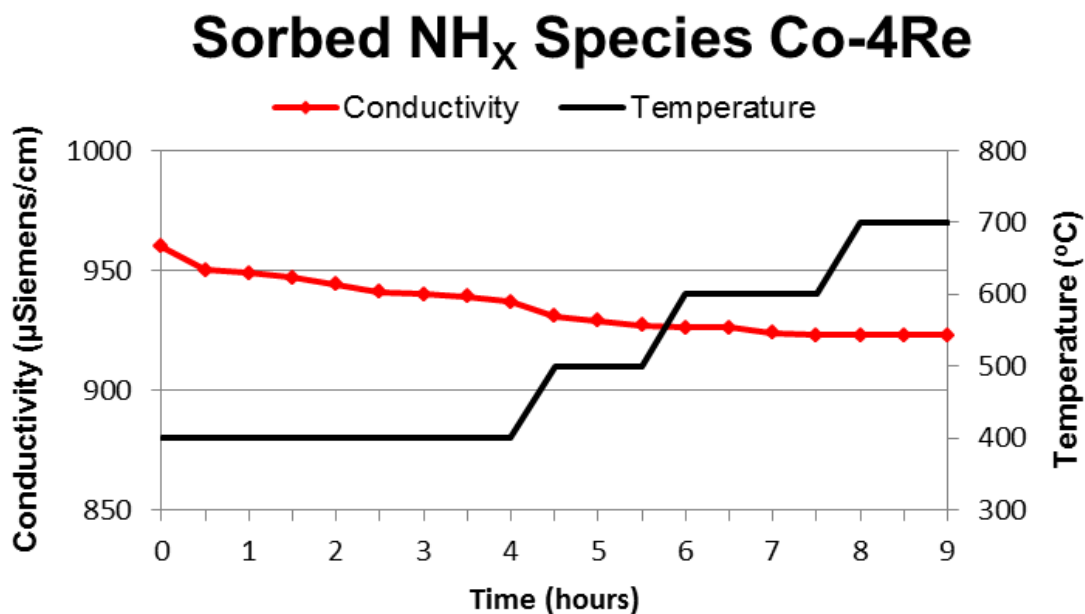
Figure 3.4-7 Conductivity data for sorbed NH$_x$ species monitored as NH$_3$ production over Co-4Re as a function of increasing temperature under H$_2$/Ar.

Reaction Temperature and Time	NH$_3$ Production Rate (μmol h^{-1} g^{-1})
400 $^{\circ}$C (0.0-0.5 h)	42
400 $^{\circ}$C (0.5-4.0 h)	9
500 $^{\circ}$C (4.0-4.5 h)	26
500 $^{\circ}$C (4.5-5.5 h)	9
600 $^{\circ}$C (5.5-6.0 h)	4
600 $^{\circ}$C (6.0-7.5 h)	4
700 $^{\circ}$C (7.5-8.0 h)	0
700 $^{\circ}$C (8.0-9.0 h)	0

Table 3.4-7 Ammonia production activity of Co-4Re under H$_2$/Ar as a function of increasing temperature.

The ammonia formation rate when using H$_2$/N$_2$ contrasted strongly with that using H$_2$/Ar as shown in Figure 3.4-8.
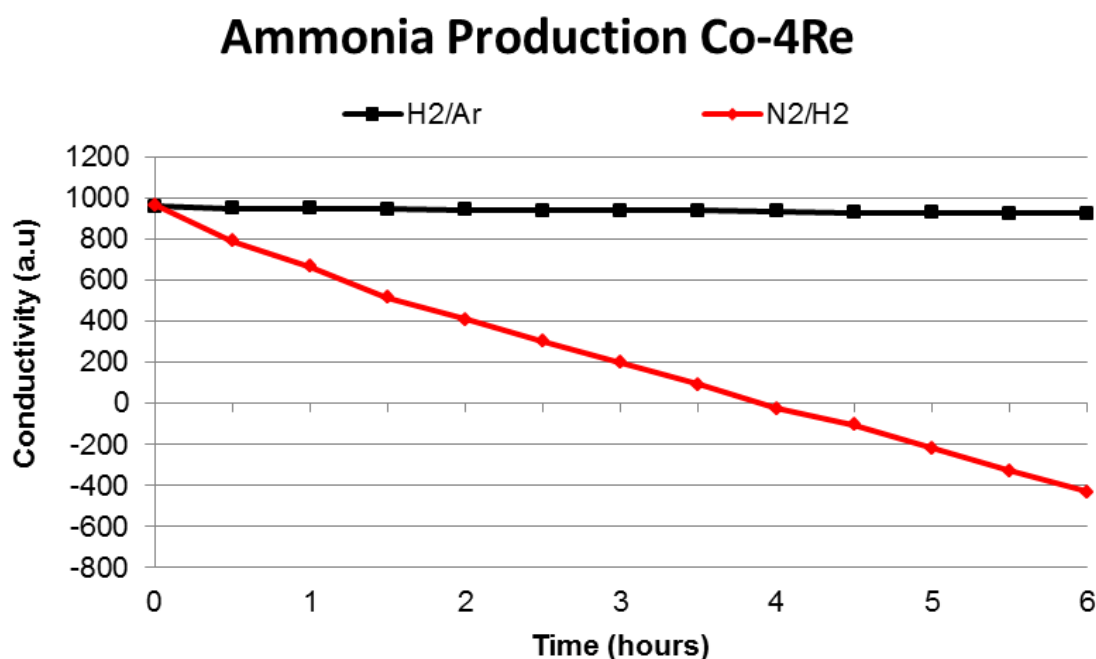
Figure 3.4-8 Comparison of conductivity for Co-4Re ammonia production using H_2/N_2 vs. H_2/Ar at 400 $^{\circ}$C.

Figure 3.4-8 highlights the catalytic ammonia synthesis activity exhibited by Co-4Re under H_2/N_2. It can be observed that there is a significant decrease in the conductivity value in the case of the H_2/N_2 reaction, consistent with the formation of ammonia and the profile indicates a steady state reaction rate. The ammonia synthesis rate which was derived from this reaction was comparable to that reported by Aika and Kojima for the steady state reaction (492 µmol h^{-1} g^{-1} at atmospheric pressure and 350 $^{\circ}$C)[59] and is presented in the table below. The initial ammonia synthesis rate quoted in Table 3.4-8 for the reaction using H_2/N_2 is much higher than the steady state rate, which is achieved after 30 minutes on stream. This increased initial rate could again be attributed to the hydrogenation of sorbed NH_x species generated by the ammonolysis or by the H_2/N_2 pre-treatment. Aika and Kojima describe the first 30 minutes of reaction under the same conditions as a stabilisation period, suggesting that similar results were observed in the early stages of the reaction.

Sample and Reaction Conditions	NH$_3$ Production Rate (µmol h^{-1} g^{-1})
Co-4Re, 400 $^{\circ}$C (H_2/N_2, 0.0-0.5 h)	747
Co-4Re, 400 $^{\circ}$C (H_2/N_2, 1.0-6.0 h)	472
Co-4Re, 400 $^{\circ}$C (H_2/Ar, 0.0-0.5 h)	44
Co-4Re, 400 $^{\circ}$C (H_2/Ar, 1.0-6.0 h)	9

Table 3.4-8 Ammonia production rates of Co-4Re under both H_2/Ar and H_2/N_2 at 400 $^{\circ}$C.

3.4.4.2   XRD Patterns.

The Co-4Re starting material appears to be slightly more amorphous than the H_2/N_2 and temperature programmed H_2/Ar post-reaction diffraction patterns.

The pattern of the Co-4Re material is similar to that obtained for the post-reaction H_2/N_2 Re_3N sample, in the fact that broad reflections are again observed centring around 40° 2θ. It is apparent that the H_2/N_2 and the temperature programmed H_2/Ar patterns are not dissimilar from the starting material with no obvious shifts to indicate changing unit cell volumes, although the intensities of reflections do increase which may possibly be due to the fact that the samples become crystalline upon application. All samples contain both Co and Re metal phases which are evident in Figure 3.4-9 and either indicated by a star or circle respectively.
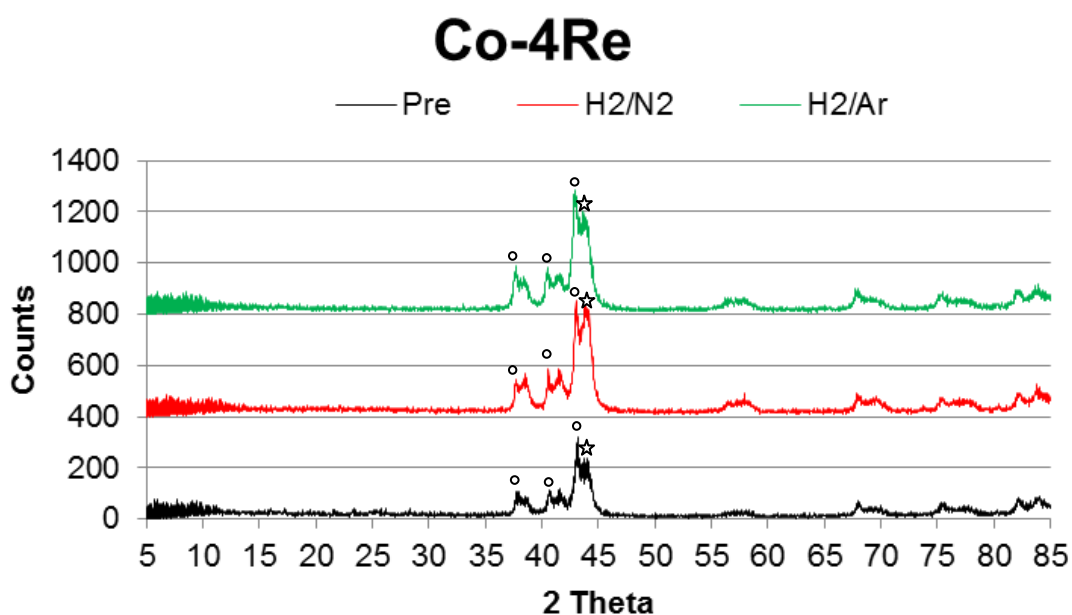
Figure 3.4-9 Pre- and Post-reaction XRD patterns of Co-4Re (Co ☆ , Re ○).

3.4.5 Ru/MgAl$_2$O$_4$ and BaRu/MgAl$_2$O$_4$.

Ruthenium is known to be an excellent catalyst for ammonia synthesis. [113-115, 242,243] Under moderate temperatures and pressures it is considerably more active than the commercial iron based catalyst. Various high surface area materials such as alumina, magnesia, zeolites, boron nitrides and activated carbon have all been investigated as supports for the ruthenium phase. The only ruthenium based catalyst to find industrial application is a promoted ruthenium catalyst supported on activated carbon, which was

commercialized by Kellogg in the mid 1980's.[129]   The unpromoted catalyst was found to be inactive in ammonia synthesis but activity dramatically increased on the addition of a promoter such as potassium, caesium or barium. Kowalczyk *et al* investigated the effect of alkali and barium promoters on a ruthenium catalyst supported on graphitized carbon.[251] It was found that barium enhanced ammonia synthesis activities on the catalyst but by which effect (structural or electronic) was unclear and there is much debate within this area.[113,251]   Within the Russian literature, there is further evidence to suggest that the addition of barium may be advantageous to ammonia synthesis activities. Studies by Panov and co-workers have found that barium nitride exhibits a high nitrogen isotopic exchange activity that is more than two orders of magnitude greater than either Fe or Ru when they are compared at 323 ^{o}C.[123,252]

In this work, Ru-based systems have only been investigated for comparative purposes. A number of supports were investigated, including MgO, BN, Al_2O_3 and $MgAl_2O_4$. Only the most active material has been presented for this reason.

3.4.5.1   Reaction Data.

As ruthenium based systems are only being studied for comparative purposes, temperature programmed H_2/Ar reactions were not investigated, as it was evident in the isothermal H_2/Ar reaction that there is a limited amount of ammonia produced. The ammonia which is apparently produced during this reaction may possibly be attributed to the hydrogenation of sorbed NH_x species residues which have accumulated during the pre-treatment phase of the reaction under H_2/N_2.   It is evident from Figures 3.4-10 and 3.4-11 that ruthenium based systems are highly active for catalytic ammonia synthesis. As has been referred to above, reports that low levels of barium dopants enhance the catalytic ammonia synthesis activity of ruthenium has been published.   However, from the results presented in Table 3.4-9 it would appear that the dopant levels of barium applied in fact slightly hinder the production of ammonia. This was also the case for other supports that were studied. Studies by Hansen *et al* have suggested that the effect of barium promotion is location sensitive, and dependent on the relative affinities of the promoter for either the support or the metal.[253] Despite this the rate of ammonia production remains much higher than that of the other materials investigated in this work.
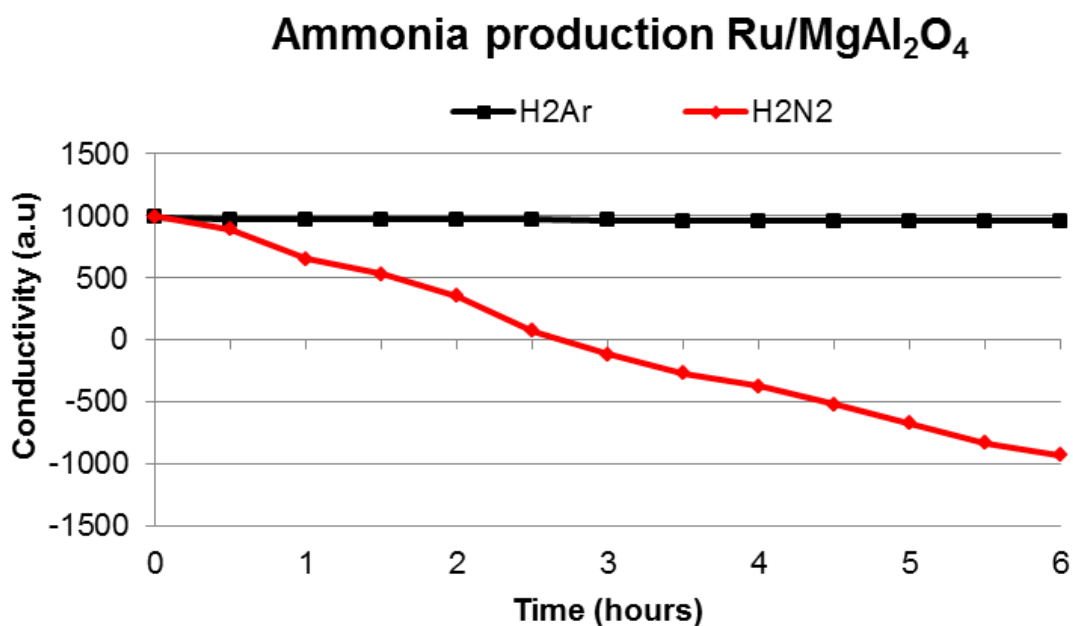
Figure 3.4-10 Comparison of conductivity for 5 % Ru/ MgAl$_2$O$_4$ ammonia production using H$_2$/N$_2$ vs. H$_2$/Ar at 400 ^{o}C.
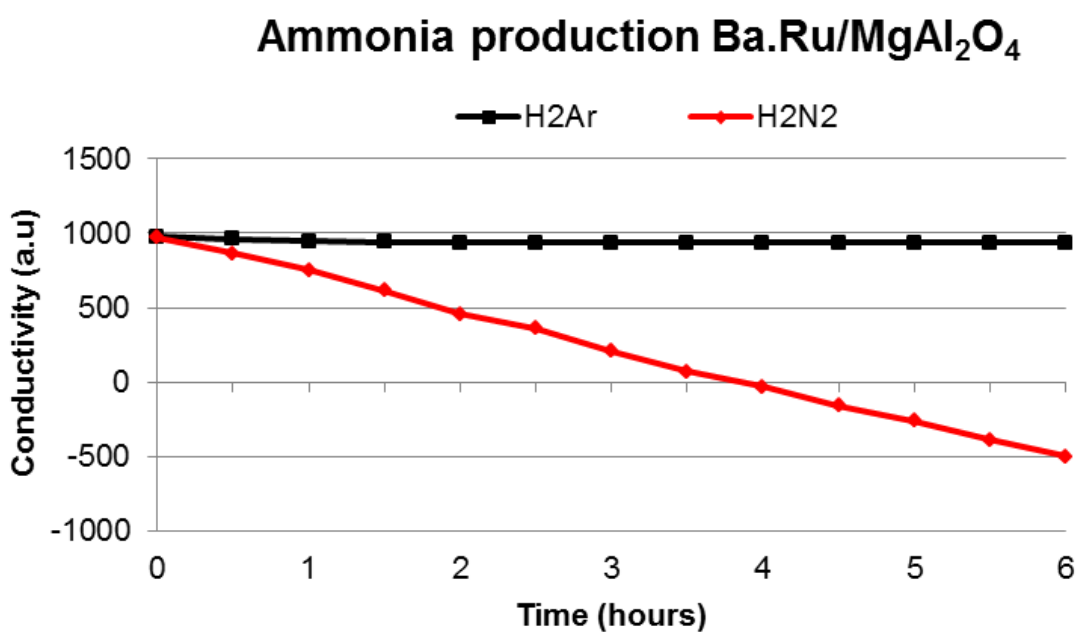
Figure 3.4-11 Comparison of conductivity for Ba.Ru/MgAl$_2$O$_4$ ammonia production using H$_2$/N$_2$ vs. H$_2$/Ar at 400 ^{o}C.

Sample and Reaction Conditions	NH$_3$ Production Rate (μmol h^{-1} g^{-1})	
	Ru/MgAl$_2$O$_4$	Ba.Ru/MgAl$_2$O$_4$
400 ^{o}C (H$_2$/N$_2$, 0.0-0.5 h)	467	480
400 ^{o}C (H$_2$/N$_2$, 1.0-6.0 h)	710	562
400 ^{o}C (H$_2$/Ar, 0.0-0.5 h)	62	63
400 ^{o}C (H$_2$/Ar, 1.0-6.0 h)	6	4

Table 3.4-9 Ammonia production rates of Ru/MgAl$_2$O$_4$ and Ba.Ru/MgAl$_2$O$_4$ under both H$_2$/Ar and H$_2$/N$_2$ at 400 ^{o}C.

3.4.5.2 XRD Patterns.

Diffraction patterns of the unpromoted ruthenium catalyst largely resemble the support material, which itself corresponds to MgAl$_2$O$_4$. Additionally due to the amorphous appearance of the material, it is hard to unambiguously assign ruthenium metal reflections, with prominent reflections occurring at approximately 43° and 62° 2θ. Despite this, reflections at these 2θ values appear to grow in intensity in the post-reaction samples and may possibly be a result of agglomeration of Ru metal.
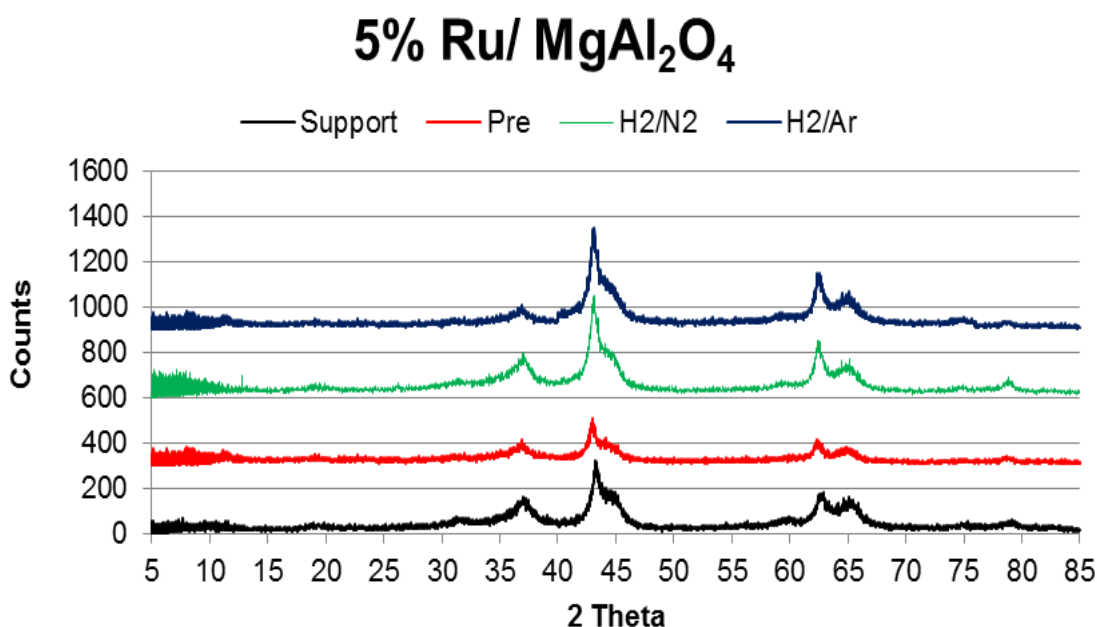
Figure 3.4-12 Pre- and Post-reaction XRD patterns of 5 % Ru/MgAl$_2$O$_4$. (JCPDS 0021-1152 and 033-0853 MgAl$_2$O$_4$).

Again in the promoted ruthenium samples, the pre- and post- reaction diffraction patterns are almost identical to that of the support. However, additional reflections are observed at

25 $^{\circ}$ and 26 $^{\circ}$ 2θ in some cases.   These reflections are difficult to assign with any degree of certainty and may either be Ba metal or Ba_3N_2 both of which have reflections centring on 25 $^{\circ}$ and 26 $^{\circ}$ 2θ.
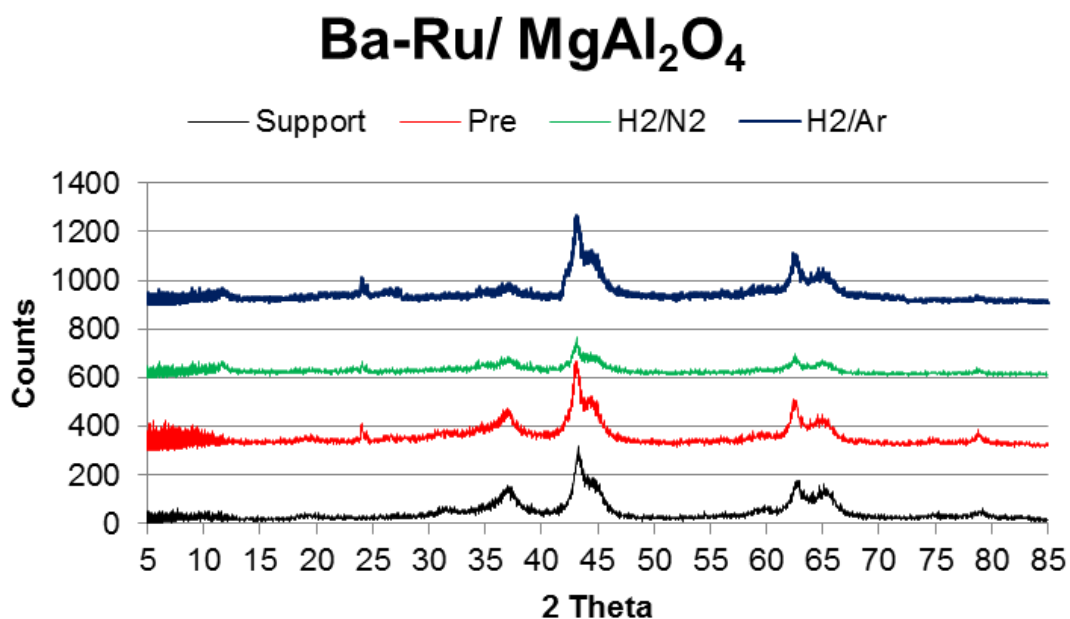
Figure 3.4-13 Pre- and Post-reaction XRD patterns of Ba-5 % Ru/MgAl$_2$O$_4$.

The diffraction pattern of the sample treated with H_2/N_2 appears to be more amorphous than either the pre- reaction sample or the sample treated under isothermal H_2/Ar conditions. This would suggest that there is more disorder within the material.

3.4.6 Summary Miscellaneous Systems.

Tables 3.4-10 and 3.4-11 give a summary of the nitrides investigated within this section, with ammonia production rates under selected conditions are presented in Table 3.4-10 whilst Table 3.4-11 presents the nitrogen content pre- and post-reaction of each material as well as the surface areas of the pre-reaction material.

3.4.6.1 Summary of Ammonia Production Rate.

Material	NH$_3$ Production Rate (μmol h^{-1} g^{-1})		
	H$_2$/N$_2$, 400 ^{o}C 1-6 h.	H$_2$/N$_2$, 400 ^{o}C, 0.5 h	H$_2$/Ar, 400 ^{o}C, 0.5h
Mg$_3$N$_2$	190	481	323
TiFe$_2$N$_x$	16	135	67
Co-4Re	472	747	44
Ru/ MgAl$_2$O$_4$	710	467	108
Ba.Ru/ MgAl$_2$O$_4$	562	480	63

Table 3.4-10 Summary of NH$_3$ production rates for the miscellaneous systems

3.4.6.2   Summary Pre/Post-Reaction N Data and Surface Areas.

Material	BET Surface Area (m^2 g^{-1})	Nitrogen Content (wt.%)			
		Calculated Stoichiometric	Pre-reaction	Post-reaction (H$_2$/Ar) 700°C	Post-reaction (H$_2$/N$_2$) 400°C
Mg$_3$N$_2$	6	27.74	23.50	14.10	19.80
TiFe$_2$N$_x$	13	4.44-11.22	1.30	0.94	1.09
Co-4Re	5	0	0	0	0
Ru/MgAl$_2$O$_4$	123	0	0	0	0
Ba.Ru/ MgAl$_2$O$_4$	111	0	0	0	0

Table 3.4-11 Summary of pre- and post-reaction nitrogen content, and surface area of pre-reaction samples for miscellaneous systems.

3.5 Summary

In this chapter the reactivity of lattice nitrogen over a range of nitride materials and was established via the comparison of ammonia synthesis activities using stoichiometric H$_2$/N$_2$ mixtures with H$_2$/Ar mixtures. The activities of these materials were subsequently

compared to a supported Ru catalyst, known to be one of the most active systems for ammonia synthesis.   Figure 3.5-1 illustrates the nitrides which have been investigated.

These studies have been conducted in order to establish which nitride materials would be suitable for participation in the proposed Mars-van Krevelen reaction. On the basis of the likely reactivity of benzene, 400 ^{o}C seems a probable upper limit for the target process, so it is therefore necessary for the potential candidate systems to either de-nitride at or below 400 ^{o}C or to exhibit the ability to form ammonia at this temperature. It was evident that on moving left to right along the transition metals that the corresponding nitrides became more thermally unstable, which could in theory prove to be advantageous in the development of a novel nitrogen transfer reagent. The adsorption-desorption cycle could be conducted at different temperature in separate steps thus possibly overcoming any thermodynamic and kinetic limitations imposed.

1 H																	2 He
3 Li	4 Be		Atomic Number SYMBOL									5 B	6 C	7 N	8 O	9 F	10 Ne
11 Na	12 Mg											13 Al	14 Si	15 P	16 S	17 Cl	18 Ar
19 K	20 Ca		21 Sc	22 Ti	23 V	24 Cr	25 Mn	26 Fe	27 Co	28 Ni	29 Cu	30 Zn	31 Ga	32 Ge	33 As	34 Se	35 Br	36 Kr
37 Rb	38 Sr		39 Y	40 Zr	41 Nb	42 Mo	43 Tc	44 Ru	45 Rh	46 Pd	47 Ag	48 Cd	49 In	50 Sn	51 Sb	52 Te	53 I	54 Xe
55 Cs	56 Ba	* 57-70	71 Lu	72 Hf	73 Ta	74 W	75 Re	76 Os	77 Ir	78 Pt	79 Au	80 Hg	81 Tl	82 Pb	83 Bi	84 Po	85 At	86 Rn
87 Fr	88 Ra	** 89-102	103 Lr	104 Rf	105 Db	106 Sg	107 Bh	108 Hs	109 Mt	110 Uun	111 Uuu	112 Uub		114 Uuq				

Figure 3.5-1 Periodic Table displaying the metal nitrides and metals of the alloys which have been investigated in this chapter.

Figure 3.5-2 illustrates the ammonia formation rates exhibited by the various materials in the initial 30 minutes on stream and the rate thereafter.
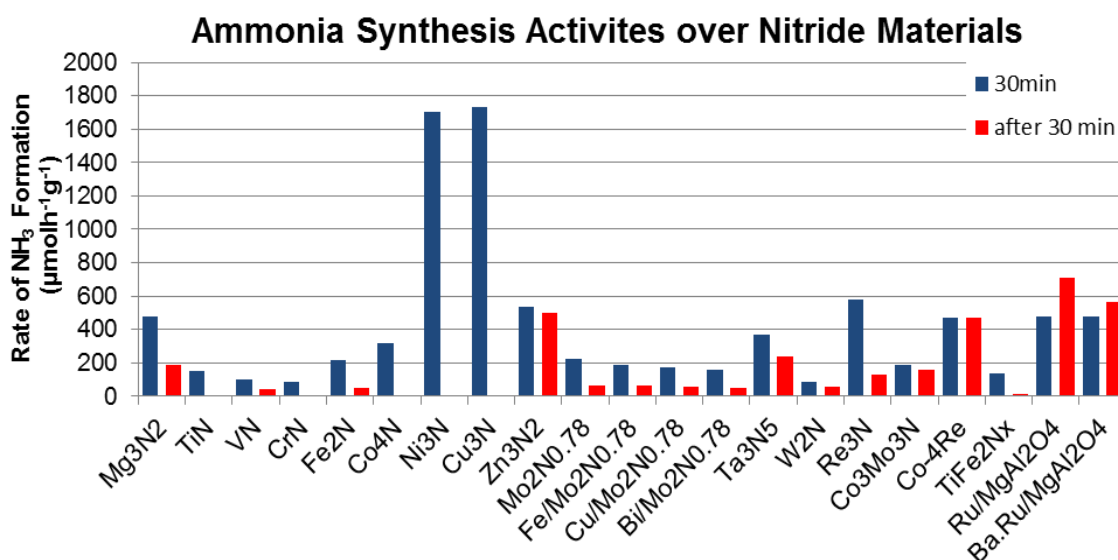
Figure 3.5-2 H$_2$/N$_2$ ammonia production rates over a range of different materials which have been investigated within this chapter. (Blue) initial 30 minutes on stream (Red) after initial 30 minutes.

It is evident that both nickel and copper nitrides exhibit a much higher rate of ammonia formation in the first 30 minutes on stream than any of the other materials investigated. However, it is apparent that this activity is not sustained and the reaction rapidly ceases. Attempts to stabilise these materials proved ineffective. Of the first row transition series, zinc nitride appears to be a promising candidate exhibiting ammonia synthesis rates almost comparable to ruthenium. However, this material also decomposes upon reaction. Vanadium and iron are the only the only two nitrides of the first transition metal series which exhibit a sustainable ammonia synthesis activity. Despite this, their activities however these are much lower than the activities found for the ruthenium-based systems. It is also apparent that the only 'comparable' ammonia synthesis activities to Ru are those which are exhibited by Zn$_3$N$_2$ and Co-4Re.

The introduction of iron as a dopant was shown to have a slight promotional effect on the ammonia synthesis activity of β-Mo$_2$N$_{0.78}$. Tantalum, tungsten and rhenium nitrides all exhibit sustainable ammonia synthesis activity at 400 ^{o}C under H$_2$/N$_2$. Alloyed Co-4Re exhibits a very high ammonia synthesis activity, albeit not as active as investigated ruthenium systems.

It is clear from the data presented that nitrogen can be removed from these materials at high temperatures under hydrogen. It is interesting to note that using a specific temperature profile only nitrides of the later metals of the Periodic Table are found to decompose fully to the pure metal. All other post-reaction materials retained nitrogen and the XRD patterns

either showed that no apparent structural change had occurred within the material, i.e. in the case of TiN, VN and CrN, or that the material contained a mixture of constituent metal and nitrided species. Nevertheless, the loss of nitrogen, and therefore its potential to be employed in nitrogen transfer reactions is evident. Despite the vast excess of hydrogen in the gas-phase, the nitrogen which is lost from these materials predominantly occurs in the form of N_2.

However, in order to function as a nitrogen transfer reagent, it is essential that the nitrogen which is depleted from the nitride, upon reaction, is subsequently restored.   Figure 3.5-3 illustrates the systems which demonstrated a loss of nitrogen, upon reaction, within this chapter (highlighted blue) and which will be further described for possible re-nitridation in the next chapter.

1 H																	2 He
3 Li	4 Be			Atomic Number SYMBOL								5 B	6 C	7 N	8 O	9 F	10 Ne
11 Na	12 Mg											13 Al	14 Si	15 P	16 S	17 Cl	18 Ar
19 K	20 Ca		21 Sc	22 Ti	23 V	24 Cr	25 Mn	26 Fe	27 Co	28 Ni	29 Cu	30 Zn	31 Ga	32 Ge	33 As	34 Se	35 Br	36 Kr
37 Rb	38 Sr		39 Y	40 Zr	41 Nb	42 Mo	43 Tc	44 Ru	45 Rh	46 Pd	47 Ag	48 Cd	49 In	50 Sn	51 Sb	52 Te	53 I	54 Xe
55 Cs	56 Ba	* 57-70	71 Lu	72 Hf	73 Ta	74 W	75 Re	76 Os	77 Ir	78 Pt	79 Au	80 Hg	81 Tl	82 Pb	83 Bi	84 Po	85 At	86 Rn
87 Fr	88 Ra	** 89-102	103 Lr	104 Rf	105 Db	106 Sg	107 Bh	108 Hs	109 Mt	110 Uun	111 Uuu	112 Uub		114 Uuq				

Figure 3.5-3 Periodic Table highlights in blue the nitride materials which lose nitrogen upon heat treatment and will be further investigated.

4. Re-nitridation Studies.

4.1 Introduction.

A major aim of this study was to investigate direct N transfer from nitride lattices to substrate and hence the potential capacity for the materials to act as nitrogen transfer reagents.   However, in order to function as a nitrogen transfer reagent, it is essential that the nitrogen which is depleted from the nitride, upon reaction, is subsequently restored.

As previously discussed in Chapter 3, this type of mechanism is frequently encountered in oxidation catalysis via metal oxides. However to date very little attention has been directed to nitrogen analogues. The only examples can be found in the work of Itoh and co-workers, which have been previously been discussed in Chapter 3,[90-92] and by Gregory and co-workers, in which, the ternary nitride Co_3Mo_3N was reported to reversible lose and take up nitrogen under similar reaction conditions to those described in this thesis.[126]

The systems which have been studied in this chapter are of significant interest as they were found to either lose a significant amount of nitrogen or reduce completely to the corresponding metal upon reaction at 400 ^{o}C or below (400 ^{o}C being the maximum temperature for the envisaged nitrogen transfer process). However if these materials were found to be active in the synthesis of aniline, it would be necessary for the nitrides to be subsequently restored to their original phase in order to be cyclically operated.

As was discussed by Wise and Markel, it is preferable to apply H_2/N_2 mixtures rather than NH_3 for the nitridation of materials for large scale applications.[41] Accordingly within this chapter regeneration of depleted nitrides using NH_3 and H_2/N_2 is discussed in relation to the number of select nitrided systems identified at the end of Chapter 3.

4.2 Results and Discussion.

As mentioned above, re-nitridation of materials is a fundamental issue associated with the envisaged nitrogen transfer process. From an industrial perspective it would be preferable to nitride or re-nitride under N_2 alone; however this has inherent problems due to the relatively inert nature of N_2. With the exception of β-$Mo_2N_{0.78}$, all the materials were prepared under ammonia and therefore initial re-nitridation studies were conducted in ammonia. Table 4.2-1 lists the materials which have been examined for re-nitridation

under NH_3 and H_2/N_2 following de-nitridation by high temperature H_2/Ar treatment, as described in Chapter 3.

Material	Restoration of nitrogen dificient materials in different nitriding atmospheres.	
	NH_3	H_2/N_2
VN	Yes	No
Fe_2N	Yes – partially	No
Co_4N	No	No
Ni_3N	Yes-partially	No
Cu_3N	No	No
Zn_3N_2	Yes-partially	No
Ta_3N_5	Yes	No
$\beta\text{-}Mo_2N_{0.78}$	-	Yes
Fe/ $\beta\text{-}Mo_2N_{0.78}$	-	Yes
Cu/ $\beta\text{-}Mo_2N_{0.78}$	-	Yes
W_2N	Yes	No
Re_3N	Yes – partially	No

Table 4.2-1 Summary Table indicating the results obtained from studies to restore nitrogen deficient nitrides following de-nitridation by to high temperature H_2/Ar treatment.

4.2.1 VN.

Vanadium nitride has been shown to be one of the more active binary nitrides for ammonia production at 400 ^{o}C - the maximum operating temperature for the target process, as described in Chapter 3. However subsequent nitrogen analysis indicated that a significant amount of nitrogen was lost upon reaction (approximately 25 % of the initial nitrogen content) and appeared to be independent of reaction conditions.

Despite this, vanadium nitride may potentially be active for similar nitrogen transfer applications. It is therefore necessary to investigate whether the nitrogen lost, upon reaction, can subsequently be replenished from a nitrogen source in keeping with the envisaged Mars-van Krevelen type process.

4.2.1.1 XRD Patterns.

As discussed in Chapters 3, cubic VN does not appear to undergo a significant phase change upon reaction as determined by XRD analysis. However V_2O_3 reflections (indicated by small stars) can be observed in the temperature programmed H_2/Ar diffraction pattern, which as previously mentioned, may occur on discharge of the material from the reactor. It is clear that the oxide is reduced under both NH_3 and H_2/N_2 due to the

absence of the oxide reflections being apparent in the diffraction patterns of re-nitrided samples. The diffraction patterns of the re-nitrided samples correspond well to the freshly prepared un-reacted VN sample with no reflection shifts being evident.
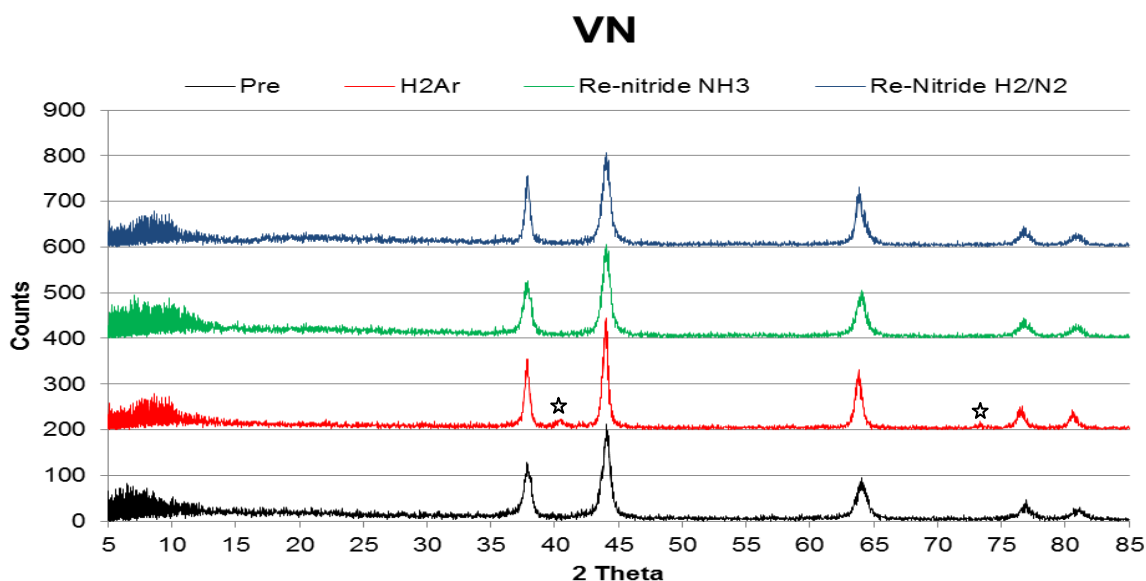
Figure 4.2-1 XRD patterns of pre- and post-temperature programmed H$_2$/Ar and re-nitrided VN samples. V metal ☆

4.2.1.2 Nitrogen Analysis.

In Chapter 3 it was shown from the conductivity versus time plots that a VN appeared to demonstrate steady state activity under H$_2$/N$_2$ at 400 ^{o}C. No sharp initial decrease in the conductivity value was observed, as had been with the other nitrides investigated and this was thought to be a result of the hydrogenation of surface NH$_x$ species.

It was also mentioned in Chapter 3, that the nitrogen lost from VN was relatively independent of reaction conditions with approximately the same amount of N being lost at either 400 ^{o}C or 700 ^{o}C. However as is evident from Table 4.2-2, there is a significant loss of nitrogen upon comparison of the pre-reaction and temperature programmed H$_2$/Ar sample. Upon treatment with H$_2$/N$_2$ under re-nitridation conditions, at 700 ^{o}C only a further limited nitrogen loss was observed, however this is within experimental error $\pm$ 0.03 wt.%. On the other hand, when nitrogen deficient VN is reacted in an ammonia atmosphere the lost nitrogen seems to be replaced and a nitrogen content closer to the stoichiometric value is achieved. However this is not apparent from the XRD analysis.

Sample and Reaction conditions	Calculated Stoichiometric N content (wt.%)	Pre-Reaction N Content (wt.%)	Post-Reaction N Content (wt.%)
VN (H$_2$/Ar) using temperature profile as shown in Fig. 3.2-2	21.55	18.39	14.06
VN re-nitridation NH$_3$ (700 ^{o}C, 3 h)	21.55	14.06	19.36
VN re-nitridation H$_2$/N$_2$ (700 ^{o}C, 3 h)	21.55	14.06	14.01

Table 4.2-2 Nitrogen content of pre-, post-temperature programmed H$_2$/Ar and re-nitrided VN samples.

4.2.2 Fe$_2$N.

Within this study iron nitrides appear to be promising candidates for nitrogen transfer reactions, due to the fact the nitrogen is evolved from the metal lattice at the temperatures of interest, specifically between 250 and 400 ^{o}C.

4.2.2.1 XRD Patterns.

From the temperature programmed H$_2$/Ar studies that were conducted in Chapter 3, it was shown that Fe$_2$N partially decomposed into a mixture of Fe metal and the lower iron nitride phase, Fe$_4$N, as indicated in Figure 4.2-2 by a triangle or square respectively. The nitrogen deficient phase was subsequently reacted at 500 ^{o}C (the original preparation temperature) under NH$_3$ and H$_2$/N$_2$, in an attempt to restore the nitrogen content in the post-H$_2$/Ar sample.

The XRD pattern of the sample re-nitrided under a H$_2$/N$_2$ atmosphere shows no significant difference when compared to the nitrogen deficient H$_2$/Ar sample, although a small reflection at approximately 25.3 ^{o} 2θ, possibly corresponding to Fe$_2$O$_3$ is evident. This could be a result of aerobic oxidation upon discharge of the material from the reactor.
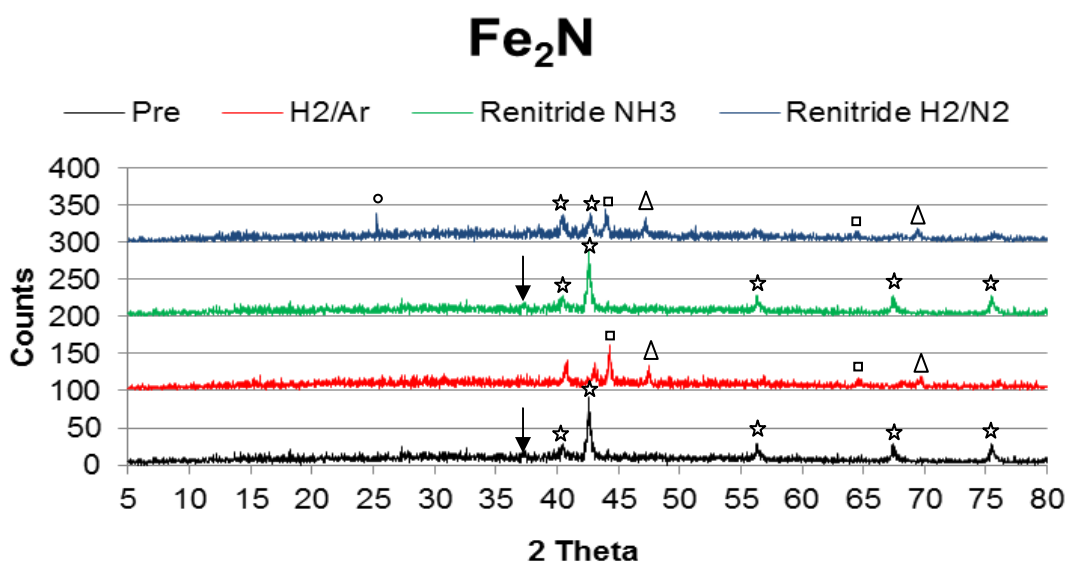
Figure 4.2-2 XRD patterns of pre-, post-temperature programmed H$_2$/Ar and re-nitrided Fe$_2$N samples. (Fe$_2$N ☆; Fe$_2$O$_3$ ○; Fe$_4$N △ ; Fe □).

However under a NH$_3$ feed gas, the nitrogen deficient sample appears to take-up nitrogen to restore the original Fe$_2$N phase, again with trace Fe$_3$N impurity being evident at approximately 37.5 $^\circ$ 2θ (indicated by an arrow in Figure 4.2-2).

Jack and Goodeve documented that iron nitrides could be prepared from direct reaction of the Fe metal under a H$_2$/N$_2$ gas mixture.[102,103] However from the studies documented within this thesis, both in the original preparation route and also in the re-nitridation studies, this has proved to be a relatively difficult method to synthesise Fe$_2$N and it may only be possible to achieve the nitride via this route under pressure.

However, it is also important to note that, as with the de-nitrided samples described in Chapter 3, the backgrounds of all samples are largely amorphous and any nitrogen which has been taken up under re-nitridation conditions may not be apparent by XRD, particularly in the case of the sample re-nitrided under H$_2$/N$_2$, as discussed in the following section.

4.2.2.2 Nitrogen Analysis.

Inspection of the data presented in Table 4.2-3 highlights that although full restoration of the original phase is not achieved under either re-nitridation conditions, a gain of nitrogen is apparent in both cases, albeit limited in the case of H$_2$/N$_2$. Additional re-nitridation studies were conducted at various temperatures, in the case of H$_2$/N$_2$, in an attempt to increase the nitrogen content in the sample. However, it was found that on increasing the

temperature the nitrogen content decreased. This could possibly be attributed to the temperatures at which the various phases of iron nitride begin to decompose to lower nitride phases and iron metal. This would indicate that higher nitride phases such as Fe_2N are only formed within a narrow temperature range making them difficult to re-nitride under H_2/N_2 gas mixtures.

On the other hand Fe_2N is partially restored to the original nitrogen composition under an ammonia atmosphere, with a nitrogen content of 6.95 wt. % compared to the original 8.59 wt.% found in the un-reacted sample. Again, as was discussed in Chapter 3, this is much closer to the stoichiometric value for Fe_3N (7.71 wt.%). However the reflections observed in the powder XRD analysis suggested that Fe_2N was formed, Figure 4.2-2.

Sample and Reaction conditions	Calculated Stoichiometric N content (wt.%)	Pre-Reaction N Content (wt.%)	Post-Reaction N Content (wt.%)
Fe_2N (H_2/Ar) using temperature profile as shown in Fig. 3.2-2	11.13	8.59	2.40
Fe_2N re-nitridation NH_3 (500 ^{o}C, 6 h)	11.13	2.40	6.95
Fe_2N re-nitridation H_2/N_2 (500 ^{o}C, 6 h)	11.13	2.40	2.57

Table 4.2-3 Nitrogen content of pre-, post-temperature programmed H_2/Ar and re-nitrided Fe_2N samples.

4.2.3 Co$_4$N.

As was discussed in Chapter 3, cobalt nitride was much more difficult to synthesise than originally envisaged. It was found that the nitride formed only within a very narrow temperature range and reaction dwell time.

Co_4N is found to rapidly decompose to Co metal, and only a limited amount of the lattice nitrogen (*ca.* 5.6%) was found to react to produce ammonia in the H_2/N_2 and H_2/Ar studies, with a significant amount being lost as N_2. Despite this, Co_4N was further investigated in benzene reactions, due to the relatively low temperature at which decomposition to Co metal occurred.

4.2.3.1 XRD Patterns.

As discussed in preceding chapters, the reflections associated with Co metal and Co_4N are almost identical making identification of phases rather difficult by XRD analysis alone.

However when combined with post-reaction nitrogen analysis, Table 4.2-3, it can be concluded that the nitride, Co_4N, does not reform under NH_3 or a H_2/N_2 gas mixtures, therefore the reflections observed in Figure 4.2-3 correspond to Co metal.
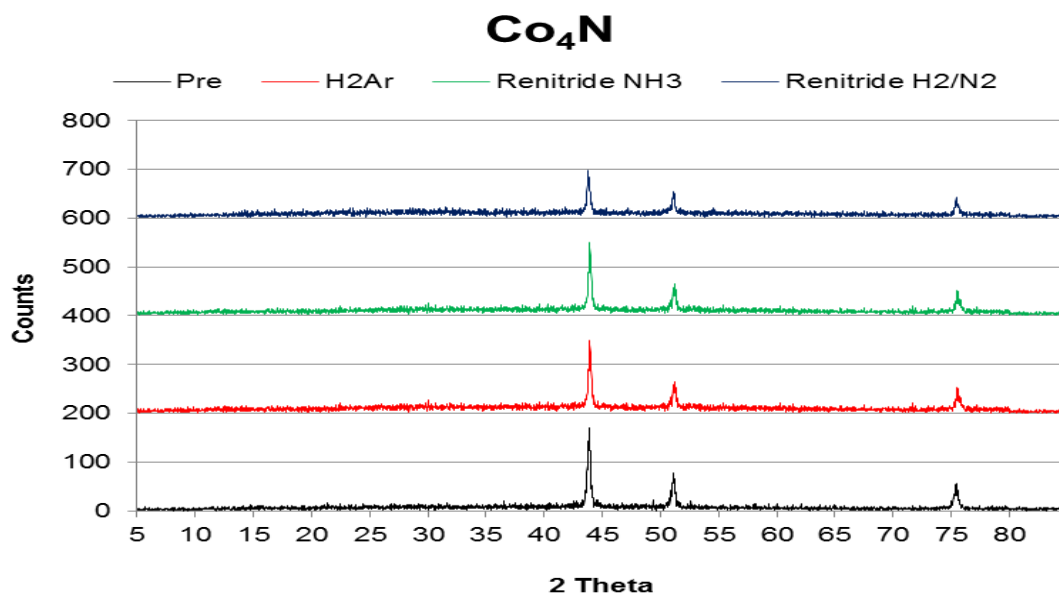
Figure 4.2-3 XRD patterns of pre-, post-temperature programmed H_2/Ar and re-nitrided Co_4N samples.

4.2.3.2 Nitrogen Analysis.

The pre-reaction sample contains a lower amount of nitrogen than the calculated stoichiometric value, as shown in Table 4.2-4. However this material was extremely difficult to prepare, and was constrained to very narrow synthesis conditions, requiring a specific temperature and time of formation, as outlined in Chapter 3. As anticipated on this basis no nitrogen is present in the samples which have undergone attempts to restore the nitrogen content, as confirmed by post-reaction analysis. This may be directly related to the inherent difficulties which were associated with the initial preparation of Co_4N which could only be synthesised within narrow temperature and time limits, as described in Chapter 3. Additionally since Co_4N reduces completely, Co metal is the starting point for re-nitridation, as opposed to the oxide which was used in the synthesis of Co_4N. The direct nitridation of Co metal is more commonly associated with sputtering or laser deposition techniques rather than those methods which are used in this work.[211, 213, 254]

Sample and Reaction conditions	Calculated Stoichiometric N content (wt.%)	Pre-Reaction N Content (wt.%)	Post-Reaction N Content (wt.%)
Co$_4$N (H$_2$/Ar) using temperature profile as shown in Fig. 3.3-4	5.60	3.17	0
Co$_4$N re-nitridation NH$_3$ (700 ^{o}C 2 h)	5.60	0	0
Co$_4$N re-nitridation H$_2$/N$_2$ (700 ^{o}C 2 h)	5.60	0	0

Table 4.2-4 Nitrogen content of pre-, post-temperature programmed H$_2$/Ar and re-nitrided Co$_4$N samples.

4.2.4 Ni$_3$N.

From the H$_2$/N$_2$ and H$_2$/Ar studies which were reported in Chapter 3, it was found that Ni$_3$N exhibits a high ammonia production activity during the first 30 minutes on stream at 250 ^{o}C. This, however, was short lived and may possibly be a result of total decomposition of the nitride to Ni metal. Consequently efforts to re-nitride this material have been attempted.

4.2.4.1 XRD Patterns.

From the post-reaction diffraction data, presented in Figure 4.2-4, it is evident that upon re-nitridation with NH$_3$ and H$_2$/N$_2$, at 480 ^{o}C, the observed reflections largely correspond to Ni metal. However, in the case of the sample re-nitrided under NH$_3$ these appear to be shifted to a slightly lower Bragg angle, 51.48 ^{o} as compared to 51.60 ^{o} 2θ for the sample treated under temperature programmed H$_2$/Ar which may indicate the incorporation of a small amount of nitrogen within the lattice. Additionally, very weak reflections can be observed at approximately 39 ^{o}, 41 ^{o} and 58 ^{o} 2θ, which can be assigned to Ni$_3$N, albeit shifted to slightly higher Bragg angles when compared to the diffraction pattern of a freshly prepared unreacted sample. These shifts may possibly be as a result of the lower nitrogen content present in the re-nitrided sample, as confirmed by nitrogen analysis.
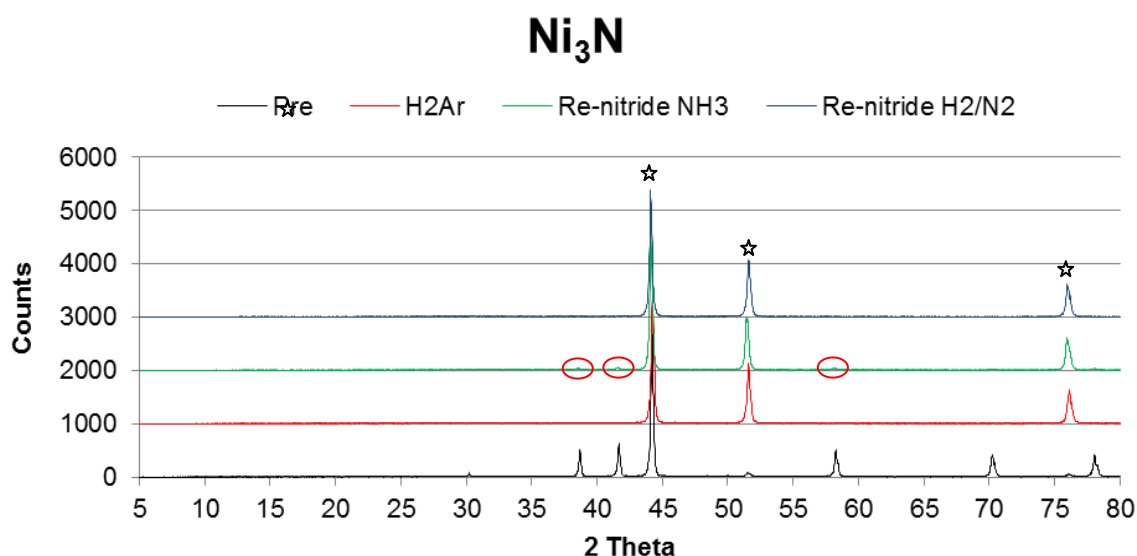
Figure 4.2-4 XRD patterns of pre-, post-temperature programmed H$_2$/Ar and re-nitrided Ni$_3$N samples. Ni metal is indcated by a ($\star$)

4.2.4.2 Nitrogen Analysis.

Samples were fully reduced to Ni metal prior to re-nitridation studies, as confirmed by XRD and elemental analysis as shown in Table 4.2-5. It is clear that the sample treated under a NH$_3$ atmosphere has partially re-nitrided, as was observed in the resultant diffraction pattern, with the nitrogen content increasing to 1.89 wt.% giving a stoichiometric value of Ni$_3$N$_{0.26}$. However, no apparent re-nitridation was observed for the sample treated under H$_2$/N$_2$. This was expected bearing in mind the sample decomposed to Ni metal at 250 ^{o}C in the H$_2$/N$_2$ study (Chapter 3).

Sample and Reaction conditions	Calculated Stoichiometric N content (wt.%)	Pre-Reaction N Content (wt.%)	Post-Reaction N Content (wt.%)
Ni$_3$N (H$_2$/Ar) using temperature profile as shown in Fig. 3.3-4	7.36	7.24	0
Ni$_3$N re-nitridation NH$_3$ (480 ^{o}C, 6 h)	7.36	0	1.89
Ni$_3$N re-nitridation H$_2$/N$_2$ (480 ^{o}C, 6 h)	7.36	0	0

Table 4.2-5 Nitrogen content of pre-, post-temperature programmed H$_2$/Ar and re-nitrided Ni$_3$N samples.

4.2.5 Cu$_3$N.

As was shown in the lattice nitrogen studies described in Chapter 3, copper nitride rapidly decomposes to copper metal when heated above 200 ^{o}C, resulting in 'holes' within the material, shown in the SEM micrographs presented in Chapter 3. As previously discussed these may be a result of sub-surface pockets of N$_2$ bursting out of the material upon heating. Previous studies in the literature document the formation of the nitride direct from the Cu metal; however, the resulting Cu from the studies conducted in Chapter 3, with this 'holed' appearance proved more difficult to re-nitride than implied.

In the case of Co$_3$Mo$_3$N, maintenance of the structure by partial de-nitridation may facilitate its regeneration. Hence partial de-nitridiation of Cu$_3$N was also attempted. As was described in Chapter 3, the loss of nitrogen from Cu$_3$N is a rapid process, however by partially de-nitriding Cu$_3$N using a lower concentration of H$_2$ (a 6% H$_2$/Ar gas mixture instead of a 3:1 H$_2$/Ar mixture) it may have been possible to restore the original nitrogen content by switching to either N$_2$ or H$_2$/N$_2$ gases after 20 minutes of H$_2$/Ar treatment. However, it did not prove possible to partially de-nitride the sample and copper metal resulted under all attempts made to do this. It may be possible that the loss of nitrogen from Cu$_3$N is sequential and once nitrogen removal is initiated it becomes independent of the reaction conditions until all nitrogen is removed and the nitride is subsequently reduced to Cu metal.

4.2.5.1 XRD Patterns.

In both NH$_3$ and H$_2$/N$_2$ re-nitridation studies, the resultant diffraction patterns are indicative of copper metal, as shown in Figure 4.2-5, and on visual inspection the samples were copper coloured.
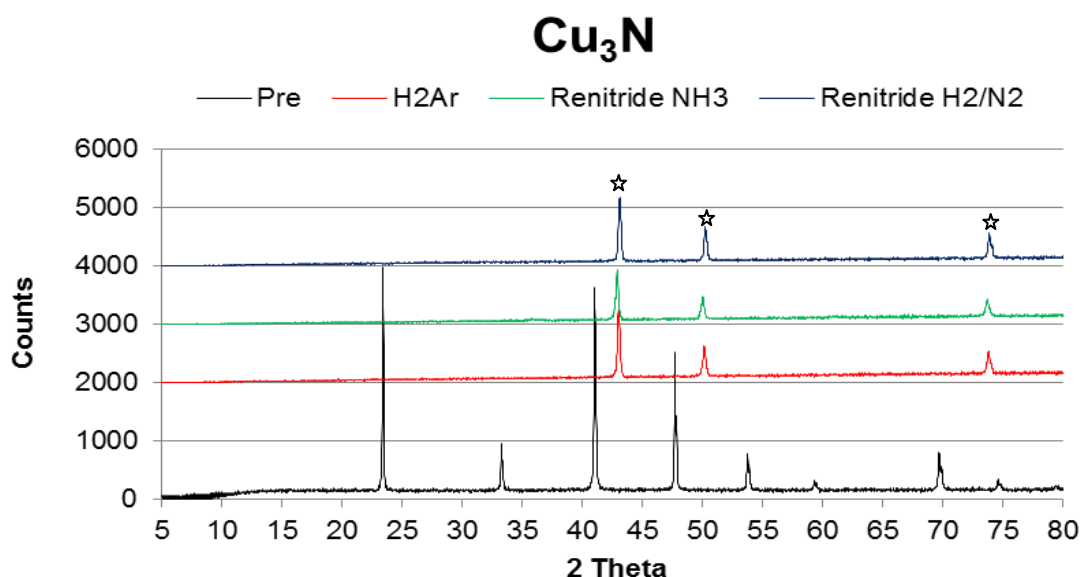
Figure 4.2-5 XRD patterns of pre-, post-temperature programmed H$_2$/Ar and re-nitrided Cu$_3$N samples. Cu metal is indacated by a (✰)

4.2.5.2 Nitrogen Analysis.

Table 4.2-6 presents the nitrogen content found in the temperature-programmed H$_2$/Ar sample and the re-nitrided samples via microanalysis. From Table 4.2-5 it is clear that nitrogen was not re-introduced into the metal lattice.

Sample and Reaction conditions	Calculated Stoichiometric N content (wt.%)	Pre-Reaction N Content (wt.%)	Post-Reaction N Content (wt.%)
Cu$_3$N (H$_2$/Ar) using temperature profile as shown in Fig. 3.3-4	6.84	6.63	0
Cu$_3$N re-nitridation NH$_3$ (300 ^{o}C, 6 h)	6.84	0	0
Cu$_3$N re-nitridation H$_2$/N$_2$ (300 ^{o}C, 6 h)	6.84	0	0

Table 4.2-6 Nitrogen content of pre-, post-temperature programmed H$_2$/Ar and re-nitrided Cu$_3$N samples.

4.2.6 Zn$_2$N$_3$.

Zinc nitride is potentially one of the more interesting nitrides which have been investigated in this work. It has been shown to be very active for the production of ammonia, albeit through its decomposition to zinc metal.

4.2.6.1 XRD Patterns.

As was previously discussed in Chapter 3, Zn_3N_2 appears to decompose to highly reactive Zn metal upon reaction, which subsequently oxidises on discharge resulting in the formation of ZnO, as confirmed by post-reaction XRD analysis. This is also apparent in Figure 5.2-6, in which the re-nitridation diffraction patterns correspond to ZnO (JCPDS 003-0888) with only trace levels of Zn_3N_2 being observed as evidenced by the presence of reflections at 43.3^o, 53.1^o and 71.2^o 2θ.

Both NH_3 and H_2/N_2 treated samples were run at 600 ^{o}C, which was temperature used for the initial synthesis of Zn_3N_2, as reported in Chapter 2.   From the XRD patterns presented in Figure 4.2-6 it is evident that the Zn reflections are not apparent in the samples treated under re-nitridation conditions, indicated by arrows in the nitrogen deficient sample. However, in the H_2/N_2 reaction sample no Zn_3N_2 reflections are observed, although they are apparent in the sample re-nitrided in NH_3, as indicated by a star in the diffraction pattern. This indicates that Zn_3N_2 becomes more fully reduced upon further heat treatment in a H_2 rich atmosphere, as confirmed with post-reaction elemental analysis, in which a further loss of N was observed.
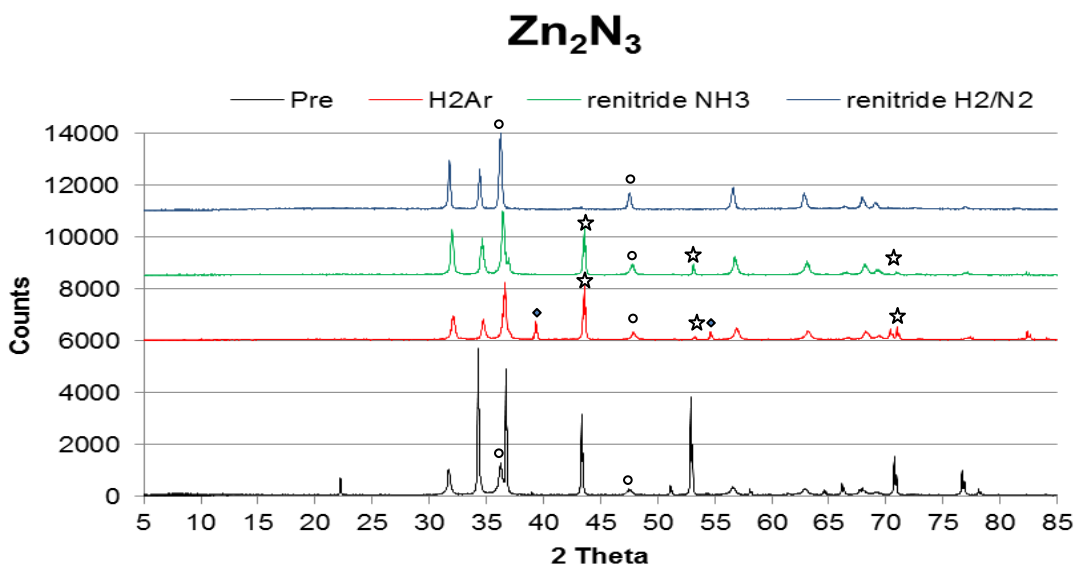
Figure 4.2-6 XRD patterns of pre-, post-temperature programmed H$_2$/Ar and re-nitrided Zn$_3$N$_2$ samples. Zn$_3$N$_2$ represented by a ✩ in H$_2$/Ar and re-nitrided diffraction patterns, Zn metal by a ⬦ and ZnO represented by ○

The reflection at approximately 36° 2θ in the diffraction pattern of the sample re-nitrided under NH_3 is slightly broader than that of the reflection observed at the same position in the post-H_2/Ar sample which may suggest that there is increased disorder within the

sample. A small ZnO reflection can be observed in the pre-reaction sample at 36° 2θ (indicated by a small circle) and it may be possible that the apparent broadening described above may be attributed to the overlap of Zn_3N_2 and ZnO reflections.

In the diffraction pattern of the sample re-nitrided under H_2/N_2, as previously mentioned, no apparent Zn_3N_2 or Zn reflections are evident. However the reflections which are observed correspond to ZnO, which occur as a result of aerobic oxidation of Zn metal upon discharge from the reactor.

4.2.6.2 Nitrogen Analysis.

On examination of the NH_3 and H_2/N_2 treated samples, it is evident that no significant amount of nitrogen has been incorporated back into the metal lattice, and in the case of the sample treated under H_2/N_2, almost total nitrogen loss has occurred. This may be a direct consequence of further exposure to heat treatment in a hydrogen rich atmosphere. This would also agree with the observed ZnO reflections evident in the diffraction pattern, Figure 4.2-6.

Sample and Reaction conditions	Calculated Stoichiometric N content (wt.%)	Pre-Reaction N Content (wt.%)	Post-Reaction N Content (wt.%)
Zn_3N_2 (H$_2$/Ar) using temperature profile as shown in Fig. 3.3-19	12.49	9.46	2.29
Zn_3N_2 re-nitridation NH_3 (600 ^{o}C, 6 h)	12.49	2.29	3.01
Zn_3N_2 re-nitridation H_2/N_2 (600 ^{o}C, 6 h)	12.49	2.29	0.86

Table 4.2-7 Nitrogen content of pre-, post-temperature programmed H$_2$/Ar and re-nitrided Zn$_3$N$_2$ samples.

From Table 4.2-7, it is clear that only a very small amount of nitrogen is replaced in the nitrogen deficient sample which has been reacted under NH_3 atmosphere, (an increase of 0.72 wt. %). This is much lower than the stoichiometric N content for Zn_3N_2. Studies employing shorter and longer reaction times were also conducted but the resultant nitrogen content in the samples was lower than that presented in Table 4.2-6.

4.2.7 Ta_3N_5.

From the H_2/N_2 and isothermal H_2/Ar studies for Ta_3N_5, described in Chapter 3, it was found that Ta_3N_5 displays a relatively high activity for ammonia production under H_2/N_2. However under H_2/Ar, ammonia production at 400 ^{o}C was limited to the first 90 minutes on stream.   Further temperature programmed studies indicated that the presence of H_2 in the feed stream results in a much more significant loss of nitrogen. The loss of nitrogen from Ta_3N_5 is generally accompanied by colour change in the sample which acts as a visual indicator to the loss of nitrogen. A similar colour change was also observed upon re-nitridation of the samples, as shown in Figure 4.2-7.
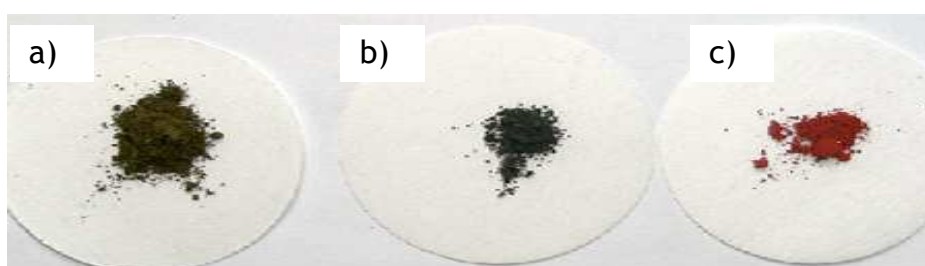
Figure 4.2-7 a) de-nitrided temperature programmed H_2/Ar b) re-nitrided H_2/N_2 c) re-nitrided NH_3

Samples from temperature programmed H_2/Ar studies were investigated for re-nitridation primarily due to the significant amount of nitrogen lost from the material during this process. It was found that upon re-nitridation in a H_2/N_2 atmosphere the colour of the sample changed from a khaki green to black, whereas in a NH_3 atmosphere the sample restored to the original red colour, implying the possibility of re-nitridation to the original phase, Ta_3N_5.

4.2.7.1 XRD Patterns.

Figure 4.2-8 presents the diffraction patterns obtained for pre-, post- temperature programmed H_2/Ar and re-nitrided reaction samples. Upon inspection of the diffraction patterns, it is noticeable that the sample re-nitrided under H_2/N_2 appears significantly different to the other diffraction patterns, which remain largely unchanged when compared to the pre-reaction pattern, although slight alterations in reflection widths can be observed in the H_2/Ar sample. The reflections observed in the re-nitrided H_2/N_2 sample correspond to TaON (JCPDS 020-1235) and are indicated by a star in Figure 4.2-8.

Furthermore in the case of the re-nitrided H_2/N_2 sample, it is apparent that there is an increase in the intensity of the background which is consistent with a greater content of amorphous phase.
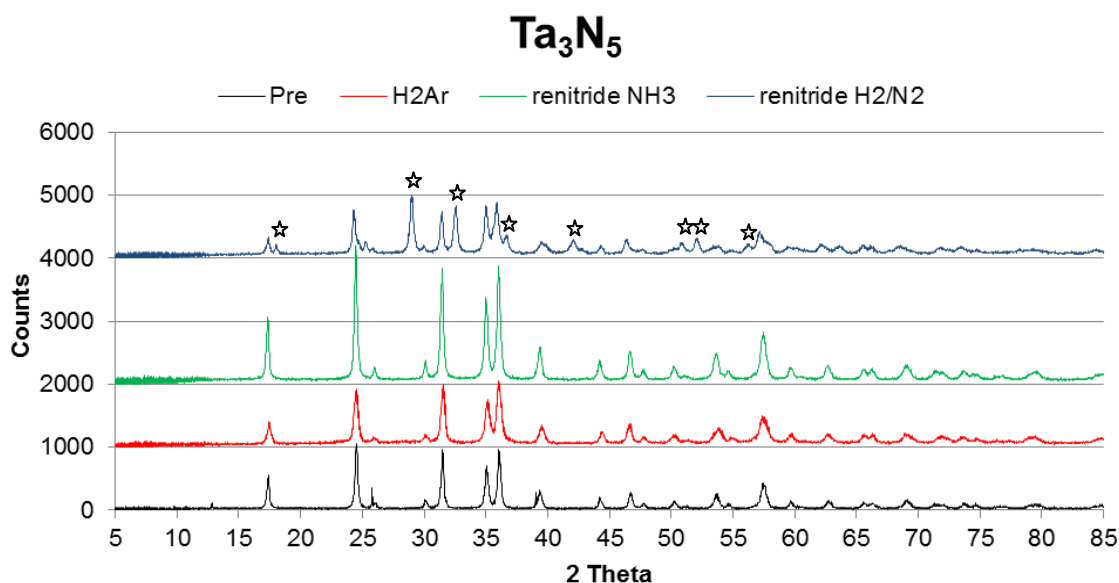
Figure 4.2-8 XRD patterns of pre-, post-temperature programmed H_2/Ar and re-nitrided Ta_3N_5 samples. TaON represented by a ☆ in H_2/N_2 re-nitrided diffraction pattern.

4.2.7.2 Nitrogen Analysis.

Attempts were made to restore the nitrogen content of the N-deficient Ta_3N_5 phase by treatment under H_2/N_2 and NH_3 and dwelling at 700 ^{o}C for 3 hours. The results of the post-reaction nitrogen analysis of the tantalum nitride samples studied under the conditions described in Chapter 3 are presented and compared with the post-reaction nitrogen contents of those "restored" materials in Table 4.2-8.

Sample and Reaction conditions	Calculated Stoichiometric N content (wt.%)	Pre-Reaction N Content (wt.%)	Post-Reaction N Content (wt.%)
Ta_3N_5 (H_2/Ar) using the temperature profile as shown in Fig. 3.2-2	11.42	11.23	7.83
Ta_3N_5 re-nitridation NH_3 (700 ^{o}C, 3 h)	11.42	7.83	11.19
Ta_3N_5 re-nitridation H_2/N_2 (700 ^{o}C, 3h)	11.42	7.83	6.49

Table 4.2-8 Nitrogen content of pre-, post-temperature programmed H_2/Ar and re-nitrided Ta_3N_5 samples.

It is clear that a further loss of nitrogen occurs under H_2/N_2 at 700 ^{o}C. This may possibly be a result of the longer heating times in a hydrogen environment, which may cause the material to become further reduced as well as the addition of oxygen as evident in Figure 4.2-8.

On the other hand, re-nitridation in ammonia results in the nitrogen content of the nitrogen deficient sample being almost totally restored after 3 hours at 700 ^{o}C, with respect to the pre-reaction sample, 11.19 and 11.23 wt. % respectively. This is both a much shorter reaction time and lower temperature than originally used to prepare the material (9 hours and 900 ^{o}C respectively). Hence the process of nitrogen loss / replenishment is fully reversible and the tantalum nitride can be readily regenerated at elevated temperature under NH_3.

4.2.8 β-Mo$_2$N$_{0.78}$.

Regardless of any application of β-Mo$_2$N$_{0.78}$ as a transfer reagent, re-nitridation is an important step following de-nitridation in order to restore the original phase. In previous studies of β-Mo$_2$N$_{0.78}$, Chapter 3, it has been observed that de-nitriding to produce Mo occurs readily but re-nitridation to restore β-Mo$_2$N$_{0.78}$ may be more difficult.

From previous investigations, as described in Chapter 3, it was found that both doped and un-doped β-Mo$_2$N$_{0.78}$ have comparable ammonia synthesis rates under H_2/N_2 at 400 ^{o}C and ambient pressure, although samples doped with Fe or Bi metal was observed to either marginally enhance or hinder the production of ammonia respectively.

Unlike the other materials in this study, β-Mo$_2$N$_{0.78}$ is prepared under H_2/N_2, rather than NH_3 which would result in the formation of γ-Mo$_2$N. For this reason, H_2/N_2 was the only re-nitridation gas employed for this system.

4.2.8.1 XRD Patterns.

As described in Chapter 3, the pre-reaction sample is consistent with the β-Mo$_2$N$_{0.78}$ phase, and was shown to fully reduce to the Mo metal with high temperature H_2/Ar treatment, as confirmed by post-reaction nitrogen analysis.

Although the original β-$Mo_2N_{0.78}$ phase is restored in the un-doped sample, it is noticeable that the reflections are slightly broader and less intense than that of the pre-reaction sample, indicating that there may possibly be greater degree of disorder within the sample.
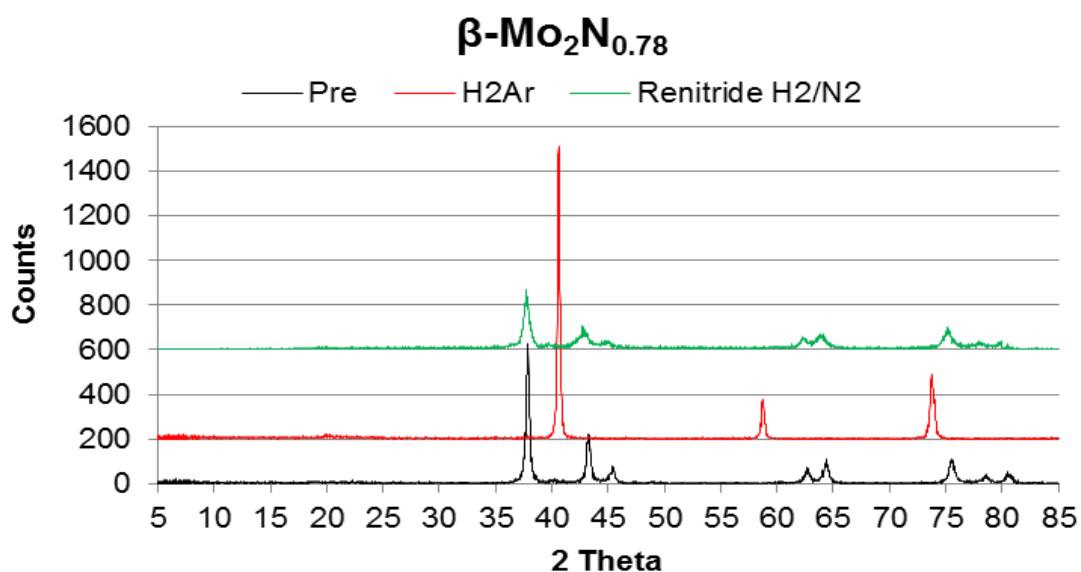
Figure 4.2-9 XRD patterns of pre-, post-temperature programmed H$_2$/Ar and re-nitrided β-Mo$_2$N$_{0.78}$ samples.

4.2.8.2 Nitrogen Analysis.

Table 4.2-9 indicates the pre- and post- reaction nitrogen contents within the β-$Mo_2N_{0.78}$ sample. As can be seen, the un-doped pre-reaction sample is comparable with the calculated stoichiometric values and it is evident that all nitrogen is removed from the sample upon reaction with H_2/Ar using the temperature profile described in Chapter 3.

As previously mentioned, the β-$Mo_2N_{0.78}$ phase is prepared under H_2/N_2 hence this was the only re-nitridation gas investigated to restore the nitrogen deficient sample. From the nitrogen data presented in Table 4.2-9 it is clear that the sample is almost totally retored to the original β-$Mo_2N_{0.78}$ at 700 ^{o}C with H_2/N_2.

Sample and Reaction conditions	Calculated Stoichiometric N content (wt.%)	Pre-Reaction N Content (wt.%)	Post-Reaction N Content (wt.%)
β-$Mo_2N_{0.78}$, (H_2/Ar) using temperature profile as shown in Fig. 3.2-2	5.38	5.58	0
β-$Mo_2N_{0.78}$, re-nitridation H_2/N_2 (700 ^{o}C, 3 h)	5.38	0	5.12

Table 4.2-9 Nitrogen content of pre-, post-temperature programmed H₂/Ar and re-nitrided β-Mo₂N₀.₇₈ samples.

4.2.9 W₂N.

In the initial H_2/N_2 and H_2/Ar studies at 400 ^{o}C W_2N showed promising potential as a nitrogen transfer reagent, primarily due to the almost steady production of ammonia under a H_2/N_2 feed gas as was illustrated in Chapter 3. In addition to this very little nitrogen was lost from the material under these conditions, in comparison to the H_2/Ar reactions.

4.2.9.1 XRD Patterns.

As discussed earlier, tungsten nitride can occur as cubic W_2N or as hexagonal WN phases. The samples prepared in this study corresponded to cubic W_2N. The observed reflections are particularly broad which would be indicative of materials with high surface area and small particle size and/or a large degree of disorder. As was shown in Chapter 3, tungsten nitride undergoes a partial decomposition to W metal under H_2/Ar at elevated temperatures, as indicated by a star in Figure 4.2-10. Due to the similarity between Mo and W it may have been reasonable to assume that it was possible to restore the original W_2N phase, under H_2/N_2, at 700 ^{o}C. However, as is evident from Figure 4.2-10, the W metal reflections become more apparent, and the nitrogen content decreases, as confirmed by post-nitrogen analysis. It is possible to almost completely restore the original phase under ammonia with no remaining W metal reflections being evident.
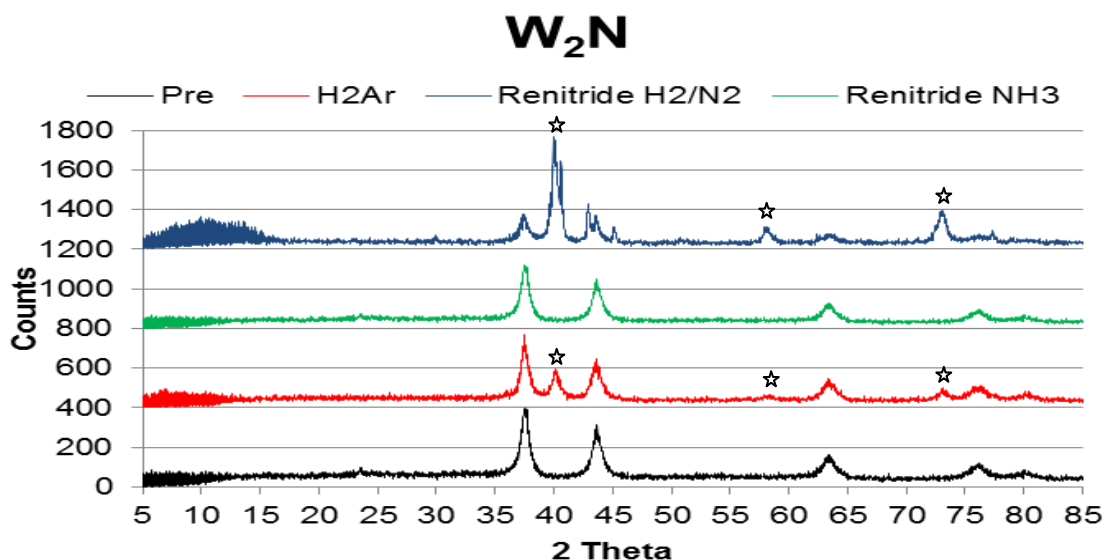
Figure 4.2-10 XRD patterns of pre-, post-temperature programmed H₂/Ar and re-nitrided W₂N samples. W metal represented by ☆

4.2.9.2 Nitrogen Analysis.

As has been previously discussed in the preceding chapter, the N content in the pre-reaction sample is relatively high with respect to the calculated stoichiometric value for W_2N and the N value is more representative of that expected from WN. However, the XRD reflections correspond to those of W_2N. It is evident that there is a significant loss of nitrogen from the material upon reaction with H_2/Ar using the temperature profile shown in Figure 3.2-2 (maximum of 700 ^oC). This is further supported by the occurrence of W metal in the post-H_2/Ar XRD pattern, confirming that lattice nitrogen is lost from the material to some extent.

A further loss of nitrogen is apparent from the sample in which re-nitridation has been attempted under H_2/N_2. This may possible be a result of the excess hydrogen present in the gas mixture causing the material to become further reduced. Again this is in agreement with the observed diffraction pattern in which the W metal reflections become more intense. Conversely under a NH_3 atmosphere the nitrogen content is almost totally restored to that of the pre-reaction material.

Sample and Reaction conditions	Calculated Stoichiometric N content (wt.%)	Pre-Reaction N Content (wt.%)	Post-Reaction N Content (wt.%)
W_2N (H_2/Ar) using temperature profile as shown in Fig. 3.2-2	3.66	6.13	4.18
W_2N re-nitridation NH_3 (700 ^{o}C, 3 h)	3.66	4.18	5.89
W_2N re-nitridation H_2/N_2 (700 ^{o}C, 3 h)	3.66	4.18	2.17

Table 4.2-10 Nitrogen content of pre-, post-temperature programmed H_2/Ar and re-nitrided W_2N samples.

4.2.10 Re₃N.

Aika and Kojima investigated Re_3N as an ammonia synthesis catalyst, comparing it with Re metal to determine whether the formation of the nitride was beneficial.[59] In that study it was reported that the initial ammonia synthesis activity was very high but the reaction subsequently subsides after 2 hours on stream. From the work presented in this thesis, rhenium nitride has been shown to exhibit production of ammonia with the H_2/N_2 feedstream at 400 ^{o}C. However, it was confirmed by both XRD and post-reaction nitrogen analysis, that the Re_3N decomposes upon reaction. It is possible that the Re_3N does not fully reduce to Re metal, as proposed in the literature but decomposes to a lower nitride phase, possibly Re_4N, although this phase has not been previously reported within the literature.

As mentioned above, rhenium nitride decomposes upon reaction and there is a significant amount of nitrogen lost when reaction is undertaken under both H_2/N_2 and H_2/Ar gas mixtures at 350 ^{o}C. The isothermally H_2/Ar reacted sample has been used to investigate the effect of re-nitridation under NH_3. NH_3 was the only regeneration gas investigated in this section of work due to the fact that H_2/N_2 reaction was observed to reduce the nitride, as described in Chapter 3.

4.2.10.1 XRD Patterns.

The Re_3N starting material appears to be largely amorphous with a very broad reflection centring upon 40 ^{o} 2θ. This is in accordance with the previously mentioned studies of Aika and Kojima as discussed previously in Chapter 3. Under H_2/Ar at 350 ^{o}C for 6 hours, almost total de-nitridation is apparent. Crystalline Re metal albeit with shifts, reflections

are evident in the post-reaction XRD pattern, Figure 4.2-11, which as postulated, may arise from formation of a lower nitride phase such as Re_4N.

Upon subsequent reaction in NH_3, it is apparent from the diffraction pattern that the material partially re-nitrides as shown in Figure 4.2-11, and a mixture of Re reflections (again shifted) and the original broad reflection are evident. This diffraction pattern is similar to those which have partially de-nitrided, as in the case of the temperature programmed H_2/Ar study.
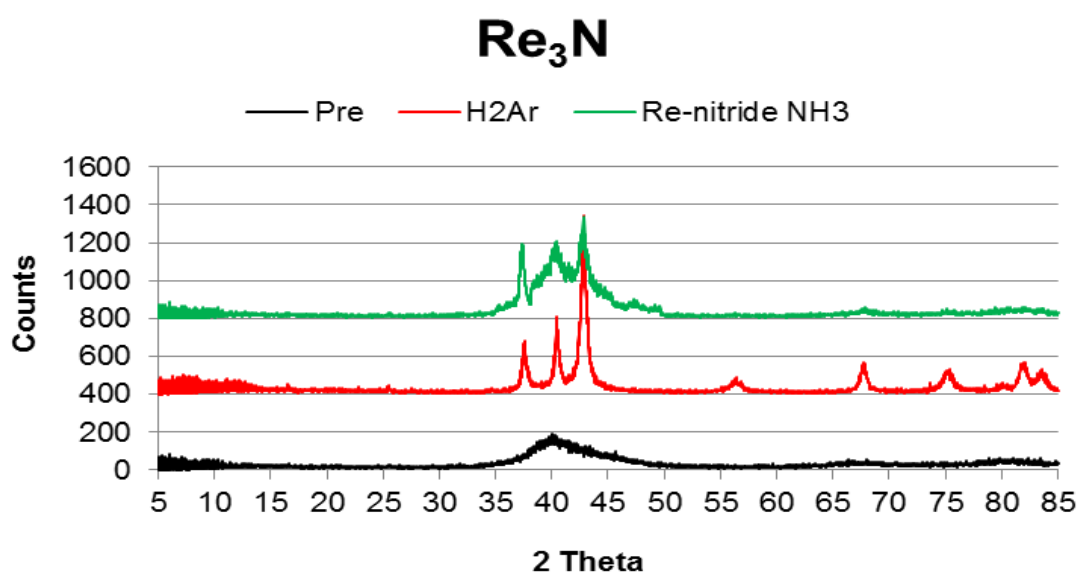
Figure 4.2-11 XRD patterns of pre-, post-isothermal H_2/Ar and re-nitrided Re_3N samples.

4.2.10.2 Nitrogen Analysis.

As can be seen from Table 4.2-11, the pre-reaction samples are in fairly good agreement with the calculated stoichiometric value for Re_3N. However, as mentioned previously, a significant amount of nitrogen is lost upon reaction in the isothermal H_2/Ar reactions which were conducted at 350 ^{o}C. Only a relatively small amount of nitrogen remained, upon re-nitridation, in ammonia. The nitrogen content increased to more than double that of the post-H_2/Ar sample.   Although the original Re_3N phase was not achieved, it is clear that it is possible to partially restore the depleted nitrogen, which may still have a potential application in a Mars van-Krevelen type process.

Sample and Reaction conditions	Calculated Stoichiometric N content (wt.%)	Pre-Reaction N Content (wt.%)	Post-Reaction N Content (wt.%)
Re_3N (H_2/Ar) using isothermal 350 ^oC	2.44	2.52	0.32
Re_3N re-nitridation NH_3 (350 ^oC, 3 h)	2.44	0.32	0.84

Table 4.2-11 Nitrogen content of pre-, post-isothermal H_2/Ar and re-nitrided Re_3N samples.

4.3 Summary of Re-Nitridation Studies.

As was discussed in the introduction to this chapter, the original nitride phase must be able to be regenerated after reaction in order to function in the envisaged nitrogen transfer process. It is therefore necessary to restore the depleted nitrogen via gas phase nitrogen species and consequently this has been investigated, as described in this chapter, through re-nitridation studies conducted in ammonia and H_2/N_2.

It was found that the re-uptake of nitrogen into the nitrogen deficient samples was largely dependent on the reaction gas employed. From the studies described, most materials exhibit either a partial or complete restoration to the original nitride phase under the gas which was used in the original synthesis.

Table 4.3.-1 provides an overview of the binary nitrides which have been investigated in this chapter and indicates under which gas mixtures either partial or total re-nitridation was observed.

On inspection of the data only the early metal nitrides (VN, β-$Mo_2N_{0.78}$, W_2N, and Ta_3N_5) were found to almost completely restore to the original nitride phase. As is evident, however, when VN, W_2N, and Ta_3N_5 are investigated in H_2/N_2 they appear to become further reduced and continue to lose nitrogen upon reaction which may possibly be attributed to the hydrogen rich atmosphere. As has previously been mentioned, β-$Mo_2N_{0.78}$ was not investigated under NH_3 as it was initially prepared under H_2/N_2

Material and Reaction Conditions	Nitrogen Analysis				
	Stoichiometric value	Pre-reaction	H$_2$/Ar	Re-nitridation	
				NH$_3$	H$_2$/N$_2$
VN (700 °C 3 h)	21.55	18.39	14.06	19.36	14.01
Fe$_2$N (500 °C 5 h)	11.13	8.59	2.40	5.95	2.57
Co$_4$N (700 °C 2 h)	5.60	3.17	0.00	0.00	0.00
Ni$_3$N (480 °C 6 h)	7.36	6.58	0.00	1.89	0.00
Cu$_3$N (300 °C 6 h)	6.84	6.63	0.00	0.00	0.00
Zn$_3$N$_2$ (600 °C 3 h)	12.49	9.46	2.29	3.01	0.86
Ta$_3$N$_5$ (700 °C 3 h)	11.42	11.23	7.83	11.19	6.49
β-Mo$_2$N$_{0.78}$ (700°C 3 h)	5.38	5.58	0.00	-	5.12
W$_2$N (700 °C 3 h)	3.66	6.13	4.18	5.89	2.17
Re$_3$N (350 °C 3 h)	2.44	2.52	0.32	0.84	-

Table 4.3-1 Pre- and post-nitrogen analysis of the binary nitrides which have been investigated in this chapter under re-nitridation conditions.

Later transition metal nitrides can be divided into two groups; those which partially re-nitride and those which remain as metals. Of the later nitrides, Fe$_2$N demonstrated the highest potential to reform the original Fe$_2$N phase. As was described earlier, Fe$_2$N decomposes to lower nitride phases upon reaction with H$_2$/Ar, however since Fe$_2$N was originally prepared from Fe metal and should then be possible to regenerate the Fe$_2$N phase from lower phases. As demonstrated by XRD analysis, the original phase is regenerated under NH$_3$ although the nitrogen content of the regenerated sample is slightly lower with respect to the original phase (5.95 and 8.95 wt.% respectively).

In the H$_2$/Ar studies described in Chapter 3, it was shown that not all nitrogen was removed from the Zn$_3$N$_2$ and Re$_3$N the samples, remaining as 2.29 wt.% and 0.32 wt.% respectively. Upon treatment with NH$_3$, the nitrogen content of both samples increased slightly as shown in Table 4.3-1. Since this increase was small it may be possible that these trace amounts can be attributed to surface NH$_x$ species.

Co$_4$N, Ni$_3$N and Cu$_3$N fully decompose to the corresponding metals upon reaction with H$_2$/Ar. However, it is only Ni$_3$N which appears to partially re-nitride, albeit to a limited extent and only in the presence of NH$_3$, as demonstrated by the presence of weak Ni$_3$N reflections in the XRD pattern, and confirmed by elemental analysis with an increase in the nitrogen content being apparent.

4.3.1 Modified Binary Systems.

As previously mentioned, Cu_3N decomposes to Cu metal upon treatment with H_2/Ar, however unlike Ni_3N no re-uptake of nitrogen is evident. Efforts to partially de-nitride Cu_3N were also undertaken as mentioned in section 4.2.5. It was anticipated that in doing so, the remaining nitrogen may help to facilitate further nitrogen uptake. However, none of these studies were successful. Another method which may help to facilitate nitrogen uptake is to introduce defects into the metal lattices of the materials. Based upon studies in which low levels of Fe dopants have been shown to significantly enhance the nitridation of niobium oxide with H_2/N_2, the importance of dopants upon the de-nitridation – re-nitridation behaviour of Cu_3N and β-$Mo_2N_{0.78}$ have been investigated.[108]

Cu_3N was doped with small amounts of lithium and palladium. Cu_3N crystallizes in a cubic anti-ReO_3 type structure and, as previously discussed in Chapter 3, has vacant interstitial sites in the centre of the crystal structure which could potentially host other metal atoms. Both lithium and palladium atoms have been reported to been successfully incorporated into this structure.[229-232] These atoms have a similar ionic radius to Cu^+ (Cu^+= 0.71 Å; Li^+ = 0.74 Å ; Pd^{2+} = 0.78 Å) and as a result can be easily accommodated by the crystal lattice. [255] It was anticipated that either the Li or Pd ions would replace some Cu ions whilst maintaining the structure of the Cu_3N, which may possibly help to facilitate re-uptake of nitrogen in to the metal, through the resultant defect structure and/or structural modification.

By doping the material with Li or Pd ions, it was thought that this could potentially help to facilitate the re-uptake of nitrogen, by occupying the vacant interstitial sites in the crystal structure and consequently introducing lattice defects which may have helped to facilitate the uptake and loss of nitrogen. However this proved ineffective and had little, if any, effect. It would appear that once reduction is initiated within the Cu_3N crystal it rapidly propagates throughout the material resulting in total elimination of nitrogen from the structure.

β-$Mo_2N_{0.78}$ on the other hand was doped with low levels of Fe, Cu and Bi. These metals have been employed as dopants for various reasons. Both Fe and Cu have been found to be active for the amination of organic compounds, which is the main focus of the work in this thesis.[169-175] Fe is also known to enhance the activation of N_2 and it was shown in Chapter 3 that ammonia production was slightly enhanced by the addition of the Fe

dopant.[256] In this study Fe may play a significant role in the loss and uptake of nitrogen. Bi has been investigated as a potential dopant as it is known to activate the C-H bond in hydrogen abstraction, however from the studies described in Chapter 3 Bi appeared to diminish ammonia production, with respect to the un-doped β-$Mo_2N_{0.78}$ sample.[176-179]

Table 4.3-2 indicates the pre- and post- reaction nitrogen contents within the doped β-$Mo_2N_{0.78}$ samples. As can be seen, Fe-doped pre-reaction samples are consistent with the calculated stoichiometric values; however the Cu and Bi samples appear to be slightly lower than expected. All samples are reduced to Mo metal by H_2/Ar in the temperature programmed regime, with all nitrogen being removed from the sample as confirmed by post-reaction nitrogen analysis.

As is evident, doped samples re-uptake nitrogen but to varying extents. As discussed previously, Bi metal appears to prevent the restoration of nitrogen into the metal lattice, with a much lower N content being observed with respect to the other samples.

Despite this, it appears that the nitrogen is restored in the other samples to give N contents close to their original pre-reaction sample. Only the Fe doped material achieves a higher nitrogen content, than the original pre-reaction sample upon re-nitridation, reaching a N content closer to the stoichiometric value. This may indicate that molybdenum nitride doped with Fe has an increased affinity for nitrogen at higher temperatures and the Fe may facilitate a nitrogen spillover effect, replenishing nitrogen loss from the molybdenum nitride phase.

Sample and Reaction conditions	Calculated Stoichiometric N content (wt.%)	Pre-Reaction N Content (wt.%)	Post-Reaction N Content (wt.%)
β-$Mo_2N_{0.78}$, (H_2/Ar) using temperature profile as shown in Fig. 3.2-2	5.38	5.58	0
β-$Mo_2N_{0.78}$, re-nitridation H_2/N_2	5.38	0	5.12
1.5% Fe / β-$Mo_2N_{0.78}$, (H_2/Ar) using temperature profile Fig. 3.2.2-2	5.38	5.31	-
1.5% Fe / β-$Mo_2N_{0.78}$ re-nitridation H_2/N_2	5.38	-	5.36
1.5% Cu / β-$Mo_2N_{0.78}$, (H_2/Ar) using temperature profile Fig. 3.2.2-2	5.38	4.39	-
1.5% Cu / β-$Mo_2N_{0.78}$, re-nitridation H_2/N_2	5.38	-	4.09
1.5% Bi / β-$Mo_2N_{0.78}$, (H_2/Ar) using temperature profile Fig. 3.2.2-2	5.38	4.66	-
1.5% Bi / β-$Mo_2N_{0.78}$, re-nitridation H_2/N_2	5.38	-	2.57

Table 4.3-2 Nitrogen content of pre-, post-temperature programmed H_2/Ar and re-nitrided doped β-$Mo_2N_{0.78}$ samples.

Fe metal appears to slightly enhance, or facilitate total re-nitridation of the original β-$Mo_2N_{0.78}$ phase, Figure 4.3-1. No shifts were observed in the re-nitrided diffraction pattern with respect to the un-reacted sample, however the reflection at approximately 81° 2θ is less intense in the re-nitrided sample. This is in good agreement with the data presented in Table 4.3-2, where it is shown that the nitrogen content of the re-nitrided sample exceeds that of the pre-reaction sample, reaching a value closer to the stoichiometric value. Although the original β-$Mo_2N_{0.78}$ phase was restored in the sample doped with Cu upon H_2/N_2 treatment, the resultant diffraction pattern is comparable to that observed in the un-doped sample, Figure 4.2-9. It is evident that the intensities of the reflections in the re-nitrided sample, as shown in Figure 4.3-2, are somewhat diminished with respect to the pre-reaction sample, which may indicate that the re-nitrided sample is less crystalline than the pre-reaction sample.
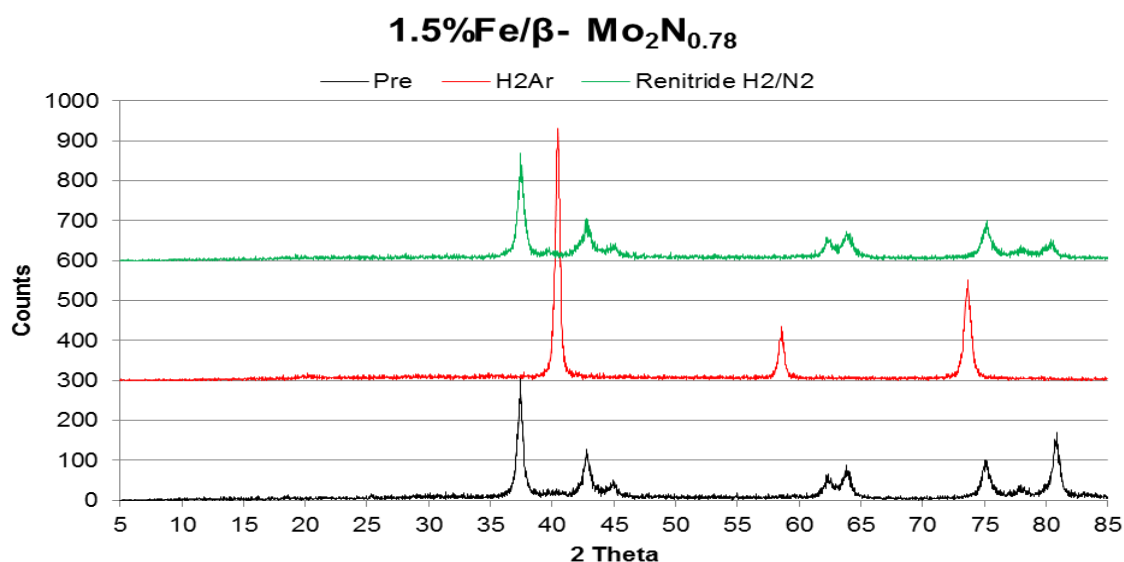
Figure 4.3-1 XRD patterns of pre-, post-temperature programmed H$_2$/Ar and re-nitrided 1.5%Fe/β-Mo$_2$N$_{0.78}$ samples.
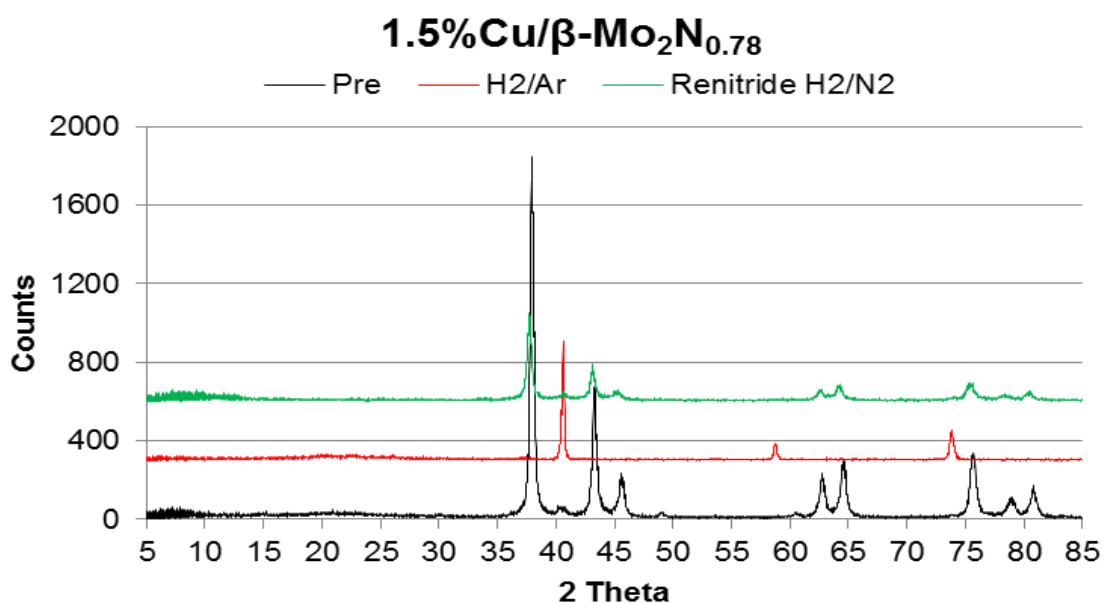
Figure 4.3-2 XRD patterns of pre-, post-temperature programmed H$_2$/Ar and re-nitrided 1.5%Cu/β-Mo$_2$N$_{0.78}$ samples.

In the case of the sample doped with Bi only partial re-nitridation is observed, Figure 4.3-3, with both β-Mo$_2$N$_{0.78}$ and Mo metal reflections being evident. This would suggest that doping β-Mo$_2$N$_{0.78}$ with Bi, in fact, impedes the re-uptake of nitrogen instead of facilitating it. As mentioned earlier it was observed in the H$_2$/N$_2$ studies conducted in Chapter 3, Bi was also observed to hinder the production of ammonia
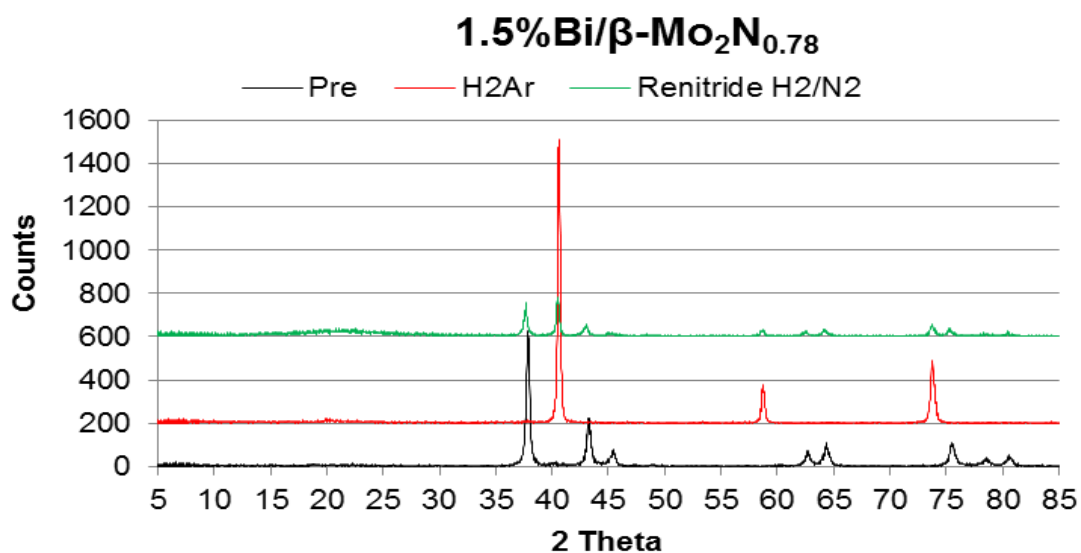
Figure 4.3-3 XRD patterns of pre-, post-temperature programmed H$_2$/Ar and re-nitrided 1.5%Bi/ β-Mo$_2$N$_{0.78}$ samples.

4.4 Summary.

As mentioned in the introduction to this chapter, regeneration of the candidate nitrides is fundamentally important in order to function as a nitrogen transfer reagents which may be applied to potential applications. Consequently, in this chapter, a range of nitrogen deficient nitrides have been investigated using NH$_3$ and H$_2$/N$_2$ to assess whether it is possible to restore the nitrogen depleted samples to their original unreacted phase.

As previously described, most nitride materials which were investigated in this chapter exhibit the potentially ability to re-uptake nitrogen, to some extent, in order to restore the original nitride phase. Co$_4$N and Cu$_3$N were the exception, in that no re-uptake of nitrogen was observed, despite efforts to increase the surface to volume ratio of the latter sample by supporting on silica. In the case of Cu$_3$N, which demonstrated very high initial ammonia production and described in Chapter 3, the effects of metal dopants was also examined. As described earlier, Cu$_3$N has a vacant interstitial site which can accommodate other metal ions. By doping Cu$_3$N with Li or Pd, as was investigated in the current study, defects are effectively introduced into the crystal lattice which can potentially have significant effects on the chemical and physical properties of the nitride. It had been anticipated that these defects may help to assist nitrogen re-uptake into the metal lattice, but this was not observed. It may be that in order to restore Co$_4$N and Cu$_3$N the original precursor has to be regenerated first (Co$_3$O$_4$ and CuF$_2$ respectively) from which the nitride is known to form. In the case of Co$_4$N this would be a relatively simple oxidation of Co metal, however to

regenerate CuF_2, HF or F_2 would be required which may have serious environmental and cost implications if to be undertaken on an industrial scale. Additionally the regeneration would ultimately be performed in a multistep process and not the two stage process which was initially envisaged for the work done in this thesis.

It was found that doping β-$Mo_2N_{0.78}$ with low levels of Fe improved re-nitridation, with respect to the un-doped sample, as shown by the nitrogen content after reaction. This is in good agreement with the findings by Wakai and co-workers in which Fe was reported to significantly improve the nitridation of niobium oxide.[108] β-$Mo_2N_{0.78}$ was the only material that could be regenerated using H_2/N_2 and this, as indicated in the introduction to this chapter, is a preferred nitriding gas for potential industrial applications, although the use of N_2 alone would be optimal.

From the results presented in this chapter, it is evident that it is possible to either partially or totally restore the original nitride phase in most of the materials investigated, with restoration of the early transition nitrides being most facile. It is therefore possible to establish candidate systems which could possibly participate in a potential Mars-van Krevelen type process. These include VN, Fe doped and undoped β-$Mo_2N_{0.78}$, Ta_3N_5 and W_2N. However, from the studies conducted in Chapter 3 it was apparent that many other nitride systems exhibit significant nitrogen loss and if suitable methods were developed to restore these nitrides, their application in nitrogen transfer may become feasible. Therefore taking the upper limit of the target process to be 400 ^{o}C, on the basis of the data presented in Chapter 3 it is possible to select candidate systems for further study. Figure 4.4-1 illustrates the potential candidate systems which will be further investigated for possible direct routes to aniline in the next chapter.

1 H																	2 He
3 Li	4 Be		Atomic Number SYMBOL									5 B	6 C	7 N	8 O	9 F	10 Ne
11 Na	12 Mg											13 Al	14 Si	15 P	16 S	17 Cl	18 Ar
19 K	20 Ca		21 Sc	22 Ti	23 V	24 Cr	25 Mn	26 Fe	27 Co	28 Ni	29 Cu	30 Zn	31 Ga	32 Ge	33 As	34 Se	35 Br	36 Kr
37 Rb	38 Sr		39 Y	40 Zr	41 Nb	42 Mo	43 Tc	44 Ru	45 Rh	46 Pd	47 Ag	48 Cd	49 In	50 Sn	51 Sb	52 Te	53 I	54 Xe
55 Cs	56 Ba	* 57-70	71 Lu	72 Hf	73 Ta	74 W	75 Re	76 Os	77 Ir	78 Pt	79 Au	80 Hg	81 Tl	82 Pb	83 Bi	84 Po	85 At	86 Rn
87 Fr	88 Ra	** 89-102	103 Lr	104 Rf	105 Db	106 Sg	107 Bh	108 Hs	109 Mt	110 Uun	111 Uuu	112 Uub		114 Uuq				

Figure 4.4-1 Periodic Table highlights in blue the nitride materials which are of interest and will be further investigated in addition to Co_3Mo_3N and Co-4Re.

5. An Investigation of Potential Direct routes to Aniline.

5.1 Introduction.

Aniline is a key intermediate compound which is used extensively within industry for the synthesis of many commodity chemicals, as well as large scale industrial applications. Around 67% of the world's aniline production is used in the manufacture of rigid polyurethanes and other materials utilized by the construction and durable goods industries. Other major uses include the manufacture of polymers, agricultural chemicals and dyes.[127]

There are several different routes for the synthesis of aniline, which generally involve converting benzene into a derivative, such as phenol,[257-259] chlorobenzene[174] and nitrobenzene,[95] which are subsequently converted to aniline. Commercially, nitrobenzene is the most frequently used feedstock for this process and was traditionally employed in a process known as the Bechamp reaction for the industrial production of aromatic amines.[95-97] This method utilizes iron and water in the presence of hydrochloric acid to reduce the nitro group to the amine, and is now almost obsolete for the reduction of nitrobenzene. A more commercially viable route was discovered in the early 1960's which improves upon the old Bechamp method - the catalytic hydrogenation of nitrobenzene – and this is still the predominant process used in the manufacture of aniline.[260-263] In this process nitrobenzene reacts with 3 mole equivalents of hydrogen gas, in the presence of a suitable catalyst. A number of different catalysts have been reported to be active including copper on silica, copper oxide, nickel sulfides and molybdenum metal.

$$C_6H_5NO_2 + 3H_2 \longrightarrow C_6H_5NH_2 + 2H_2O$$
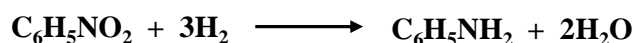
Although this route is very selective to aniline (> 99%), the nitrobenzene is generally produced by nitration of benzene using a nitric-sulfuric acid mixture, which itself requires the oxidation of ammonia to produce the nitric acid.[95] It is evident that current methods which incorporate nitrogen into organic molecules, specifically in the production of aromatic amines, proceed via an indirect process requiring a number of intermediate nitrogen inter-conversion reactions. This has several different cost and environmental implications including the energy intensive processes that are required, the inability to

recover catalysts and the use of acids on an industrial scale.[98,99]   An attractive path for the synthesis of aniline is the direct amination of benzene, as shown below:

$$C_6H_6 \; + \; NH_3 \; \rightleftharpoons \; C_6H_5NH_2 \; + \; H_2$$
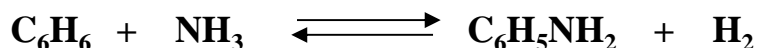
This type of process has attracted much attention recently as it avoids the use of acids on an industrial scale. Most of the efforts in this area have concentrated on the identification, development and optimisation of effective catalysts.[264-267]   The direct synthesis of aniline by this route has been documented since 1917, in the work of Wibaut, in which aniline was synthesised by passing benzene over a nickel/iron catalyst at moderate temperatures and atmospheric pressure.[265] This reaction, however, is thermodynamically limited due to the co-production of hydrogen. Various approaches have been employed to overcome this limitation including the use of gaseous oxygen as well as reducible metal oxide systems in order to remove the hydrogen as water, and thus drive the equilibrium forward. However the inclusion of O_2 can seriously impair the selectivity of the reaction. The most successful system reported to date is based upon a reducible oxide system. This is Du Pont's NiO/Ni cataloreactant system for which, reportedly, a maximum aniline selectivity of 97% is observed, at a maximum benzene conversion of only 13%. Hence this process was not commercialised and a number of serious problems exist in the stability of the cataloreactant upon multiple reduction and re-oxidation cycles. [117,268-272]

5.2 Proposed Direct Routes to Aniline.

Direct approaches to aniline formation by reaction with ammonia have been limited by the need to remove the co-product hydrogen. An alternative potential route to aniline that has been investigated in the study presented in this thesis is shown below:

$$C_6H_6 + \; N_{(a)} + \tfrac{1}{2}\,H_2 \; \longrightarrow \; C_6H_5NH_2$$
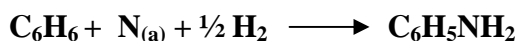
where N(a) = lattice or adsorbed nitrogen species

In this method the thermodynamic limitations may, potentially, be overcome as hydrogen is a reactant, rather than a product of the reaction.

Despite literature that documents the high activity of some metal nitrides for ammonia synthesis, there have been very few studies which investigate the use of metal nitrides as

aminating agents. Studies by Thompson *et al* have shown that early transition metal nitrides are successful in the amination of ethanol to ethylamine with ammonia resulting in high selectivities and activities comparable to those which are observed for supported platinum and nickel catalysts,[18] with activities being ranked as $VN > Mo_2N > W_2N > TiN > NbN$. Additionally a study by Mckay[111] and co-workers investigate the potential use of Co_3Mo_3N for nitrogen insertion into benzene according to the scheme outlined above. The current study is effectively an extension of this previous work and extends it to investigate a greater range of nitride materials.

The reactivity of lattice nitrogen, as probed by reduction with H_2/Ar mixtures, for a range of different nitride materials has been discussed in Chapter 3. The materials which have been further investigated in this chapter demonstrated the ability to de-nitride at temperatures at, or below, 400 ^oC which is the maximum temperature for the envisaged process based upon the probable stability of benzene.

The aim of the work reported in this chapter was to perform initial investigations into the application of nitrides as potential nitrogen carriers that would facilitate the direct activation of nitrogen to the synthesis of industrially desirable products, in particular the direct conversion of benzene to aniline. Once in the nitrided state, if direct nitrogen activation and incorporation of pathways become possible, there could be a reduction in the requirement for the use of ammonia via its inter-conversion to derivatives, as a reactant. This would be significant since commercial ammonia synthesis reportedly accounts for 1% of the global energy demand, as stated earlier.

Figure 5.2-1 shows the materials, highlighted in blue, which have demonstrated the ability to act as a possible nitrogen transfer source in the investigation as outlined in Chapters 3 and 4. These materials have subsequently been subjected to treatment with benzene and a 3:1 H_2/N_2 gas mixture, as detailed below.

Two different reaction methods were employed in testing of benzene and hydrogen over the metal nitrides, which will be discussed in turn. Both of these methods were conducted according to the procedures outlined in the relevant testing sections in Chapter 2.

1																	2
H																	He

Atomic Number
SYMBOL

Figure 5.2-1 Metal nitrides to be investigated within this chapter are highlighted in blue.

It should be noted that no aniline was observed in the reaction products of any of the reactions subsequently described in this chapter. Despite this, evidence of products other than aniline were observed using some of the materials which have been investigated. Identification of these compounds has proved to be very problematic due to the low concentrations observed and no definitive assignments have been made.

Several methods were employed in an attempt to identify the compounds which were observed. These included the use of ninhydrin indicator to ascertain whether primary or secondary amines were present in the compounds.[273] Samples were spotted onto a TLC plate and subsequently dipped into a ninhydrin solution, dried and heated with a heat gun to visualise the spot. Typically alpha amino acids and primary amines give a blue- purple whereas proline gives a yellow product and secondary amines produce a red orange coloured stain.[274-276] However this proved an ineffective method as ninhydrin itself colours to an orange/pink colour upon uncontrolled heating.

Attempts to analyse samples using Fourier transform infrared spectroscopy was also ineffective due to the low concentrations involved, and no difference was observed between the un-reacted benzene and the reaction products.

This subsequently led to samples being analysed through the use of ^{1}H NMR spectroscopy and mass spectroscopy. This helped to a certain extent in the fact that they helped to rule out the formation of aniline. Small peaks, other than benzene, were evident in some ^{1}H NMR spectra and the mass spectra obtained for the reaction products did not correspond to the mass fragments expected for aniline.

From the pulse reactions that were undertaken, UV-Vis spectroscopy was attempted for the coloured reaction products, in the understanding that it may be possible to work out the conjugation, if any, in the event of the synthesis of polycyclic aromatics and subsequently partially identify the compound or any functional groups present.

Additionally, samples were sent to the EPSRC National Mass Spectroscopy Service where GCMS was undertaken. However again, the concentrations of reaction compounds were so low that problems were encountered in the identification of compounds, which involved using their search and match library facility and no definitive assignments could be made.

Although a wide range of materials have been investigated, and some materials screened appear to be active for the synthesis of certain compounds, no definitive product identification has been possible other than the fact that the target compound, aniline, has not been synthesised in any of the reactions performed.

5.3 Benzene-Flow Reactions.

The first method which was investigated involved passing a continuous flow of benzene over the reaction material in a feedstream of H_2/N_2 and was conducted according to the procedure described in the testing section in Chapter 2. The reaction temperatures were employed based upon the performance determined in the previous chapter. In addition to this, the temperature at which the material decomposed to the corresponding metal was also taken into consideration for the more unstable nitrides. Table 5.3-1 gives an overview of the reaction temperatures used for each material.

Products from the reaction were condensed using an ice bath at the exit stream of the reactor and subsequently analysed by mass spectroscopy and ^{1}H NMR spectroscopy. The concentration of benzene flowed over the material was estimated using the vapour pressure of benzene at room temperature, and determined to be approximately 9% by volume at the ambient laboratory temperature (18 ^{o}C).

Material	Reaction Temperature	
	300 °C	400 °C
Co_3Mo_3N		X
Mg_3N_2		X
VN		X
Fe_2N		X
Co_4N	X	
Ni_3N	X	
Cu_3N	X	
Zn_3N_2		X
Ta_3N_5		X
$\beta\text{-}Mo_2N_{0.78}$		X
$Fe/\beta\text{-}Mo_2N_{0.78}$		X
$Cu/\beta\text{-}Mo_2N_{0.78}$		X
W_2N		X
Re_3N	X	
Co-4Re		X

Table 5.3-1 Overview of reaction temperatures used for each specific material.

The ^{1}H NMR spectra of benzene and aniline are presented in Figures 5.3-1 and 5.3-2 respectively. Benzene occurs as a singlet between 7-8 ppm in the spectrum,[277-280] and can be seen to occur at 7.92 ppm in the spectrum below. Small impurities are also evident at 2.49 ppm and 1.45 ppm. Mono-substituted benzenes often appear as a doublet and in the case of aniline a broad signal is also apparent at 3.72 ppm, corresponding to a NH_2 coupling.
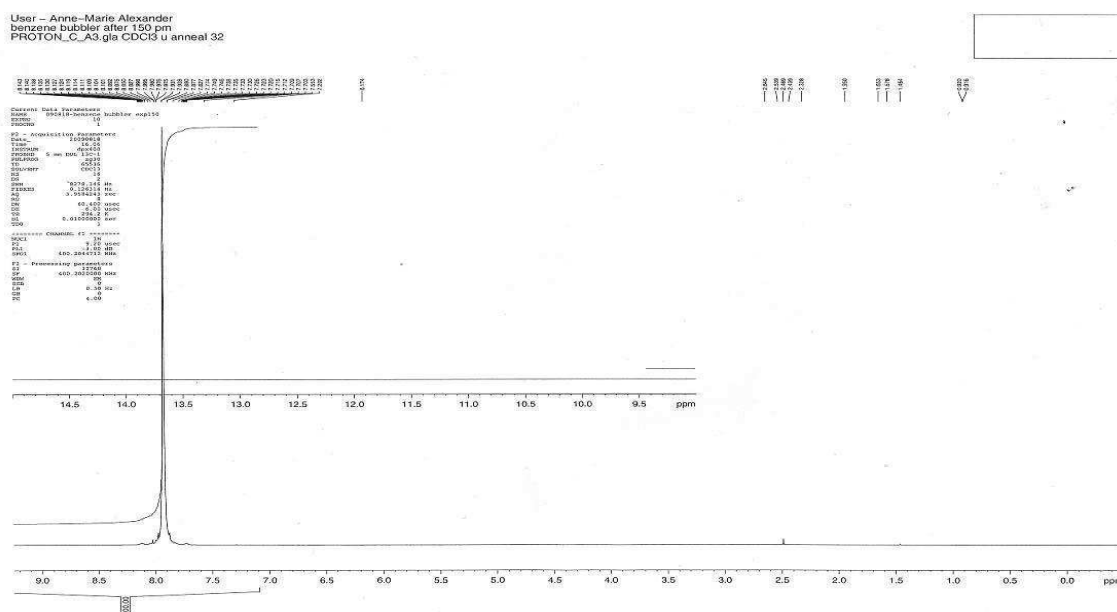
Figure 5.3-1 ^{1}H NMR spectrum of benzene in $CDCl_3$.
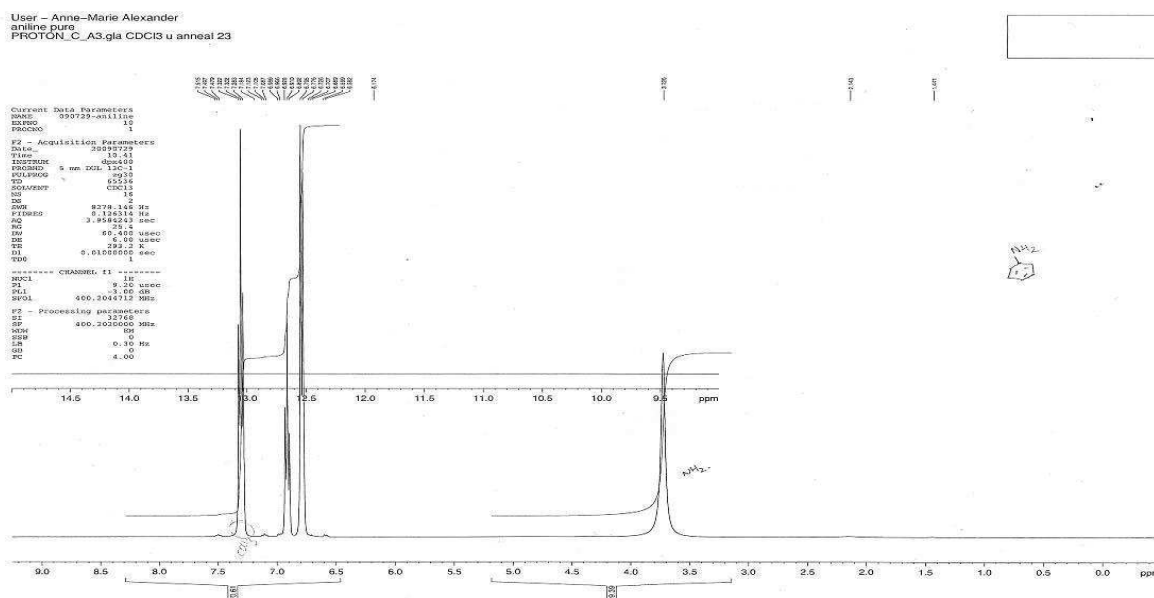
Figure 5.3-2 ^{1}H NMR spectrum of aniline in CDCl$_3$.

5.3.1 Co$_3$Mo$_3$N.

Co$_3$Mo$_3$N has attracted much attention recently as an alternative catalyst for ammonia synthesis and reports by Aika and Kojima have documented that doping Co$_3$Mo$_3$N with Cs$^+$ results in ammonia synthesis activities which have been claimed to be higher than those of commercial iron-based catalysts.[60-63,67-68] Jacobsen and co-workers have rationalised this activity in terms of a volcano relationship between the ammonia synthesis and nitrogen binding energy.[66,68] The combination of Co (with a low N$_2$ binding energy) and Mo (with a high N$_2$ binding energy) produces a CoMo alloy with an optimal nitrogen adsorption energy similar in strength to that of ruthenium, as shown in Figure 5.3-3

As described, Jacobsen *et al*. identified CoMo as a potential high-activity alloy catalyst by simple interpolation between the corresponding pure-metal components on the volcano curve (Figure 5.3-3), which was subsequently confirmed using first principle DFT calculations. They also calculated that the N$_2$ dissociation energy on this alloy is intermediate between the dissociation energies of the pure metal components. It was also concluded that the bulk nitrogen of the ternary nitride did not appear to affect the activity of the alloy and that the main role of nitrogen atoms was to induce ordering to give the required (111) surface containing both Co and Mo atoms. This would therefore imply that the bulk nitrogen was inert in this respect.[66]
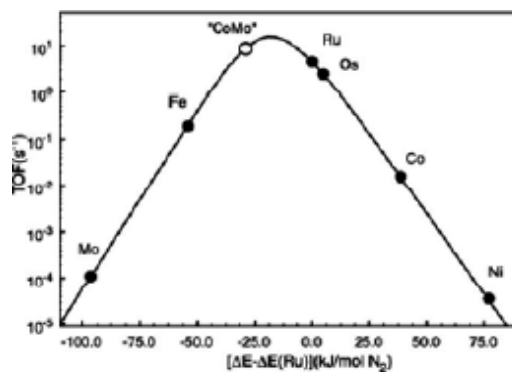
Figure 5.3-3 Calculated turnover frequencies for ammonia synthesis as a function of the adsorption energy of nitrogen for various transition metals and alloys.[66]

However, more recently Co_3Mo_3N has been shown to reversibly take-up and release nitrogen. In studies by Mckay *et al*, it has been demonstrated that it is possible to remove 50% of the lattice nitrogen under H_2/Ar at high temperature (700 ^{o}C) with the remaining nitrogen shifting to a new crystallographic position, resulting in a phase change from the Co_3Mo_3N (331) phase to the Co_6Mo_6N (661) phase.[111,124] This was subsequently confirmed by powder neutron diffraction studies.[125] In these studies it was also shown that it was possible to replenish the lost nitrogen in a reverse nitrogenation process, which can be achieved under a N_2 feedstream, therefore enabling the material to potentially participate in a Mars-van Krevelen process.[126] For this reason Co_3Mo_3N was the first material to be investigated as a potential candidate for the direct reaction of benzene to aniline.

Reactions with Co_3Mo_3N and benzene have previously been documented by Mckay and co-workers in which a temperature profile similar to that which was described for the temperature programmed H_2/Ar studies used for the early transition metal nitrides in Chapter 3. However it was found that Co_3Mo_3N underwent carburization to Co_3Mo_3C, due to the high reaction temperatures and hence a lower reaction temperature has been employed in this study. Initially studies were conducted using chlorobenzene rather than benzene itself, primarily due to the fact that it is easier to cleave the C-Cl bond in chlorobenzene than the C-H bond found in benzene.

5.3.1.1 ^{1}H NMR Spectroscopy.

Figure 5.3-4 shows the ^{1}H NMR spectrum of chlorobenzene taken from the bubbler prior to reaction, so as to directly compare the products collected from the exit stream of the reactor, Figure 5.3-5, with that of starting material.
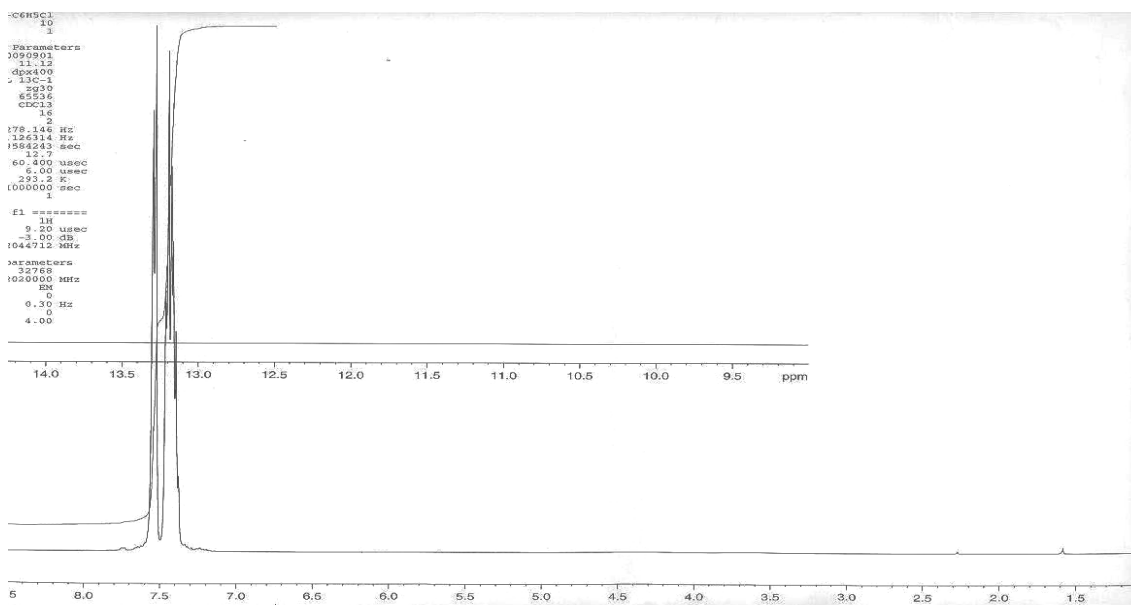
Figure 5.3-4 ^{1}H NMR spectrum of chlorobenzene in CDCI[3].

It is evident that additional peaks appear in the spectrum of the reaction products obtained. The most obvious change is a broad peak occurring at 4.82 ppm, which is highlighted in this spectrum. The shape of the peak is consistent of that would be expected from an R_2CHZ group where Z = O, N or a halogen and it is also in the region of the spectrum where this would be expected to occur. [277-280] There is a small multiplet at 0.83 ppm, and a tiny singlet at 3.30 ppm. These peaks are within the hydrocarbon region of the spectrum and may possibly be a saturated hydrocarbon species and a CH group respectively. The large peak at 1.42 ppm corresponds to water and the large singlet in the aromatic region arises due to benzene, which characteristically occurs at 7.37 ppm. As this observed peak is a singlet, and different to the doublet as seen in the ^{1}H NMR spectrum of the unreacted chlorobenzene, it may be possible that some of the chlorobenzene has undergone hydrogenation forming benzene. The small peak at 2.07 ppm also appears in the unreacted chlorobenzene and so is concluded to be an impurity.
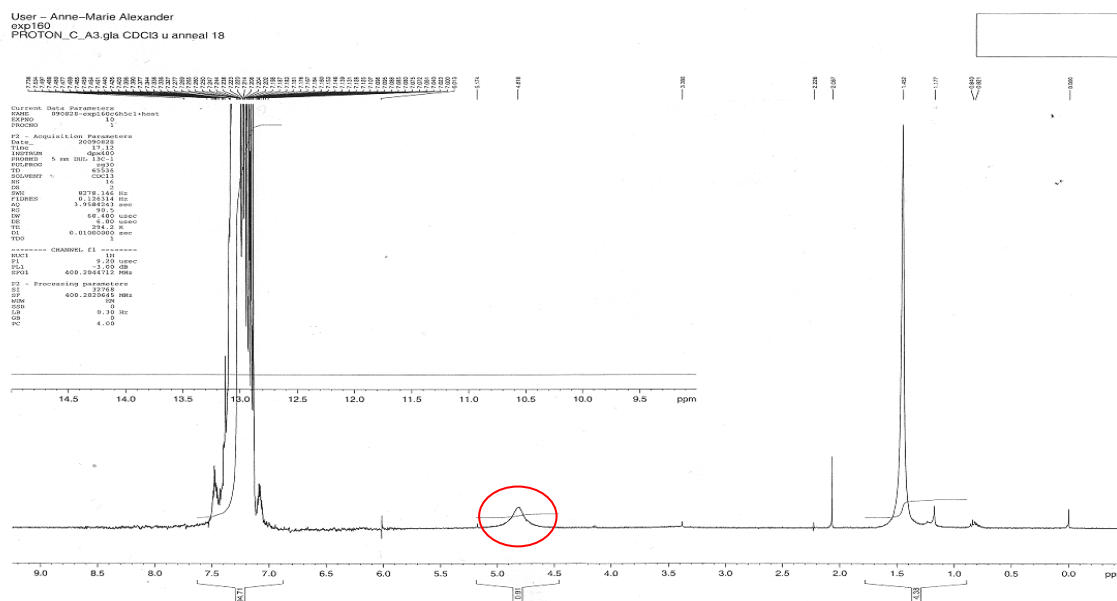
Figure 5.3-5 ^{1}H NMR spectrum of products collected after reaction of Co$_3$Mo$_3$N with H$_2$/N$_2$ and C$_6$H$_5$Cl at 400 ^{o}C for 1 h (CDCl$_3$).

Following these results, analogous reactions were undertaken with benzene to investigate whether or not it was possible to aminate the benzene directly. From Figures 5.3-6 and 5.3-7 it is apparent that a broad peak observed at 3.52 ppm, more clearly presented in Figure 5.3-7 which is an expansion of the spectrum, which is again within the same region as the broad NH$_2$ stretch observed in the aniline spectrum, Figure 5.3-2 (3.72 ppm).   In addition there is a small peak at *ca*. 0.91 ppm. Again there appears to be some impurities giving rise to small features at 2.20 ppm and 1.20 ppm. These are also present in the spectrum of benzene prior to reaction. It should be noted that the TMS signal was shifted to 0.10 ppm.
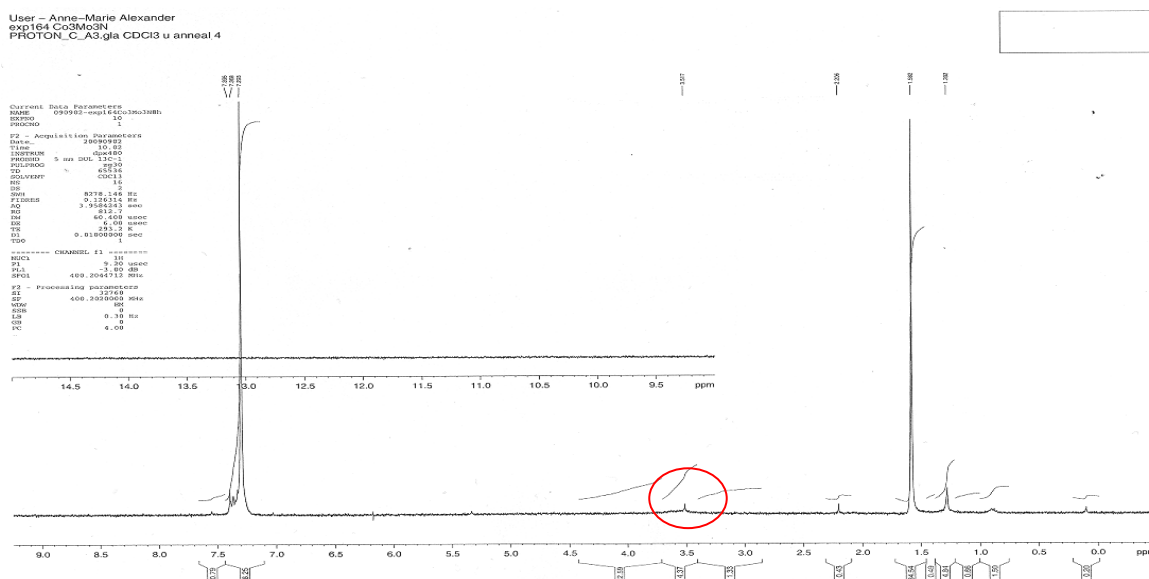
Figure 5.3-6 ^{1}H NMR spectrum of products collected after reaction of Co$_3$Mo$_3$N with H$_2$/N$_2$ and C$_6$H$_6$ at 400 ^{o}C for 1 h. (CDCl$_3$)
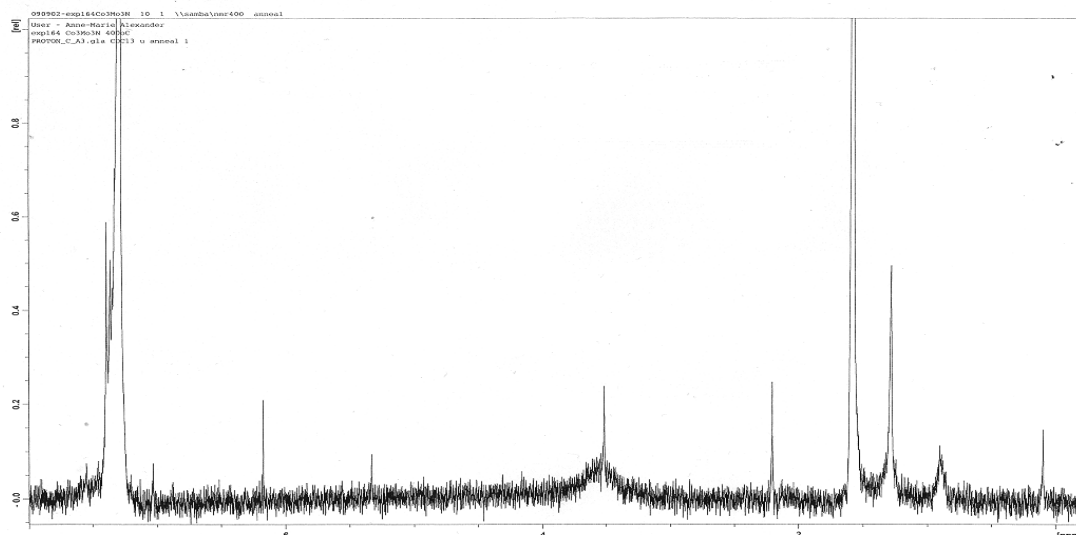
Figure 5.3-7 Expansion of Figure 5.3-6.

These reactions have been repeated several times under the same conditions and the resultant products have given the similar ^{1}H NMR spectrum on each occasion.

5.3.1.2 XRD Patterns.

The XRD patterns of the post-reaction Co$_3$Mo$_3$N samples show the same characteristic reflections to that of the pre-reaction material. However, upon close inspection, the shifts resulting from the reaction under chlorobenzene are evident.

The post-reaction chlorobenzene XRD pattern shows a shift to a higher angle 2θ, which is indicative of a decrease in the unit cell volume. This can be seen clearly in the comparison of the pre- and post-chlorobenzene reaction patterns in Figure 5.3-8, and the shifts correspond to a decrease in d-spacing from 2.125 Å in the pre-reaction sample to 2.117 Å in the post-chlorobenzene reaction. This effect does not occur in the post-benzene reaction XRD pattern where no apparent shift is observed although a small decrease in the intensities is possibly evident.
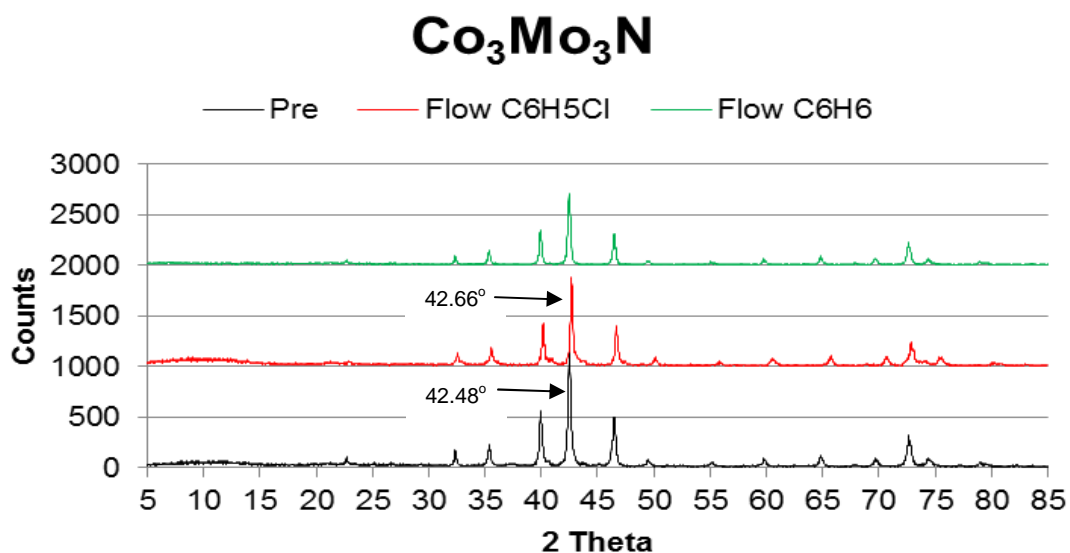
Figure 5.3-8 Pre- and post-chlorobeneze and benzene XRD patterns of Co_3Mo_3N.

Similar shifts, to a higher Bragg angle, have been observed in H_2/Ar studies and have been attributed to the loss of almost 50 % nitrogen from the material resulting in the formation of Co_6Mo_6N, which has been previously documented.[126] CHN microanalysis, Table 5.3-5, confirmed that only 1/3 of nitrogen was lost from this material when reacted under chlorobenzene, compared to almost half reported under H_2/Ar. It has been reported that on the transformation from Co_3Mo_3N to Co_6Mo_6N under H_2/Ar only two line phases are observed with no intermediate stoichiometry being evident.[126] The cause for the shifts, documented here, remains unclear and is currently under investigation. It may be possible that a chloronitride forms, which may explain why a smaller shift is observed in the diffraction pattern and also why only a third of nitrogen is lost. However it is unlikely that the Cl atoms replace the N atoms in a 1:1 ratio. The N^{3-} ion has an ionic radius of 1.71 Å, although it is anticipated that the radius of N may be smaller in the Co_3Mo_3N structure (since it will not be in the N^{3-} form), whereas Cl^- is slightly larger at 1.81 Å.[255] On this basis, if chlorine were to replace nitrogen in a 1:1 basis the shift to a lower Bragg angle would be expected. Shifts to lower Bragg angles were reported in a study by Mckay *et al*, in which the formation of Co_3Mo_3C was observed as a direct result of the reaction between Co_3Mo_3N and C_6H_6 at 700 °C, in which the carbon atoms replaced all nitrogen atoms within the crystal structure.[111] In both chlorobenzene and benzene reactions there is no evidence of carbon species being deposited on the material, either as graphite (which would have a signature (002) reflection at *ca.* 26 ° 2θ or as another carbide species. This was subsequently confirmed by CHN analysis.

5.3.2 Mg₃N₂.

As discussed in Chapter 3, Ley and co-workers reported that Mg_3N_2 releases ammonia upon reaction with protic solvents such as methanol.[100] This in turn was demonstrated to function as an alternative nitrogen source for the amination of esters to primary amides.

In the current study it was found, from the studies described in Chapter 3, that Mg_3N_2 produces a significant amount of ammonia at 400 ^{o}C, the upper limit to the proposed reaction, under both H_2/N_2 and H_2/Ar suggesting that the material undergoes a form of decomposition. This was confirmed by post-reaction nitrogen analysis.   Consequently Mg_3N_2 has been studied in the envisaged reaction with benzene.

5.3.2.1 ^{1}H NMR Spectroscopy.

It is evident that there is a large peak at 7.82 ppm, which can be ascribed to benzene. However upon closer inspection the presence of additional weaker peaks can be observed, which are different to those previously described. Expanded versions of the original spectrum, which is shown in Figure 5.3-9, are presented in Figures 5.3-10 and 5.3.11.
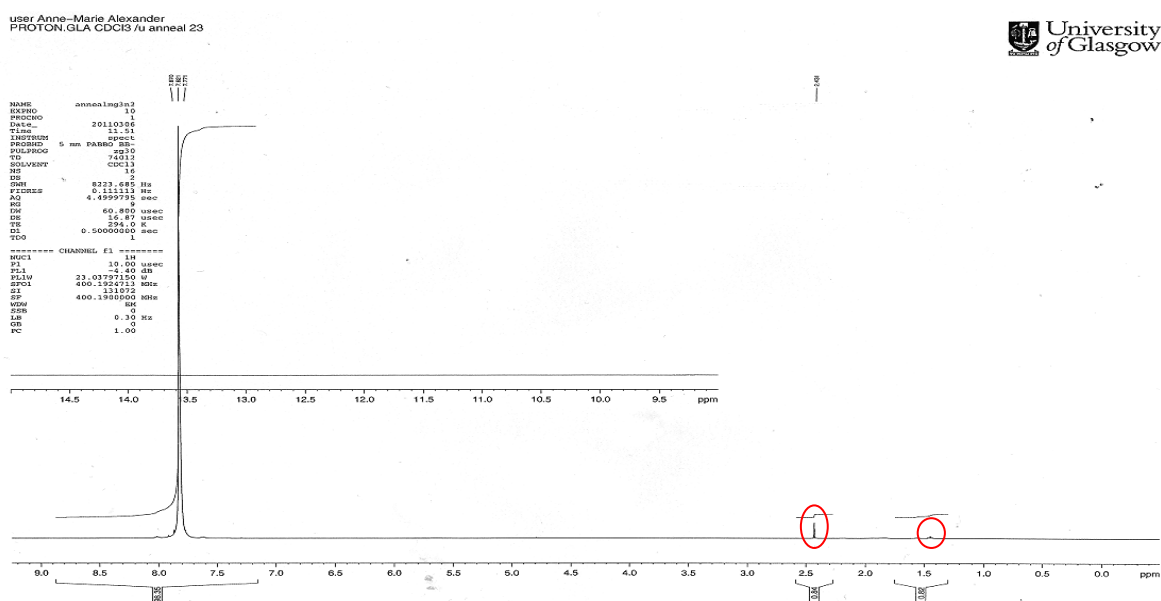
Figure 5.3-9 ^{1}H NMR spectrum of products collected after reaction of Mg₃N₂ with H₂/N₂ and C₆H₆ at 400 ^{o}C for 1 h. (CDCl₃)

From Figure 5.3-10 it is evident that there several clearly defined peaks at the lower end of the spectrum indicative of either allylic or vinylic hydrocarbon chains. In addition to this there is a singlet and quartet which appears within the aromatic region of the spectrum. These peak positions, descriptions and possible assignment are presented in Table 5.3-2.
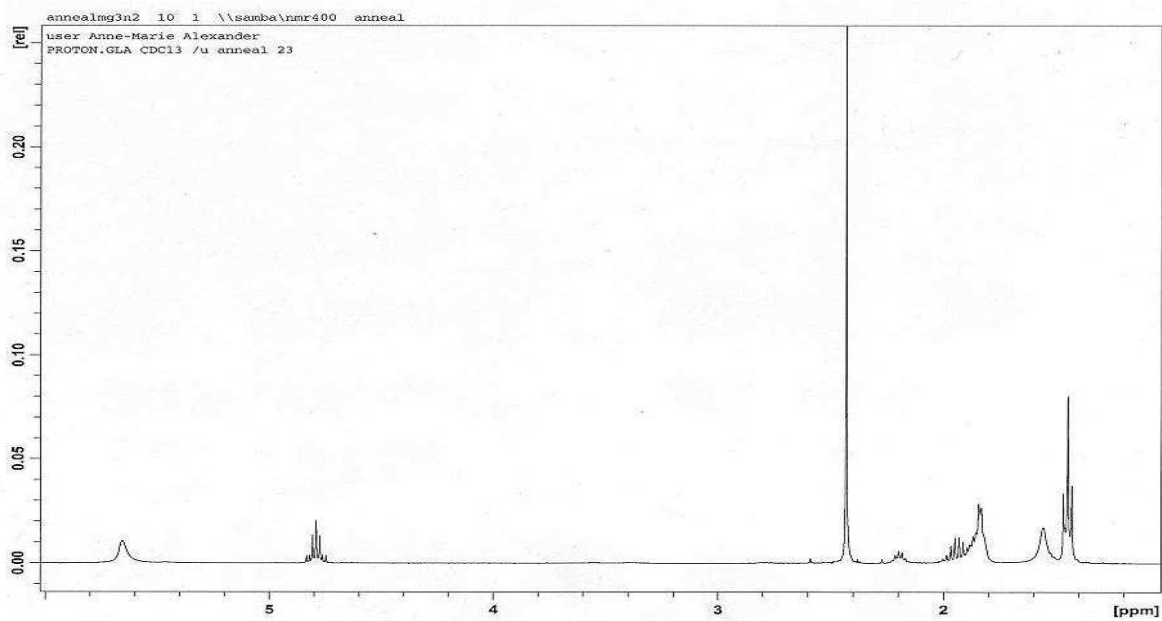
Figure 5.3-10 Expansion of upfield chemical shifts in Figure 5.3-9.
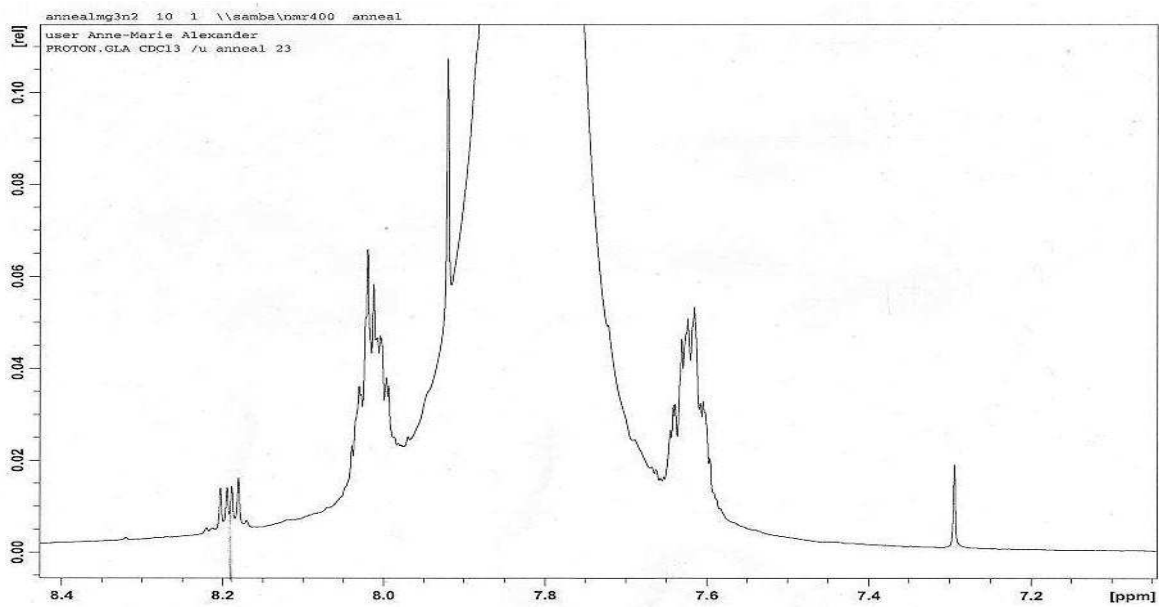
Figure 5.3-11 Expansion of downfield chemical shifts in Figure 5.3-9.

Peak Shift (ppm)	Description	Possible Assignment
1.48	triplet	C$\underline{H}$-CH$_2$
1.57	broad singlet	RN$\underline{H}_2$
1.89	doublet	C$\underline{H}$-CH
1.95	sextet	CH$_2$-C$\underline{H}$-CH$_3$
2.19	quintet	CH$_3$-C$\underline{H}$-CH or R–CH$_2$-C$\underline{H}$-CH$_2$
4.80	septet	R-(CH$_3$)CH-CH$_3$
5.64	broad singlet	RCO-N$\underline{H}_2$ or ArO$\underline{H}$
7.30	singlet	aromatic RC-C$\underline{H}$
8.19	double doublet	aromatic CH-C$\underline{H}$-CH (Ar-R group)

Table 5.3-2 Table of chemical shifts from the ^{1}H NMR spectrum, Figures 5.3-10 and 5.3-11.

From the possible fragments, assigned to each shift a possible structure may be:
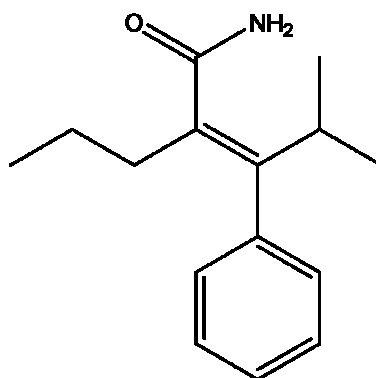
The mass fragments which obtained via mass spectroscopy are relatively high and are presented below:

71, 87, 105, 113, 127, 141, 147, 159, 175, 194, 211, 229, 233 m/z.

The overall mass of the above compound is 219. However this mass is not observed in the mass spectrum. The 175 m/z mass fragment is relatively close to the mass which would be obtained from the above compound if the propyl group were to be removed (176). As previously mentioned, Mg$_3$N$_2$ is sensitive to oxidation in air, it may be possible that the material is slightly oxidised upon loading into the reactor, which may subsequently account for the presence of oxygen in the proposed structure.

5.3.2.2 XRD Patterns.

The pre- and post-benzene reaction XRD patterns are presented in Figure 5.3-12. There is no observed shift in the reflections of the post-benzene sample and the pattern is directly comparable to that of the pre-reaction sample, with both samples matching the cubic Mg_3N_2 phase.
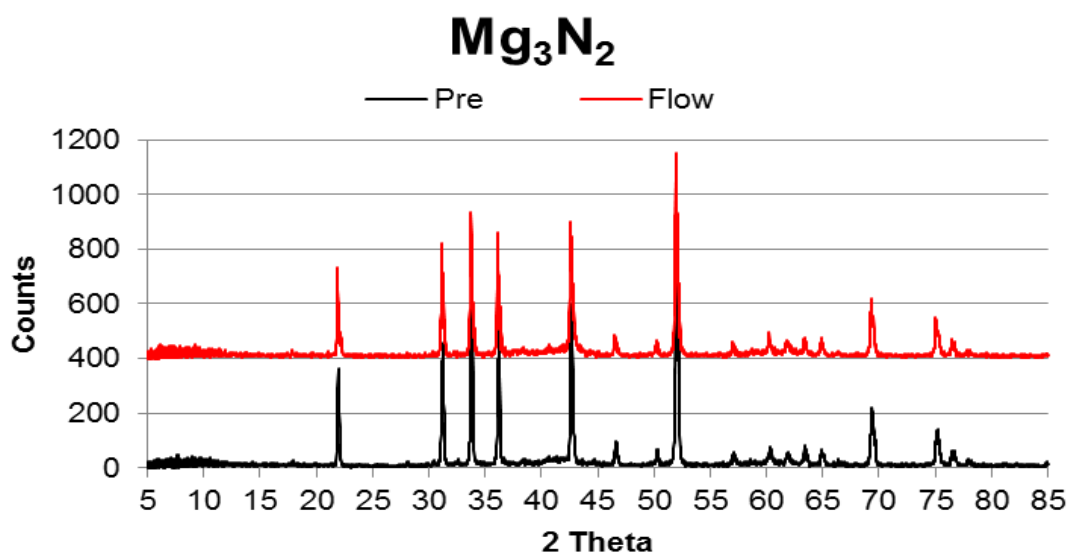
Figure 5.3-12 Pre- and Post-benzene XRD patterns of Mg₃N₂.

5.3.3 VN.

Vanadium nitride, amongst others, has been reported by Thompson and co-workers to be active in the amination of ethanol.[18]   It was shown that vanadium nitride, like platinum and supported nickel, was selective towards the ethylamine but only in the presence of ammonia, since otherwise ethene was observed to be dominant product.

Vanadium nitride was shown to be active for the production of ammonia, as described in Chapter 3, whilst it was also revealed, by subsequent post-reaction nitrogen analysis, that although a significant amount of nitrogen is lost upon reaction, only 1.8 % of the total nitrogen that was lost contributed to the formation of ammonia, with the remaining probably being lost as N_2. Vanadium nitride has subsequently been investigated as a possible aminating agent by reaction with benzene.

5.3.3.1 ^{1}H NMR Spectroscopy.

There was no apparent difference in the ^{1}H NMR spectra of the unreacted benzene and that for the products collected at the exit of the reactor, and so it is concluded that no products were formed.

5.3.3.2 XRD Patterns.

As with the lattice nitrogen studies, documented in Chapter 3, the XRD patterns of samples before and after reaction with benzene were confirmed to be cubic VN. Although there is a limited amount of nitrogen lost from the material, as confirmed by CHN analysis, it may be possible that only loosely bound surface NH_x species are removed at 400 ^{o}C, which may not be a sufficient temperature to activate the lattice nitrogen for it to then subsequently react with benzene. However, above 400 ^{o}C it is possible that benzene will decompose into carbon and hydrogen and so the temperatures above this value were considered to be outside the target range of the desired direct amination process as stated in the introduction to this chapter.
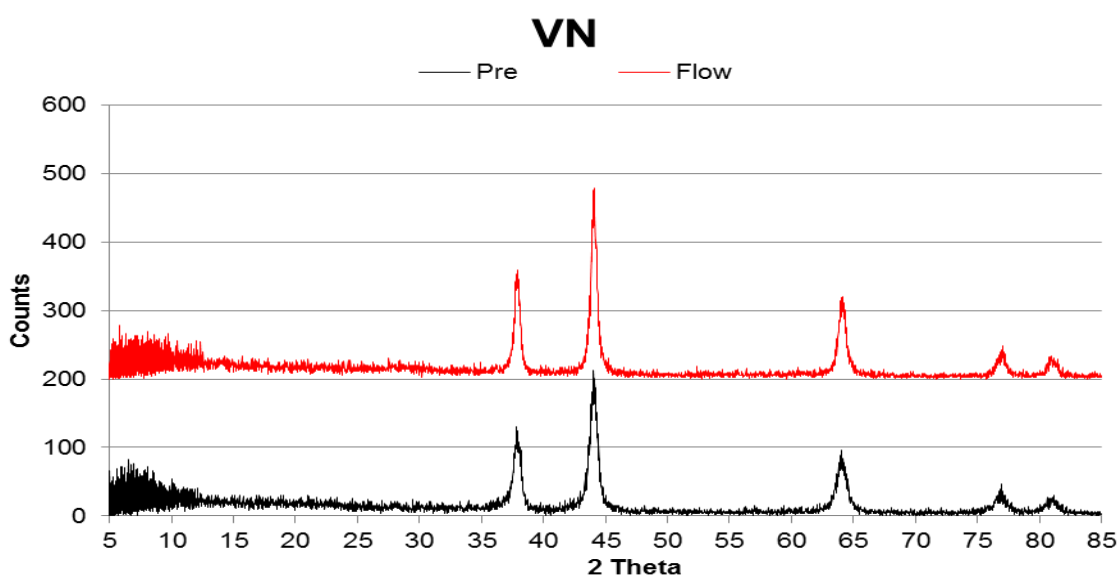
Figure 5.3-13 Pre- and Post-benzene reaction XRD patterns of VN.

5.3.4 Ta$_3$N$_5$.

In Chapter 3 Ta$_3$N$_5$ was shown to be active for the synthesis of ammonia at 400 ^{o}C under H_2/N_2. It was found that under these conditions a very limited amount of nitrogen was lost from the material, when compared to the sample reacted under isothermal H_2/Ar. It may be

possible that the N_2 present in the H_2/N_2 feed gas suppresses the hydrogenation of the lattice N in Ta_3N_5. Another possible explanation is that the N_2 in the feed gas fills the voids created upon hydrogenation of lattice N.

It was also demonstrated through a Ar-H_2/Ar switching experiment, that although a small degree of ammonia was produced under an Ar only feed the presence of H_2 caused a much more significant drop in the conductivity value, which consequently demonstrates the reactivity of the lattice nitrogen in this material.

To the writer's knowledge there is currently no literature available which has reported the use of Ta_3N_5 as an aminating regent or in nitrogen transfer type applications. From the data presented in Chapter 3, summarised above, Ta_3N_5 may be an interesting potential candidate for nitrogen transfer applications.

5.3.4.1 ^{1}H NMR Spectroscopy.

Again, no obvious change was observed in the post-reaction ^{1}H NMR spectrum of the reactant benzene. It was therefore concluded that no reaction occurred.

5.3.4.2 XRD Patterns.

The XRD patterns of the pre- and post-benzene reactions are essentially the same, indicating that the phase remains unchanged. However it is evident that the reflections which correspond to TaN (indicated by a star) present in the pre-reaction sample, samples do not appear in the post-benzene sample. This was also observed in the diffraction patterns of the post-H_2/Ar reaction samples (reported in Chapter 3), and may be attributed to the samples becoming more reduced upon reaction. Furthermore, some reflections appear slightly broader in the post- benzene sample, such as those at approximately 30 ^{o} and 35 ^{o} 2θ, possibly indicating that there is a slight increase in the disorder within the sample, which is also consistent with the apparent increase in intensity of the background. This could possibly arise due to the loss of nitrogen from the sample, as confirmed by CHN analysis, giving rise to a post-reaction stoichiometry corresponding to $Ta_3N_{3.99}$. No evidence of any additional carbon containing species was found after reaction.
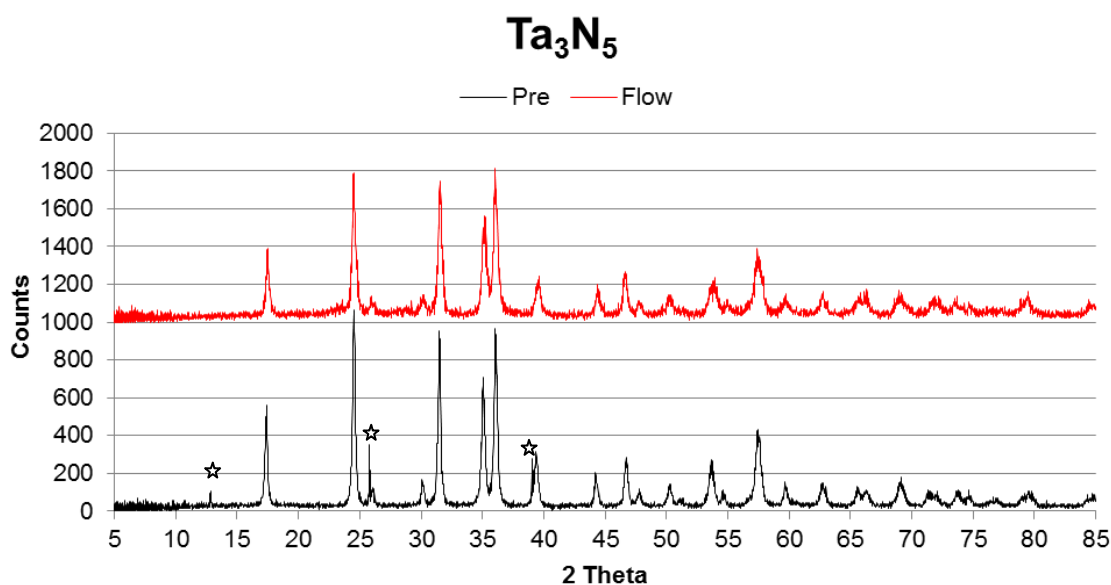
Ta$_3$N$_5$

Figure 5.3-14 Pre- and Post- benzene reaction XRD patterns of Ta$_3$N$_5$. TaN reflections are indicated by a ☆

5.3.5 β-Mo$_2$N$_{0.78}$.

5.3.5.1 ^{1}H NMR Spectroscopy.

In the spectra obtained of the benzene reactant, no change was observed upon reaction for the un-doped and doped β-Mo$_2$N$_{0.78}$ samples. Hence it was concluded that no product formation occurred.

5.3.5.2 XRD Patterns.

After reaction with C$_6$H$_6$ and H$_2$/N$_2$ it is evident, in the case of the un-doped β-Mo$_2$N$_{0.78}$ sample, that there are some shifts to a lower Bragg angle present in the post-reaction diffraction pattern with respect to that determined pre-reaction, Figure 5.3-15. This would generally be indicative of an increasing unit cell volume. In the instance of reactions with benzene it may be possible that some of the nitrogen is replaced by carbon which may induce a shift to a lower 2θ value due to the increased size of the carbon radius (N^{-3} 1.71 Å, atomic N radius 0.65 Å and C^{-4} 2.60 Å, atomic C radius 0.70 Å).[255] The presence of carbon in the sample was subsequently confirmed by post elemental analysis which revealed that both nitrogen and carbon was present being 3.31 wt.% and 1.32 wt.% respectively. Aside from the shift to a lower angle, no significant difference in the phase composition and no evidence of graphite was observed.
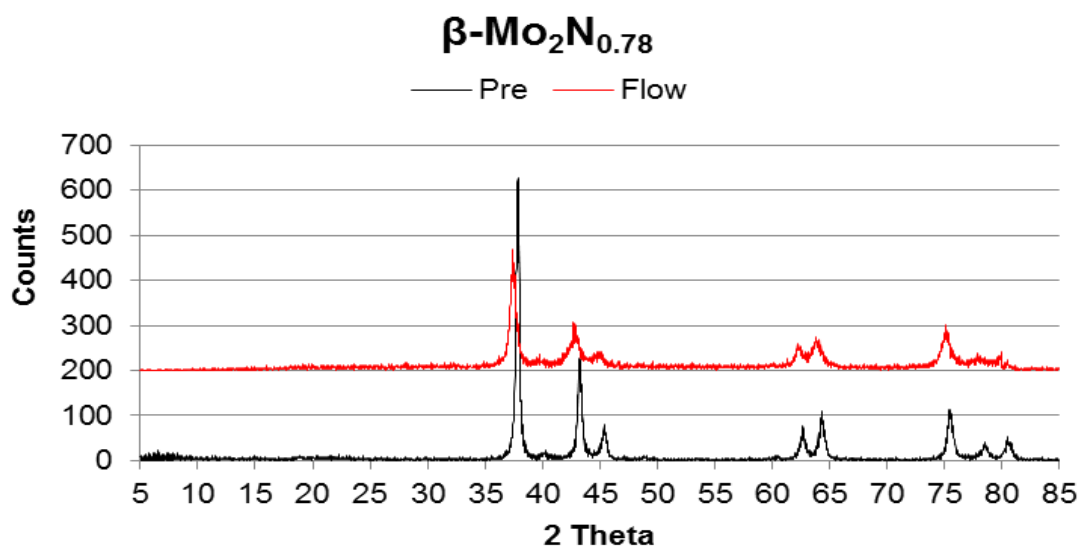
$\beta\text{-Mo}_2\text{N}_{0.78}$

Figure 5.3-15 Pre- and Post-benzene reaction XRD patterns of β-Mo₂N₀.₇₈.

The pre- and post-benzene diffraction patterns for the Fe doped $\beta\text{-Mo}_2\text{N}_{0.78}$ are presented in Figure 5.3-16. It is apparent that there are small changes in the intensity of the reflections at *ca.* 82 ^{o} 2θ. In addition there is also a small reflection which can be observed in both diffraction patterns at approximately 25 ^{o} 2θ in the pre-reaction sample and 26° 2θ in the post-benzene sample. The reflection is more apparent in the post-benzene diffraction pattern, which may indicate the presence of graphite which would correspond to a reflection at 26° 2θ.

1.5%Fe/β- Mo₂N₀.₇₈
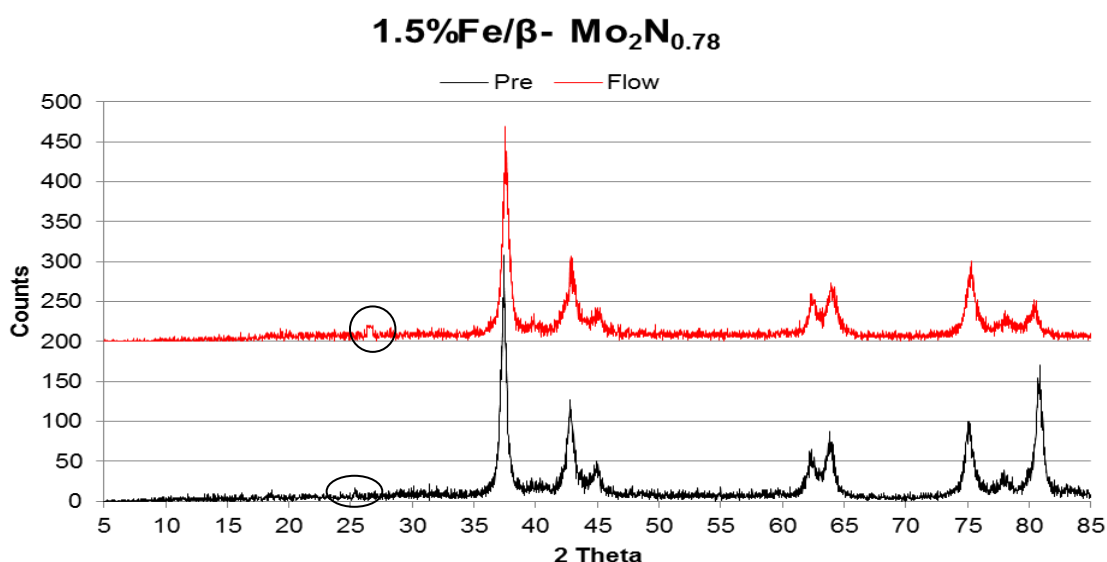
Figure 5.3-16 Pre- and Post-benzene reaction XRD patterns of 1.5 wt.% Fe/β-Mo₂N₀.₇₈.

The post-reaction XRD pattern of the Cu doped $\beta\text{-Mo}_2\text{N}_{0.78}$ sample resembles the pre-reaction sample, although the Mo reflections are more apparent. In addition it is clear that

the intensities of the reflections decrease and the reflections become slightly broader with respect to those observed in the pre-reaction sample. This may be a result of the material becoming slightly more disordered upon reaction with benzene. No apparent graphite reflections are observed in the post-reaction Cu doped sample and the absence of carbon in the sample was subsequently confirmed by elemental analysis, Table 5.3-5.
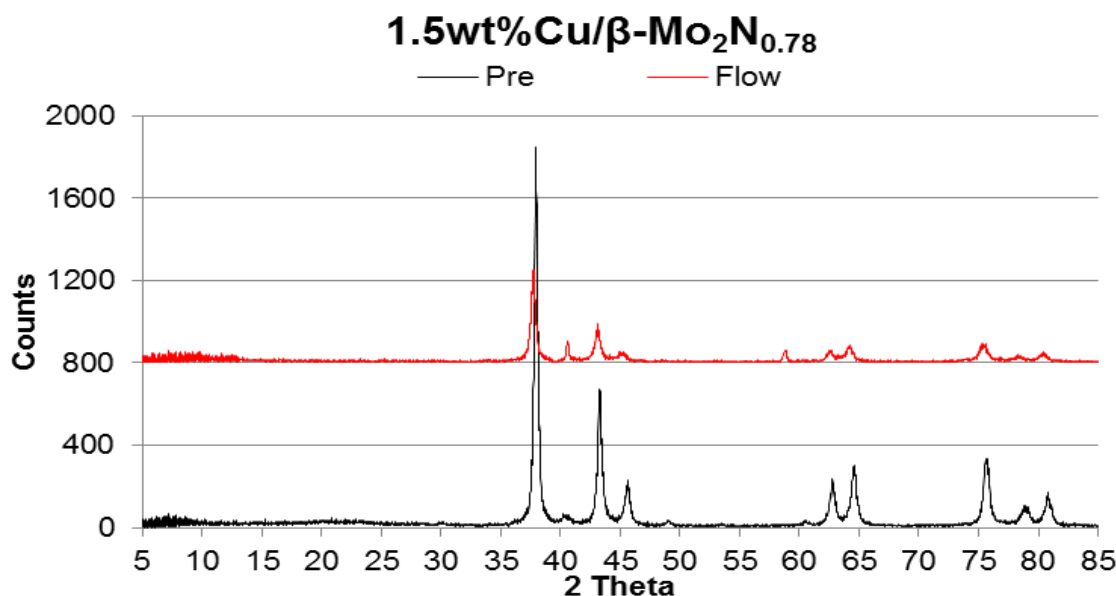
Figure 5.3-17 Pre- and Post-benzene reaction XRD patterns of 1.5 wt.% Cu/β-Mo$_2$N$_{0.78}$

5.3.6 W$_2$N.

There are several examples of tungsten nitride being used for amination reactions. Within the patent literature, Bowmen *et al* reported on the use of WN and W$_2$N, amongst others, for the amination of primary and secondary alcohols, for example the amination of monoethanolamine by diethenetriamine which resulted in a mixture of polyethlenepolyamines.[282] More recently Thompson *et al* also reported on the synthesis of ethylamines, as discussed in section 5.3.3, using W$_2$N.[18]

W$_2$N was shown to be active for the production of ammonia, as demonstrated in the studies described in Chapter 3, and is subsequently investigated in this chapter for the envisaged reaction with benzene.

5.3.6.1 ^{1}H NMR Spectroscopy.

From the ^{1}H NMR spectrum of products which were collected from this experiment, it was evident that no reaction with the benzene had taken place.

5.3.6.2 XRD Patterns.

The diffraction patterns of the pre- and post-benzene reactions are very similar, with a very small shift to a lower 2θ angle observed in the post-benzene reaction XRD pattern. This shift corresponds to a lattice d spacing of 2.400 Å compared with 2.394 Å observed in the pre-reaction sample. The shift to a lower angle is indicative of an increasing unit cell volume. However it was shown by post-reaction elemental analysis that a small amount of nitrogen was lost upon reaction (0.56 wt.%), which would normally result in the shift moving to a higher Bragg angle, and there was no indication of carbon present. The explanation for this effect is currently unclear but sample displacement effects in the XRD sample holder cannot be ruled out.
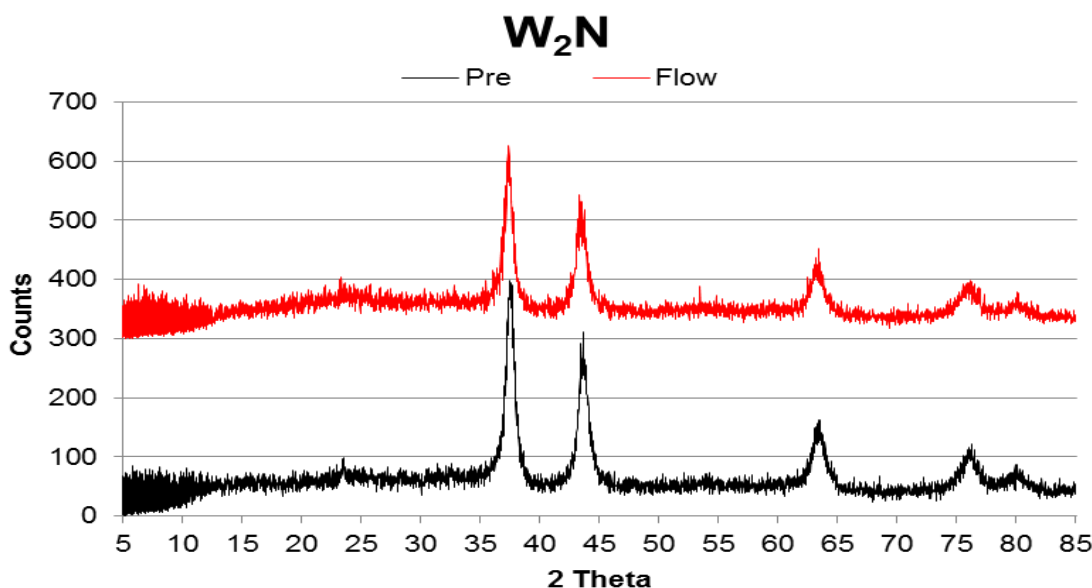
Figure 5.3-18 Pre- and Post- benzene reaction XRD patterns of W$_2$N.

5.3.7 Fe$_2$N.

Iron catalysts have been long known for their activity for ammonia synthesis.[210-213] In the present investigation, Fe$_2$N was found to be active for NH$_3$ synthesis at ambient pressure as detailed in Chapter 3. It was shown by XRD analysis that upon reaction Fe$_2$N decomposes to lower nitride phases such as Fe$_3$N and Fe$_4$N as well as Fe metal, demonstrating the evolution of nitrogen upon reaction. This has been well documented and is described in much detail by Goodeve and Jack.[102,103]

Although there is an abundance of literature related to the structure and ammonia synthesis activities of iron nitrides, there is very little related to amination type reactions.

5.3.7.1 ^{1}H NMR Spectroscopy.

Fe_2N was reacted with benzene at 400 ^{o}C. Upon analysis of the reaction products by ^{1}H NMR spectroscopy, no evidence of any product formation could be found.

5.3.7.2 XRD Patterns.

The post-reaction XRD pattern of Fe_2N, Figure 5.3-19, is clearly different to the pre-reaction sample. It is also evident that there is a broad reflection occurring at approximately 26 ^{o} 2θ, this is a signature reflection of graphite (indicated by a star). Additional weaker reflections at 54 ^{o} and 77 ^{o} 2θ also match graphite. The broad reflection at 26 ^{o} 2θ possibly indicates that the graphite in the sample is very disordered or it may also be possible that there are very few layers of graphite present in the sample. The number of layers in the sample can be estimated using the Scherrer equation. Taking the inter-planar spacing of graphite to be 3.35 Å, and that the apparent crystallite size of the reflection was calculated to be 63.50 Å, this corresponds to 19 layers of graphite present in the post-reaction sample. The presence of carbon was confirmed by CHN analysis to be 2.13 wt.%. It may be possible that graphite is not the only reflection which occurs at 26 ^{o} 2θ, a weak Fe_2O_3 reflection (JCPDS 039-1346) also occurs at this position. The larger reflections at 44 ^{o} and 65 ^{o} 2θ, correspond to Fe metal; however identification of other Fe metal peaks is difficult due to the overlap of reflections which may correspond to lower iron nitride phases, such as Fe_4N and Fe_3N. The pre-treated sample was confirmed to be pure phase Fe_2N by XRD, with a small impurity at 41° 2θ, which could possibly correspond to Fe_3N.
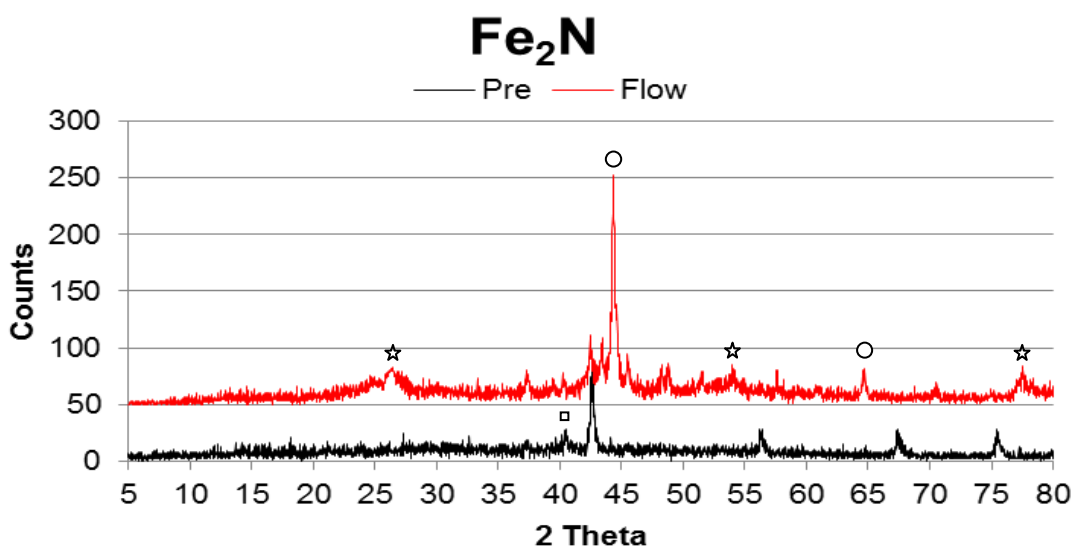
Figure 5.3-19 Pre- and Post-benzene reaction XRD patterns of Fe₂N. unambiguously assigned reflections are represented as the following, Fe metal ○, Fe₃N □ graphite ☆.

5.3.8 Re₃N.

From the studies conducted in Chapter 3, Re_3N has shown to be active for the production of ammonia, and had a greater ammonia production rate between 1-6 hours on stream than most of the other nitride systems which were investigated, with the exception of Zn_3N_2, Ta_3N_5, Mg_3N_2 and Co_3Mo_3N. As was mentioned in Chapter 3 the catalytic literature for Re_3N is scarce, although it has been shown to be active for catalytic hydrodenitrogenation reactions.[73] There is no evidence within the literature to suggest that Re_3N has previously been investigated for amination of organic compounds or for its potential use in nitrogen transfer applications.

5.3.8.1 ¹H NMR Spectroscopy.

Upon reaction, weak product peaks can be observed in the spectrum, as shown in Figure 5.3-20. Expanded spectra are presented in Figures 5.3-21 and 5.3-22.
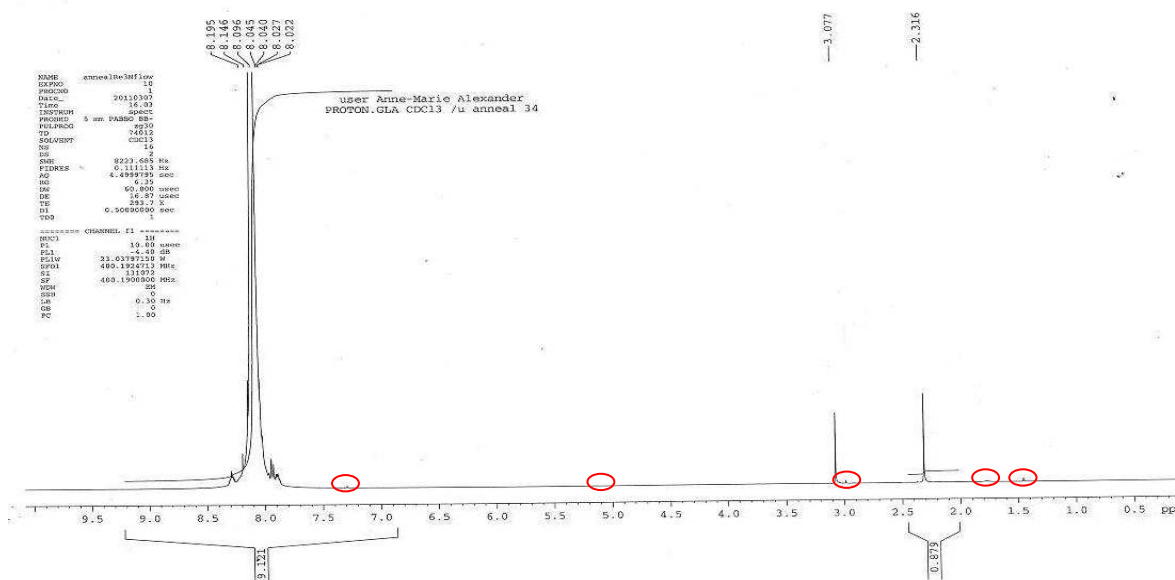
Figure 5.3-20 ^{1}H NMR spectrum of products collected after reaction of Re$_3$N$_2$ with H$_2$/N$_2$ and C$_6$H$_6$ at 400 ^{o}C for 1 h. (CDCl$_3$)

It is apparent that most of these additional peaks occur at the upfield end of the spectrum, and a small peak is apparent at 7.39 ppm occurring in the in the aromatic region of the spectrum.   The peaks at the upfield end of the spectrum are indicative of small hydrocarbon species. These peak positions, descriptions and possible assignment are presented in Table 5.3-3.
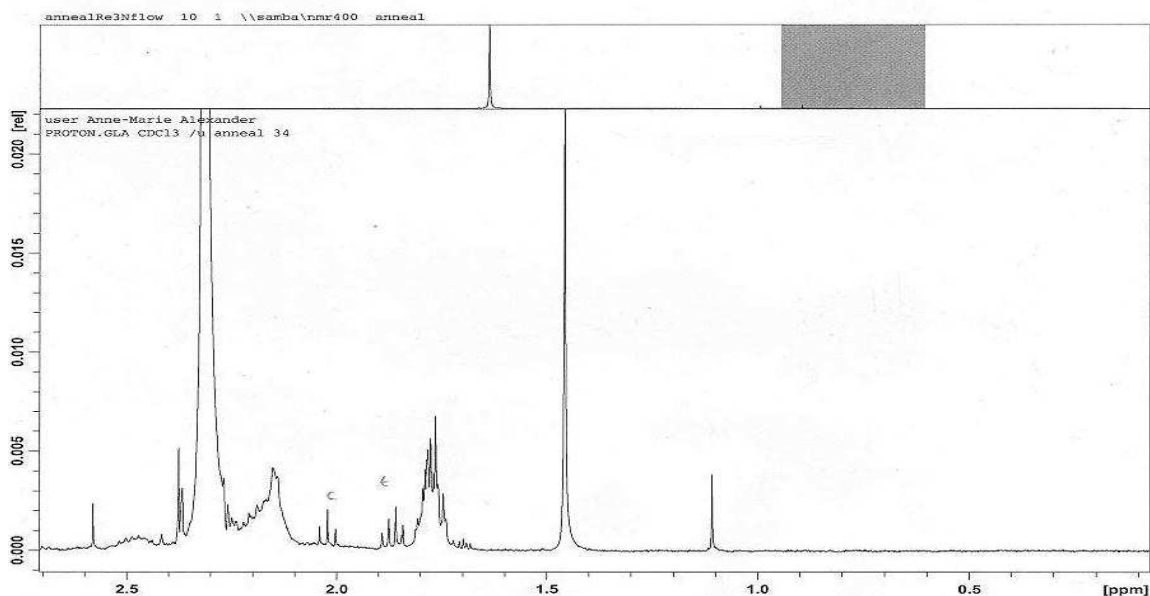
Figure 5.3-21 Expansion of shifts from 0-2.7 ppm in Figure 5.3-20.
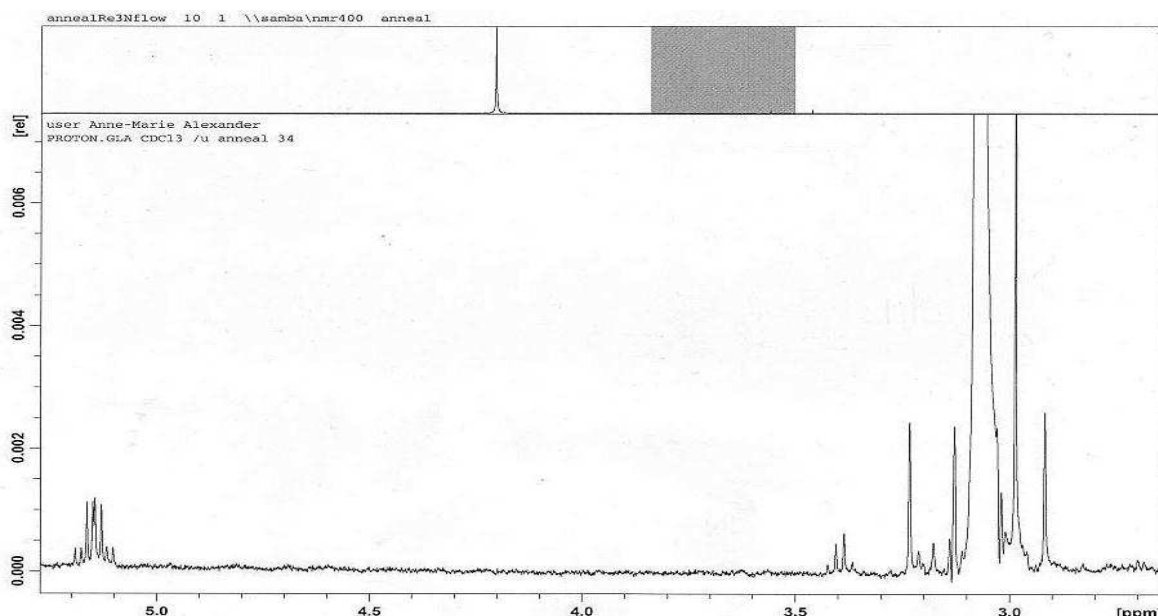
Figure 5.3-22 Expansion of shifts from 2.7-5.3 ppm in Figure 5.3-20.

Peak Shift (ppm)	Description	Possible Assignment
1.11	singlet	C-C$\underline{H}$
1.67	multiplet	?
1.87	quartet	C$\underline{H}$-CH$_3$
2.02	triplet	C$\underline{H}$-CH$_2$
2.39	doublet	C$\underline{H}$-CH
3.38	quartet	C$\underline{H}$-CH$_3$
5.15	multiplet	CH$_3$-C$\underline{H}$-CH$_2$-R
7.29	singlet	Aromatic CH

Table 5.3-3 Table of chemical shifts observed in ^{1}H NMR spectrum presented in Figures 5.3-21 and 5.3-22.

From the possible fragments, with the exception of the multiplet at 1.67 ppm, assigned to each shift a possible structure may be:
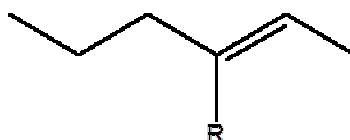
Again some of the mass fragments which were observed from the spectrum were relatively high, with respect to the target molecule aniline (93), and are presented below:

71, 78, 43, 51, 50, 83, 121, 149, 167, m/z

As observed previously the mass at 71 is again evident, which as described may be a result of a dehydrogenated benzene ring and the mass at 78 is unreacted benzene. The mass observed at 43 m/z may be attributed to CH_3- CH_2-CH_2 whilst the mass at 83 m/z may correspond to the hydrocarbon chain which is observed in the proposed fragment; CH_3-CH_2-CH_2-CH_2-CR=CH-CH_3

5.3.8.2 XRD Patterns.

The XRD pattern which was obtained for the post-benzene reaction sample demonstrates it to have partially de-nitrided, as shown by the patterns presented in Figure 5.3-23. A mixture of Re reflections (again shifted) and the original broad reflection are evident. Additional sharper reflections are also apparent in the diffraction pattern. These reflections at 17 ^{o}, 26 ^{o}, 28 ^{o}, 30 ^{o} and 35 ^{o} 2θ, as indicated by a star, correspond to ReO_3 (JCPDS 040-1155), may possibly be a result of oxidation of Re metal on discharge from the reactor.
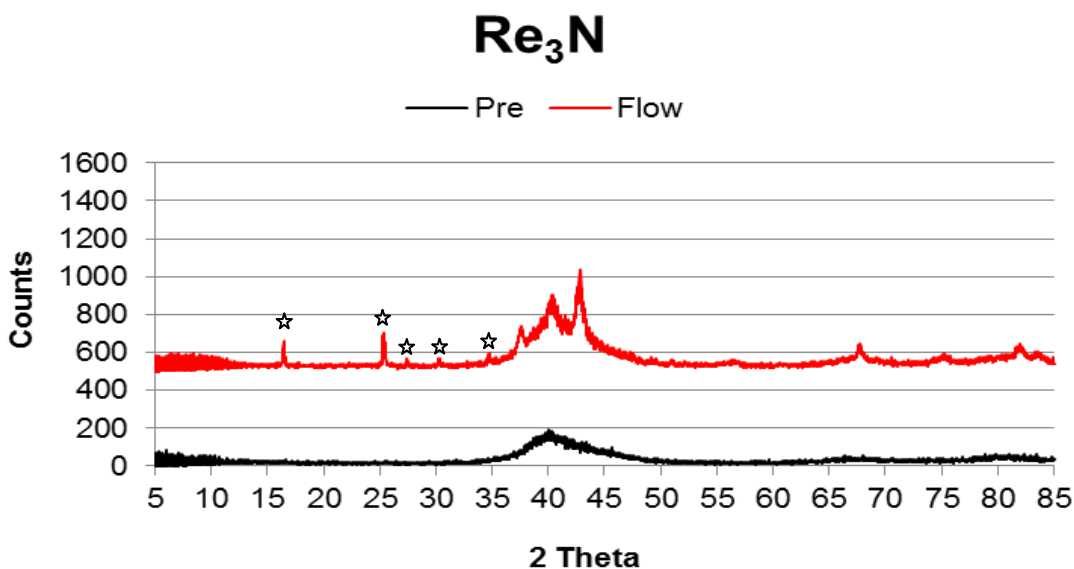
Figure 5.3-23 Pre- and Post- benzene reaction XRD patterns of Re$_3$N. ReO$_3$ reflections indicated by ☆.

5.3.9 Co$_4$N.

Cobalt nitride was shown to produce only a limited amount of ammonia from the H_2/Ar and H_2/N_2 studies conducted in Chapter 3. However it was shown that although a significant amount of nitrogen was lost from the material upon reaction, only 5.6 % of the total nitrogen lost from the material contributed to the formation of ammonia, with the remainder probably being lost as N_2. Cobalt nitride was also shown to rapidly decompose

upon reaction to Co metal and, as mentioned in Chapter 3, was difficult to prepare requiring very narrow synthesis conditions.

However as the decomposition temperature of the nitride is well below that of the maximum temperature for the envisaged process (250 ^{o}C and 400 ^{o}C respectively) it may be possible to react the nitrogen with benzene by employing high ramp rates and short reaction times (100 ^{o}C min^{-1} and 1 hour respectively).

However in a study by Rausch and co-workers, a supported Co catalyst was shown to be active for the amination of ethanol.[283] In that investigation it was shown that gas phase hydroamination of ethanol and ammonia over a supported Co metal catalyst yielded a large range of reaction products including ethylamines and diethylimine.

5.3.9.1 ^{1}H NMR Spectroscopy.

From the ^{1}H NMR spectrum of products which were collected from this experiment, it was evident that no reaction with the benzene had taken place.

5.3.9.2 XRD Patterns.

Again, as described for the H$_2$/Ar and H$_2$/N$_2$ studies presented in Chapter 3, identification of phases proved difficult by XRD, as Co metal, Co$_4$N and CoC$_x$ (JCPDS 044-0962) all have reflections centring on similar Bragg angles. However, a small shift to a higher 2θ angle was observed at *ca.* 44 ^{o} 2θ. On the whole there is no significant difference between the pre- and post-reaction diffraction patterns. The post-benzene carbon and nitrogen analysis can be used to determine if this material has decomposed to Co metal or whether the transformation to a carbide has occurred, from the CHN data presented in Table 5.3-5 it is evident that the nitride has decomposed to Co metal and no carbon is present in the post-benzene reaction sample.
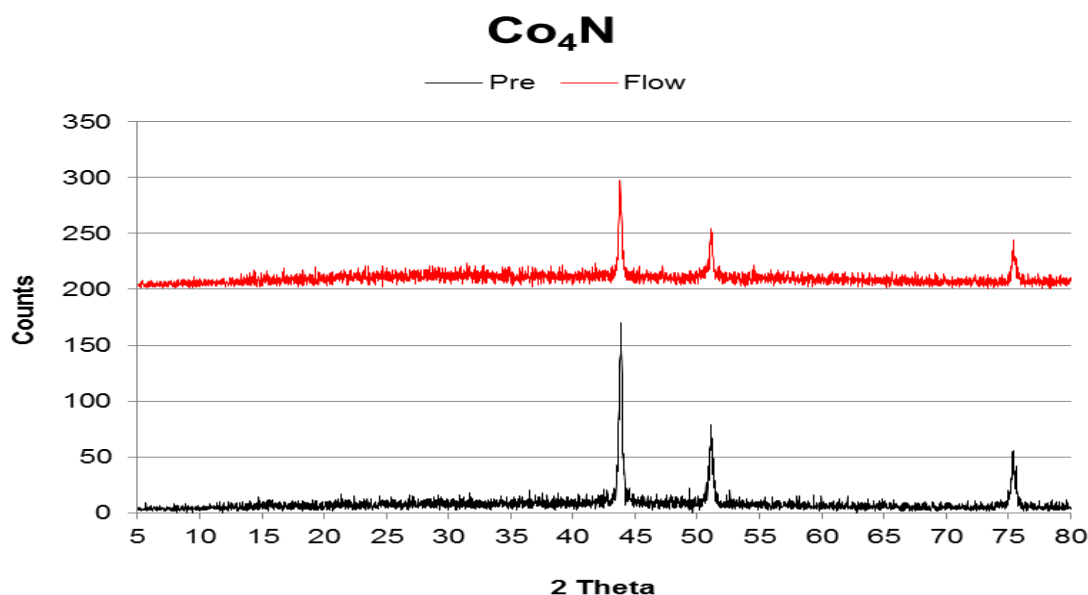
Co₄N

Figure 5.3-24 Pre- and Post- benzene reaction XRD patterns of Co₄N.

5.3.10 Ni₃N.

As previously discussed, Ni_3N decomposes to Ni metal upon reaction. As was observed in the studies in Chapter 3 a significant amount of ammonia is produced within the first half hour on stream. However, this ceases almost immediately with very little or no ammonia produced thereafter. As the material decomposes below the desired reaction temperature for the benzene reactions it may be possible, as described in the case for Co_4N and Cu_3N, to react the nitrogen with benzene, upon decomposition of the nitride to Ni metal, by employing high temperature ramp rates.

5.3.10.1 ^{1}H NMR Spectroscopy.

Ni_3N was reacted with both benzene and chlorobenzene feeds at 300 ^{o}C. However there was no indication that amination or any other reaction had occurred in these instances. The ^{1}H NMR spectra of post-reaction trapped samples corresponded to the respective reaction solvents, demonstrating the absence of detectable products of reaction.

5.3.10.2 XRD Patterns.

Upon inspection of the post-reaction XRD patterns, Figure 5.3-25, it is clear that there are some differences between the pre- and post-reaction samples. In the case of the reaction with chlorobenzene, the nitride decomposes to the Ni metal, which is confirmed by CHN analysis, whereas in the case of the reaction with benzene, under the same reaction

conditions, there is evidence of very weak reflections occurring at *ca.* 26 $^{\circ}$ and 48 $^{\circ}$ 2θ arising as a result of reaction. These reflections are consistent with graphite, although very weak. The presence of carbon is confirmed in the post-reaction sample by CHN analysis. From this it was found that the post-reaction sample contained a mixture of carbon and nitrogen at levels of 2.4 wt.% and 1.1 wt.% respectively. The percentage of carbon in the sample is much lower than the value for stoichiometric Ni_3C which is 6.77 wt.%. It is difficult to ascertain whether or not the carbide has formed due to the similarity in reflections which are observed in the XRD. However there is a possible shift to a higher 2θ value which is indicative of a decreasing unit cell volume. This shift corresponds to a d spacing of 2.317 Å compared to 2.324 Å (which is found in the pre-reaction Ni_3N sample) or 2.280 Å (which relates to the (110) reflection of the Ni_3C phase as given by JCPDS file number 026-1080). It may be possible that in this instance a carbonitride has formed. Similar shifts are also observed in the Ni metal reflections present. It is also apparent in the post-benzene diffraction pattern that although both Ni and Ni_3N reflections are evident, the intensities of these reflections are also comparable in size to the reflections in which only Ni metal reflections are observed, as in the post-chlorobenzene sample, or those in which only Ni_3N reflections are evident, as in the pre-reaction sample. This indicates that both products are present in the sample.
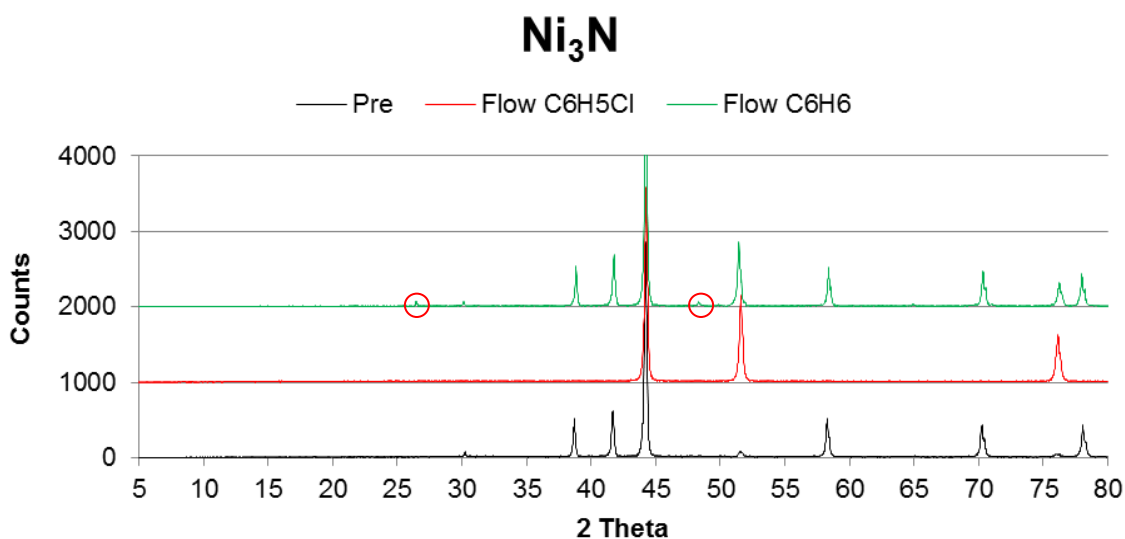
Figure 5.3-25 Pre- and Post-chlorobenzene and benzene reaction XRD patterns of Ni₃N.

5.3.11 Cu₃N.

Copper itself is a good aminating agent with examples being found in the patent literature and documented in organic synthesis.[169-173,235,236] In a study by Burgers and van Bekkum it was found that copper exchanged zeolites were highly active for the direct conversion of chlorobenzene to aniline in the presence of ammonia, where isolated Cu atoms were thought to be the active sites.[174] More recently Xu and Wolf reported that aryl halides could be aminated in the presence of catalytic amounts of copper salts to form anilines and their derivatives at low temperatures.[175]   However there are no literature studies documenting that Cu₃N has been used for this purpose.

Copper nitride along with some of the other more unstable nitrides such as Ni_3N, Co_4N and Re_3N, as was previously shown in Chapter 3, decomposes at a relatively low temperature. It was for this reason that a high ramp rate (100 ^{o} C min^{-1}) was employed in the experiments for this material described in this chapter. Copper nitride has been reacted with both chlorobenzene and benzene in flow reactions; however, an additional study in which Cu₃N was refluxed with chlorobenzene was also investigated, primarily due to the lower stability of Cu₃N.

5.3.11.1 ^{1}H NMR Spectroscopy.

In the reflux reaction with chlorobenzene and Cu₃N, the resultant ^{1}H NMR spectrum, matched chlorobenzene, and even after expansion of the baseline, no additional peaks were observed. From previous literature studies, it has been shown that Cu₃N is fairly stable up to temperatures of 250 ^{o}C beyond which it starts to decompose, so it is perhaps not surprising that no apparent reaction occurred during refluxing (at temperature 200 ^{o}C). Therefore it could be concluded that there was no active nitrogen to participate in the reaction at this temperature.

The ^{1}H NMR spectrum of the products obtained from the reaction of Cu₃N with chlorobenzene and H_2/N_2 at 400 ^{o}C, is shown in Figure 5.3-26, and on first inspection does not appear to be different from that of benzene. A large peak can be observed at corresponding to unreacted C_6H_5Cl, however there is also evidence of additional very weak peaks. Upon expansion of this spectrum, Figure 5.3-27, these peaks correspond to a small doublet at 6.17 ppm, two broad singlets at 4.08 ppm and 1.95 ppm, which may possibly be attributed to either Cl, NH or an OH group attached to CH-R group, and a triplet at 1.68 ppm, which may correspond to a CH-CH₂ group.[277-280]
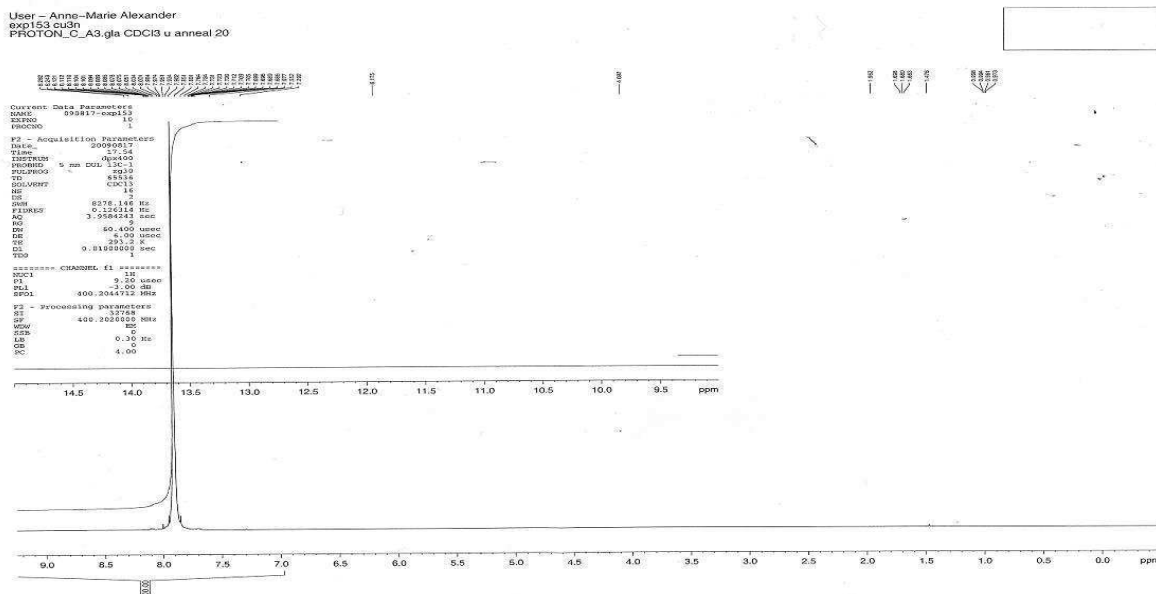
Figure 5.3-26 ^{1}H NMR spectrum of products collected after reaction of Cu₃N with H₂/N₂ and C₆H₅Cl at 400 °C for 1 h (CDCl₃).
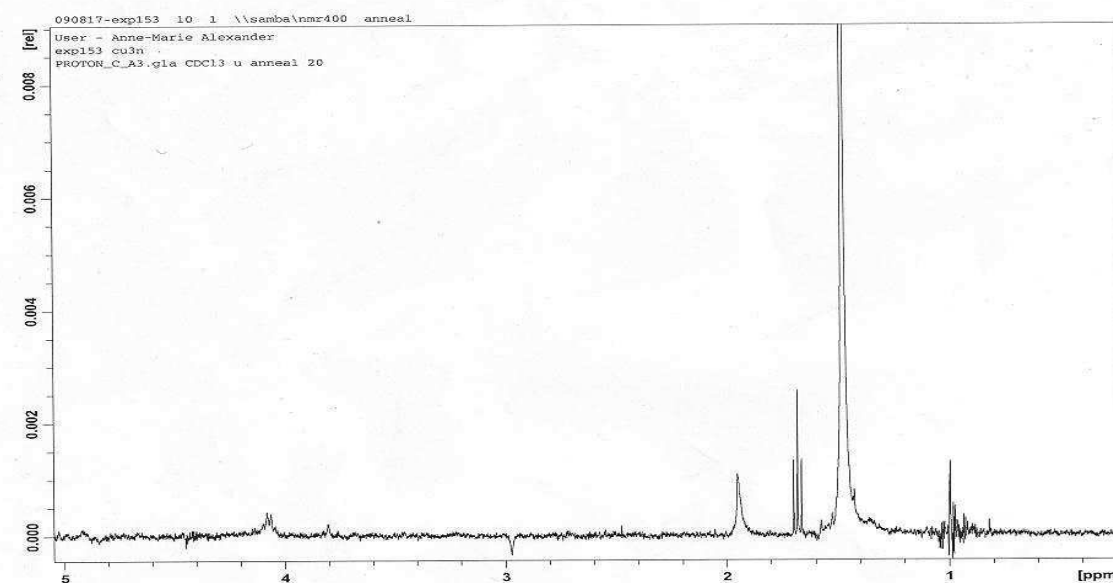
Figure 5.3-27 Expansion of the upfield region of the ^{1}H NMR spectrum in Figure 5.3-26.

Further investigations employed a flow of benzene over the material and the ^{1}H NMR spectrum obtained from the reaction products are presented in Figures 5.3-28 and 5.3-29. It is clear that there are several very weak peaks at the upfield end of the spectrum which correspond to the production of hydrocarbons. On expansion of this spectrum it was found that the peak at 1.05 ppm is a triplet, which would suggest the presence of a CH_2 coupling and a further peak is apparent at 3.67 ppm, this is split into a quartet and indicative of a CH_3 coupling. There is an additional peak which can be observed at approximately 4.70 ppm, but this peak is much larger than those described above and

probably corresponds to water in the solvent. There is no indication of the presence of any aromatic species other than unreacted C_6H_6.
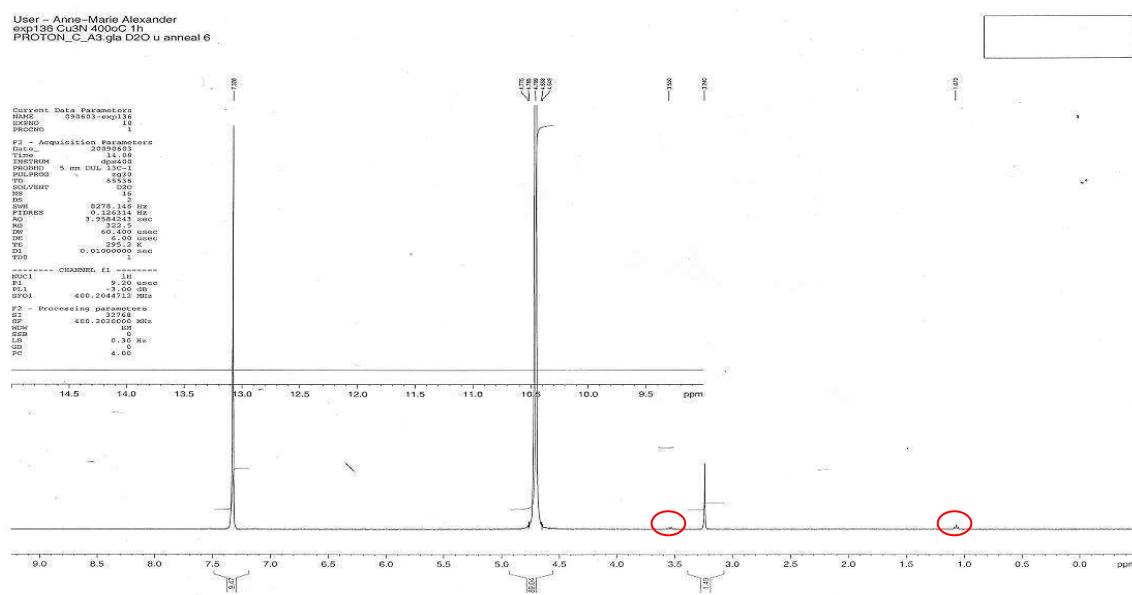
Figure 5.3-28 ^{1}H NMR spectrum of products collected after reaction of Cu_3N with H_2/N_2 and C_6H_6 at 400 °C for 1 h (D_2O).
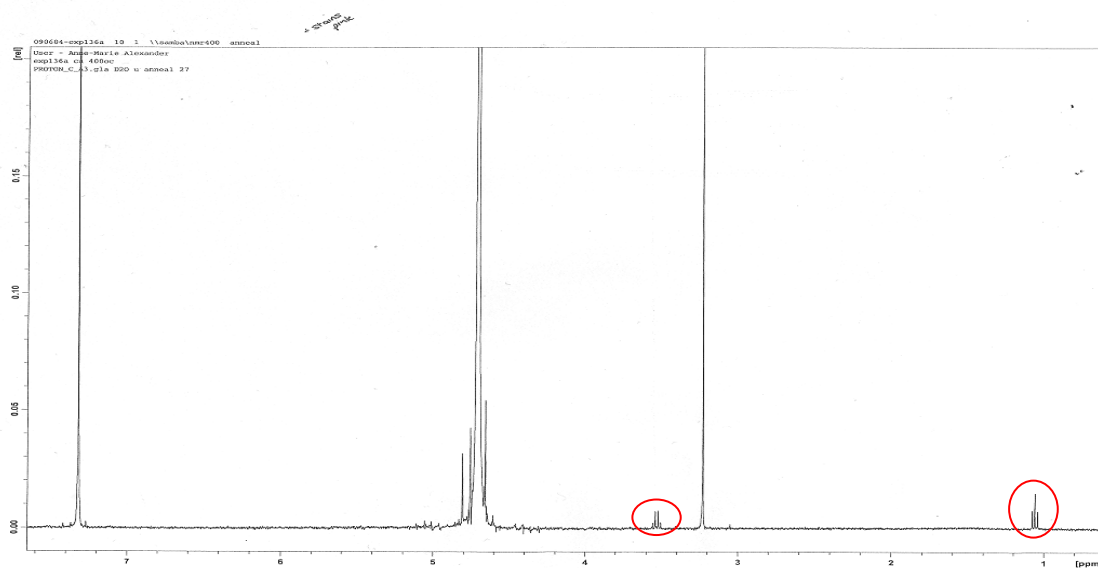
Figure 5.3-29 Expansion of Figure 5.3-28.

5.3.11.2 XRD Patterns.

As can be seen from Figure 5.3-30 the samples which have been reacted with benzene and chlorobenzene in the flow reactions have decomposed to Cu metal. Subsequent CHN analysis confirmed that all the nitrogen had been removed from the material. In the case of the chlorobenzene reflux reaction, the post-reaction diffraction pattern corresponds to that of the copper nitride, which would again suggest, that the reaction temperature has not been high enough to cause the nitride to lose nitrogen, as discussed earlier.
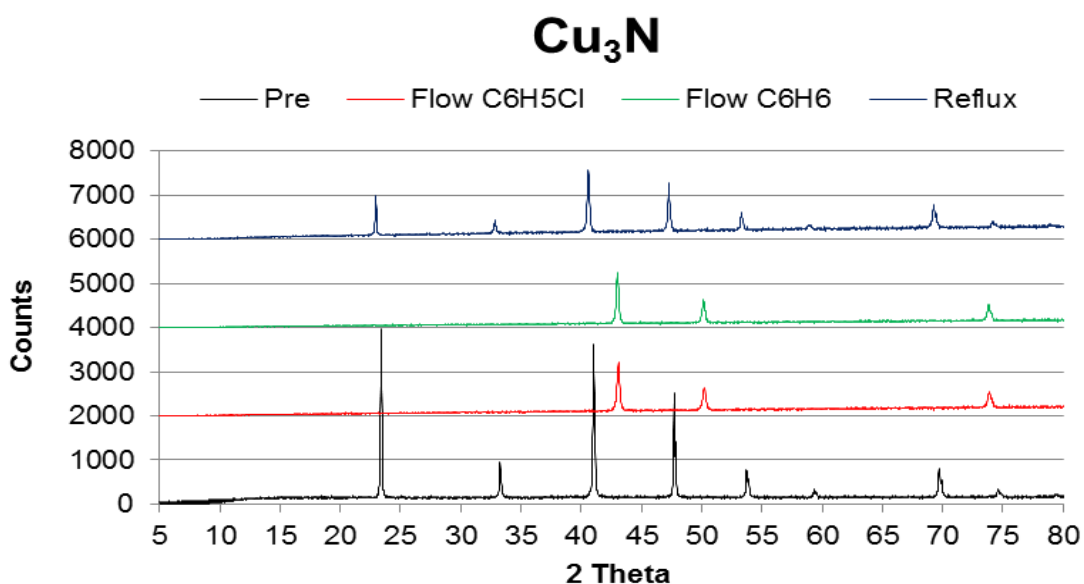
Figure 5.3-30 Pre- and Post-chlorobenzene and benzene reaction XRD patterns of Cu₃N

5.3.12 Zn₃N₂.

As was demonstrated in Chapter 3, zinc nitride shows an initial high activity for the production of ammonia at 400°C, which subsequently ceases after 6 hours on stream. This result was surprising as it was anticipated that Zn_3N_2 may behave similarly to Cu_3N. As the catalytic literature for Zn_3N_2 is scarce, and mainly concentrates on the structural and optical properties rather than catalytic aspects, it is again unclear whether Zn_3N_2 will be a suitable candidate for the amination of benzene, or indeed for similar Mars-van Krevelen type related processes.

5.3.12.1 ^{1}H NMR Spectroscopy.

Zn_3N_2 showed significant activity in the studies which were described in Chapter 3. Further to this, it was also one of the few materials which also exhibited additional peaks in the ^{1}H NMR spectrum of the post-benzene reaction product, as shown in Figures 5.3-31 and 5.3-32.

Expansion of the ^{1}H NMR spectrum highlights the presence of a triplet at 1.03 ppm and a quartet at 3.53 ppm, these are indicative of a CH_2 and CH_3 group respectively. These peaks are similar to those which were observed in the ^{1}H NMR spectrum of the Cu_3N reaction with benzene. In addition to these, there is a very broad peak which is apparent at approximately 6.78 ppm, which was not observed in the case of the Cu_3N reaction. This peak may correspond to a N or O containing heterocycle, however this remains unclear.[277-

[280] These types of compounds, i.e. pyridine, pyrolle and furan have a characteristic broad peak between 6.7 and 7.2 ppm. NH and OH groups, which have a similar broad appearance, occur at lower or higher shifts of around 3.6-4.8 ppm and 7-9 ppm respectively.[277-280]
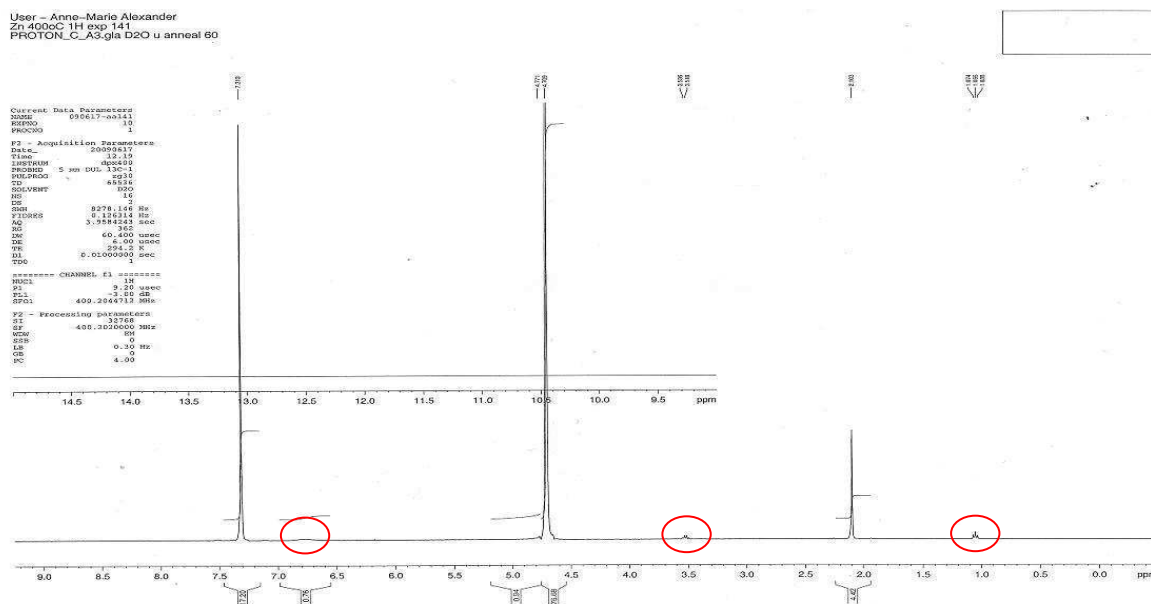
Figure 5.3-31 ^{1}H NMR spectrum of products collected after reaction of Zn$_3$N$_2$ with H$_2$/N$_2$ and C$_6$H$_6$ at 400 ^{o}C for 1 h. (D$_2$O)
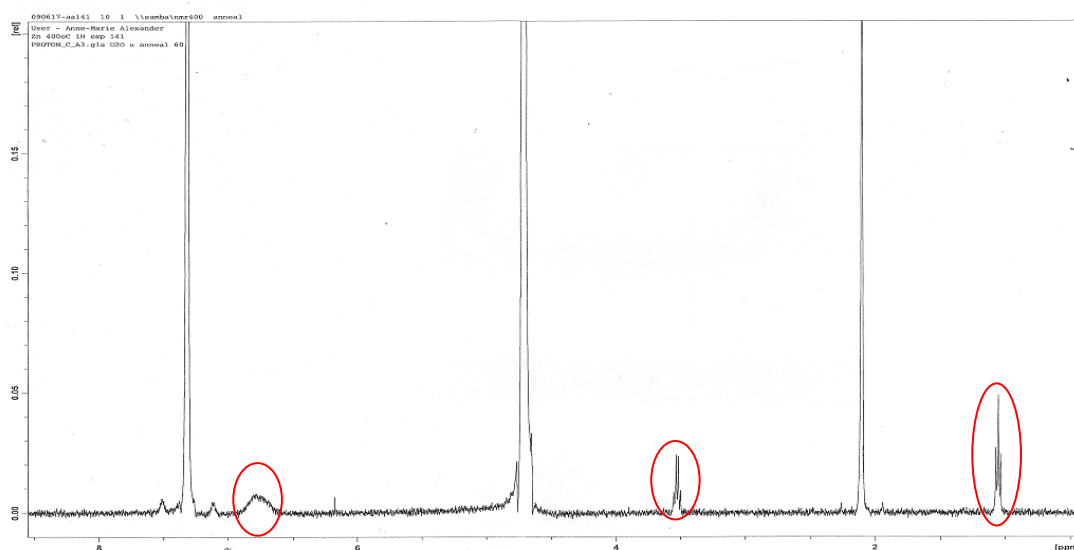
Figure 5.3-32 Expansion of Figure 5.3-31

5.3.12.2 XRD Patterns.

Although pre-reaction Zn$_3$N$_2$ has a relatively high nitrogen content, it is slightly lower than expected from stoichiometric Zn$_3$N$_2$, as was discussed in Chapter 3, and this may be attributed to the presence of ZnO in the sample as confirmed by XRD analysis with a ZnO

reflection observed at *ca*. 36 ^{o} 2θ. In addition, a small Zn metal impurity was detected at *ca*. 39 ^{o} 2θ. However, the remaining reflections matched those of cubic Zn_3N_2. The Zn reflection becomes more apparent in the post- benzene reaction pattern, which would be expected in the case of decomposition of the nitride. Again, as was seen in H_2/Ar studies reported in Chapter 3, the formation of ZnO is evident in the post-reaction XRD patterns, as has been previously discussed this may be due to the increased susceptibility of Zn metal to oxidise on discharge due to its increased reactivity.
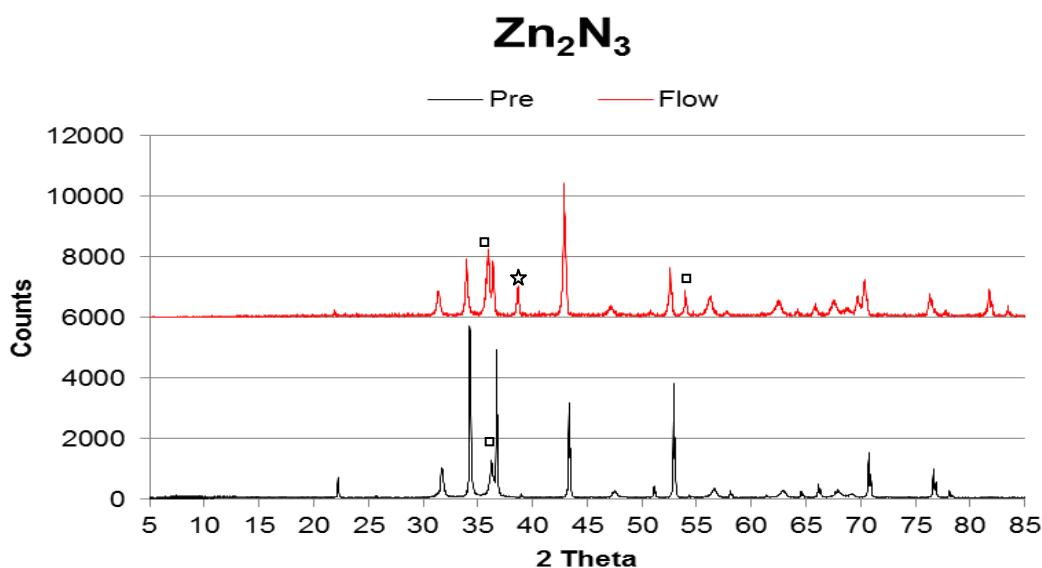
Figure 5.3-33 Pre- and Post-reaction XRD patterns of Zn_2N_3 The symbols used show characteristic reflections Zn metal (☆) and ZnO (▫) that can be clearly identified without ambiguity. (JCPDS 035-0762 Zn_2N_3).

5.3.13 Co-4Re.

Co-4Re is a relatively unstudied material and has demonstrated good potential as an ammonia synthesis catalyst, as reported in the studies by Aika and Kojima and subsequently in the H_2/N_2 reaction performed in Chapter 3.[59] Initially this work has centred solely on nitride based materials, however Co-4Re has been investigated as a nitrogen transfer reagent based upon the significant ammonia synthesis activity exhibited in Chapter 3. This material has a much higher activity than the other materials investigated, with the exception of the Ru based materials and Zn_3N_2. However Zn_3N_2 appears to decompose to Zn metal upon reaction and the production of ammonia ceases after 6 hours on stream. Co-4Re, on the other hand, has been tested for 16 hours under ammonia synthesis conditions with no apparent decrease in activity. It is for this reason that Co-4Re is being investigated under benzene reaction conditions.

5.3.13.1 ^{1}H NMR Spectroscopy.

Only upon expansion of the ^{1}H NMR spectrum obtained from the products of reaction between Co-4Re and C_6H_6 with H_2/N_2 are very weak product peaks observed. As with the other reaction products, the sample mainly consists of un-reacted benzene, which swamps the trace compounds which have been observed in some of the proton spectra. This was one of the main reasons that these experiments were only run for one hour, in an attempt to prevent any reaction products being diluted with excess un-reacted benzene. Figures 5.3-35 to 5.3-37 illustrates the peaks which were observed on expansion of the proton spectrum of Co-4Re.
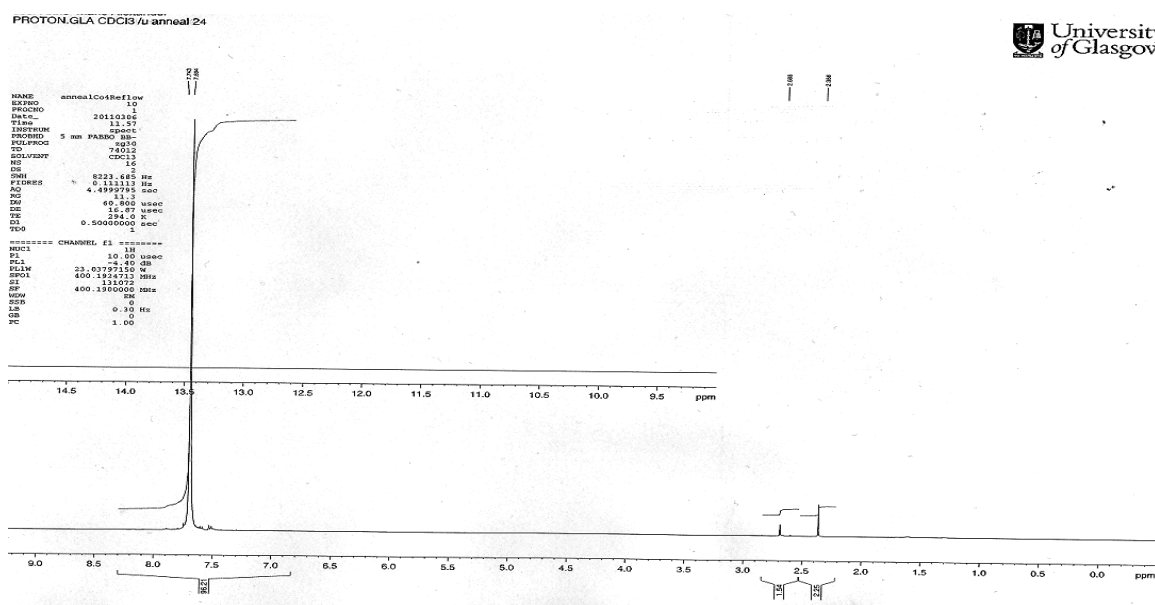
Figure 5.3-34 ^{1}H NMR spectrum of products collected after reaction of Co-4Re with H_2/N_2 and C_6H_6 at 400 $^\circ$C for 1 h. (CDCl$_3$)

Again, it is evident that most of the peaks are concentrated at the lower end of the spectrum, indicating the possible presence of hydrocarbon species. Additionally there are some peaks which are also present in the aromatic region of the spectrum, aside from the large benzene peak. However, it is obvious that these peaks overlap with benzene peak, making identification or possible assignment difficult. Table 5.3-4 provides an overview of the peak shifts along with a possible proton assignment to the respective shifts.
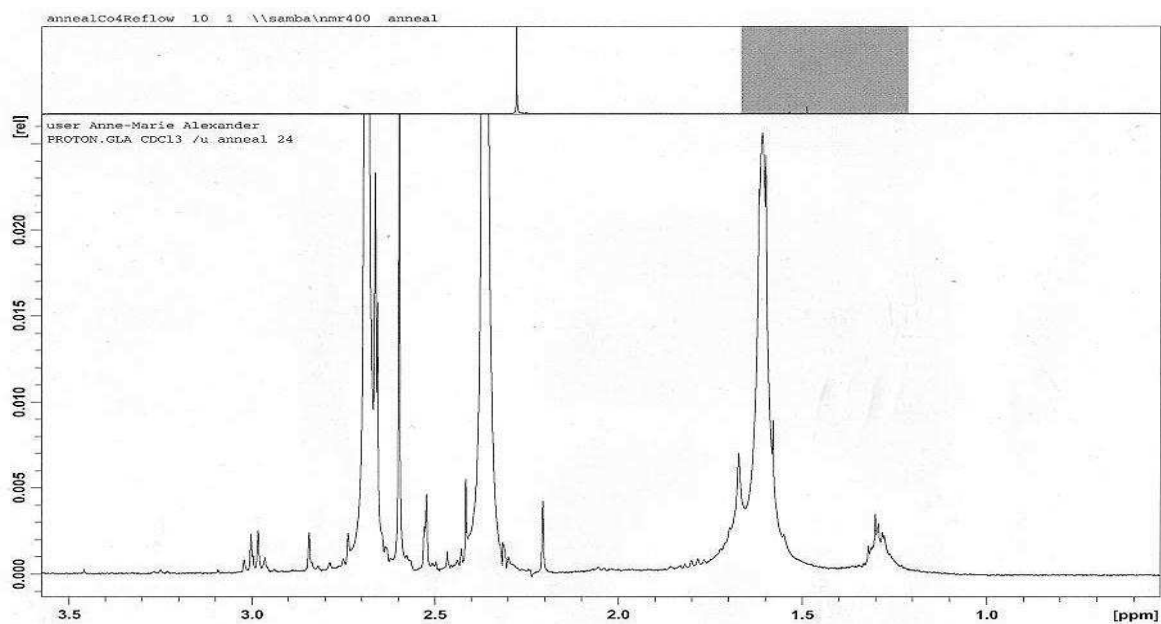
Figure 5.3-35 Expansion of shifts from 0.0-3.5 ppm in Figure 5.3-34.
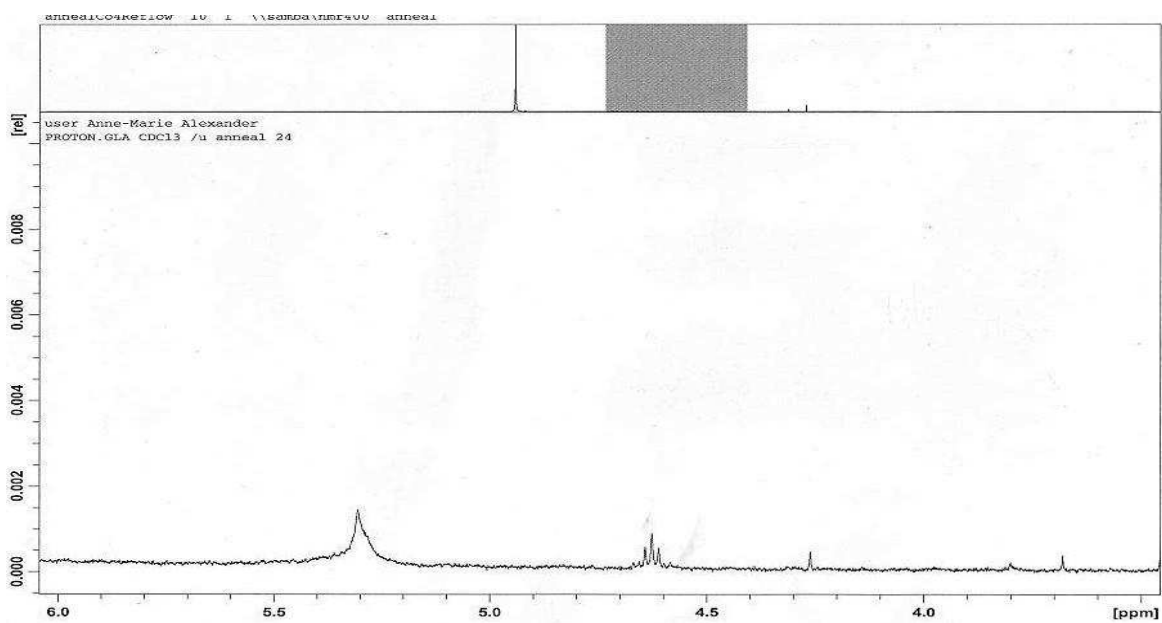
Figure 5.3-36 Expansion of shifts from 3.5-6 ppm in Figure 5.3-34.
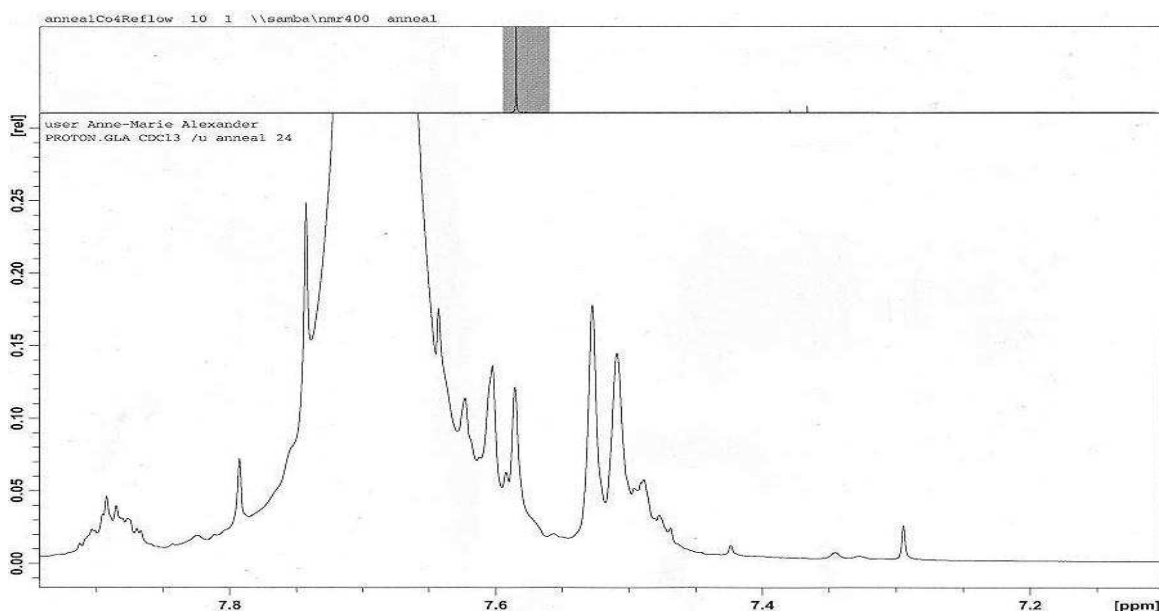
Figure 5.3-37 Expansion of shifts from 7.10-7.95 ppm in Figure 5.3-34.

Peak Shift (ppm)	Description	Possible Assignment
1.28	triplet of doublets	CH_2-C$\underline{H}$-CH
2.99	quartet	CH_3-C$\underline{H}$
3.67	singlet	C-C$\underline{H}$
4.26	singlet	C-C$\underline{H}$
4.63	triplet	CH_2-C$\underline{H}$
5.30	broad singlet	R-N$\underline{H}_2$ or R-O$\underline{H}$
7.29	singlet	Aromatic CH
7.50	possible doublet	Aromatic CH-C$\underline{H}$-CH (protons in same environment)
7.60	possible triplet	Aromatic CH-C$\underline{H}$-CH (protons in different environments)
7.88	multiplet	may be C_6H_5-R (overlapping signals from each proton)

Table 5.3-4 Table of chemical shifts observed in ^{1}H NMR spectrum presented in Figures 5.3-35 to 5.3-37.

It may be possible that one of the compounds present in the reaction products is nitrobenzene. As can be seen from the diagram below nitrobenzene has similar shifts to that observed in the ^{1}H NMR spectrum, and would have a similar splitting pattern with the H_a protons splitting into a doublet at 8.2 ppm; H_b protons splitting into a triplet at 7.6 ppm (as H_c and H_a protons are in different chemical environments) and H_c splitting into a doublet at 7.8 ppm. As protons a and c are ortho and para, respectively, to the NO_2 group

(electron withdrawing) this results in a downfield shift and consequently signals may overlap resulting in the appearance of a multiplet, if the resolution is not high enough to completely separate the signals.[277-280]
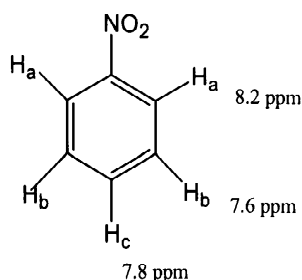
5.3.13.2 XRD Patterns.

The post-benzene reaction diffraction pattern of the Co-4Re material is similar to that obtained for the pre-reaction sample with no obvious shifts to indicate changing unit cell volume. As seen in the H_2/N_2 and H_2/Ar studies, the intensities of reflections in the post-reaction sample increase in intensity, which as previously mentioned may be as a result of the material becoming more crystalline upon application. As mentioned in Chapter 3, the pre–reaction samples contain both Co and Re metal phases, which are indicated by a star or circle respectively in Figure 5.3-38. As has been previously discussed in Chapter 3, Co-4Re becomes more crystalline upon reaction which is evident in Figure 5.3-38. This appears to be the only significant difference which is apparent between the diffraction patterns of the unreacted and post-benzene reaction samples. Additionally there was no evidence of graphitic species on the surface of the material which was consistent with the post-reaction CHN analysis.
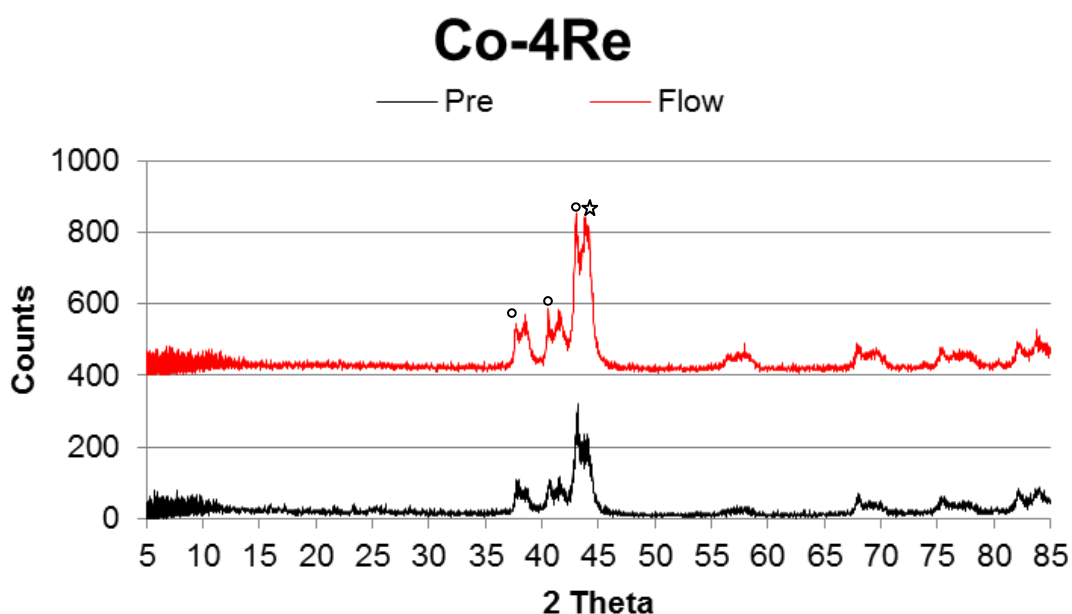
Figure 5.3-38 Pre- and Post-benzene reaction XRD patterns of Co-4Re (Co ☆, Re ○).

5.3.14 Post-Reaction Carbon and Nitrogen Analysis.

The post- reaction carbon and nitrogen contents of the nitrided materials were determined by combustion microanalysis, and are shown in Table 5.3-6

It is apparent that all of the materials which have been investigated in this section lose nitrogen, to varying extents, from their structure upon reaction with benzene and H_2/N_2. However it is also evident that certain materials also contain carbon after reaction.

As can be observed from the data presented in Table 5.3-6 Mg_3N_2 loses a significant amount of nitrogen upon reaction, however no apparent reflection shifts were observed in the diffraction patterns between the pre- and post-benzene reaction samples. Additionally, as mentioned previously, Mg_3N_2 is air and moisture sensitive and the sample may undergo oxidation prior to elemental analysis, which is a factor that needs to be considered upon analysis of the elemental data.

Elemental analysis confirmed the fact that carbon species were present in the post-benzene Fe_2N, Ni_3N and Fe doped β-$Mo_2N_{0.78}$ samples. Both carbon and nitrogen are evident in both the Ni_3N and Fe doped β-$Mo_2N_{0.78}$ samples. It is interesting to note in the case of the Fe doped β-$Mo_2N_{0.78}$ sample, the same wt.% of carbon is also apparent in the Fe_2N. Fe is known to be an active catalyst in the cracking of hydrocarbons and is frequently used for

Fischer-Tropsch reactions.[95] It may be possible that the Fe metal causes the benzene to decompose and thus deposits accumulate on the material surface.

As mentioned above, both carbon and nitrogen are evident in the post-benzene Ni_3N sample but not in the chlorobenzene sample in which decomposition to Ni metal is apparent. As was discussed in section 4.3.10, it is difficult to ascertain whether both carbide and nitride phases are present within the sample due to the close proximity of the reflections, although the presence of a tiny reflection at approximately 26° 2θ is present, which would be charateristic of graphite.

From the table overleaf it is clear that both carbon and nitrogen are present in the sample, although these are both much lower than the calculated stoichiometric values for nitrogen and carbon in Ni_3N and Ni_3C (7.36 wt.% and 6.38 wt.% respectively). As mentioned, it may be possible that a carbonitride phase exists, however this is remains unclear.

Nitride Material (400 °C, * 300 °C)	Calculated Stoichiometric N Content wt.%	Pre-reaction N Content wt.%	Nitrogen and Carbon content (wt.%)			
			Post-reaction			
			Observed N Content wt.%		Observed C Content wt.%	
			C_6H_6	C_6H_5Cl	C_6H_6	C_6H_5Cl
Co_3Mo_3N	2.92	2.93	2.55	1.97	-	-
Mg_3N_2	27.74	23.50	18.73		-	
VN	21.55	17.39	14.86		-	
Fe_2N	11.13	7.86	0.90		2.13	
Co_4N *	5.60	3.68	0.40		-	
Ni_3N *	7.36	6.58	1.10	0.09	2.40	-
Cu_3N *	6.84	6.05	0.00	-	-	-
Zn_3N_2	12.49	9.80	5.45		-	
Ta_3N_5	11.42	11.23	9.11		0.07	
β-$Mo_2N_{0.78}$	5.38	5.41	3.31		1.32	
Fe/ β-$Mo_2N_{0.78}$	5.38	5.58	2.73		2.13	
Cu/ β-$Mo_2N_{0.78}$	5.38	4.39	2.29		-	
W_2N	3.66	6.13	5.57		-	
Re_3N *	2.44	2.50	1.31		-	
Co-4Re	n/a	n/a	n/a		n/a	

Table 5.3-5 Pre- and Post-benzene reaction nitrogen and carbon content of materials investigated using a flow of benzene and H_2/N_2 at the reaction temperature specified in the text.

5.4 Benzene-Pulse Reactions.

The second method investigated as a potential synthesis route to aniline adopted a series of alternate benzene and ammonia pulses into a carrier gas which were subsequently passed over the reaction material.   These pulse studies were undertaken with the ultimate aim to overcome the limitation posed by direct reaction of ammonia and benzene.   Direct amination of benzene is equilibrium limited by the loss of hydrogen as discussed in the

introduction to this chapter. By pulsing ammonia the dehydrogenation stage can possibly be separated from the amination stage. NH_x residues adsorbed onto the surface of the reagent may react with the following pulse of benzene. In doing so, this lifts the equilibrium limitation by the potentially separating hydrogen loss from nitrogen addition in the reaction and potentially enables increased benzene conversion to aniline.

Pulse reactions were conducted as described in the testing section in Chapter 2. The materials which were investigated in the benzene-flow reaction have also been studied within this section and, as with the benzene–flow reactions, different reaction temperatures were applied taking into account the thermal stability of the materials. The temperature at which each material was studied is summarised in Table 5.4-1 below.

Nitride Material	Reaction Temperature H_2/N_2 (Ar and H_2/Ar for specific materials *)		
	250 ^{o}C	350 ^{o}C	400 ^{o}C
Co_3Mo_3N *		X	
Mg_3N_2*		X	X
VN		X	X
Fe_2N		X	X
Co_4N	X	X	
Ni_3N	X	X	
Cu_3N *	X	X	
Zn_3N_2 *		X	
Ta_3N_5		X	X
β-$Mo_2N_{0.78}$		X	X
Fe/β-$Mo_2N_{0.78}$		X	X
Cu/β-$Mo_2N_{0.78}$ *		X	X
W_2N		X	X
Re_3N *	X	X	
Co-4Re *		X	

Table 5.4-1 Overview of reaction temperatures used for each specific material. * indicates samples reacted in a H_2/Ar feed stream.

Of the materials presented in Table 5.4-1, it was found that the only materials to present indication of reaction, either in the form of apparent coking in the post-reaction bed packing granules or by ^1H NMR spectroscopy, were the same materials which displayed changes in the proton spectra of the benzene-flow reactions.   These materials are

Co_3Mo_3N, Mg_3N_2, Cu_3N, Zn_3N_2, Re_3N and Co-4Re. For this reason, these are the only materials which will be described in this section.

The other materials studied showed no indication of reaction with benzene other than small amounts of carbon being evident in the post-reaction elemental analysis. These CHN results have also been included in Table 5.4-2 at the end of this section. The ^{1}H NMR spectra of these materials were found to match that of the control ^{1}H NMR spectrum which is shown in Figure 5.4-1, along with a small additional peak between 7.89 and 8.05 ppm consistent with benzene.
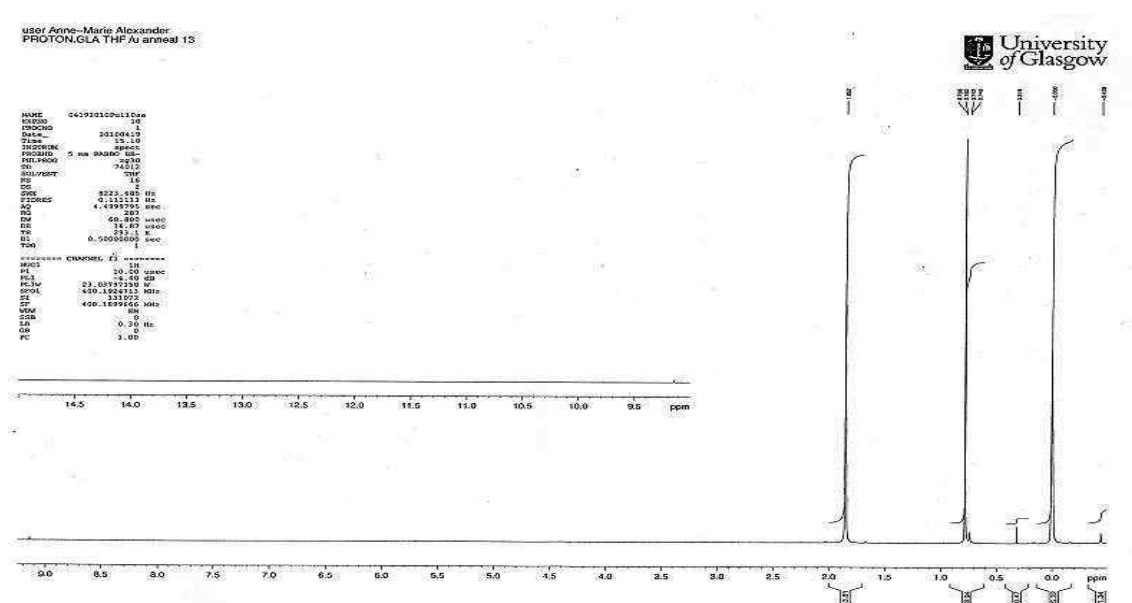
Figure 5.4-1 Control ^{1}H NMR spectrum used for benzene-pulse reactions.

The control ^{1}H NMR spectrum was obtained as a result of soaking unreacted silica packing granules in THF, which was the only solvent that dissolved the 'coked' material observed in some of the post-reaction packing granules of certain materials investigated. This solvent was therefore used for consistency. The two large peaks 0.79 ppm and 1.85 ppm correspond to THF with TMS referencing to 0 ppm.

Figure 5.4-2 illustrates the colours which were observed from the products obtained from the coked post-reaction bed packing granules. This 'coking' was only observed in the reactions which employed a H_2/N_2 feed gas for certain materials. It was not observed in the reactions which were conducted under an Ar only or H_2/Ar feedstream. It is apparent that most catalytic aminations occur in the presence of hydrogen, and it has been documented that its presence improves the yield of amines and prevents the catalyst deactivating by preventing the formation of nitrides, i.e. during disproportionation of

reactants and products which may consequently lead to incorporation of nitrogen into the metal lattice, instead of the formation of the amine.[283, 284] It is therefore surprising that no apparent reaction products are observed when using a H_2/Ar feed, and that they are only evident when using a 5 % H_2/N_2 feed, especially considering all other reaction conditions remain the same this may be indicative that a source of gas-phase N_2 is required to generate them. Furthermore, the order that NH_3 and C_6H_6 were pulsed into the reactor did not appear to make a difference.

Figure 5.4-2 Products obtained from H_2/N_2 pulse with C_6H_6 and (from left to right) Mg_3N_2, Re_3N, Cu_3N, Zn_3N_2 and Co-4Re.

Similar colours were reported in a study by Schulz, in which the deactivation of a zeolite catalyst during methanol conversion was investigated.[285] It was shown that during the reaction 'coke' forms on the surface of the zeolite subsequently blocking pores and hence deactivating the catalyst. It was reported that different at different temperatures different types of 'coke' were observed. For instance, it was noted that between 270-300 ^{o}C the catalysts had attained a yellow colour, which on exposure to air turned pink, which was reported to indicate the presence of highly unsaturated organic compounds, such as ethyl-trimethly-benzene and isopropyl-dimethyl-benzene. At higher temperatures (above 400 ^{o}C) the catalyst had been found to have three distinguishable zones; black, grey and blue in colour. The blue zone was thought to be associated with minor coking by olefins, such as ethene and propene.[285]

5.4.1 Co_3Mo_3N.

5.4.1.1 ^{1}H NMR Spectroscopy.

It is evident that the obtained spectrum, Figure 5.4-3, is very different to that of the control, which is presented in Figure 5.4-1. Two large multiplets at 1.62 ppm and 3.51 ppm correspond to THF and appear to mask some of the other shifts. However it is clear that there is an abundance of peaks at the lower end of the spectra, indicative of small chain hydrocarbons. This spectrum is very difficult to interpret and may possibly be due to the fact that multiple components are present within the sample. Attempts to purify the mixture were undertaken through use of thin layer chromatography. A variety of different

solvent systems were investigated to try and achieve a good separation, and clearly identify the number of compounds within the sample. However, this proved difficult as the TLC spot appeared to either 'run' on the silica or remain on the baseline as a 'whole' spot. This would possibly be due to the sample either being too concentrated or that the polarity of the compounds are in fact very similar to each making them difficult to separate. Figure 5.4-4 shows an expansion of Figure 5.4-3.
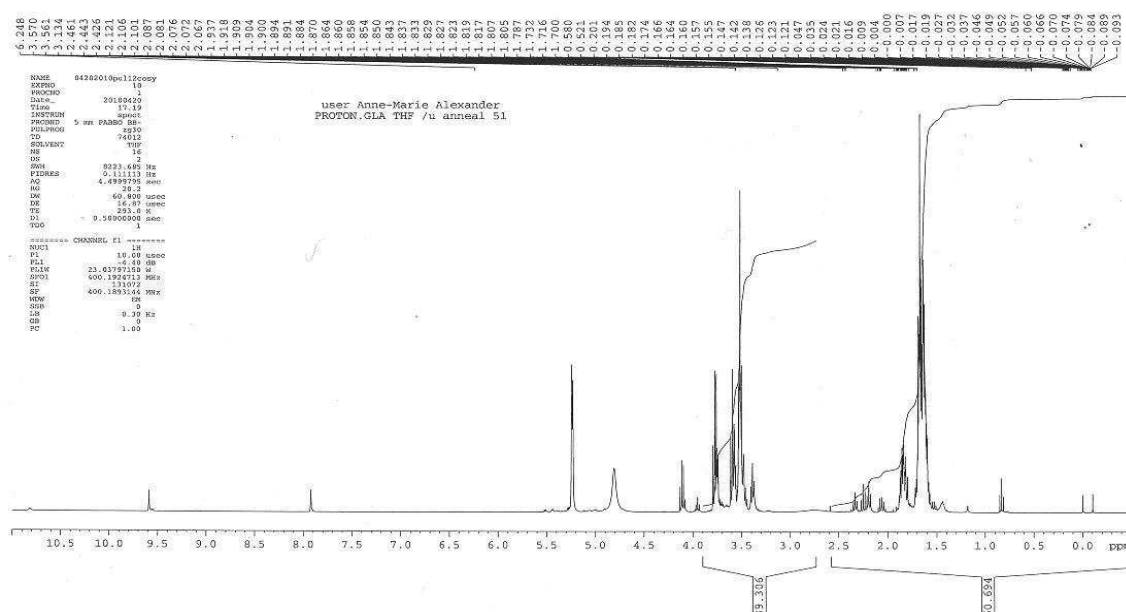
Figure 5.4-3 ^{1}H NMR spectrum of products collected after pulse reaction of Co$_3$Mo$_3$N with H$_2$/N$_2$ and C$_6$H$_6$ at 400 ^{o}C for 3 h (THF-d8).

From the spectrum, below, it is apparent that there are several triplets, occurring at 0.91 ppm and 2.38 ppm which would possibly be indicative of a CH$_2$ coupling; whilst it is difficult to assign the multiplets at 1.65 ppm, 2.05 ppm and 2.20 ppm.
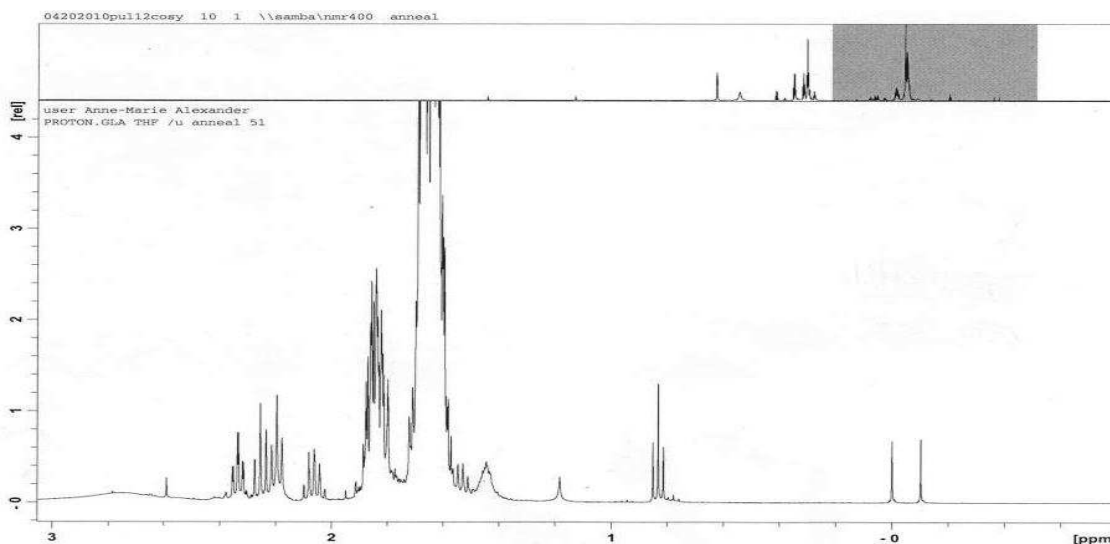
Figure 5.4-4 Expansion of the chemical shifts from -1.0-3.0 ppm in Figure 5.4-3.

The region which is covered in spectrum a) in Figure 5.4-5 is generally associated with protons that are coupled to either N, O or halogen atoms and often exhibit a broadening of mark up areatheir peak shape.[277-280] The two multiplets at approximately 3.58 ppm and 3.75 ppm are difficult to identify, it is evident that a triplet occurs at 3.38 ppm; a triplet of doublets corresponding to a $CH_2CH=CH$ group at 3.95 ppm and a quartet at 4.12 ppm, which may possibly be a CH or CH_2 group coupled to a CH_3 group. This is slightly higher than would be expected from standard ethyl group which would generally appear between 1-2 ppm, and it may be that a more electronegative atom, such as an O or N atom, is in close proximity.
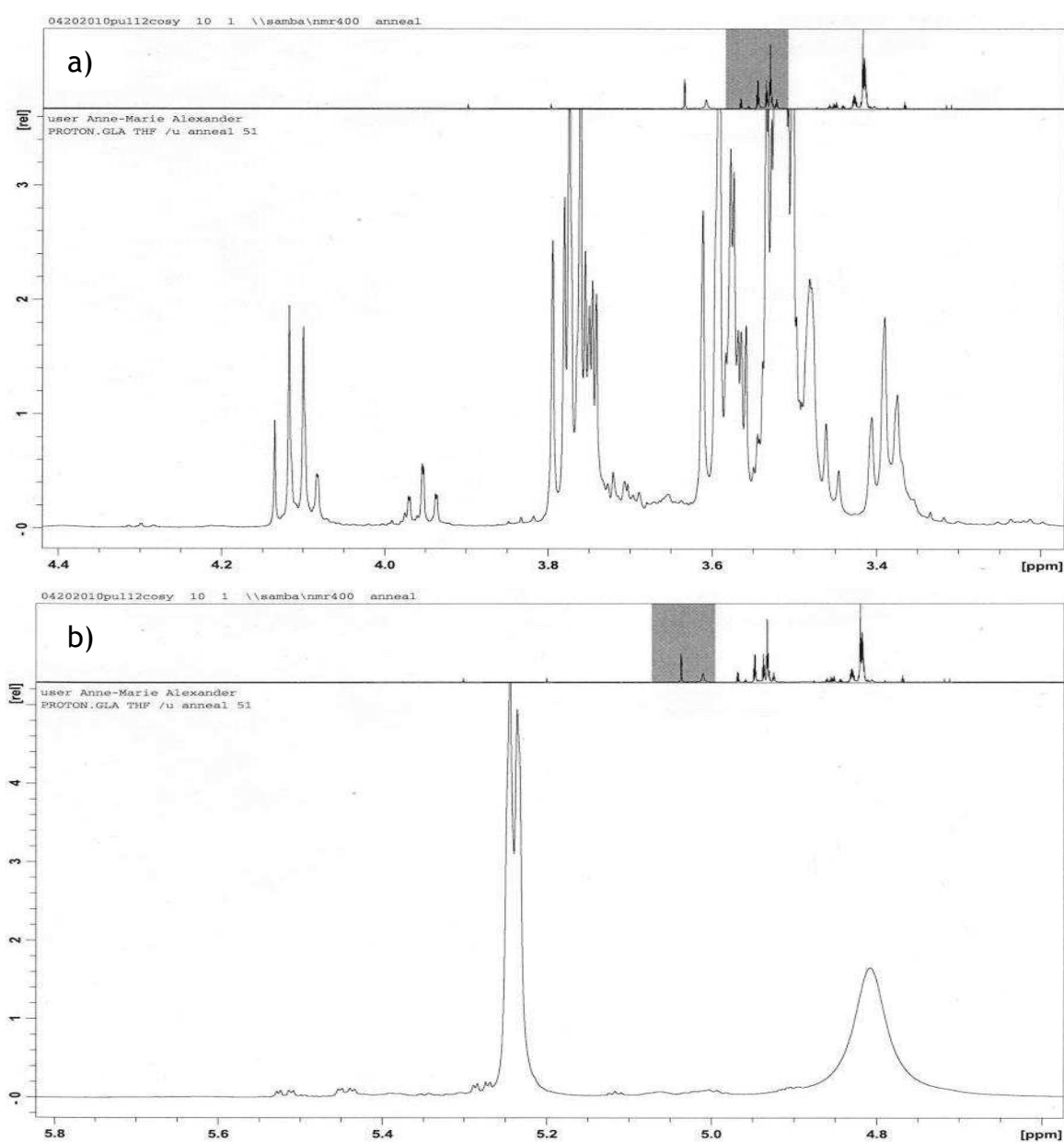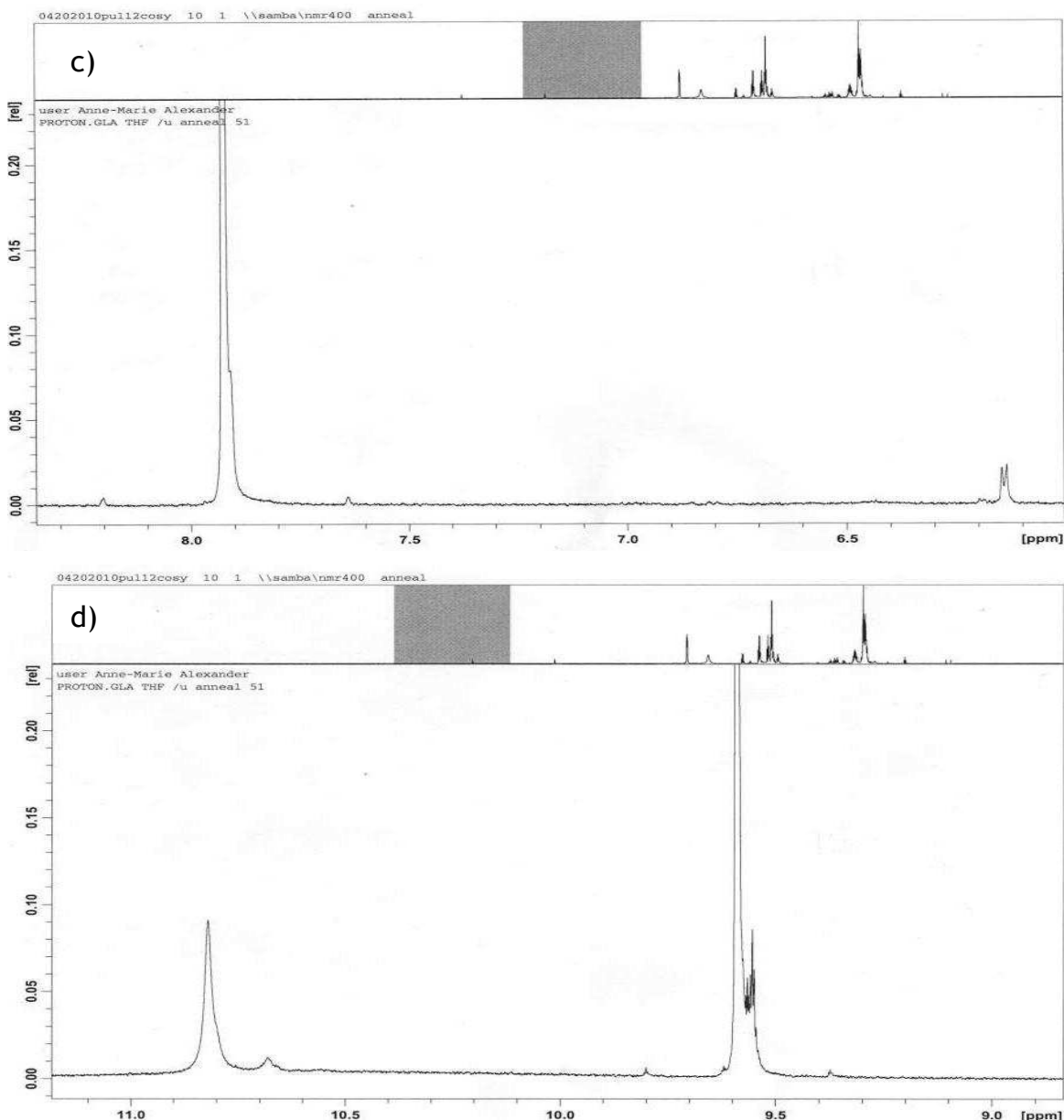
Figure 5.4-5 Expansions of Figure 5.4-3 at different shifts in the spectrum where peaks are observed a) 3.2-4.4ppm b) 4.6-5.8 ppm c) 6-8.5ppm d) 9-11ppm.

Spectra b-d indicate that a OH or NH_2 group may possibly be present within the sample, which is identified by a broad peak occurring at 4.81 ppm, characteristic of the presence of a RNH or ROH group, further reflections can also be observed at the higher end of the spectrum. Peaks which appear at higher chemical shifts are usually indicative of the presence of either a CO or COOH group.[277-280]

5.4.1.2 XRD Patterns.

It is evident that small shifts to higher Bragg angles occur in both post-reaction samples, as shown in Figure 5.4-6. This type of shift in the Bragg reflection is indicative of a decrease unit cell volume and thought to be, in this instance, as a result of loss of nitrogen from the sample. The shift which is observed under a H_2/Ar feed gas is consistent with that which

has been previously documented by Mckay and co-workers. In the case of the H_2/N_2 sample, the observed shift from 42.48 ^{o} to 42.68 ^{o} 2θ, is not as significant as is in the case of H_2/Ar, however it is clear that a degree of loss of nitrogen has occurred. This was subsequently confirmed by post-reaction CHN analysis, in which it was found that nitrogen had been removed from the sample in addition to the addition of 0.70 wt.% of carbon. This is much lower than the stoichimetric value for carbon in Co_3Mo_3C which would be 2.52 wt.%. However there are no apparent reflections in the diffraction pattern to indicate the presence of carbon species such as graphite. Consequently, it may be possible that this shift is attributed to the formation of a carbonitride phase.
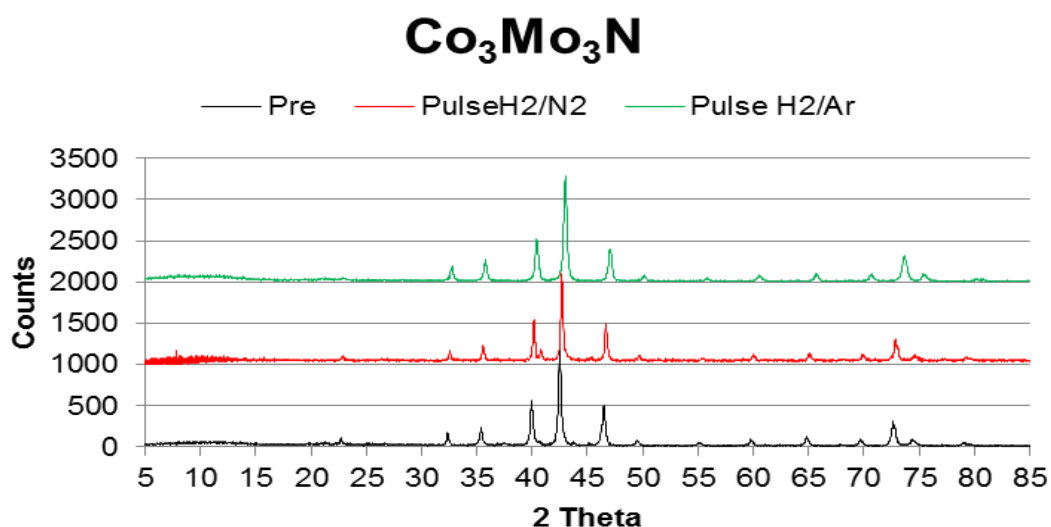
Figure 5.4-6 Pre-and Post-H_2/N_2 and H_2/Ar XRD patterns of Co_3Mo_3N from benzene/ammonia-pulse reaction.

5.4.2 Mg_3N_2.

5.4.2.1 ^{1}H NMR Spectroscopy.

The reaction products which were obtained from this reaction, coating the post-reaction packing granules, were light yellow in colour and dissolved in chloroform unlike most of the other reaction products which appeared to only dissolve in THF. It is apparent from the spectra that there are no peaks in the aromatic region, apart from a small peak at 7.21 ppm, which can possibly be attributed to unreacted benzene.
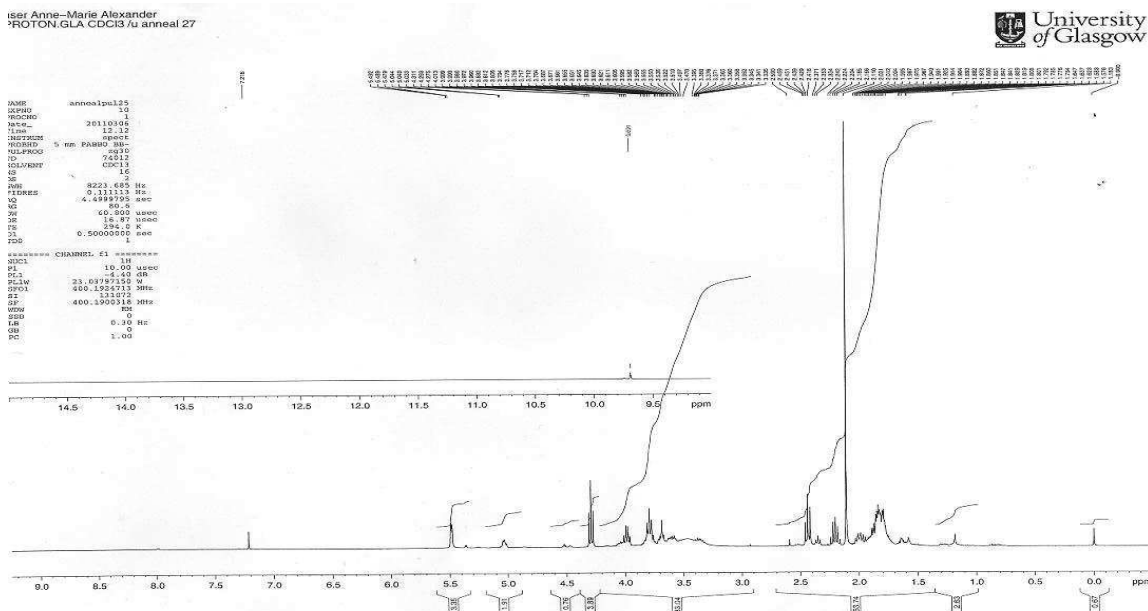
Figure 5.4-7 ¹H NMR spectrum of products collected after pulse reaction of Mg₃N₂ with H₂/N₂ and C₆H₆ at 400 °C for 3 h (CDCl₃).

On expansion of this spectrum the splitting pattern becomes more evident, Figure 5.4-8 a-c. However as the spectrum is relatively complex it is difficult to accurately determine the compound or compounds within the sample, although the compound or compounds are most likely to be unsaturated hydrocarbon(s) due to the number of peaks within 1.5-2.5 ppm and 3.5-5.5 ppm, which are typically regions where allylic or vinylic proton peaks are observed.[277-280]
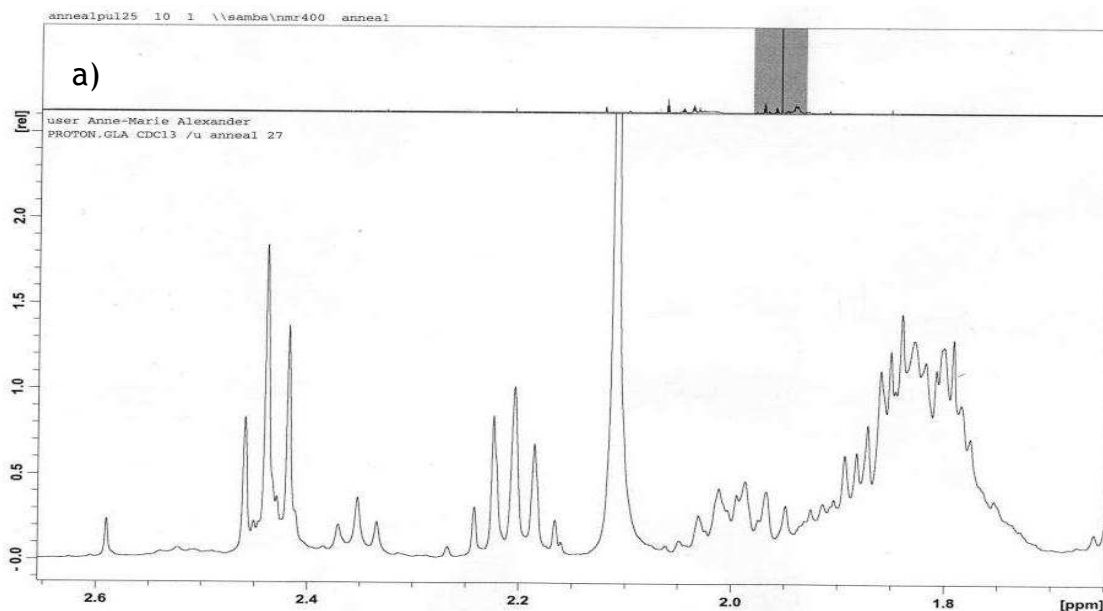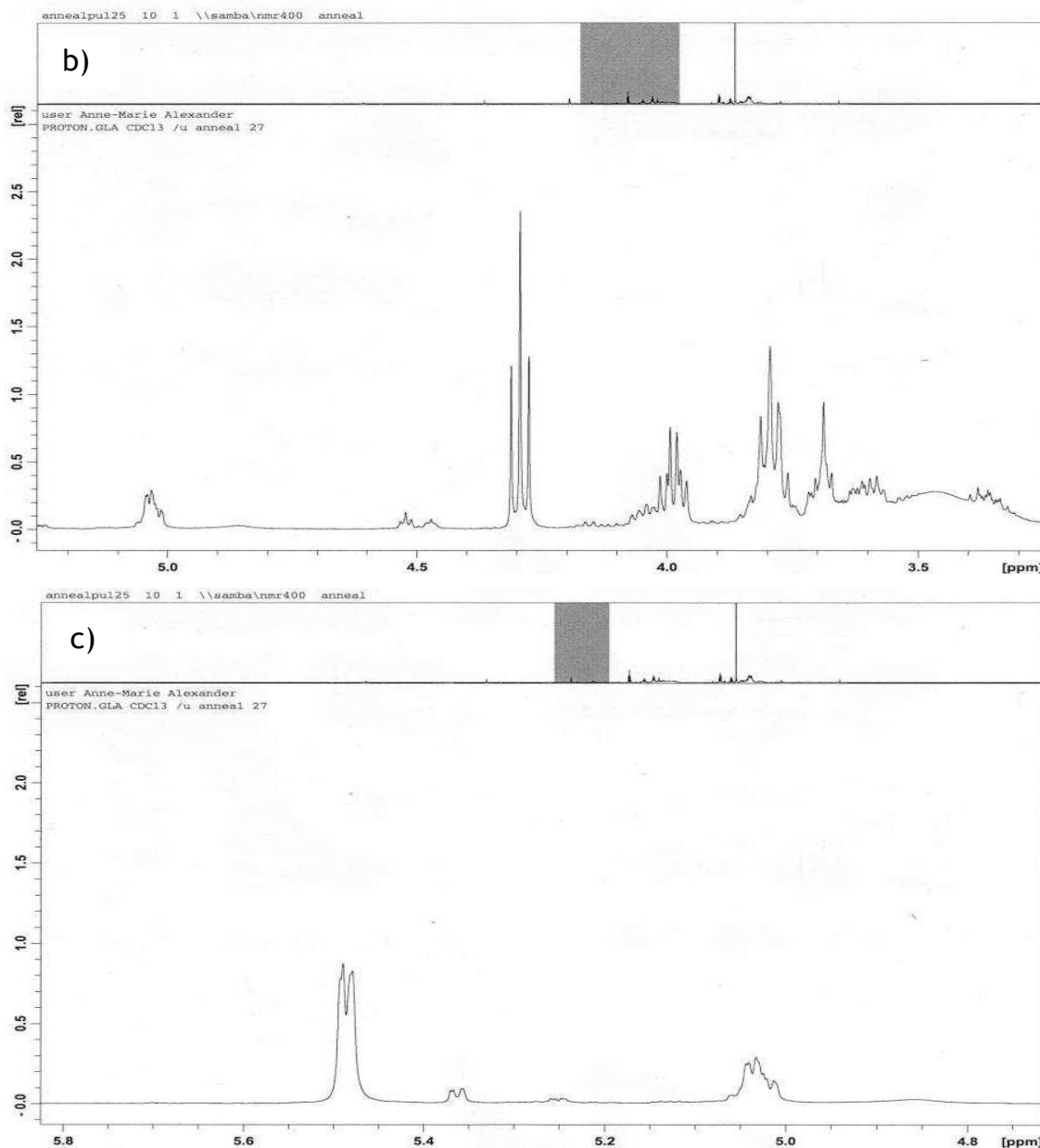
Figure 5.4-8 Expansions of Figure 5.4-7 at different shifts in the spectrum where peaks are observed a) 1.2-2.8 ppm b) 3.3-5.2 ppm c) 4.6-5.8 ppm.

5.4.2.2 XRD Patterns.

Again as has been found in both lattice (Chapter 3) and the benzene flow studies, Mg_3N_2, does not appear to undergo any significant bulk phase change upon reaction, with no apparent shift in Bragg angle to indicate an increase or decrease in the unit cell volume, nor does the material appear to decompose to Mg metal, as has been seen with some other nitride materials which have been investigated. All three samples match to cubic Mg_3N_2, and it is apparent from the XRD patterns that the reflections are sharp and indicative of well crystalline material.

Figure 5.4-9 Pre-and Post-H₂/N₂ and H₂/Ar XRD patterns of Mg₃N₂ from benzene/ammonia-pulse reaction.

5.4.3 Re₃N.

5.4.3.1 ¹H NMR Spectroscopy.

Figure 5.4-10 shows the ¹H NMR spectrum which was obtained for the reaction of Re₃N and benzene. As is evident, the spectrum is very complex making identification of compounds difficult, and although relatively similar to that which was observed in the case of Co₃Mo₃N, differences can be observed. The most apparent difference is a small broad peak at 4.91 ppm, which could possibly be RNH₂ group, which has an approximate chemical shift of between 5-8 ppm[277-280] and a collection of very weak peaks in the aromatic region at approximately 7.32 ppm, and 6.25 ppm, which have been expanded in Figure 5.4-11.

Figure 5.4-10 ¹H NMR spectrum of products collected after pulse reaction of Re₃N with H₂/N₂ and C₆H₆ at 400 °C for 3 h (THF-d8).

Upon expansion of the aromatic region, Figure 5.4-11 a), it is evident a substituted aromatic fraction is present in the reaction products, with a small triplet and two doublets being apparent. However, the remaining peaks overlap to such an extent that it is unclear which positions a substitution may occur and how many protons are associated with this aromatic species. A small doublet is also evident at 6.24 ppm

Furthermore the peak which can be observed at 8.05 ppm may possibly be unreacted benzene and additional peaks at approximately 9.69 ppm, and at 9.67 ppm, Figure 5.4-11 b), comprise a doublet of doublets and a doublet of triplets respectively. Due to the peak position, it may also be possible that this corresponds to substituted benzene which has an oxygen atom present in the structure.
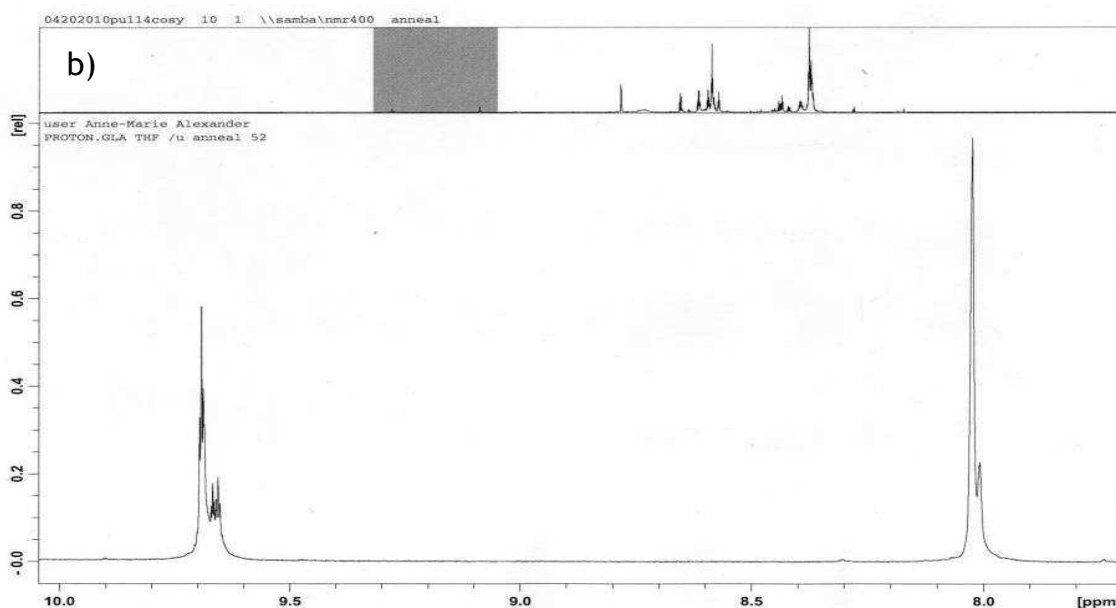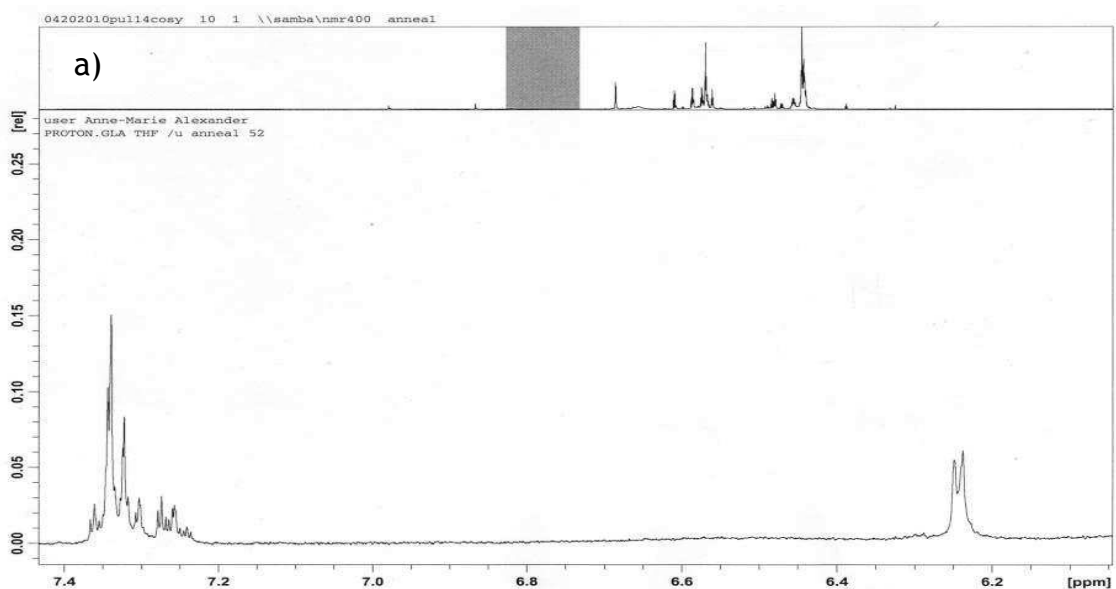
Figure 5.4-11 Expansions of Figure 5.4-10 at different shifts in the spectrum where peaks are observed a) 6.3-7.4 ppm b) 7.9-10.0 ppm

From the above spectra it is probable that there is more than one compound present in the reaction products.

5.4.3.2 XRD Patterns.

As seen in previous studies the "Re$_3$N" starting material appears to be largely amorphous with a very broad reflection centring upon 40 $^\circ$ 2θ. Under H$_2$/N$_2$ at 350 ^{o}C for 3 h, almost total de-nitridation is apparent resulting in crystalline Re metal, with similar shifts which have been previously reported in Chapter 3, Figure 5.4-12. The H$_2$/Ar pulse sample only partially de-nitrides and can be seen in the Figure with a mixture of Re reflections (again shifted) and the original broad reflection being evident in the post-reaction XRD pattern.
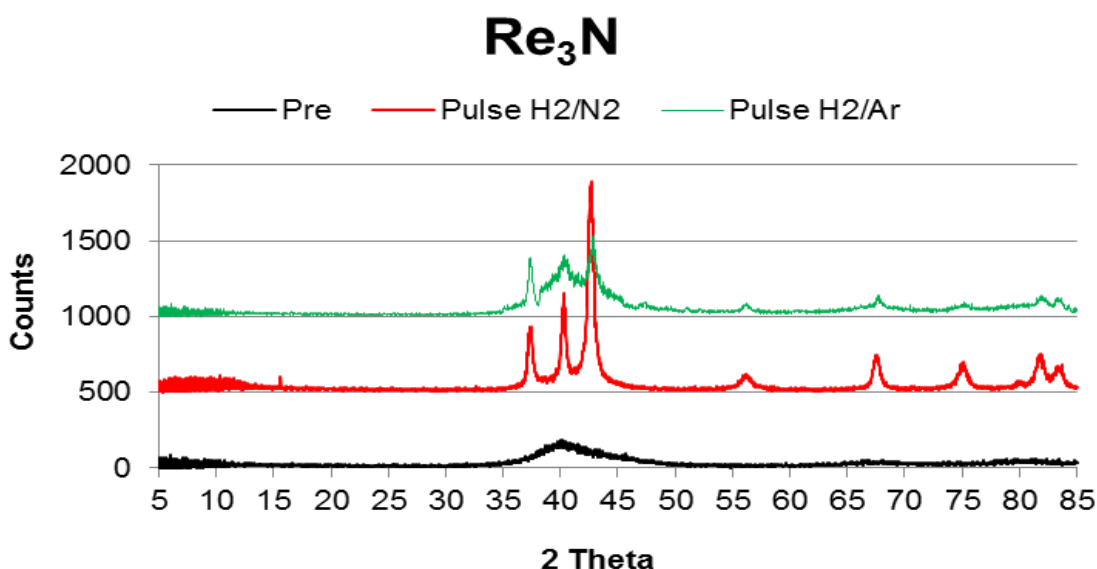
Figure 5.4-12 Pre-and Post-H$_2$/N$_2$ and H$_2$/Ar XRD patterns of Re$_3$N from benzene/ammonia-pulse reaction.

5.4.4 Cu$_3$N.

5.4.4.1 ^{1}H NMR Spectroscopy.

The reaction product obtained from the pulse reaction of Cu$_3$N and benzene with H$_2$/N$_2$, was bright blue in colour, which was a visual indication that a reaction had taken place. The ^{1}H NMR spectrum for these reaction products was very similar to that obtained for the products of the Co$_3$Mo$_3$N reaction, and is shown in Figure 5.4-13. It is interesting that both colours were also similar; however the colour of the products acquired in the pulse

reaction with Cu_3N was much more intense than that observed in the case from the Co_3Mo_3N pulse reaction. It may be possible that Cu_3N is more reactive towards benzene than Co_3Mo_3N thus leads to increase in the concentration of products which may result in the more intense colour.

The two characteristic THF peaks are apparent at approximately 1.61 and 3.49 ppm. As with the Co_3Mo_3N reaction product, a number of peaks are concentrated at the lower end of the spectrum, some of which appear to be masked by the THF signals. Additionally there is a peak centring around 9.59 ppm, as well as another at 7.95 ppm, which can be attributed to un-reacted benzene. It is probable that the spectrum presented in Figure 5.4-13 is compiled of several different compounds and one of which may potentially have a CHO group in its structure, this would give rise to a chemical shift between 9 and 10 ppm, and hence account for the peak observed at 9.59 ppm.

Furthermore the two singlets centring on 4.80 and 5.25 ppm may possibly be protons attached to a tertiary C=C bond, or it may also be possible that these peaks correspond to $CONH_2$ or ROH groups.[277-280]

It is not possible to accurately determine which compounds are in this sample by the spectrum alone as it is too complex. As previously mentioned it is most likely that the sample contains more than one reaction product.
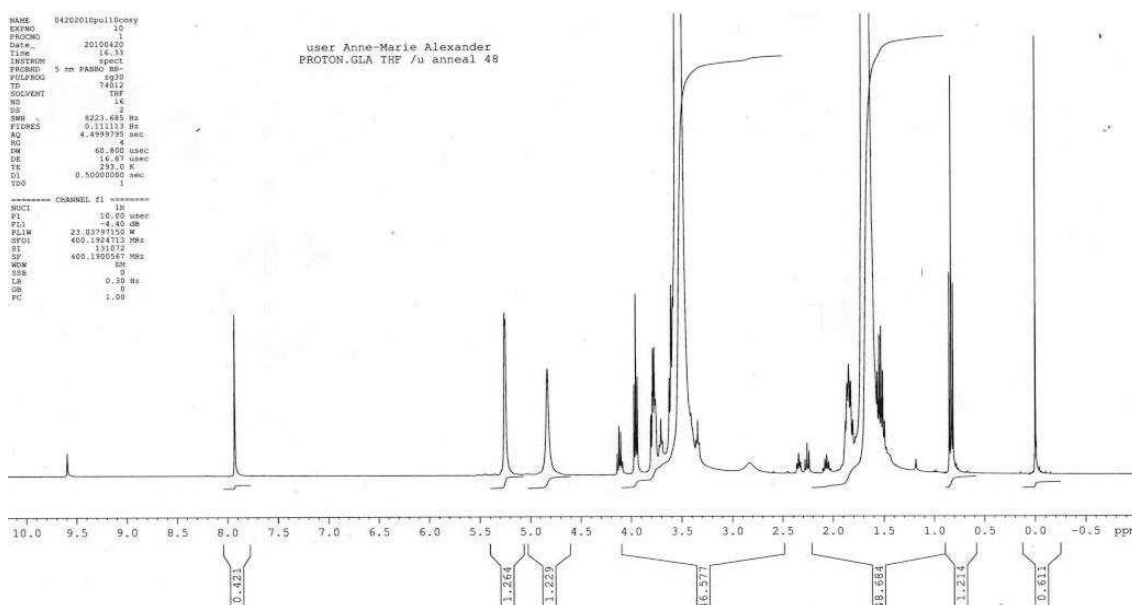
Figure 5.4-13 ^{1}H NMR spectrum of products collected after pulse reaction of Cu_3N with H_2/N_2 and C_6H_6 at 400 ^{o}C for 3 h (THF-d8).

5.4.4.2 XRD Patterns.

In the case of the pulse reaction under a H_2/Ar feedstream, copper nitride decomposed to the copper metal as expected due to the reaction being conducted at 350 ^{o}C, which is above the sample decomposition temperature. However, under H_2/N_2, it is clear from the diffraction pattern shown in Figure 5.4-14, that the nitride did not undergo complete decomposition, with a mixture of copper nitride and copper metal phases being evident. This was surprising due to the fact that copper nitride apparently decomposes to copper metal at temperatures above 250 ^{o}C, as was observed in the other studies documented in this thesis.
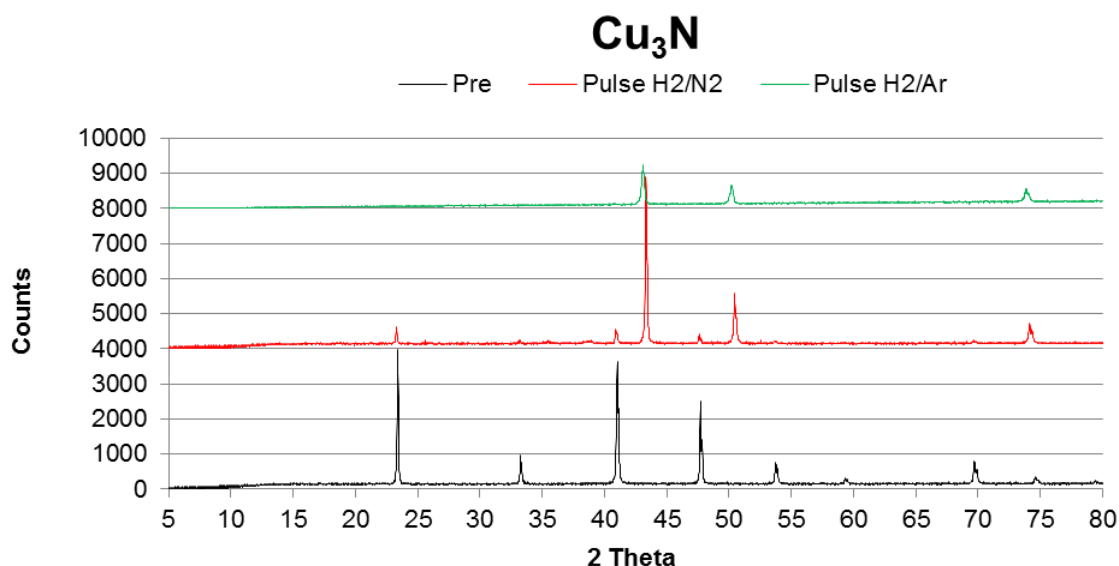
Figure 5.4-14 Pre-and Post-H_2/N_2 and H_2/Ar XRD patterns of Cu$_3$N from benzene/ammonia-pulse reaction.

5.4.5 Zn$_3$N$_2$.

5.4.5.1 ^{1}H NMR Spectroscopy.

As for the Co$_3$Mo$_3$N and the Cu$_3$N samples the reaction product, once dissolved off the post-reaction packing material, was blue in colour. Likewise a similar ^{1}H NMR spectrum was obtained with the same chemical shifts to that observed in the Cu$_3$N reaction products. Chemical shifts greater than 9 ppm are generally associated with elements that have a high electronegativity, such as oxygen. The resultant peak at 9.61 ppm is indicative that an oxygen atom may be present in one of the reaction products. This may have arisen due to the fact that trace amounts of ZnO are present in the pre-reaction Zn$_3$N$_2$ sample, as

confirmed by XRD anaysis in Figure 5.4-15, and subsequently the benzene may have reacted with these oxide species to produce oxygen containing products.

Figure 5.4-15 ^{1}H NMR spectrum of products collected after pulse reaction of Zn_3N_2 with H_2/N_2 and C_6H_6 at 400 ^{o}C for 3 h (THF-d8).

5.4.5.2 XRD Patterns.

As was observed for the H_2/N_2 and H_2/Ar studies, the presence of ZnO is apparent in all samples. It is thought to occur as a result of aerobic oxidation of zinc metal upon discharge of the sample. It is also apparent that, in the case of the H_2/Ar pulse reaction, the characteristic Zn_3N_2 peak at approximately 23 ^{o} 2θ is significantly diminished so that it is very weak in comparison to other reflections. However there does not appear to any significant shift in the reflections, despite the significant loss of nitrogen upon reaction, confirmed by post-reaction CHN analysis.

Figure 5.4-16 Pre- and Post-H$_2$/N$_2$ and H$_2$/Ar XRD patterns of Zn$_2$N$_3$ from benzene/ammonia-pulse reaction. The symbols used show characteristic reflections of Zn metal (☆) and ZnO (□) that can be clearly identified without ambiguity.

5.4.6 Co-4Re.

5.4.6.1 ^{1}H NMR Spectroscopy.

The reaction product obtained from the post-reaction bed granules was red/brown in colour, and as with the other spectra that have been described in this section, the ^{1}H NMR spectrum is very complex, Figure 5.4-17, and therefore identification of species is problematic.   However unlike the other spectra, it is evident that two large peaks in the aromatic region corresponding to a triplet at 7.16 ppm and a multiplet at 7.08 ppm, as benzene is generally represented by a singlet between 7-8 ppm, and within this body of work has been generally observed at *ca.* 8 ppm, the presence of a triplet and multiplet within the aromatic region would be indicative of a substituted benzene. Due to the upfield shift, with respect to the previously observed benzene peaks (*ca.* 8 ppm), this may indicate that the substituent group is electron donating such as NH$_2$ or OCH$_3$.   If an electron withdrawing group were attached, for instance OH or NO$_2$, a shift to a more downfield position would be expected.   Additionally a broad peak can be observed at 3.78 ppm, which is slightly masked by the neighbouring THF signal at 3.62 ppm, and another at 5.00 ppm. These may potentially correspond to a NH or NH$_2$ groups. The peak at 3.78 ppm is slightly larger than that at 5.00 ppm and may either be a result of the two peaks belonging to different compounds or that there is more protons associated with the peak at 3.78 ppm. When these are peaks are compared to those observed in the aniline spectrum in Figure

4.3-2, there is a relatively good match. However, as mentioned previously, it is difficult to establish if this is a compound present in the reaction products.
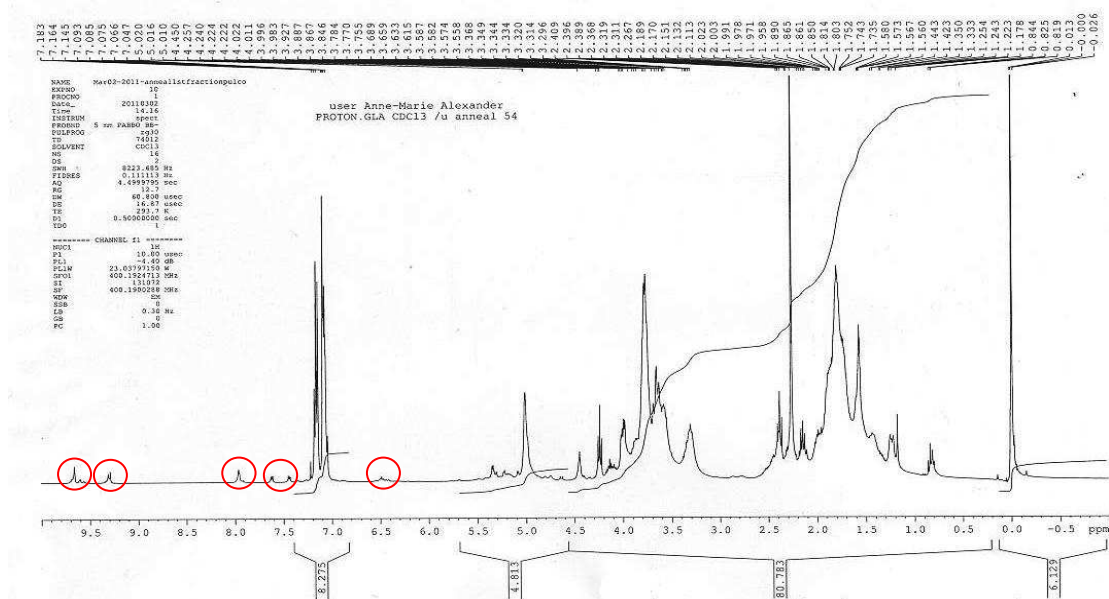

Figure 5.4-17 ^{1}H NMR spectrum of products collected after pulse reaction of Co-4Re with H$_2$/N$_2$ and C$_6$H$_6$ at 400 ^{o}C for 3 h (THF-d8).

It is also evident that there are additional smaller peaks observed in the aromatic region, which have been expanded for clarity in Figures 5.4-18 and 5.4-19. It is apparent that the very weak peaks centring at 6.46 ppm, appear to correspond to a triplet and a doublet, however the resolution of these peaks is relatively low.

Figure 5.4-18 Expansions of Figure 5.4-17 at different shifts in the spectrum where peaks are observed a) 6.4-6.7 ppm
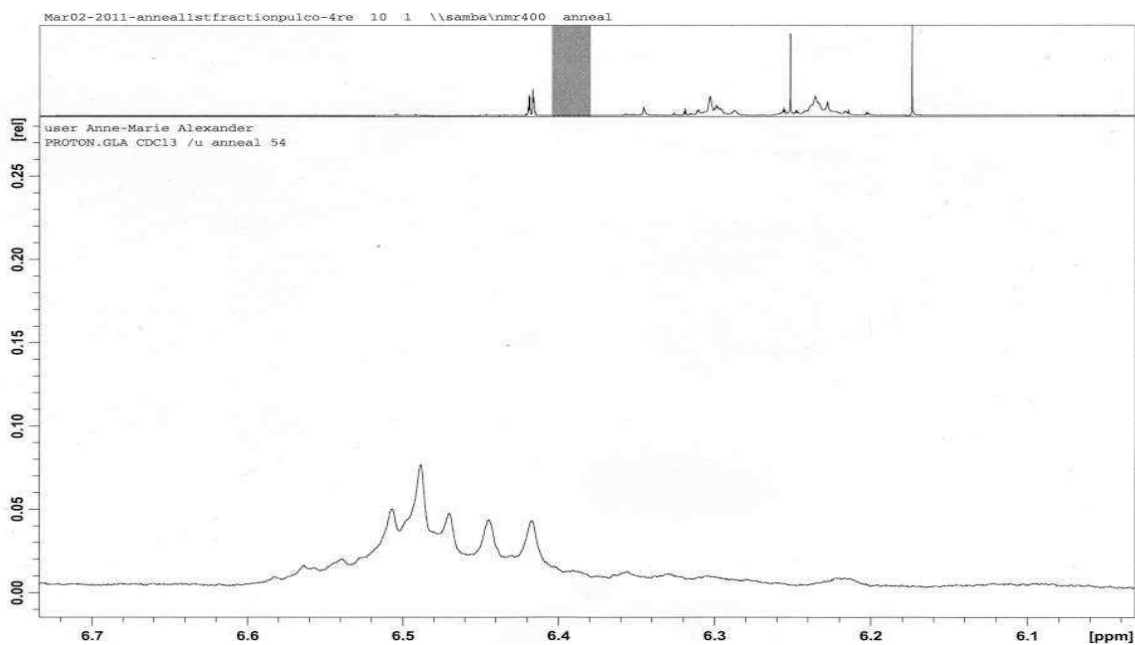
The peak centring at 7.96 may be attributed to unreacted benzene, whilst the two doublets of doublets at 7.43 ppm and 7.72 ppm may be the result of a di-substituted phenyl, with one substituent being very electron withdrawing, such as a NO_2 group, this would subsequently cause two doublet of doublets to be observed in the ^1H NMR spectrum, a consequence of the resonance within the aromatic ring.

As previously mentioned the presence of electron withdrawing substituents result in downfield chemical shifts of the proton signals. This would therefore explain the presence of peaks observed at 9.28 ppm and approximately 9.66 ppm, Figure 5.4-19 b).
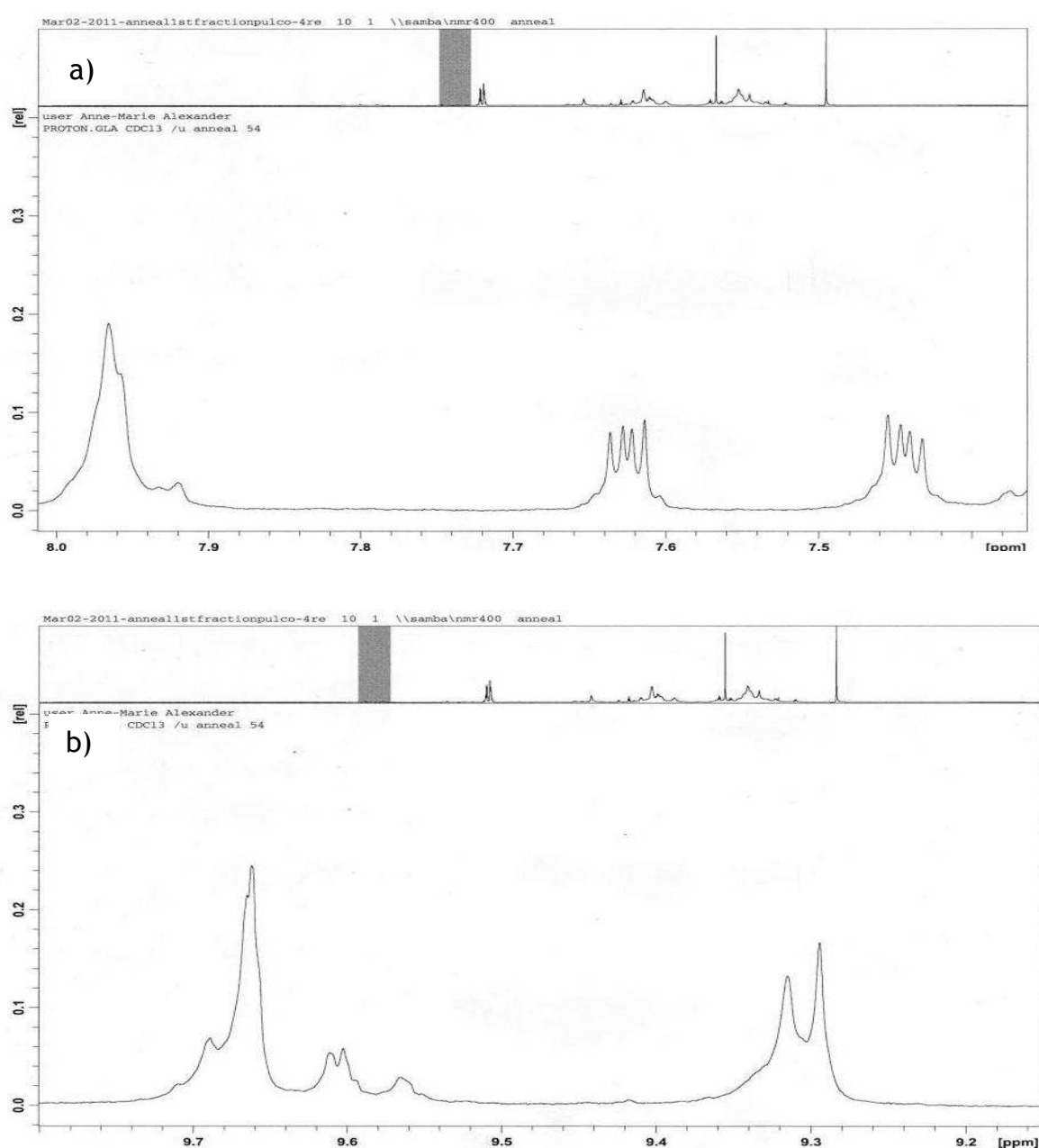
Figure 5.4-19 Expansions of Figure 5.4-17 at different shifts in the spectrum where peaks are observed a) 7.4-8.0 ppm b) 9.2-9.8 ppm

5.4.6.2 XRD Patterns

As with the previous studies investigating Co-4Re, as discussed in Chapter 3, the post-benzene diffraction patterns match to the pre-reaction diffraction pattern, although the system again appears to become more crystalline upon reaction. Both pre- and post-reaction samples contain a mixture of Co metal and Re metal phases which are indicated in Figure 4.4.6- 2, by a star or circle respectively.
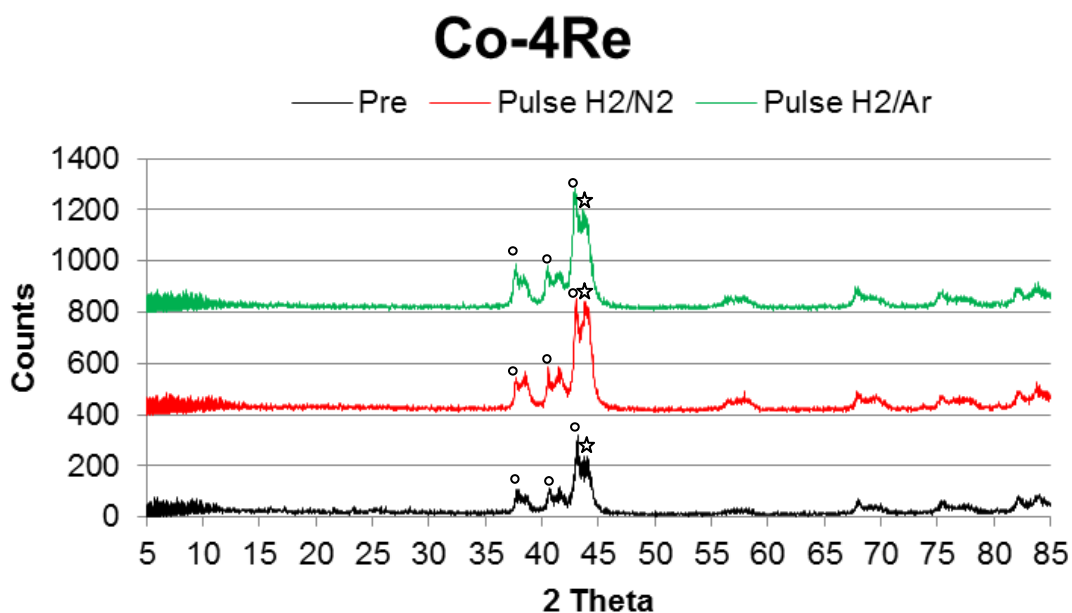
Figure 5.4-20 Pre-and Post-H$_2$/N$_2$ and H$_2$/Ar XRD patterns of Co-4Re from benzene/ammonia-pulse reaction– (Co ☆ Re ○)

5.4.7 Post-Reaction Carbon and Nitrogen Analysis

The post-reaction carbon and nitrogen contents of the benzene pulse reaction samples were determined by combustion microanalysis, and are provided in Table 5.4-2. The nitrogen content of the pre-reaction sample and the stoichiometric value for each material are also presented for comparative purposes.

As was observed in the benzene flow-reactions, both Fe$_2$N and Fe doped β-Mo$_2$N$_{0.78}$ show an increased carbon content when compared to the other materials investigated, and again the presence of graphite was evident in the post-reaction XRD, although this may not be a true graphitic reflection in the   case of Fe doped β-Mo$_2$N$_{0.78}$ as has been previously discussed. The presence of carbon is also evident in the post-reaction Co$_3$Mo$_3$N sample, which have given rise to the small shift to increased Bragg angle apparent in the post-

reaction XRD pattern, this may also explain why only 1/3 of the nitrogen is lost from the material instead of a loss of almost 50 % previously reported under a H_2/Ar atmosphere; Zn_3N_2 and un-doped β-$Mo_2N_{0.78}$ samples. Trace amounts were also observed in Ni_3N, Cu_3N, Ta_3N_5 and Cu doped β-$Mo_2N_{0.78}$ samples, however were undetected by XRD analysis.

It is apparent that both Ni_3N and Cu_3N do not fully reduce to the corresponding metal as has been previously observed, despite the reaction temperature being above that in which decomposition has been previously observed in the benzene flow reactions and in the studies conducted in Chapter 3. It may be possible that by pulsing the NH_3 sequentially the nitrides are regenerated to an extent.

Again Zn_3N_2 displays a significant loss of nitrogen upon reaction, and is comparable to losses which have been previously reported in the reactions investigated in Chapter 3.

When the nitrogen contents of the Zn_3N_2 post-flow and post-pulse reactions are compared it is clear that the nitrogen content is lower in the pulse reaction sample (being 5.45 wt.% and 3.14 wt.% respectively). However it is also apparent, as mentioned earlier, that carbon is present within the post-pulse reaction sample, although the presence of carbon is not apparent by XRD analysis. It may possibly that the carbon replaces some of the nitrogen in the metal lattice.

Nitrogen and Carbon content (wt.%)

Material (350 ^{o}C)	Calculated Stoichiometric N Content wt%	Pre-reaction N Content wt%	Post-reaction Observed N Content wt%		Observed C Content wt%	
			H$_2$/N$_2$	H$_2$/Ar	H$_2$/N$_2$	H$_2$/Ar
Co$_3$Mo$_3$N *	2.92	2.93	1.79	1.63	0.70	0.54
Mg$_3$N$_2$ *	27.74	23.50	18.73	17.41	-	-
VN	21.55	17.39	14.92		-	
Fe$_2$N	11.13	7.86	3.71		0.92	
Co$_4$N	5.60	3.68	-		-	
Ni$_3$N	7.36	6.58	1.72		0.05	
Cu$_3$N *	6.84	6.05	0.92	0.21	0.02	-
Zn$_3$N$_2$ *	12.49	9.80	3.14	2.36	0.21	0.37
Ta$_3$N$_5$	11.42	11.23	8.43		0.02	
β-Mo$_2$N$_{0.78}$	5.38	5.41	3.48		0.35	
Fe/β-Mo$_2$N$_{0.78}$	5.38	5.58	4.12		0.75	
Cu/β-Mo$_2$N$_{0.78}$	5.38	4.39	1.10		0.04	
W$_2$N	3.66	6.13	5.48		-	
Re$_3$N *	2.44	2.50	0.52	0.38	-	-
Co-4Re *	n/a	n/a	-	-	-	-

Table 5.4-2 Pre- and Post-benzene reaction nitrogen and carbon content of materials investigated by a series of benzene and ammonia pulses in H$_2$/N$_2$ and H$_2$/Ar gas feeds.

5.4.8 Summary

The work which was conducted in this chapter was undertaken to investigate the possibility of direct synthesis of aniline from benzene. Initial studies involved passing a flow of benzene over the material and condensing the effluent gas, which subsequently led on to reactions whereby benzene and ammonia were sequentially pulsed into a feed gas and over the reaction material. Although it is clear that some of the materials, which have been investigated in the current study have produced some interesting results with respect to the organic species in which have been produced these currently remain unidentified, it is evident that these materials have not synthesised the target molecule, aniline.

Further studies need to be conducted in order to identify the compounds produced from the pulse reactions; it may be that there is scope to develop these new and novel syntheses routes in the preparation of organic compounds.

From the results presented in this chapter several nitride based systems appear to be of interest, these include Re_3N, Cu_3N Zn_3N_2, Co_3Mo_3N and Co-4Re.

As was discussed in the introduction to this chapter, much effort has been done in an effort to characterise these unknown products. Several different characterisation techniques were used, all of which provided little if no information regarding structural characterisation. This as has been mentioned may be a result of the low concentrations of products, which were obtained.

In the initial studies with the benzene flow reactions a ninhydrin stain was used in order to identify whether primary amines were present in the sample, which stain blue-purple upon reaction with ninehydrin. This colour was not observed in the spotted TLC plates however a pink/orange spot was observed in some instances. It has been reported that some secondary amines stain this colour with ninehydrin, however it was also discovered that ninehydrin itself also dries, on the TLC plate, to the same pink/orange colour with prolonged heating and therefore this test was discarded as being unreliable.

Additionally, infrared and UV-Vis spectroscopies were also undertaken. It was thought that the infrared spectroscopy would provide information regarding the presence of NH_x groups in the reaction products. The spectra which were obtained matched that of the un-reacted benzene despite the presence of additional peaks in the ^{1}H NMR spectra. UV-Vis spectroscopy was employed so as to assess the level of conjugation, if any, within the coloured pulse reaction samples. Benzene has a characteristic band at 295 nm and on the basis that coloured compounds generally have an absorbance between 400-700 nm it would therefore be possible to assess the level of conjugation, and identify any functional groups present in the product reaction sample.

This subsequently led to samples being analysed through the use of ^{1}H NMR spectroscopy and mass spectroscopy. Although these methods were useful to a certain extent the spectra which were obtained were often very complex making product identification difficult. Samples were also purified in the event that more than one compound was present in the reaction products. This involved initially spotting TLC plates and finding an appropriate

solvent system in order to achieve a good separation between the components, however it was found that the spots streaked on the TLC regardless of the solvent system investigated. The most efficient system that was investigated was a 1 % methanol: chloroform system, which was subsequently used in a drip column to separate the reaction products. It was found that most coloured reaction products had more than one component. It proved difficult to completely separate them, and as a result complex ^{1}H NMR spectra were subsequently observed.

6. Conclusions

In this thesis, a series of nitride-based materials have been screened and the reactivity of lattice nitrogen present within them was assessed. Throughout this research project, the experimental work was conducted with the aim of developing a potential nitrogen transfer reagent in order to synthesise aniline via the direct conversion of benzene and has been split into three distinct sections. The first section of work investigated the hydrogenation of lattice nitrogen in order to assess the possibility of producing reactive species. It was necessary at this point to establish which materials were reactive and lost nitrogen from the metal lattice at or below 400 ^{o}C, the maximum temperature for the envisaged reactions with benzene. From the data presented, the removal of nitrogen from some of these materials and its potential for reaction was evident.   In order to truly act as a nitrogen transfer reagent in a process akin to the Mars-van Krevelen process, observed in metal oxide based reactions, it was necessary for the nitrogen deficient material to be regenerated, and hence this was the second section examined. Finally the reaction of benzene and hydrogen over bulk binary nitrides in an attempt to trap the reactive NH_x species, for the production of aniline was investigated.   To the author's knowledge, this is the largest systematic study which has been undertaken in this area. Valuable insights into all the different processes were obtained and are summarised in this section.

- On moving left to right along the first row transition metal series, the corresponding nitrides became more thermally unstable, which could in theory prove to be advantageous in the development of a novel nitrogen transfer reagent.

- Correspondingly, upon moving across the first transition metal series, it was found that ammonia production increased during the first 30 minutes on stream with Cu_3N exhibiting the highest ammonia production rates during the first half hour of reaction. However, with the exception of VN, Fe_2N and Zn_3N_2 which exhibited an almost steady state ammonia synthesis after 30 minutes, no further ammonia production was observed.

- On descending a group, the ammonia production activity of the corresponding nitride also increases, which is subsequently sustained for longer than the 30 minutes observed in the case of the first series.

- On comparing the ammonia synthesis activities of binary metal nitrides with Ru based systems, it was found that only Zn_3N_2 has a 'comparable' activity to Ru. Although Re_3N has an initial rate which is similar to that observed by Ru based systems, whilst Cu_3N and Ni_3N have an initial ammonia production rate which is more than double that observed by Ru.

- Hydrogenation of lattice nitrogen in the binary nitride systems has been shown to be a function of temperature. Increasing the temperature under H_2/Ar appears to differentiate between weakly and strongly bound nitrogen species. Despite the vast excess of hydrogen in the gas-phase, the nitrogen lost from these materials predominantly occurs in the form of N_2.

- The loss of nitrogen, and therefore its potential to be employed in nitrogen transfer reactions, is evident. Nitrides of the later transition metals, Co_4N, Ni_3N and Cu_3N, and also β-$Mo_2N_{0.78,}$ are found to decompose fully to the parent metal, with heat treatment. All other nitrides retained nitrogen.

- It was demonstrated that that the nitrogen content in most of the nitrogen deficient samples investigated, with the exception of Cu_3N and Co_4N, could either be partially or wholly restored under the nitriding gas used to prepare the original nitride phase, thereby confirming the possibility that the materials may potentially function as nitrogen transfer reagents.

- Reactions investigating the possibility of direct synthesis of aniline from benzene were undertaken over materials which either displayed a loss of nitrogen or demonstrated the ability to synthesise ammonia at 400^oC or below. Initial studies involved passing a flow of benzene over the material and condensing the effluent gas, which subsequently led on to reactions whereby benzene and ammonia were sequentially pulsed into a feed gas and over the reaction material.

- Certain materials produced interesting results, namely Zn_3N_2, Cu_3N, Re_3N, Co_3Mo_3N, Mg_3N_2 and Co-4Re, and further work is required in order to characterise the products obtained primarily due to the fact that product identification by ^{1}H NMR spectroscopy, mass spectroscopy and GCMS, proved difficult as a consequence of the low concentrations of products within the samples. The main focus of this screen was to produce aniline and this was not achieved.

- Nitrides such as Ni_3N, Fe_2N, un-doped and Fe doped β-$Mo_2N_{0.78}$ and Co_3Mo_3N show a higher tendency for carburisation as benzene is passed over the material. XRD analysis of the Ni_3N, Fe_2N and Fe doped β-$Mo_2N_{0.78}$ post-reaction samples indicate the presence of an extra reflection, attributed to graphite, and provides an explanation for the excess carbon present in the post-reaction sample, whilst the XRD diffraction patterns of un-doped β-$Mo_2N_{0.78}$ and Co_3Mo_3N exhibit small shifts to either higher or lower Bragg angles respectively. This may arise from the insertion of C atoms into the crystal structure and consequently forming a carbonitride phase.

Below is diagram of the Periodic Table to illustrate the range of materials which have been investigated. Those which are highlighted in blue those nitrides (or elements in the case of Co-4Re and Co_3Mo_3N) exhibit some interesting features, in terms of the reaction products which were observed, and are worthy of further investigation.

1 H																	2 He
3 Li	4 Be		**Atomic Number** **SYMBOL**									5 B	6 C	7 N	8 O	9 F	10 Ne
11 Na	12 Mg											13 Al	14 Si	15 P	16 S	17 Cl	18 Ar
19 K	20 Ca		21 Sc	22 Ti	23 V	24 Cr	25 Mn	26 Fe	27 Co	28 Ni	29 Cu	30 Zn	31 Ga	32 Ge	33 As	34 Se	35 Br	36 Kr
37 Rb	38 Sr		39 Y	40 Zr	41 Nb	42 Mo	43 Tc	44 Ru	45 Rh	46 Pd	47 Ag	48 Cd	49 In	50 Sn	51 Sb	52 Te	53 I	54 Xe
55 Cs	56 Ba	* 57-70	71 Lu	72 Hf	73 Ta	74 W	75 Re	76 Os	77 Ir	78 Pt	79 Au	80 Hg	81 Tl	82 Pb	83 Bi	84 Po	85 At	86 Rn
87 Fr	88 Ra	** 89-102	103 Lr	104 Rf	105 Db	106 Sg	107 Bh	108 Hs	109 Mt	110 Uun	111 Uuu	112 Uub		114 Uuq				

This is the first study to screen such a large range of both binary and ternary nitride systems in this manner. By assessing the nitrogen desorption properties of each binary nitride, both with respect to across the Periodic Table, it is therefore possible to potentially develop a more suitable second-generation catalyst based upon the periodic trends identified.

In terms of this 1st generation screening process it is possible to establish possible 2nd generation ternary and quaternary nitride candidate systems, based upon the lattice nitrogen reactivity and also the thermal stability of the binary nitrides. It would be interesting to continue this work and possibly probe the effect and activity of mixed systems to either increase activity or increase the thermal stability of the material. For

instance, if it were possible to make a ternary ZnTi system, the combination of an unstable system (Zn) and a stable system (Ti) would be achieved. Another system which may prove interesting would be a Ta based ternary nitride, perhaps involving Cu or Ni. Ta_3N_5 was very interesting in the fact that it had very desirable ammonia synthesis properties, was relatively stable in a H_2/N_2 atmosphere and could also be regenerated to the original phase after being depleted of N. However, no reaction was observed with benzene. Cu_3N and Ni_3N on the other hand decompose to the corresponding metal at low temperatures; they are difficult to restore to the original nitride phase, and Cu_3N appears to be active in the synthesis of organic based compounds. These compounds may have a similar valence electron count as CoMo ($15e^-$); $15e^-$ (ZnTi), $16e^-$ (CuTa) and $15e^-$ (NiTa) which may potentially influence the properties of the material, with respect to their activity and performance as a nitrogen transfer reagent, if electronic parameters are of significance.

List of references

1.   R. Niewa, H. Jacobs, Chem. Rev., 96 (1996) 2053

2.   R. Niewa, F. J. DiSalvo, Chem. Mater., 10 (1998) 2733

3.   E. Kroke, M. Schwarz, Co-ord. Chem. Rev., 248 (2004) 493

4.   A. Simon, Co-ord. Chem. Rev., 163 (1997) 253

5.   "The Chemistry of Transition Metal Carbides and Nitrides", S. T. Oyama (ed.), Blackie Academic and Professional, Glasgow, (1996).

6.   www.webelements.com (August 2010)

7.   D. H. Gregory, J. Chem. Soc. Dalton Trans., (1999) 259.

8.   S. T. Oyama, G. L. Haller, Catalysis, Spec. Per. Rep., Vol. 5, RSC London, (1982) 333

9.   S. T. Oyama, Catal. Today, 15 (1992) 179

10.   R. B. Levy, M. Boudart, Science, 181 (1973) 547

11.   E. Furimsky, Appl. Catal. A: Gen., 1 240 (2003) 1

12.   J. S. J Hargreaves, D. Mckay, Catalysis, 19 (2006) 85

13.   S.T. Oyama J. Solid State Chem., 96 (1992) 442

14.   L. Ramqvist, J. Appl. Phys., 42 (1971) 2113

15.   J. Monnier, H. Sulimma, A. Dalai, G. Caravaggio, Appl. Catal. A: Gen., 382 (2010) 176

16.   A. P. Caricato, M. Fernandez, G. Leggieri, A. Luches, M. Martino, F. Romano, Appl. Surf. Sci., 253 (2007) 8037

17.   C. Shi, A. M. Zhu, X. F. Yang, C. T. Au, Appl. Catal A: Gen., 276 (2004) 223

18.   M. K. Neylon, S. K. Bej, C. A. Bennett, L. T. Thompson, Appl. Catal. A: Gen., 232 (2002) 13

19.   M. K. Neylon, S. Choi, H. Kwon, K. E. Curry, L. T. Thompson, Appl. Catal. A: Gen., 183 (1999) 253

20.   M. Nagai, Appl. Catal. A: Gen., 322 (2007) 178

21.   G. Paniconi, Z. Stoeva, H. Doberstein, R. I. Smith, B. L. Gallagher, D. H. Gregory Solid State Sci., 9 (2007) 907

22.   A. Baiker, M. Maciejewski, J. Chem. Soc, Faraday Trans. 1, 80 (1984) 2331

23.   W. Lengauer, J. Alloys. Compd., 186 (1992) 293

24.   H. A. Wriedt, J. L. Murray, Bull. Alloy Phase Diag., 4, 8 (1987) 378

25.   Z. G. Chen, L. Cheng, G. Lu, J. Zou, Chem. Eng. Journal, 165 (2010) 714

26.   D. J. As, Microelectronics Journal, 40 (2009) 204

27.   M. G. Moreno-Armenta, G. Soto, N. Takeuchi, J. Alloys. Compd., 509 (2011) 1471

28.   G. Husnain, F. Tao, Y. Shu-De, Physica B, 405 (2010) 2340

29.   B. Yuan, J. X. Liu, G. J. Zhang, Y. M. Kan, P. L. Wang, Ceramics International, 35 (2009) 2155

30.   R. Marchand, Y. Laurent, J. Guyader, P. L'Haridon, P. Verdier, J. Euro. Ceramic Soc., 8 (1991) 197

31.   "Kirk-Othmer Encyclopedia of Chemical Technology", ed. M. E. Howe-Grant, John Wiley and Sons, Inc., New York, 4th ed., Vol 17 (1992) pg 108

32.   L. Volpe, M. Boudart, J. Solid State Chem., 59 (1985) 332

33. R. Marchand, X. Gouin, F. Tessier, Y. Laurent, "The Chemistry of Transition Metal Carbides and Nitrides", ed. S. T. Oyama, Blackie Academic and Professional, Glasgow, (1996) Chapter 13, pg 252

34. D. Mckay, J. S. J. Hargreaves, J. L. Rico, J. L. Rivera and X. L. Sun, J. Solid State Chem., 181 (2008) 325.

35. D. H. Gregory, J. Chem. Soc., Dalton Trans., (1999) 259

36. Z. Wei, Q. Xin, P. Grange, B. Delmon, J. Catal., 168 (1997) 176

37. J. G. Choi, R. L. Curl, L. T. Thompson, J. Catal., 146 (1994) 218

38. C. H. Jaggers, J. N. Michaels, A. M. Stacy, Chem. Mater., 2 (1990) 150

39. A. Y. Garin, L. Kienle, G. V. Vajenine, J. Solid State Chem., 179 (2006) 2339

40. R. Marchand, F. Tessier, F. J. DiSalvo, J. Mater. Chem., 9 (1999) 297

41. R. S. Wise, E. J. Markel, J. Catal., 145 (1994) 344

42. M. Nagai, Y. Goto, A. Miyaka, M. Kiyoshi, K. Hada, K. Oshikawa, S. Omi, J. Catal., 182 (1999) 292.

43. S. W. Gong, H. K. Chen, W. Li, B. Q. Li, Appl. Catal. A: Gen., 279 (2005) 257

44. A. G. Cairns, J. G. Gallagher, J. S. J. Hargreaves, D. Mckay, E. Morrrison, J. L. Rico, K. Wilson, J. Alloys Compd., 479 (2009) 851

45. S. Chouzier, P. Afanasiev, M. Vrinat, T. Cseri, M. Roy-Auberger, J. Solid State Chem., 179 (2006) 3314

46. P. Afanasiev, Inorg. Chem., 41 (2002) 5317

47. M. Wu, J. Alloys Compd, 486 (2009), 223

48. B. Song, J. K. Jian, H. Q. Bao, M. Lei, H. Li, G.Wang, Y. P. Xu, X. L. Chen, Appl. Phys. Lett., 92 (2008) 192511

49. B. Song, X. Chen, J. Han, J. Jian, W. Wang, H. Zuo, X. Zhang, S. Meng, Inorg. Chem., 48 (2009) 10519

50. K. T. Jacob, R. Verma, R. M. Mallya, J. Mater. Sci., 37 (2002) 4465

51. B. Mazumder, A. L. Hector, Top. Catal., 52 (2009) 1472

52. C. J. H. Jacobsen, J. J. Zhu, H. Lindelov, J. Z. Jiang, J. Mater. Chem., 12 (2002)

53. M. R. Hillis, C. Kemball, M. W. Roberts, Trans. Faraday Soc., 62 (1966) 3570

54. D. A. King, F. Sebba, J. Catal., 4 (1965) 253

55. D. A. King, F. Sebba, J. Catal., 4 (1965) 430

56. J. G. Choi, J. Ha, J. W. Hong, Appl. Catal. A: Gen., 168 (1998) 47

57. N. Segal, F. Sebba, J. Catal., 8 (1967) 113

58. N. Segal, F. Sebba, J. Catal., 8 (1967) 105

59. R. Kojima, K. I. Aika, Appl. Catal. A: Gen., 209 (2001) 317

60. R. Kojima, K. I. Aika, Chem. Lett, (2000) 514

61. R. Kojima, K. I. Aika, Appl. Catal. A: Gen., 215 (2001) 149

62. R. Kojima, K. I. Aika, Appl. Catal. A: Gen., 218 (2001) 121

63. R. Kojima, K. I. Aika, Appl. Catal. A: Gen., 219 (2001) 157

64. C. J. H. Jacobsen, M. Brorson, T. Sehested, H. Teunissen, E. Turnqvist, U.S Patent 6235676, (1999).

65. C. J. H. Jacobsen, Chem. Commun., (2000) 1057

66. C. J. H. Jacobsen, S. Dahl, B. S. Clausen, S, Bahn, A. Logadottir, J. K. Norskov, J. Am. Chem. Soc., 123 (2001) 8405

67.   A. Boisen, S. Dahl, C. J. H. Jacobsen, J. Catal., 208 (2002)180

68.   S. Dahl, A. Logadottir, C. J. H. Jacobsen, J. K. Norskov, Appl. Catal. A: Gen., 222 (2001) 19

69.   W. J. McGill, F. Sebba, J. Catal., 2 (1963) 104

70.   S. T. Oyama, J. Catal., 133 (1992) 358

71.   M. Olea, M. Florea, I. Sack, R. Prada Silvey, E. M. Gaigneaux, G. B Martin, P. Grange, J. Catal., 232 (2005) 152

72.   Z. Yao, A. Zhu, J. Chen, X. Wang, C. T. Au, C. Shi, J. Solid State Chem., 180 (2007) 2635

73.   P. Clark, B. Dhandapani, S. T Oyama, Appl. Catal. A: Gen., 184 (1999) L175

74.   V. Sundaramurthy, A. K. Dalai, J. Adjaye, Appl. Catal. A: Gen., 335 (2008) 204

75.   S. Ramanathan, S. T. Oyama, J. Phys. Chem., 99 (1995) 16365

76.   K. Milad, K. J. Smith, P. C. Wong, K. A. R. Mitchell, Catal. Lett., 52 (1998) 113

77.   H. Imamura, K. Mizuno, K. Ohishi, E. Suda, K. Kanda, Y. Sakata, S. Tsuchiya , J. Alloys Compd, 275–277 (1998) 903

78.   A. Orlov, M. S. Tikhov, R. M. Lambert , Comptes Rendus Chimie, 9 (2006) 794

79.   D. Wu, M. Long, W. Cai, C. Chen, Y. Wu, J. Alloys Compd., 502 (2010) 289

80.   X. Yang, C. Cao, L. Erickson, K. Hohn, R. Maghirang, K. Klabunde, J. Catal., 260 (2008) 128

81.   C. Liu, X. Tang, C. Mo, Z. Qiang, J. Solid State Chem., 181 (2008) 913

82.   H. Zhang, Y. Chen, L. Fu, J. Ma, J. Alloys Compd, 499 (2010) 269

83.   M. Hara, G. Hitoki, T. Takata, J. N. Kondo, H. Kobayashi, K. Domen, Stud. Surf. Sci. Catal., 145 (2003) 169

84.   T. Morikawa, R. Asahi, T. Ohwaki, K. Aoki, Y. Taga, Jap. J. Appl. Phys., 40 (2001) L561

85.   G. Hitoki, T. Taneka, J. N. Kondo, M. Hara, H. Kobayashi, K. Domen, Chem. Commun., (2002) 1698

86.   B. Avasarala, P. Haldar, Electrochimica Acta, 55 (2010) 9024

87.   B. Wu, Y. Fu, J. Xu, G. Lin, M. Hou, J. Power Sources, 194 (2009) 976

88.   V. D. Noto, E. Negro, S. Lavina, S. Gross, G. Pace, Electrochimica Acta, 53 (2007) 1604

89.   H. Zhong, H. Zhang, G. Liu, Y. Liang, J. Hu, B. Yi, Electrochemistry Commun., 8 (2006) 707

90.   M. Itoh, K. Machida, M. Yamamoto, K. Hirose, G. Adachi, J. Alloys Compd., 364 (2004) 208

91.   M. Itoh, K. Machida, K. Hirose, T. Sakata, H. Mori, G. Adachi, J. Phys. Chem. B, 103 (1999) 9498

92.   M. Itoh, K. Machida, H. Nakajima, K. Hirose, G. Adachi, J. Alloys Compd., 288 (1999) 141

93.   P. Mars, D. W. van-Krevelen, Chem. Eng. Sci. Spec. Suppl., 41 (1954) 263

94.   T. Xiao, A. Hanif, A. P. E. York, Y. Nishizaka, M. L. H. Green, Phys. Chem. Chem. Phys., 4 (2002) 4549

95.   "Industrial Organic Chemistry", eds. K. Weissermel, H. J. Arpe, VCH, Weinheim, 3rd ed. (1997)

96.   R. S. Downing, P. J. Kunkeler, H. van Bekkum, Catal. Today, 37 (1997) 12

97.   C. Haas, European Chemical News, (2004) 16

98.   "Kirk-Othmer Encyclopedia of Chemical Technology" ed. M. E. Howe-Grant, John Wiley and Sons, Inc., New York, 4th ed., Vol 2, pg 638

99.   "Fundamentals of Industrial Catalytic Processes", eds. C. H Bartholomew, R. J Farrauto, Wiley, 2nd ed., (2006) pg 372

100. G. E. Veitch, K. L. Bridgwood, S. V. Ley, Organic. Lett., 10 (2008) 3623

101. Z. Zhang, R. Liu, Y. Qian, Mater. Research Bulletin, 37 (2002) 1005

102. C. Goodeve, K. H. Jack, Disc. Farday Soc., 4 (1948) 82

103. K. H Jack, Acta. Cryst., 5 (1952) 404

104. A. G. Gordon, D. H. Gregory, A. J. Blake, D. P. Weston, M. O. Jones, Int. J. Inorg. Mat., 3 (2001) 973

105. G. Paniconi, Z. Stoeva, R. I Smith, P. C. Dippo, B. L. Gallagher, D. H. Gregory, J. Solid State Chem. 181 (2008) 158

106. F. Zong, H. Ma, C. Xue, W. Du, X. Zhang, H. Xiao, J. Ma, F. Ji, Mat. Lett., 60 (2006) 905

107. L. Volpe, M. Boudart, J. Phys. Chem., 90 (1986) 4874.

108. Y. Wakai, T. Hara, K. K. Bando, N. Ichikuni, S. Shimazu, Top. Catal., 52 (2009) 1517

109. S. J. Henderson, A. L. Hector, J. Solid State Chem., 179 (2006) 3518

110. R. Kojima, K. I Aika, Appl. Catal A: Gen., 209 (2001) 317

111. J. S. J. Hargreaves, D. Mckay, J. Molecular Catal. A: Chem., 305 (2009) 125

112. G. Y Huang, J. D. Lin, Z. X. Xu, D. W. Liao, Chinese Chem. Lett., 16 (2005) 273

113. D. Szmigiel, H. Bielawa, M. Kurtz, O. Hinrichsen, M. Muhler, W. Raróg-Pilecka, S. Jodzis, Z. Kowalczyk, L. Znak, J. Zielinski, J. Catal., 205 (2002) 205

114. D. Szmigiel, W. Raróg-Pilecka, E. Mi´skiewicz, M. Gli'nski, M. Kielak, Z. Kaszkur, Z. Kowalczyk, Appl. Catal A: Gen., 273 (2004) 105

115. B. Fastrup, Catal. Lett., 48 (1997) 111.

116. E. Truszkiewicz, W. Raróg-Pilecka, K. Schmidt-Szalowski, S. Jodzis, E. Wilczkowska, D. Lomot, Z. Kaszkur, Z. Karpin´ski, Z. Kowalczyk, J. Catal., 265 (2009) 181

117. P. Desrosiers, S. Guan, A. Hagemeyer, D. M. Lowe, C. Lugmair, D. M. Poojary, H. Turner, H. Weinberg, X. Zhou, R. Armbrust, G. Fengler, U. Notheis, Catal. Today, 81 (2003) 319

118. G. E. Keller, M. Bhasin, J. Catal., 73 (1982) 9

119. R. Contractor, J. Ebner, M. J. Mummey, Studies Surf. Sci. Catal., 55 (1990) 553

120. "Heterogeneous Catalytic Oxidations: Fundamental and Technological Aspects of the Selective and Total Oxidation of Organic Compounds", ed. B. K. Hodnett, Wiley, (2000) 135

121. P. Tetenyi, in "Isotopes in Heterogeneous Catalysis", eds. J. S. J. Hargreaves, S. D. Jackson, G. Webb, Imperial College Press, London, (2006) Chapter 4.

122. J. M. Gracia, F. F. Prinsloo, J. W. Niemantsverdriet, Catal. Lett., 133, (2009) 257

123. G. I. Panov, G. K. Boreskov, A. S. Kharitonov, E. M Moroz, V. I Sobolev, Kinetics Catal., 25, (1984) 101

124. D. Mckay, D. H. Gregory, J. S. J. Hargreaves, S. M. Hunter, X. L. Sun, Chem. Commun., (2007) 3051

125. S. M. Hunter, D. Mckay, R. I. Smith, J. S. J. Hargreaves, D. H. Gregory, Chem. Mater., 22 (2010) 2898

126. D. H. Gregory, J. S .J Hargreaves, S. M. Hunter, Catal. Lett., 141 (2011) 22

127. "Kirk-Othmer Encyclopedia of Chemical Technology", ed. M. E. Howe-Grant, John Wiley & Sons, Inc., New York, 4th ed., Vol 2, pg 426

128. "Catalytic Ammonia Synthesis – Fundamentals and Practice",ed. J. R. Jennings, Plenium Press, New York (1991)

129. Kellogg Co., U.S. Patent 4568532, (1984)

130. R. B. Strait, Nitrogen Methanol, 238 (1999) 37

131. R. B. Strait, S. A. Knez, in: International Conference Exhibition, Caracas, 28 February–2 March, 1999.

132. S. R. Tennison, in "Catalytic Ammonia Synthesis: Fundamentals and Practice", ed J. R. Jennings, Plenum Press, New York, (1991) pg 303

133. T. Koerts, R. A. van Santen, J. Chem. Soc., Chem. Commun., (1991) 1281

134. T. Koerts, M. J. A. Deelen, R. A. van Santen, J. Catal., 138 (1992) 101

135. S. Ramanathan, S. T. Oyama, J. Phys. Chem. 90 (1986) 4874

136. C. Stampfl, A. J. Freeman, Phys. Rev. B, 71 (2005)

137. S. Burns, J. G. Gallagher, J. S. J. Hargreaves, P. J. F. Harris, Catal. Lett., (2007) 122

138. F. H. Ribeiro, R. A. Dalla Betta, M. Boudart, E. Iglesia, J. Catal., 130 (1991) 498

139. M. J. Ledoux, C. Pham Huu, J. Guille, H. Dunlop, J. Catal., 134 (1992) 383

140. K. E. Curry, L. T. Thompson, Catal. Today, 21 (1994) 171

141. F. H. Ribeiro, R. A. Dalla Betta, M. Boudart, J. Baumgartner E. Iglesia, J. Catal., 130 (1991), 86

142. K. Hori, M. Mori, J. Am. Chem. Soc., 120 (1998) 7651

143. M. Mori, J. Organometallic Chem., 689 (2004) 4210

144. H. Zhang, F. Li, Q. Jia, Ceramics Int., 35 (2009) 1071

145. C. Wang, Y. Dai, H. Gao, X. Ruan, J. Wang, B. Sun, Solid State Commun., 150 (2010) 1370

146. X. Cui, Z. Yu, M. Ma, P. K. Chu, Surf. Coat. Tech., 204 (2009) 418

147. Z. Wu, F. Dong, W. Zhao, S. Guo, J. Hazardous Mat., 157 (2008) 57

148. Z. Zhang, J. B. M. Goodall, D. J. Morgan, S. Brown, R. J. H. Clark, J. C. Knowles, N. J. Mordan, J. R. G. Evans, A. F. Carley, M. Bowker, J. A. Darr, J. Euro. Ceramic Soc., 29 (2009) 2343

149. D. Li, H. Haneda, S. Hishita, N. Ohashi, Mat. Sci. Eng. B, 117 (2005) 67

150. S. Kaskel, K. Sclichte, T. Kratzke, J. Mol. Catal. A: Chem., 208 (2004) 291

151. C. R. Lotz, F. Sebba. Trans. Faraday Soc., 53 (1957) 1246

152. B. M. Biwer, S. L. Bernasek, Appl. Surf. Sci., 2 (1986) 41

153. C. C. Jiang, T. Goto, T. Hirai, J. Alloys Compd., 190 (1993) 197

154. S. Kaskel, K. Sclichte, G. Chaplais, M. Khanna, J. Mat. Chem., 13 (2003) 1496

155. C. C. Lee, Y. Hu, M. W. Ribbe, Science, 329 (2010) 642

156. L. A. Nikonova, S. A. Isaeva, N. I. Pershikova, A. E. Shilov, J. Mol. Catal., 1 (1975/76) 367

157. R. Kapoor, S. T. Oyama, J. Solid State Chem., 99 (1992) 303

158. H. Kwon, S. Choi, L. T. Thompson, J. Catal., 184 (1999) 236

159. E. Erturk, H. J. Heuvel, H. G. Dederichs, Surf. Coat. Technol., 39-40 (1989) 435

160. R. R. Aharonov, B. F. Coll, R. P. Fontana, Surf. Coat. Technol., 61 (1993) 223

161. K. Sugiyama, K. Hayashi, J. Sasaki, O. Ichiko, Y. Hashiguchi, Surf. Coat. Technol., 66 (1994) 505

162. C. Liu, A. Leyland, S. Lyon, A. Matthews, Surf. Coat. Technol., 76- 77 (1995) 623

163. T. Fujihana, Y. Okabe, K. Takahashi, M. Iwaki, Nucl. Instr. Meth. Phys. Rev. B, 45 (1990) 669

164. C. Gautier, J. Machet, Thin Solid Films, 295 (1997) 43

165. F. Elstner, C. Gautier, H. Moussaoui, O. Piot, J. Machet, Phys. Stat. Sol. A, 158 (1996) 505.

166. P. S. Herle, M. S. Hegde, N. Y. Vasathacharya, S. Philip, M. V. Rama Rao, T. Sripathi, J. Solid State Chem., 134 (1997) 120

167. H. Jehn, P. Ettmayer, J. Less Common Metals, 58 (1978) 85

168. A. G. Cairns, J. G. Gallagher, J. S. J. Hargreaves, D. Mackay, J. L. Rico and K. Wilson, J. Solid State Chem.,183 (2010) 613

169. T. L. Renken, M. W. Forkner, U.S patent 0227632, (2008)

170. C. E. Habermann, U.S patent 4772750, (1988)

171. S. J. Carter, M. D. Cliffton,U.S Patent 4965384, (1990)

172. J. W. Mitchell, R. P. Underwood, M. E. Ford, G. A. Vedage, H. X. Li, European Patent 150559 A1, (2005)

173. M. Yasuhara, Y. Tatsuki, M. Nakamura, F. Matsunaga, European Patent 0293483 B1, (1993)

174. M. H. W. Burgers, H. van Bekkum, J. Catal., 148 (1994) 68

175. H. Xu, C. Wolf, Chem. Commun., (2009) 3035

176. R. K. Gasselli, in "Handbook of Heterogenous Catalysis", eds. G. Ertl, H. Knözinger, J. Weitkamp, Wiley, New York, Vol. 5 (1997) pg. 2302.

177. R. K. Gasselli, Top. Catal., 21 (2002) 79.

178. J. D. Burrington, R. K. Gasselli, J. Catal., 59 (1979) 79

179. J. D. Burrington, C. T. Kartisek, R. K. Gasselli, J. Catal., 81 (1983) 489

180. M. Liu, W. You, Z. Lei, T. Takata, K. Domen, C. Li, Chinese J. Catal., 27 (2006) 556

181. M. Hara, G. Hitoki, T. Takata, J.N. Kondo, H. Kobayashi, K. Domen, Catal. Today, 78 (2003) 555

182. K. Maeda, N. Nishimura, K. Domen, Appl. Catal. A: Gen., 370 (2009) 88

183. C. Yue, M. Trudeau, D. Antonelli, Chem. Commun., (2006) 1918

184. C. Yue, L. Qiu, M. Trudeau, D. Antonelli, Inorg. Chem., 46 (2007) 5084

185. J. G. Choi, Appl. Catal. A: Gen., 184 (1999) 189

186. H. Böhm, F. A. Pohl, Wiss. Ber. AEG-Telefunken, 41 (1968) 46

187. R. Kiessling, L. Peterson, Acta Metallurgica, 2 (1954) 675

188. W. Ensinger, M. Kiuchi, Surf. Coat. Technol., 84 (1996) 425

189. C. Shi, X. F. Yang, A. M. Zhu, C. T. Au, Catal. Today, 93-95, (2004) 819

190. J. A. Melo-Banda, J. M. Domínguez, G. Sandoval-Robles, Catal. Today, 65 (2001) 279

191. J. Monnier, H. Sulimma, A. Dalai, G. Caravaggio, Appl. Catal. A: Gen., 382 (2010) 176

192. A. Mittasch, in " Advances in Catalysis and Related Subjects" eds W. G. Frankenburg, V. I. Kowmarewsky, E. K. Rideal, Academic Press, New York, Vol 2 (1950) pg. 81

193. Z. Knor, C. Edelmann. J. Rudny, J. Stachurski, App. Surface Sci., 25 (1986) 107

194. Z. Yao, X. Zhang, F. Peng, H. Yu, H. Wang, J. Yang, Int. J. Hydrogen Energy, 36 (2011) 1955

195. M. S. Platanov, S. B. Anisimov, J. Gen. Chem., 1360 (1937)

196. J. P. McGeer, H. S. Taylor, J. Am. Chem. Soc., 73 (1951) 273

197. N. D. Spencer, G. A. Somorjai, J. Catal., 78 (1982) 148

198. E. B. Yeh, L. H. Schwartz, J. B. Butt, J.Catal., 91 (1985) 241

199. R. B. Anderson, Adv. Catal., 5 (1953) 355

200. E. P. Perman, Proc. Roy. Soc., 76 (1905) 167

201. A. Ozaki, K. Aika, in "Catalysis Science and Technology" eds J.R. Anderson, M. Boudart, Springer, Berlin, Vol 1 (1981) pg 106

202. K. Tamaru, in "Catalytic Ammonia Synthesis: Fundamentals and Practice", ed J. R. Jennings, Plenum Press, New York, (1991) pg. 13

203. A. Mittasch, E. Kuss, O. Emert, Z. Elektrochem, 34 (1928) 829

204. H. Y. Zhu, J. Alloys Compds., 240 (1996) L1

205. G. I. Panov, A. S. Kharitonov, React. Kinet. Catal. Lett., 29 (1985) 267

206. C. J. H Jacobson, J. Jiang, S. Mǿrup, B. S. Clausen, H. Topsǿe, Catal. Lett., 61 (1999) 115

207. A. Leineweber, J. Aufrecht, E. J. Mittemeijer, Int. J. Mat. Res., 97 (2006) 753

208. A. Leineweber, H. Jacobs, F. Huning, H. Lueken, H. Schilder, W. Kockelmann, J. Alloys Compds., 288 (1999) 79

209. A. Leineweber, T. Liapina, T. Gressmann, M. Nikolussi, E. J. Mittemeijer, Adv. Sci. Tech., 46 (2006) 32

210. Z. W. Yao, A. M. Zhu, C. T. Au, C. Shi, Catal. Lett., 130 (2009) 63

211. M. Hasegawa, T. Yagi, Solid State Commun., 135 (2005) 294

212. X. Wang, H. Jia, W.T. Zheng, Yan Chen, S. Feng Thin Solid Films, 517 (2009) 4419

213. J. S. Fang, L. C. Yang, C. S. Hsu, G. S.Chen, Y. W. Lin, J. Vac. Sci. Technol. A, 22 (2004) 698

214. R. Juza, W. Sachsze, Z. Anorg. Allg. Chem., 251 (1943) 201

215. K. Peter, J. Solid State Chem., 176 (2003) 530

216. D. Vempaire, S. Miraglia, J. Pelletier, D. Fruchart, E. K. Hill, L. Ortega, A. Sulpice, F. Fettar, J. Alloys Compds, 480 (2009) 225

217. I. M. Neklyudov, A. N. Morozov, Physica B, 350 (2004) 325

218. A. Leineweber, H. Jacobs, S. Hull, Inorg. Chem., 40 (2001) 5818

219. A. Baiker, D. Monti, Y. S. Fan, J. Catal. 88, (1984) 81

220. S. R. Tennison, in "Catalytic Ammonia Synthesis: Fundamentals and Practice", ed J. R. Jennings, Plenum Press, New York, (1991) 350

221. N. Kieda, G. L. Messing, J. Mat. Sci. Lett., 17 (1998) 299

222. T. Maruyama, T. Morishita, Appl. Phys. Lett., 69 (1996) 890

223. K. J. Kim, J. H. Kim, J. H. Kang, J. Crystal Growth, 222 (2001) 767

224. D. M. Borsa, D. O. Boerma, Surf. Sci., 548, (2004) 95

225. P. Blaha, J. Redinger, K. Schwarz, Phys. Rev. B, 31 (1985) 2316

226. W. R. L. Lambrecht, Phys. Rev. B, 62 (2000) 13538

227. N. Ashley, R. Grimes, K. McClellan, J. Mater. Sci., 42 (2007) 1884

228. R. Juza, H. Hahn, Z. Anorg. Allg. Chem., 241 (1939) 172

229. U. Zachwieja, H. Jacobs, J. Less Common Mat., 161 (1990) 175

230. U. Zachwieja, H. Jacobs, J. Less Common Mat., 170 (1991) 185

231. R. Juza, K. Langerand K. von Benda, Angew Chem., 80 (1968) 373

232. F. Gulo, A. Simon, J. Kohler, R. K. Kremer, Angew Chem. Int., 43 (2004) 2032

233. M. G. Moreno-Armenta, A. Martínez-Ruiz, N. Takeuchi, Solid State Sci., 6 (2004) 9

234. H. Hahn, Phys. Rev. B, 53 (1996) 12684

235. K. M. Parida, D. Rath, S. S. Dash, J. Mole. Catal. A: Chem., 318, (2010) 85

236. C. Dume, W. F. Hölderich, Appl. Catal. A: Gen., 183, (1999)167

237. R. Juza, H. Hahn, Z. Anorg. Allg. Chem., 224 (1940) 125

238. Z. Li, P.Wang, H. Chen, X. Cheng, Physica B, 406 (2011)1182

239. R. Long, Y. Dai, L.Yu, B. Huang, S. Han, Thin Solid Films, 516 (2008) 1297

240. F. Zong, H. Ma, C. Xue, H. Zhuang, X. Zhang, H. Xiao, J. Ma, F. Ji, Solid State
     Commun., 132 (2004) 521

241. D. E. Partin, D.J. Williams, M.O'Keeffe, J. Solid State Chem.,132 (1997) 56

242. A. Ozaki, K. Aika and H. Hori, Bull. Chem. Soc. Jap., 44 (1971) 3216

243. Q. C. Xu, J. D. Lin, J. Li, X. Z. Fu, Z. W. Yang, W. M. Guo, D. W. Liao, J. Molecular Catal. A: Chem., 259 (2006) 218

244. H. Lorenz, I. Orgzall, E. Hinze, Diamond Relat. Mater., 4 (1995) 1046

245. L. Chen, M. Huang, T. Luo, Y. Gu, L. Shi, Z. Yang, Y. Qian, Mater. Lett., 58 (2004) 3634

246. I. P. Parkin, A. M. Nartowski, Poylhedron, 17 (1998) 2617

247. J. Hao, Y. Li, Q. Zhou, D. Liu, M. Li, F. Li, W. Lei, X. Chen, Y. Ma, Q. Cui, G. Zou, J. Liu, X. Li, Inorg. Chem., 48, (2009) 9737

248. E. Schwab, E. Wicke, Z. Physik. Chem., 122 (1980) 217

249. B. M. Biewer, S. I. Bernasek, Appl. Surf. Sci., 25 (1986) 41

250. R. Kojima, H. Enomoto, M. Muhler, K. Aika, Appl. Catal. A: Gen., 246 (2003) 311

251. Z. Kowalczyk, M. Krukowski, W. Raróg-Pilecka, D. Szmigiel, J. Zielinski, Appl. Catal. A: Gen., 248 (2003) 67

252. A. S. Kharitonov, G. K. Boreskov, G. I. Panov, Yu. D. Pankratiev, React. Kinet. Catal. Lett., 22 (1983)

253. T. W Hansen, P. I. Hansen, S. Dahl, C. J. H. Jacobsen, Catal. Lett., 84 (2002) 7

254. K. Suzuki, T. Kaneko, H. Yoshida, H. Morita, H. Fujimori, J. Alloys Compd., 224 (1995) 232

255. "Handbook of Chemistry and Physics" eds R. C. Weast, M. J. Astle, W. H. Beyer, C.R.C Press Inc., Florida, 67th ed, F-157

256. T. A. Bazhenova, A. E. Shilov, Coord. Chem. Rev., 144 (1995) 69

257. M. Gans, Hydrocarbon Proc., 55 (1976) 145

258. M. Yashuhara, F. Matsunaga, Mitsui Petrochemicals Industries Ltd., European Patent 321-275-A2, (1989)

259. A. A. Shutz, L. A. Cullo, Aristech Chemical Corp., PCT Patent. WO 9305010A1, (1993)

260. O. C. Karakalitis, Jr., C. M. Vanderwaart, F. Houghton, U.S Patent 2891094 (1959)

261. M. Sada, T. Zinno, Y. Otsuka, T. Ohrui, German Patent 1133394 (1973)

262. H. J. Pistor, H. Sperber, G. Poehler, A. Wegerich, German Patent 2320658 (1962)

263. H. Thelen, K. Halcour, U. S. Patent 3882048 (1975)

264. J. Becker, W. F. Holderich, Catal. Lett., 54 (1998) 125

265. N. I. Kuznetsova, L. I. Kuznetsova, L. G. Detusheva, V. A. Likholobov, G. P. Pez, H. Cheng, J. Molecular Catal. A: Gen.,161 (2000) 1

266. T. Chen, C. Hu, Z. Fu, A. Tian, Chinese Sci. Bulletin, 47 (2002) 1937

267. C. Hu, L. Zhu, Y. Xia, Ind. Eng. Chem. Res., 46 (2007) 3443]

268. E. N Squire, U.S Patent 2948755, (1960)

269. E. N. Squire, U.S Patent 3919155, (1975)

270. T. W DelPesco, U.S Patent 4001260, (1977)

271. T. W. DelPesco, U.S Patent 4031106, (1977)

272. W. F. Holdrich, Appl. Catal. A: Gen., 194-195 (2000) 487

273. P. J. Cashman, J. D. Beede, J. Forens. Sci. Soc., 19 (1979) 137

274. V. J. Harding, R. M. MacLean, J. Biological Chem., 25 (1916) 337

275. "Thin Layer Chromatography - Physical and Chemical Detection Methods: Fundamentals and Reagents I" eds. H. Jork, W. Funk, W. Fischer, H. Wimmer, VCH, Weinheim, Vol 1 (1990) pg 354

276. "Thin Layer Chromatography – A Laboratory Handbook" eds. E. Stahl, Academic Press Inc., New York, (1965) pgs 405 and 496

277. "Organic Chemistry" eds. J. Claydon, N. Greaves, S. Warren, P. Wothers, Oxford University Press, (2001) Chapter 11

278. "Organic Chemistry" ed. P. Y. Bruice, Pearson Education (2004) Chapter 14

279. "Handbook of Chemistry and Physics" eds. R. C Weast, M. J. Astle, W. H. Beyer. C.R.C Press Inc., Florida, 67th ed, F-209

280. H. E. Gottlieb, V. Kotlyar, A. Nudelman, J. Org. Chem., 62 (1997) 7512

281. J. C. Slater, J. Chem. Phys., 41 (1964) 3199

282. R. G. Bowman, M. H. Tegen, G. E. Hartwell, U. S. Patent 4922024, (1990)

283. A. K. Rausch, E. van Steen, F. Roessner, J. Catal., 253 (2008) 111

284. A. Baiker, Heterogeneous Catal. and Fine Chem., (1988) 283

285. H. Schulz, Catal. Today, 154 (2010) 183